# The physiology of alien chloroplasts: light adaptation mechanisms in cytoplasmic hybrids of the Solanaceae family.

Yeates, Anna M.

# The physiology of alien chloroplasts: light adaptation mechanisms in cytoplasmic hybrids of the Solanaceae family

Anna M. Yeates

---

Submitted in partial fulfilment of the requirements of the degree of Ph.D. at the

School of Biological and Chemical Sciences,
Queen Mary, University of London

September 2014

Queen Mary
University of London

# Author's declaration

I, Anna M. Yeates, confirm that the research included within this thesis is my own work or that where it has been carried out in collaboration with, or supported by others, that this is duly acknowledged below and my contribution indicated. Previously published material is also acknowledged below.

I attest that I have exercised reasonable care to ensure that the work is original, and does not to the best of my knowledge break any UK law, infringe any third party's copyright or other Intellectual Property Right, or contain any confidential material.

I accept that the College has the right to use plagiarism detection software to check the electronic version of the thesis.

I confirm that this thesis has not been previously submitted for the award of a degree by this or any other university.

The copyright of this thesis rests with the author and no quotation from it or information derived from it may be published without the prior written consent of the author.

## Support of work by others

- The cybrid lineage on which this work is based was created in the laboratory of Dr Mikhajlo Zubko (Zubko et al., 1996). Their method for creating the plants is described here in §2.7.1.
- Dr Giulia Mastroianni performed all ultra-thin sectioning for electron microscopy (described in §2.11.2).
- Freeze fracture was done in collaboration with Dr Petra Ungerer (§2.11.3).
- Electron microscopy was performed in collaboration with Dr Petra Ungerer and Dr Giulia Mastroianni (§2.11.4).
- Proteomic work (in-gel sample processing and LC-MS/MS) was performed at Cambridge Centre for Proteomics (CCP, Biochemistry department, University of Cambridge, Cambridge, UK; http://proteomics.bio.cam.ac.uk), facility manager, Dr Mike Deery. The procedure is described in §2.10.1.

## Meetings at which the work was presented

### Poster presentations

- Plant Organellar Signalling conference, from algae to higher plants. FEBS. Primošten, Croatia. 31/08 - 03/09/11
- Postgraduate symposium, Queen Mary, University of London. 20/02/12
- Light Harvesting, satellite meeting of the International Congress on Photosynthesis. ISPR. St Louis, Missouri, USA. 08 - 11/08/13
- International Congress on Photosynthesis. ISPR. St Louis, Missouri, USA. 08 - 11/08/13
- Harvest meeting, Marie Curie Initial Training Network, Chania, Crete. 18 - 21/09/13

### Seminar presentations

- Postgraduate symposium, Queen Mary, University of London. 04/03/11
- Harvest meeting, Marie Curie Initial Training Network. Cambridge, UK. 18/09/11
- Plastid Preview meeting, University of Manchester, UK. 07/09/12
- Biochemical Society christmas meeting, University of Sheffield, UK. 17/12/12
- Postgraduate symposium, Queen Mary, University of London. 18/02/13
- Biochemical Society christmas meeting, Queen Mary University, London. 16/12/14

---

*Signed* Anna M. Yeates

*date* September 26th, 2014

# Abstract

The investigation presented here is of a new plant model for photosynthesis research. The plant's novelty is a hybrid cytoplasm which was engineered to contain the nuclear genome of *Nicotiana tabacum* (tobacco) and the chloroplast genome of *Hyoscyamus niger* (henbane). For photosynthesis research the implications of cytoplasmic hybridisation centre on the nuclear and chloroplast encoded pigment-protein complexes of the photosynthetic machinery in the thylakoid membrane of the chloroplast.

We investigate how the energy input from nuclear-encoded light harvesting complexes to the chloroplast-encoded core complexes is regulated in the cybrid plants, when light limits or exceeds photochemical capacity. When light limited, the phenomenon of state transitions (ST) serves to redress the imbalance of light input at PSI and PSII. In excess light, non-photochemical quenching (NPQ) mechanisms are activated in order to safely dissipate potentially harmful energy that has been absorbed by the system.

Our investigation at first indicated that the cybrid plants had a greater capacity for NPQ compared to wildtype *N. tabacum* and *H. niger*. LHCII aggregation, xanthopyll cycle activity and PsbS were investigated for a possible reasons for the increase. However no difference or contradictory evidence was found. NPQ measurements were repeated and showed large variability and no significant difference in NPQ capacity compared to the wildtype parent species. The reason for the variability in the cybrid results could not be resolved but is suggested to be due to heightened environmental sensitivity.

STs were found to be consistently inhibited in cybrids. Investigation of cybrid LHC isoelectric points and molecular weight revealed novelties. LHCs were then subjected to proteomic analysis that indicated possible truncation at the N-terminus, and thus the possible removal of a phosphorylation site that crucial for the initiation of ST.

We also investigate the ability of the $Nt(Hn)$ cybrid to adjust to high and low intensity light environments in terms of acclimation at the level of the whole plant, leaf, tissue, cell, chloroplast, thylakoid membrane, pigment, and electron transport rates.

# Acknowledgements

Firstly, I would like to thank my Ph.D. supervisor, Professor Alexander Ruban for giving me this project and for helping me through it with advice, patience and encouragement. I have thoroughly enjoyed being a member of his engaging, inspiring and dynamic lab group and I deeply appreciate that he has made so many resources freely available to me.

I would also like to thank Dr Erica Belgio who has guided me through all of the laboratory work, the theory and the written work, and as a result I will probably always remain indebted to her for her time, patience and insatiable desire for understanding and to be understood. When we no longer see each other regularly, there will be an Erica shaped gap in my life.

I would like to thank Dr Chris Duffy for his occasional mentoring, he is always interested and interesting and I will miss not working near him. Thank you also to the ever cheerful Dr Petra Ungerer who has untiringly come to my aid in the lab, in particular in the freeze fracture, thin section and TEM work. Thank you also to Dr Giulia Mastroianni for her work in ultra-thin sectioning and electron microscopy.

It is a great pleasure to also acknowledge the support I received from Dr Snjezana Juric who thankfully pushed me in to the lab at the very start, and from Heike Brinkman for her advice about plant growth and her guidance with GISH, although we never got it to work. I have also had several helpful discussions with Dr Ruth Rose, Dr Katerina Petrou, Dr Matt Johnson and members of the Marie Curie European Harvest Network.

I would like to express my gratitude for the proteomic work that was performed at Cambridge Centre for Proteomics, and the helpful assistance from the staff there, particularly Dr Mike Deery the facility manager. Finally, thank you to Dr Mikhajlo Zubko for donating the cybrid seeds from the exciting, novel plant line that he created and upon which this work is based, and for introducing me to them in a visit to Manchester University at the beginning of my Ph.D.. I acknowledge the BBSRC for funding this project.

# Abbreviations and symbols

| | |
|---|---|
| aa | amino acid |
| AL | actinic light (Dual PAM) |
| Ax | antheraxanthin |
| ATP | adenosine triphosphate |
| Bis-Tris | 2-[bis(2-hydroxyethyl)amino]-2-(hydroxymethyl)propane-1,3-diol |
| bp | base pair |
| BSA | bovine serum albumin |
| C | $Nt(Hn)$ cytoplasmic hybrid plant |
| C- | carboxyl-terminus of the protein |
| $\beta$-carot. | $\beta$-carotene |
| CCP | Cambridge Centre for Proteomics |
| °C | degree Celsius |
| CEF | cyclic electron flow |
| Chl | chlorophyll |
| Chl $a$ | chlorophyll $a$ |
| Chl $b$ | chlorophyll $b$ |
| cmc | critical micelle concentration |
| CORR | co-location for redox regulation |
| CP24 | $\sim$ 24 kDa apoprotein of the PSII antenna complex (minor antenna) |
| CP26 | $\sim$ 26 kDa apoprotein of the PSII antenna complex (minor antenna) |
| CP29 | $\sim$ 29 kDa apoprotein of the PSII antenna complex (minor antenna) |
| CP43 | $\sim$ 43 kDa apoprotein of the PSII core complex (internal antenna) |
| CP47 | $\sim$ 47 kDa apoprotein of the PSII core complex (internal antenna) |
| cpDNA | chloroplast DNA |
| cTP | chloroplast transit peptide |
| cybrid | cytoplasmic hybrid plant |
| Cyt $b_6f$ | cytochrome $b_6$ protein |
| D1 | PSII core component D1 |
| D2 | PSII core component D2 |
| Da | Dalton |
| DCMU | 3-(3,4-dichlorophenyl)-1,1-dimethylurea |

| | |
|---|---|
| $\alpha$-DM | n-Decyl-$\beta$-D-maltopyranoside (detergent) |
| $\beta$-DM | n-Dodecyl-$\beta$-D-maltopyranoside (detergent) |
| DNA | deoxyribonucleic acid |
| DTT | 1,4-dithiothreitol |
| Dun. | indicates that the organism was named by Dunal |
| $e^-$ | electron |
| e.g. | exempli gratia (lat), meaning "for example" |
| EDTA | ethylendiamine tetraacetic acid |
| ETC | electron transport chain |
| ETR | electron transport rate |
| ExPASy | Expert Protein Analysis System |
| Fd | ferredoxin |
| $F_m$ | maximal fluorescence |
| $F_o$ | minimal fluorescence |
| $F_s$ | steady state fluorescence |
| $F_s$I | steady state fluorescence with FR light in State I |
| $F_s$I' | fluorescence in State I, shortly after FR light removal |
| $F_s$II | fluorescence just after FR reappliction |
| $F_s$II' | steady state fluorescence after acclimation to FR light |
| FF | freeze fracture |
| FNR | ferredoxin:$NADP^+$ oxidoreductase |
| FPLC | fast pressure liquid chromatography |
| FR | the inbuilt far red light source in DUAL PAM |
| x g | centrifugal force |
| GC | (Sanyo) controlled environment growth cabinet |
| GE | growth environment, either HL or LL |
| GTP | guanosine triphosphate |
| h | hour |
| H | Henbane (*Hyocyamus niger*) |
| HEPES | N-2-hydroxyethypiperazin-N'-2-ethansulfonate |
| HL | high intensity light growth environment |
| HPLC | high pressure liquid chromatography |
| IEF | iso-electric focusing |
| ISPR | International Society of Photosynthesis Research |
| KCl | potassium chloride |
| kDa | kilodalton |
| $KH_2PO_4$ | potassium dihydrogen phosphate |
| L. | indicates that the organism was named by Linnaeus |
| L | litre |

| | |
|---|---|
| LC MS-MS | liquid chromatography followed by tandem mass spectrometry |
| LED | light emitting diode |
| LEF | linear electron flow |
| LHC | pigment-protein light harvesting complex |
| *lhca* | gene for PSI chlorophyll a/b-binding protein |
| *lhcb* | gene for LHCII chlorophyll a/b-binding protein |
| LHCII | major, trimeric light harvesting complex of PSII |
| LL | low intensity light growth environment |
| $LN_2$ | liquid nitrogen |
| lTP | lumen transit peptide |
| Lut | lutein |
| MeOH | methanol |
| MES | 2-(N-morpholino)-ethane sulphonic acid |
| $MgCl_2$ | magnesium chloride |
| $MgSO_4$ | magnesium sulphate |
| Mill. | indicates that the organism was named by Miller |
| min | minute |
| ML | fluorescence measuring light (Dual PAM) |
| mL | millilitre |
| MS | mass spectrometry |
| mtDNA | mitochondrial DNA |
| MW | molecular weight |
| Mya | million years ago |
| N- | amino-terminus of the protein |
| $Na_2HPO_4$ | sodium hydrogen carbonate |
| $NADP^+$ | nicotinamide adenine dinucleotide phosphate, oxidised |
| NADPH | nicotinamide adenine dinucleotide phosphate, reduced |
| NaOH | sodium hydroxide |
| NCBI | National Centre for Biotechnology Information |
| Nx | neoxanthin |
| nm | nanometer |
| NPQ | non-photochemical quenching of chlorophyll fluorescence |
| ns | nanosecond |
| NSL | non-saturating light |
| $OD_\lambda$ | optical density at a wavelength denoted in subscript |
| OEC | oxygen evolving complex |
| PAM | pulse amplitude modulation |
| PAR | photosynthetically active radiation (0.4-0.7 $\mu$m) |
| PBS | phosphate buffered saline |

| | |
|---|---|
| $OsO_4$ | osmium tetroxide |
| Pc | plastocyanin |
| PCR | polymerase chain reaction |
| PDB | Protein Data Bank |
| PEG | polyethyleneglycol |
| $\Delta$ pH | trans-thylakoid membrane pH |
| pI | isoelectric point |
| PGR | plant growth regulator hormone |
| pmf | proton motive force |
| PTM | post-translational modification |
| PQ | plastoquinone |
| PSI | photosystem I holocomplex |
| PSII | photosystem II holocomplex |
| PTFE | polytetrafluoroethylene |
| $Q_A$ | primary quinine acceptor at PSII |
| $Q_B$ | secondary quinine acceptor at PSII |
| RC | reaction centre of the photosystem |
| RLC | rapid light curve |
| RNA | ribonucleic acid |
| RNC | ribosome-nascent chain |
| ROS | reactive oxygen species |
| rpm | rotations per minute |
| RT | room temperature |
| Rubisco | ribulose-bis-phosphate carboxylase |
| s | second |
| SD | standard deviation |
| SDS | sodium dodecyl sulfate |
| SDS-PAGE | sodium dodecyl sulfate polyacrylamide gel electrophoresis |
| SE | standard error |
| SL | saturating light |
| SP | saturating pulse |
| SPP | stromal processing peptidase |
| SR | Signal-Recognition-Particle (SRP) Receptor |
| SRP | Signal Recognition Particle |
| ST | state transitions |
| STI | state I, LHCII is functionally attached to PSII |
| STII | state II, LHCII is functionally attached to PSI |
| T | tobacco (*Nicotiana tabacum*) |
| TEM | transmission electron microscopy |

| | |
|---|---|
| TEMED | tetramethylethylenediamine |
| TPP | thylakoidal processing peptidase |
| TIC | translocon at the inner envelope membrane of chloroplasts |
| TOC | translocon at the outer envelope membrane of chloroplasts |
| Tricine | N-[2-hydroxy-1,1-bis(hydroxymethyl)-ethyl]glycin |
| Tris | 2-Amino-2-hydroxymethyl-propane-1,3-diol |
| UniProt | Universal Protein resource |
| V | electromotive force (voltage) |
| VALAP | Vaseline, lanolin and paraffin sealer |
| Vx | violaxanthin |
| v/v | volume per volume |
| w/v | weight per volume |
| XC | xanthophyll cycle |
| Zx | zeaxanthin |
| $\lambda$ | wavelength |
| $\mu$L | microlitre |
| $\Phi$ | quantum yield |

# Contents

---

## Materials and Methods

---

## Results and Discussion

# List of Figures

# List of Tables

# Introduction

# An overview of the thesis

A novel combination of a nuclear genome from *Nicotiana tabacum* L. (tobacco) with a chloroplast subgenome from *Hyoscyamus niger* L. (henbane), has been established in a stable, sexually reproducible plant lineage. The result is a cytoplasmic hybrid (cybrid) of *N.tabacum*-nuclear-encoded and *H.niger*-chloroplast-encoded proteins. The plant's denomination is $Nt(Hn)$, following the cybrid naming convention which gives the initials of the nuclear parent, followed by those of the chloroplast parent in brackets. For photosynthesis research, the implications of an engineered merger of inter-specific plant subgenomes, centres around the photosynthetic machinery, its function and its regulation.

A plant nuclear genome encodes for $> 99$ % of the cell proteins, including most of those comprising the chloroplast. The chloroplast genome, in contrast, encodes for only about one hundred proteins, which are synthesised and utilised within the chloroplast. Most notably, the chloroplast genome encodes for the photosystem (PS) I and PSII reaction centre proteins. The photochemical reaction centre is the core component of the photosystem supercomplex, of which the other subunits are nuclear-encoded pigment-protein light harvesting complexes (LHCs) that collect light for photochemistry, while also regulating energy input to the reaction centre.

Sunlight is a highly variable source of energy and so the ability of a plant to regulate light harvesting by plastically coupling its structural and functional phenotype to its light environment is essential for optimal primary production. Acclimation to the long-term light environment is dependent upon the cooperative government of nuclear and chloroplast gene expression and protein degradation pathways. While to deal with short-term, unpredictable fluctuations in natural light, photosynthetic organisms have evolved molecular mechanisms that require the rapid and precise interaction of nuclear- and chloroplast- encoded proteins in the thylakoid membrane.

The cybrid plant offers an intriguing model for the study of light-regulation physiology, both at the level of interaction between the inter-specific proteins in the thylakoid membrane, and in the concerted action of the inter-specific sub-genomes for the regulated expression, and degradation, of the chloroplast proteins. This thesis presents the initial investigation of these aspects in this newly conceived

model (the *Nt*(*Hn*) cybrid), and as far as we are aware, it is the first investigation of either light acclimation or light harvesting regulation by molecular mechanisms in any cybrid plant.

The study started with two broad objectives. Firstly, we aimed to assess the acclimation of the *Nt*(*Hn*) cybrid to the long-term light environment, through phenotypic analysis of the whole plant, leaf, cell, chloroplast, thylakoid, membrane proteins, pigments and electron transport rates. And secondly, we aimed to investigate the mediation of short-term light fluctuations by the molecular mechanisms of state transitions, and non-photochemical quenching (NPQ). In most cases analyses were performed on plants that were grown under high light (HL) and under low light (LL) which allowed us to also see how the long-term acclimation effects short-term function.

In Chapter 1, we describe the chloroplast, thylakoids and the pigment-protein complexes that comprise the photosynthetic machinery of the light reactions in higher plants. Next, the photosynthetic mechanism is described, again, with our main focus bearing on the light-reactions. The topic of plant regulation in a changing light environment is reviewed with particular attention paid to the mechanisms of NPQ and state transitions. Our understanding of chloroplast evolution and the nuclear-chloroplast relationship is then considered and lastly, we introduce the cytoplasmic hybrid plant as a research topic.

Chapter 2 describes the Materials and Methods used for this investigation. We also describe the protocol used by Zubko et al. (1996) for the construction of the *Nt*(*Hn*) cybrid (§2.7.1). In §2.9.1 we include some background information on the principle of Pulse Amplitude Modulated (PAM) chlorophyll fluorometry and its use in monitoring photosynthetic and regulatory functions. In the experimental work, the wildtype *N.tabacum* plant was used as the main control, although in most procedures wildtype *H.niger* was also tested for comparison.

Chapters 3-6 are the Results and Discussion chapters. The investigation began with a general characterisation of the *Nt*(*Hn*) model (Chapter 3) in relation to wildtype *N.tabacum* and wildtype *H.niger*. Plant growth, seed germination rates and flower morphology are described. The chloroplast and mitochondrial genome analyses by Zubko et al. (1996, 2001), is presented in the discussion.

Our assessment of *Nt*(*Hn*) acclimation to long-term growth in LL and HL, is presented in Chapter 4. This included growth rate and plant size analysis, histological examination of leaf tissue, measurements of cell size and chloroplast size. Cell and chloroplast size ratios and numbers of chloroplasts per cell were investigated using confocal images of isolated leaf cells. Thin section transmission electron microscopy analysis of the chloroplasts and thylakoid membrane organisation was also performed. Molecular acclimation of the photosynthetic membrane was as-

sessed through protein stoichiometry and pigment composition analysis. Lastly, electron transport rates in LL and HL plants were investigated at various light intensities using rapid light curves.

The work presented in Chapter 5 is a main focus of our investigation. Here we assess the regulatory molecular mechanisms that occur in response to fast changes in light availability. Protective NPQ was measured from chlorophyll fluorescence traces according to standard procedures. Components known to be involved in the NPQ mechanism: PsbS, the xanthophyll cycle and the aggregation of trimeric LHCII, were each investigated. State transitions, a mechanism effective when light limits photochemistry, were also measured.

Interesting differences in the capacity for short term light regulation were found between *Nt*(*Hn*) and the wildtype parent plants. The investigation of possible explanations for the novel *Nt*(*Hn*) phenotype, comprised the subject of Chapter 6. This chapter includes an extensive investigation of the PSII major antenna through several techniques and proteomic work. A general discussion in Chapter 7 serves to draw the results together.

# Chapter 1

# State of the art

## 1.1 Photosynthesis, an overview

Photosynthesis is the conversion of solar energy into bioenergy followed by its subsequent use in the production of high-energy biomass from inorganic carbon. It is one of only two known mechanisms that secures energy and carbon for the biological world. The second mechanism, chemosynthesis, is found only in microorganisms at deep sea vents (Cavanaugh, 1983) and within the Earth's crust (Lever et al., 2013). This means that almost the entirety of the organic biomass that exists and has existed on Earth and the energy consumed by or trapped within it, was originally arrived at through photosynthesis: a biomolecular mechanism that occurs in some groups from the Bacteria domain and in the plants and algae of the Eukarya domain (Blankenship, 2002; Sugiura et al., 2014).

Two sequences characterise photosynthesis. In the first, the primary or 'light reactions', light energy is absorbed, trapped and conserved in the chemical bonds of reduced nicotinamide adenine dinucleotide phosphate (NADPH) and adenosine triphosphate (ATP), generating a gain in reducing power and a source of Gibbs free energy respectively. In the second sequence or 'dark reactions' this energy is used for the construction of carbohydrate ($C_6H_{12}O_6$) from ambient carbon dioxide ($CO_2$). The whole process can be summarised as a light-dependent redox reaction in a general formulation first devised by van Niel et al. (1942):

$$CO_2 + 2\,H_2A \xrightarrow{photons} (-CH_2O-) + H_2O + 2\,A \tag{1.1}$$

where -$CH_2O$- represents a unit of carbohydrate and $H_2A$ describes a general oxidisable species.

About 2.2-2.8 billion years ago, the ability to cleave electrons from $H_2O$ with deposition of $O_2$ as a waste product ($H_2A$ and 2 A in Eq. 1.1, respectively), de-

veloped in the ancient ancestors of modern day cyanobacteria (Des Marais et al., 2000; Renger, 2007), resulting in several profound consequences for life on Earth. Prokaryotic oxygenic photosynthesis eventually gave way to eukaryotic photosynthesis, an estimated 1.7 billion years ago (Leitch and Leitch, 2013) when a unicellular heterotroph engulfed and endosymbiotically incorporated a cyanobacterial cell. This then underwent an evolutionary transformation into the obligate organelle now recognised as the chloroplast (de Alda et al., 2014; Wicke et al., 2011). From this apparently singular endosymbiotic event all extant eukaryotic photoautotrophs are thought to have descended (McFadden and van Dooren, 2004; Palmer, 2000; Wicke et al., 2011).

The exhaust of $O_2$ into the atmosphere consequently accelerated, profoundly altering life on Earth. Anaerobic organisms were driven to near total extinction while the development of the oxidising atmosphere fulfilled a bioenergetic prerequisite for the origination of all multicellular life, propelling biodiversification of aerobic lifeforms (Canfield, 2014; Greiner et al., 2011; Schirrmeister et al., 2013). In addition, the coincidental development of the Earth's ozone ($OO_2$) layer provided the protective blanket against ultra-violet (UV) radiation that was necessary for the expansion of terrestrial biodiversity (Barber, 2014; Greiner et al., 2011).

## 1.2 The Machinery for Photosynthesis in Plants

### 1.2.1 The Chloroplast

Eukaryotic photosynthesis takes place exclusively in chloroplasts. Depending on the cell type and organism, chloroplasts may number up to 200 per cell. In Fig 1.1a, a scanning electron micrograph (SEM) of a leaf cross section reveals numerous chloroplast within the mesophyll cells of the leaf. In Fig 1.1b a single chloroplast is presented with its internal structures indicated. A double-membrane bounds the chloroplast compartment that is typically about 5-10 $\mu$m in diameter. The stroma, a colourless liquid, fills the internal space in which there is suspended a structure called thylakoids (§1.2.2).

As already mentioned, the chloroplast organelle is an ancestral remnant of a once-free living organism of the ancient cyanobacterial lineage. Now, the large majority of the endosymbiont's genetic material resides in the cell nucleus while the chloroplast retains a small, conserved fraction that encodes about 100 proteins. Therefore, in order to import the roughly 3000 nuclear encoded proteins needed to construct a fully functional chloroplast (Jarvis, 2008), the chloroplast envelope is necessarily richly embedded with protein import machinery (Soll and Schleiff, 2004; Jarvis, 2008). These molecular gateways are referred to as Toc (translocon

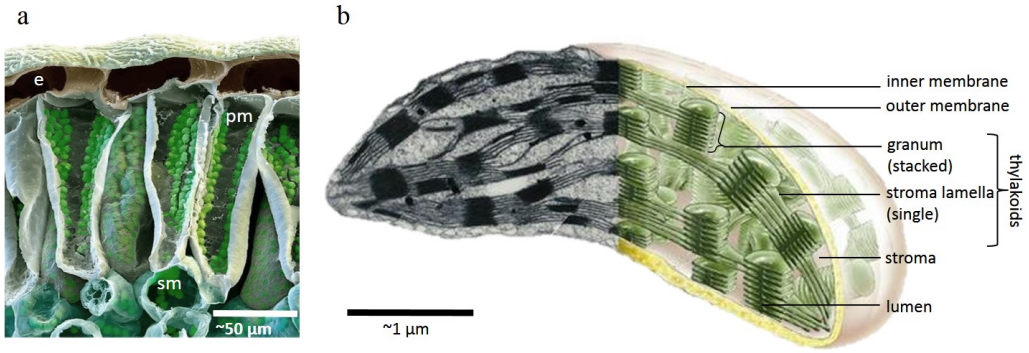


**Figure 1.1:** The chloroplast. **a)** A scanning electron micrograph (falsely coloured) of a leaf cross-section in which palisade mesophyll (pm), spongy mesophyll (sm) and upper epidermal cells (e) are apparent. Chloroplasts (coloured bright green) can be seen inside the mesophyll cells. The image was adapted from Hensel (2006). **b)** A single chloroplast imaged by TEM with an extension into a schematic diagram to represent the internal structures 3-dimensionally. Adapted from Pearson Education online archives.

at the outer envelope membrane of chloroplasts) and Tic (translocon at the inner envelope membrane of chloroplasts) machinery (Jarvis and López-Juez, 2013). The evolutionary history of the chloroplast is discussed more fully in §1.5.

### 1.2.2 Thylakoids

Thylakoids are an extensive membranous system that bound a continuous, internal space called the lumen (Fig. 1.1b). Their structure is highly oblate, typically spanning the chloroplast laterally, while only reaching a height of about 4-10 nm in the lumen (Ruban, 2012; Pribil et al., 2014). During photosynthesis, $H^+$ ions are pumped across the membrane into the lumen in order to build the pH gradient necessary for ATP synthesis (§1.3), it is therefore important that the lumenal space is osmotically intact and impermeable to uncontrolled ion movement, to maintain its acidification (Blankenship, 2002).

Thylakoids are found in two morphologically distinct arrangements, either folded into cylindrical stacked structures called grana which have a diameter of 300 - 600 nm (Kirchhoff et al., 2013) and may comprise 5-50 discs (Pribil et al., 2014), or else as separate layers called stroma lamella, that bridge between the grana (Figs 1.1b, 1.2). Until recently the architecture of the grana-lamella junctions was in debate (Kouřil et al., 2012; Pribil et al., 2014; Mustárdy et al., 2008; Shimoni et al., 2005). Now, studies using electron tomography have visualised the grana, resolving much of the ultrastructure (Austin and Staehelin, 2011; Daum et al.,

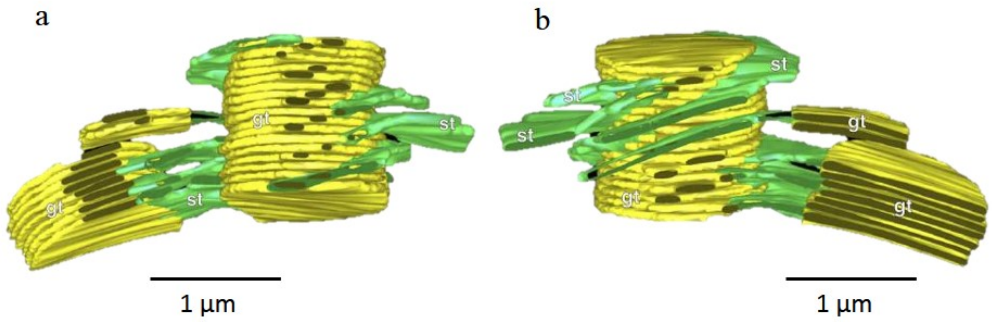


**Figure 1.2:** Electron tomographs of a section of chloroplast thylakoids shown in **a)** from 'front' view, and in **b)** after 180 ° rotation of a). The grana (gt) are coloured *yellow* and the stroma thylakoids (st) are coloured *green*. The figure is reproduced and with modification from (Austin and Staehelin, 2011).

2010; Daum and Kühlbrandt, 2011). Fig 1.2, presents electron tomograhs from Austin and Staehelin (2011), the findings show a helical arrangement of the stroma lamellae with the granal stacks.

The thylakoid membrane is a lipid bilayer with a high concentration of unsaturated fatty acid residues (Ruban, 2012; Jarvis and López-Juez, 2013) which impart a fluidity that is thought to be important for i) structural plasticity, necessary for rearrangement of the thylakoids into grana or lamellae and ii) the lateral movement of the protein complexes that are embedded within the surface (Benning, 2009; Kirchhoff et al., 2013).

The embedded structures are the various pigment-protein complexes (see §1.2.4.1 and §1.3.3) which together, perform the light reactions. Their organisation is heterogeneous according to the arrangement of the photosynthetic surface, with Photosystem II (PSII) and the Light Harvesting Complex II antenna (LHCII) enriching the grana, while Photosystem I (PSI) and ATP-synthase inhabit the stroma lamellae. The reason for the heterogeneity is unresolved, although the bulky protrusions of PSI and ATP-synthase are thought to be the basis for their exclusion from the compact grana (Pribil et al., 2014; Suorsa et al., 2013).

### 1.2.3 Pigments

Photosynthetic pigments are located within the protein structures that are embedded in the thylakoid membrane. The vast majority are the green chlorophyll (Chl) pigments, typically occurring in the thylakoids in concentrations of over 0.2 M (Ostroumov et al., 2014). Higher plants utilise two of the five Chl groups, the blueish-green Chl *a* and the yellowish-green Chl *b*. A second pigment class, the

red-orange carotenoids, is also utilised for photosynthetic function, with, among others, the role of broadening the absorption cross-section.

In Fig 1.3a,b, the structure of Chl *a* is shown. Chl *b* differs only by the substitution of a methyl group for an aldehyde group, as indicated. The molecule is a cyclic tetrapyrole with a large planar, porphyrin "head" that has an area of about 14 Å × 14 Å (1.4 nm × 1.4 nm; Nobel, 2009). A central $Mg^{2+}$ atom is coordinately bound by four inward orientated nitrogen atoms of the tetrapyrole ring. A long, flexible, hydrophobic phytol tail, about 20 Å (2 nm) in length, extends from the forth ring of the head and functions to anchor and orientate the molecule (Ruban, 2012; Nobel, 2009; Fig 1.3b).

The carotenoids are linear pigment molecules, represented by $\beta$-carotene in Fig 1.3c. They are divided into the pure hydrocarbons known as carotenes or those that contain oxygen which are known as xanthophylls. Of the former group, $\beta$-carotene is the main pigment in plants, from the latter, antheraxanthin (Ax), violaxanthin (Vx), zeaxanthin (Zx), neoxanthin (Nx) and lutein (Lu) are present. The first three, Ax, Vx and Zx, differ from each other only by the number of epoxy groups and as such, through de/epoxidation, their stoichiometry is adjusted in a process known as the xanthophyll cycle (see §1.4.2.2).

The photosynthetic pigments all contain alternating double-single bonds, which creates a strong $\pi$-conjugation and therefore strong absorption extinction coefficients (Ruban, 2012). In the chlorophylls there are 12 double carbon bonds in the head, while in carotenoids usually $\geq$9 double/single bond alternate along the length (Fig. 1.3c). The linear arrangement in the carotenoid gives a broader and weaker conjugation compared to chlorophyll (Nobel, 2009). Absorption spectra for Chl *a*, Chl *b*, and $\beta$-carotene are presented in Fig 1.3d.

The role of the pigment molecules in photosynthesis is multi-part. Primarily, they are i) the absorbers of light and as such can be considered to be the life blood of photosynthesis. Other roles, are ii) the transfer of excitation energy to the reaction centre, iii) the generation of electron transfer by charge separation, iv) the degradation of excess energy to heat and v) structural stabilisation the complexes (Li, 2006; Scheer, 2008).

All pigments can absorb light but only the reaction centre chlorophylls are specialised to transduce light into chemical energy. Emerson and Arnold (1932) were the first to realise this when they discovered that, functionally, Chl works in groups, with roughly 250 Chl molecules delivering energy to one reaction centre (Hall et al., 1999). The reaction centres of PSII and PSI contain Chl *a* molecules called P680 and P700 respectively, where P stands for primary donor and the number refers to the absorption maximum (Croce and van Amerongen, 2014). After donating an electron, $P680^+$ is the strongest biological oxidising agent and

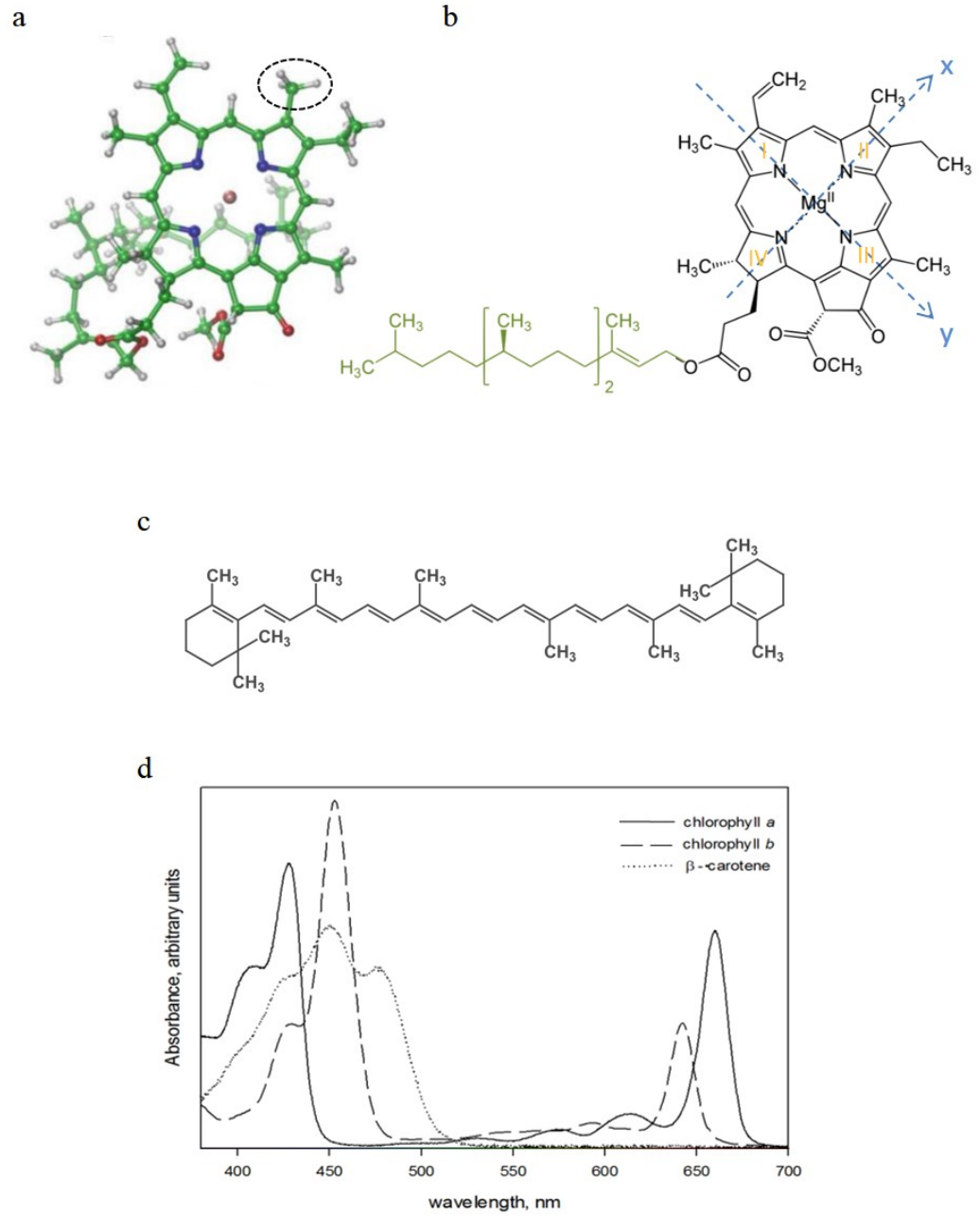


**Figure 1.3:** Photosynthetic pigment structure and spectral properties. **a)** The molecular structure of Chl *a*. The structure is identical to Chl *b*, apart from the substitution of the ringed methyl group ($R-CH_3$) for an aldehyde group ($R-CHO$). The image is adapted from Müh and Renger (2014). **b)** The chemical structure of Chl *a*, the phytol tail is in green, adapted from Berg et al. (2002). **c)** The structural formula of $\beta$-carotene from Berg et al. (2002). **d)** Absorption spectra of Chl *a* and Chl *b* in diethyl ether and of $\beta$ - carotene in hexane. Data were taken from the PhotochemCAD database (Dixon et al., 2005; Du et al., 1998).

when in an excited state (*), P700* is the strongest biological reducing agent (McDonald, 2003; Rappaport et al., 2002). These are properties that firmly place the reaction centre pigment molecules at the very start of every single food chain.

### 1.2.4 The Thylakoid Membrane Complexes

Four large, membrane-bound, multi-subunit complexes, PSII, Cytochrome $b_6f$ (Cyt $b_6f$), PSI and ATP-synthase, are the principle components involved in transforming light energy into biologically available energy. PSII and PSI are considered to be the two photosynthetic units of higher plants, they each have pigment-binding light harvesting systems, that deliver absorbed energy to a reaction centre located within a core complex, where light energy is transformed into chemical energy.

The structures are represented in Fig 1.4 which highlights their composition as multiple subunit complexes of mixed nuclear-encoded and chloroplast-encoded origin. In Table 1.1 the protein components of each complex are listed and the location of the encoding gene, in the nucleus or chloroplast, is indicated (see §1.5 for discussion about thylakoid membrane complex gene location). Each complex is described below.

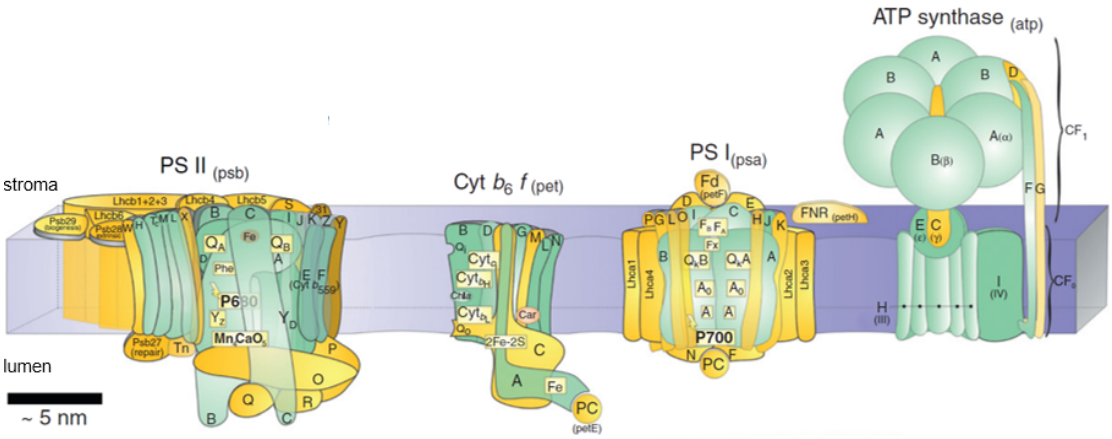


**Figure 1.4:** A schematic model of the thylakoid membrane proteins of higher plants. *In vivo*, PSII and Cyt $b_6f$ occur in dimers, here they are presented in monomeric form in order to expose the respective components. The protein subunits are colour coded to show the location of the gene that encodes them, in either of the nucleus (*yellow*) or the chloroplast (*green*), see §1.5 for a discussion. The figure is taken from Allen et al. (2011).

#### 1.2.4.1 Light Harvesting Antennas

Free pigments absorb but do not harvest light, instead the energy is released from the absorbing molecule as heat or fluorescence (Beddard and Porter, 1976).

For light harvesting, pigment molecules must be held, arranged and specifically orientated in a protein 'scaffold' to allow the transfer of energy to neighbouring pigment molecules until it eventually reaches the reaction centre and initiates charge separation. The pigment-protein complexes thus function as antennas that increase the absorption cross-section of the photosystem reaction centre. The subunits of the PSII and PSI light harvesting systems are of two distinct types: those that are directly linked to the reaction centre, with which they form the core, and those that are bound to the core complex and which are known as the light harvesting complexes (LHCs).

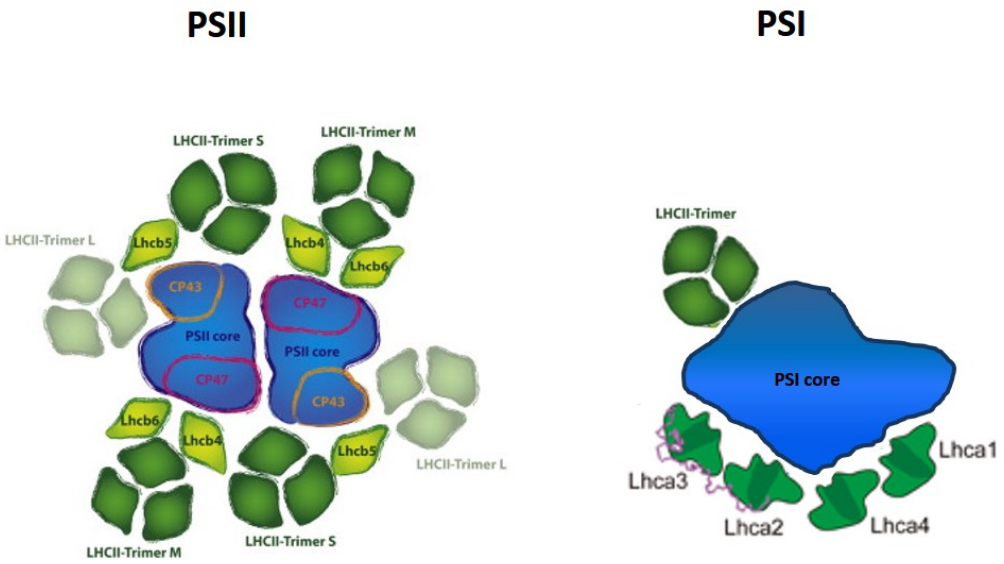


**Figure 1.5:** A schematic overview of the various light harvesting antenna components, and their arrangement, in the PSI and PSII supercomplexes, as viewed from above. The PSII complex shown here represents what is thought to be the complete macrostructure of the PSII dimer, designated as C2S2M2(L2) (Boekema et al., 1999), where C = core and S, M and L refer to the binding of the 'LHCII trimers' (*dark green*) as strongly, moderately or loosely bound, respectively. LHCII is generally associated with PSII although it is also found at PSI under certain conditions. The PSII figure is taken from Ballottari et al. (2012) and PSI was adapted from Minagawa (2013).

Fig 1.5 shows an overview of the main antenna components of the PSII and PSI supercomplexes (Ballottari et al., 2012; Minagawa, 2013). Six types of LHC are known for PSII (Lhcb1-6). These are the major Light-Harvesting Complex II (LHCII), a trimeric complex, composed of varying combinations of the three monomers, Lhcb1-3 (Pietrzykowska et al., 2014) and the minor antennas: Lhcb4 (CP29), Lhcb5 (CP26) and Lhcb6 (CP24). These complexes bind variable numbers

of Chl *a*, Chl *b* and carotenoid pigments. The core antenna subunits, proximal to the reaction centre, are CP43 and CP47 (Bricker and Frankel, 2002).

The peripheral PSI antenna complexes, collectively known as LHCI, are arranged in a crescent shape around the core and comprise four pigment-binding polypeptides called Lhca1-4, each encoded by a single *lhca* gene (Morosinotto and Bassi, 2007). Recent work by Mazor et al. (2015), resolved the PSI supercomplex at 2.8 Å. They found that, collectively, Lhca1-4 bound 52 Chl *a*, 9 Chl *b* and 10 carotenoids (Mazor et al., 2015), totalling about 48 % of the total PSI pigment complement, with the remaining pigments situated in the core, forming a robustly integral antenna (Nelson and Ben-Shem, 2004). The arrangement contrasts that of PSII where the large majority (85 %) of the Chl are bound by the peripheral LHC complexes (Ruban, 2012). Furthermore, the 'robustness' of the PSI superstructure contrasts the 'looseness' and flexibility of the PSII superstructure (Ruban, 2012).

An interesting feature of the PSI antenna is the presence of so-called 'gap' or 'linker' pigments that are bound at the interfaces of the antenna polypeptides and at the interface between the antenna and the core complexes, compared to the more usual arrangement where the pigments are bound only within the complexes (Morosinotto and Bassi, 2007). Recently, two additional Lhca proteins have been identified in *Arabidopsis thaliana*, Lhca5 and Lhca6 (Ganeteg et al., 2004; Klimmek

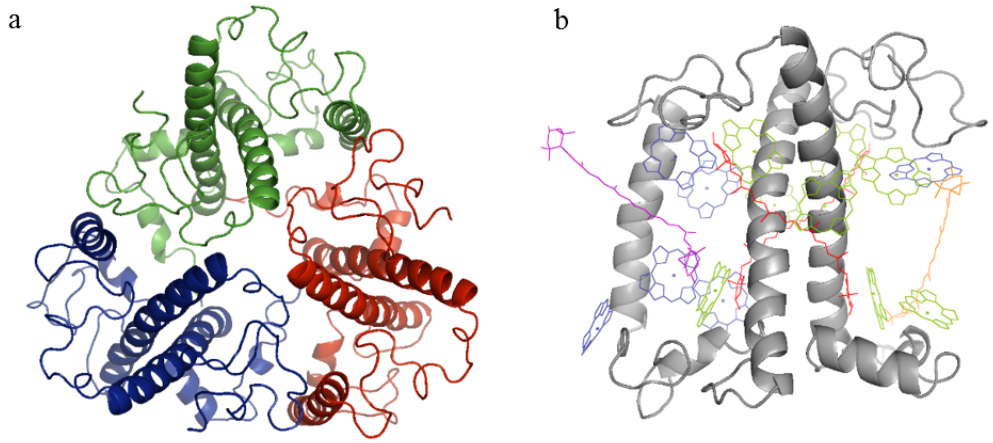


**Figure 1.6:** The LHCII complex. **a)** The trimeric form as viewed from the stroma, with individual protein monomers shown in different colours (Standfuss et al., 2005; PDB 2BHW). **b)** An LHCII monomer, as seen from the side, with bound pigment molecules (Liu et al., 2004; PDB 1RWT). The phytol tails of the chlorophylls have been removed for easier viewing. The polypeptide is shown in grey and the pigments are coloured as follows: Chl *a*, green; Chl *b*, blue; lutein, red; violaxanthin, orange and neoxanthin, purple.

et al., 2006). The exact docking site and function of these proteins is not currently known although suggestions are that they could play a role in the electron transfer from PSI to Cyt $b_6f$ during cyclic electron flow (Schöttler and Toth, 2014; see §1.3.3.2).

Although the LHCII antenna complex is considered to be a component of PSII, evidence shows that a small, mobile portion is capable of functionally and reversibly, attaching to PSI in a process known as state transitions (see §1.4.2.3) (Ruban, 2012). This small portion is thought to be located at the grana edges although the bulk of LHCII is located predominantly within the granal stacks. LHCII constitutes about half of the protein mass of the thylakoid membrane (van Amerongen and Croce, 2007) and is the most abundant membrane protein on Earth (Remelli et al., 1999). High resolution crystal structures have been obtained for LHCII at 2.72 Å (Liu et al., 2004) and 2.5 Å (Standfuss et al., 2005). Fig 1.6 presents a structural model of the LHCII trimer proteins and a single LHCII monomer with bound pigment molecules. Each monomer binds eight Chl *a*, six Chl *b* and four carotenoids: two luteins, located at the centre, a neoxanthin molecule which protrudes into the thylakoid membrane and one violaxanthin/zeaxanthin molecule that is involved in an enzymatic xanthophyll cycle described in §1.4.2.2 (van Amerongen and Croce, 2007).

#### 1.2.4.2 Photosystem II

PSII is a water-splitting plastoquinone oxidoreductase. The structure of PSII from cyanobacteria has been resolved at 1.9 Å (Umena et al., 2011). However, high resolution structural information about plant PSII has been more difficult to obtain due to the problems involved in purifying the complex (Caffarri et al., 2009). A combination of approaches, including electron crystallography (Rhee et al., 1997), electron microscopy (Nield et al., 2000; Hankamer et al., 1999), x-ray crystallographic studies of smaller PSII components (Pan et al., 2011) and biochemical methods (Caffarri et al., 2009), have found good agreement between the PSII model for plants and the high resolution model derived for cyanobacteria (Ballottari et al., 2012; Caffarri et al., 2009; Nickelsen and Rengstl, 2012; Nield et al., 2000; Nield and Barber, 2006).

In Fig 1.7, the structure of the cyanobacterial PSII dimer from *Thermosynechococcus vulcanus* is shown. Each monomer of the dimer is associated, either permanently or transiently, with nearly forty protein components, (Shi, Hall, Funk and Schröder, 2012) most of which are of low molecular weight. The core complex, contains four large, intrinsic membrane subunits: D1 (PsbA), D2 (PsbD), CP47 (PsbB) and CP43 (PsbC) and three extrinsic subunits at the lumenal side which

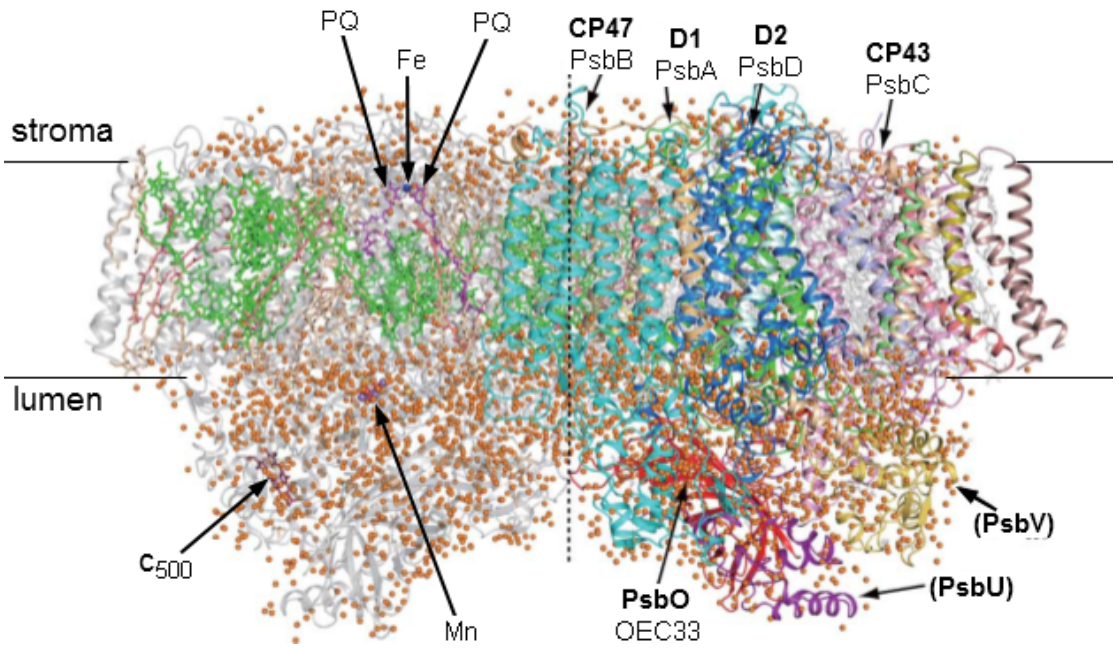


**Figure 1.7:** A side view of the molecular structure of the PSII dimer from cyanobacteria. On the right side, the protein subunits are coloured individually and the cofactors are in grey, while on the left side the proteins are in grey and the cofactors are coloured. Water molecules are represented by orange balls. The dashed line indicates the pseudo line of separation of the two dimers. The figure is taken from Umena et al. (2011).

make up the oxygen evolving complex (OEC). PsbO (OEC33) is common to all oxygenic photosynthesisers whilst the other two subunits are PsbU and PsbV (Cyt $c_{550}$) in cyanobacteria and PsbP (OEC24) and PsbQ (OEC17) in plants and green algae (Fig 1.7). The exact location of PsbP and PsbQ in the PSII structure is still uncertain (Bricker et al., 2012) although new insights into their position and interactions have been reported (Bricker and Frankel, 2011; Ido et al., 2014). A large number of small subunits are also present including PsbE (Cyt $b_{559}$ $\alpha$) and PsbF ($\beta$ subunits) (Shi, Hall, Funk and Schröder, 2012).

In plants, the primary core proteins, D1 and D2, have five transmembrane spanning $\alpha$-helices and bind six molecules of Chl *a* and two molecules of pheophytin *a* (a metal-free Chl *a* molecule in which the $Mg^{2+}$ ion has been replaced with two $H^+$ atoms). The D1 and D2 proteins bind all the redox active co-factors that are involved in the conversion of excitation (physical) energy, into biochemical energy (Barber, 2014). These cofactors include a special Chl *a* dimer (P680), pheophytin *a* (Pheo), a firmly bound plastoquinone (PQ) molecule ($Q_A$) and a second PQ

molecule ($Q_B$) which exits the core complex after receiving two electrons from $Q_A$, and two protons from the stroma. CP47 and CP43 each have six transmembrane $\alpha$-helices (Rhee et al., 1997, 1998) and bind 16 and 13 Chl *a* respectively (Ferreira et al., 2004; Umena et al., 2011). They have been shown to associate directly with the core and are also thought to have direct interaction with the oxygen evolving centre (OEC) (Bricker and Frankel, 2002). The OEC is a cluster of metal ions, $Mn_4Ca^{2+}$, and is the site of water oxidation. As already mentioned, in plants the OEC is formed of polypeptides PsbO, a Mn-stabilising structure, PsbP and PsbQ and lies extrinsically to the core, protruding into the lumenal space of the thylakoid (Fig 1.7).

#### 1.2.4.3 Cytochrome $b_6f$

The Cyt $b_6f$ complex of oxygenic photosynthesisers, is a plastoquinone-plastocyanin oxidoreductase (Cramer et al., 2011) with a central position between PSII and PSI in the linear electron transport chain. It is also responsible for the transfer of

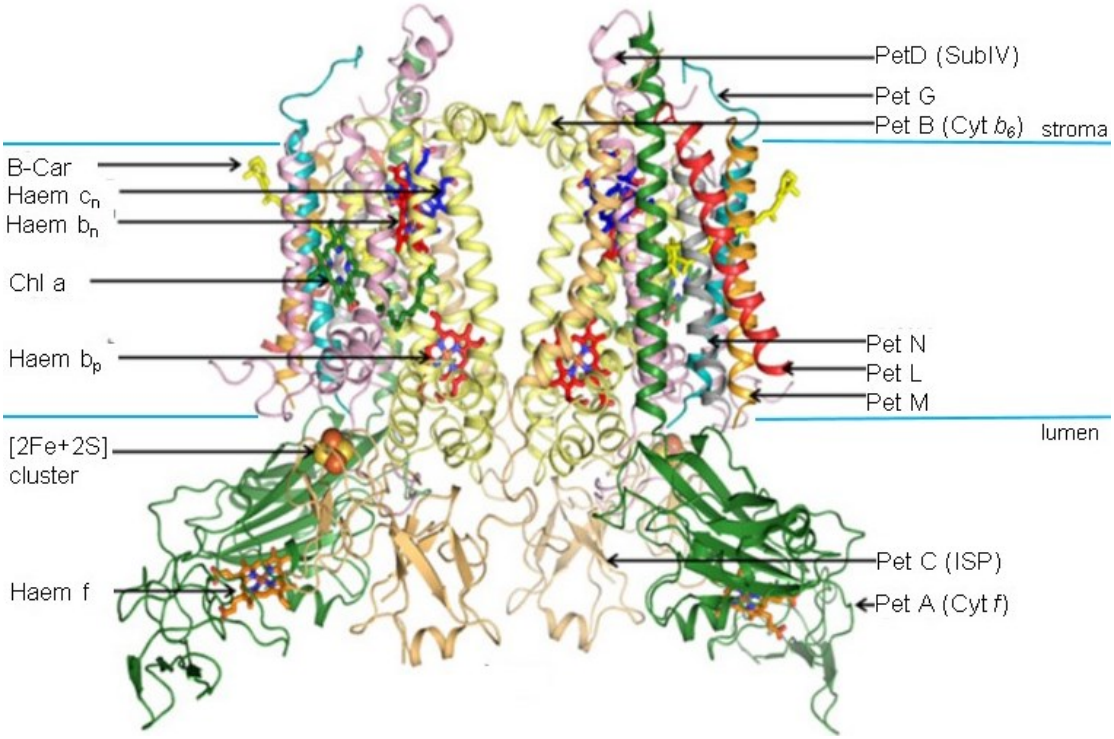


**Figure 1.8:** The Cytochrome $b_6f$ complex of oxygenic photosynthesis as viewed from the side. The protein subunits PetL, PetM and PetN are indicated as are seven cofactors that comprise the following: four haems; one iron-sulphur cluster ($Fe_2S_2$) of the Rieske iron-sulphur protein (ISP); one Chl *a* and one $\beta$-cartotene. Figure adapted from Cramer et al. (2011); Baniulis et al. (2008)

protons into the thylakoid lumen from the stroma during linear electron transport (§1.3.3.1) and cyclic electron transport (§1.3.3.2). The complex is a symmetric dimer, each monomer comprising eight polypeptide subunits (Baniulis et al., 2008) which are the products of the *pet* genes, and seven prosthetic groups.

The Cyt $b_6f$ complex is shown in Fig 1.8. The four prominent subunits are i) cytochrome $b_6$ (PetB) subunit which contains three haems: two b-type haems, haem$b_n$ bound on the negative or stromal side of the complex, haem$b_p$ bound on the positive or lumenal side of the complex and a c-type haem, haem$c_n$, also bound on the negative-side; ii) the cytochrome $f$ protein (PetA) which binds haem$f$; iii) the Rieske iron-sulphur ($Fe_2S_2$) protein (PetC) and iv) Subunit IV (PetD). Four smaller subunits, PetG, L, M and N, are present at the periphery of each monomer (Baniulis et al., 2008; Cramer et al., 2011). Cyt $b_6f$ also binds a single Chl $a$ and a single $\beta$-carotene molecule the function of which is not yet determined (Baniulis et al., 2008; Kurisu et al., 2003).

#### 1.2.4.4 Photosystem I

PSI is a plastocyanin-ferredoxin oxidoreductase, pictured in Figs 1.5 and 1.9. It has two distinct moieties: the core complex and a belt of four Lhca transmembrane antennas (Fig 1.5). Unlike PSII, PSI is a monomeric complex, the most recent report on its structure, at 3.3 Å by Amunts et al. (2010), describes 18 protein sub-units (Fig 1.9). 14 of the proteins comprise the core while the remaining four constitute Lhca1-4. Encoding is by the *psa* genes. In addition, Amunts et al. (2010) report that each PSI contains 173 Chl molecules, 15 carotenoids, 2 phyloquinones and 3 $Fe_4S_4$ clusters.

The two largest core subunits are PsaA and PsaB. They form a heterodimer that coordinates the reaction centre components which consists of six Chl $a$ molecules including the heterodimeric Chl *a/a'* P700 pigments (Jordan et al., 2001), these are organised into two near-identical 'branches' held by PsaA (Branch-A) and PsaB (Branch-B). Each branch also holds another Chl $a$ molecule ($A_0$) and a phylloquinone ($A_1$). The final redox active co-factor of the reaction centre is $F_X$, an iron-sulphur ($Fe_4S_4$) cluster that is held between the two halves of the core reaction centre (Amunts et al., 2007, 2010; Busch and Hippler, 2011; Nelson and Ben-Shem, 2004). $F_A$, and $F_B$ are two further $Fe_4S_4$ clusters that function as the terminal components of the PSI electron transport chain and are held by the smaller protein subunit PsaC (Amunts et al., 2007) (see Fig 1.15 for further details of the PSI RC components). PsaA/B heterodimer also binds about 80 Chls in total, which function as intrinsic light-harvesting antennae (Amunts and Nelson, 2009).

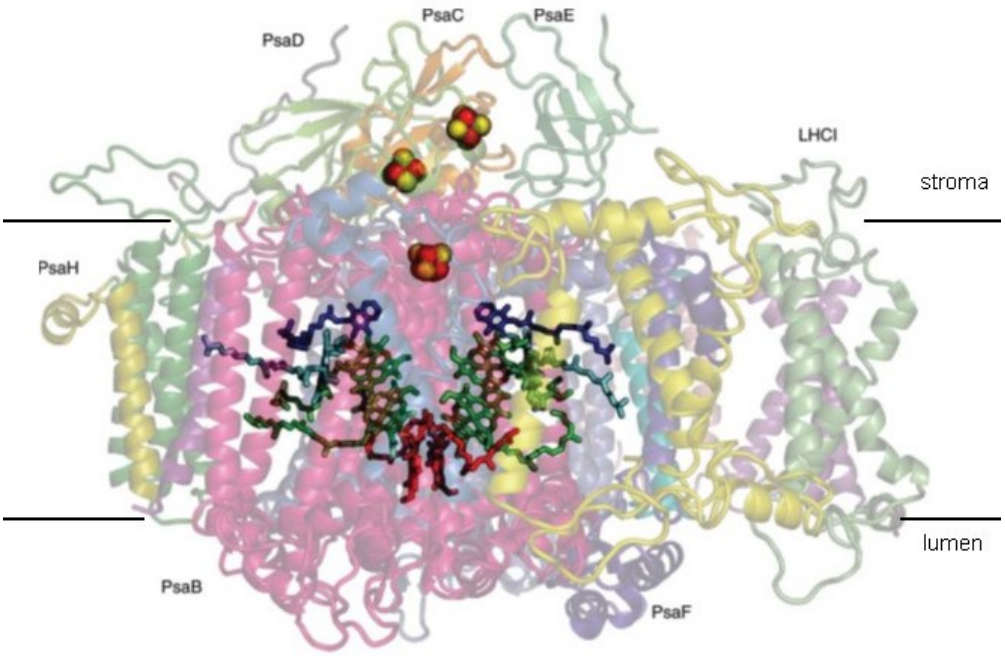


**Figure 1.9:** Molecular structure of plant PSI as viewed from the plane of the membrane. The 16 polypeptide chains and one LHCI peptide are labelled and shown in lower contrast to highlight the cofactors. The carotenoids, lipids and most of the Chl molecules are removed. The cofactors involved in electron transport (P700, $A_0$, $A_1$, $F_X$, $F_A$, and $F_B$), are shown in the following colours: Chl *a* (P700), red; other Chls, green; quinones, blue and the iron-sulphur clusters are red-yellow. Figure taken from Nelson and Yocum (2006)

.

PsaF and PsaN are positioned lumenally and interact with the electron carrier plastocyanin (Pc) and both proteins have been shown to bind the Lhca antenna units (Amunts et al., 2007; Busch and Hippler, 2011). The smaller subunits, PsaC, PsaD and PsaE are closely positioned and extend into the stroma forming the binding site for ferredoxin (Fd), the soluble electron transporter that links to ferredoxin-$NADP^+$ reductase (FNR) (Fig 1.9). Subunits PsaH, L, O, P and I provide a platform for the attachment of the Lhca 1-4 proteins (Busch and Hippler, 2011).

#### 1.2.4.5 ATP-synthase

ATP-synthase, also known as the $F_1F_o$ complex, is ubiquitous to all energy-transducing membranes (Nelson and Ben-Shem, 2004). In general it has been found to be structurally and functionally conserved across the prokaryotic bacte-

ria and eukaryotic mitochondria and chloroplasts, with some differences evident between subunits and subunit stoichiometry (Futai and Kanazawa, 1983; Böttcher and Gräber, 2000). The large-scale architecture of the ATP-synthase complex is represented in Fig 1.10, in which two distinctive regions can be observed: an intermembrane, hydrophobic region called $F_o$, and a larger, hydrophilic region that protrudes into the stroma called $F_1$, for chloroplast ATP-synthase, these subsections are referred to as $CF_o$ and $CF_1$ respectively.

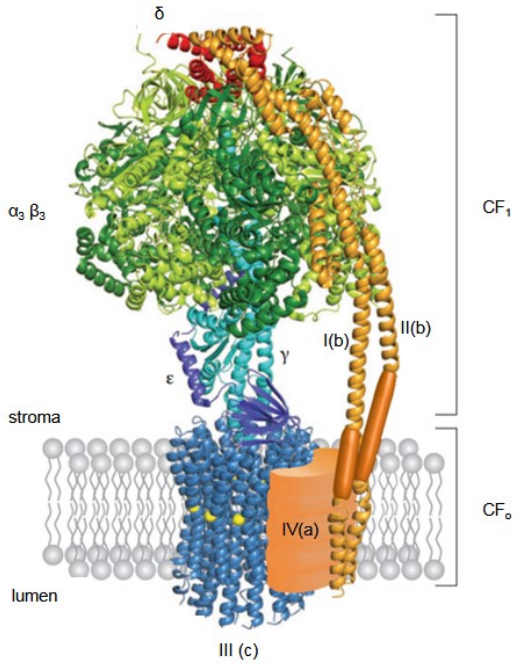


**Figure 1.10:** The molecular structure of ATP-synthase as viewed from the plane of the membrane. The image was constructed by von Ballmoos et al. (2009) using the determined structures of individual subunits that are available in the Protein Data Bank (PDB) and which were derived from various organisms. Here we have re-labelled the components using the nomenclature used for chloroplast (C) ATP-synthase. The subunits are coloured as follows, $CF_o$: I(b) and II(b) (orange), III(c) (blue) and IV(a) (peach), and five subunits of $CF_1$ are $\alpha$ (dark green), $\beta$ (light green), $\gamma$ (turquoise), $\delta$ (red) and $\varepsilon$ (purple).

The $CF_1$ portion of the complex is built of subunits $\alpha$, $\beta$, $\gamma$, $\delta$ $\varepsilon$ (Süss and Schmidt, 1982; Abrahams et al., 1994; Groth and Pohl, 2001). In the large 'head' structure (Fig 1.10), 3 $\alpha$ and 3 $\beta$ units ($\alpha_3\beta_3$) are positioned alternately in a ring-like structure forming a large, hexagonal 'head' (Abrahams et al., 1994). The long stalk-like, $\gamma$ subunit extends through the core of the $\alpha_3\beta_3$ head, filling the central shaft, while the other end protrudes into subunit III of the $CF_o$ region (Gibbons et al., 2000). Subunit III, is a ring formation of 'c' proteins, which varies

in number between taxonomic groups (von Ballmoos et al., 2009; Lolkema and Boekema, 2003; Meier et al., 2007; Seelert et al., 2000), although so far, Subunit III has consistently been found to be a multimer of 14 'c' proteins in chloroplast ATP-synthase (Seelert et al., 2000; Balakrishna et al., 2014). The peripheral b proteins of subunits I and II form a stator that connects the $CF_1$ and the $CF_o$ regions.

## 1.3 The Photosynthetic Mechanism in Plants

The photosynthetic process can be divided into four phases: i) light absorption and energy transfer to the reaction centre, ii) charge separation and primary electron transfer, iii) energy stabilisation by secondary processes and iv) carbohydrate synthesis (Blankenship, 2002). The first three phases are the 'light-reactions' and take place at the thylakoid membrane. The forth phase comprises the so-called 'dark reactions' that occur in the stroma and are collectively known as the Calvin-Benson cycle. Each phase is described below.

### 1.3.1 Light absorption, delivery to the reaction centre and other mechanisms for deexcitation of Chl*

Photosynthesis begins with the absorption of a photon of light energy by a pigment molecule that is bound within a photosystem, transforming the molecule from a ground state to an excited state (Chl* or Car*). An excited state describes an elevated energy level of the molecule (or atom). This event is the transformation of the electro-magnetic energy of a photon into an internal energy of the pigment molecule. For this to happen, the energy content of the light that is incident on the absorbing surface must strictly complement the energy needed to raise an electron from the highest occupied molecular orbital (HOMO) to the lowest unoccupied molecular orbital (LUMO) (Ruban, 2012).

#### 1.3.1.1 Resonant excitation energy transfer

As mentioned already, photo-induced charge separation ($Chl^+$) occurs only in the few Chls that form the reaction centre. The vast majority of the pigment molecules, which are held within the light harvesting system, function collectively to deliver the energy that they absorb to the reaction centre, thus greatly increasing the reaction centre absorption cross-section. The transfer process is high-speed, on average taking roughly 150 ps for excitation energy transfer from the site of photon absorption somewhere in the large supermolecular structure, to the event of charge

separation at the reaction centre (Croce and van Amerongen, 2014), the process also has near 100 % efficiency (Blankenship, 2002; Müh and Renger, 2014).

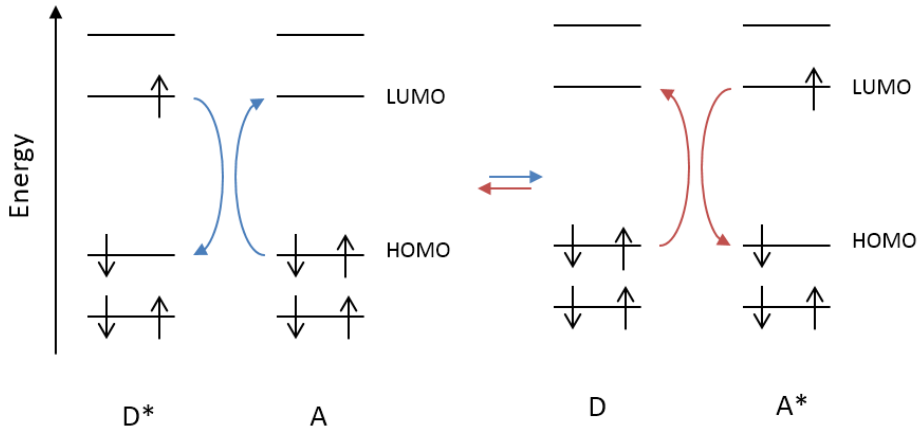


**Figure 1.11:** A molecular orbit diagram of radiationless exciton transfer between a donor molecule (D) and an acceptor molecule (A). See main text for discussion. The figure was redrawn from Müh and Renger (2014).

Excitation energy transfer (EET) is a radiationless process described by Förster resonance energy transfer theory (FRET; Förster, 1948, 2012; Nobel, 2009). When an electron is promoted to a higher molecular orbital by the absorption of a photon, a defect electron (hole) is left at the lower level (Müh and Renger, 2014). The electron and hole can be described as a pair of charged particles that attract each other. This bound electron-hole pair is the exciton that stores the energy of the absorbed photon (Müh and Renger, 2014). In Fig 1.11 a simplified molecular orbital diagram describes the process of radiationless exciton transfer as a simultaneous excitation-deexcitation of a donor-acceptor pair (Müh and Renger, 2014).

The transfer of an exciton to the neighbouring antenna subunit, is from a specific site in the subunit called the terminal emitter. For example, in each monomer of the LHCII trimer, the terminal emitter is a group of three Chl *a* molecules, Chl *a*610, Chl *a*611 and Chl *a*612 located on the outside of the trimer (Duffy et al., 2012). The pigments within the antenna complex are orientated in such a way as to promote efficient transfer of the exciton to the terminal emitter, which then transfers it to a neighbouring antenna subunit, until it reaches the reaction centre. The transfer of absorbed energy to the reaction centre is nearly 100 % efficient (Beddard and Porter, 1976; Horton and Ruban, 2005).

### Other pathways for deexcitation of Chl*

Although not strictly part of the 'photosynthetic mechanism' it is important to describe the several alternative pathways for deexcitation of Chl*, as the efficiency of the photochemical process to some extent depends on the probability of photochemistry with respect to these other excited state decay processes (Belgio, 2009). In Fig 1.12, the decay pathways are represented as competitive mechanisms for relaxation of $^1\text{Chl}^* \rightarrow {}^1\text{Chl}$, and can be summarised as follows: 1) re-emission of the energy as Chl fluorescence, 2) transfer of the exciton to the photosynthetic reaction centre (already described in §1.3.1) followed by utilisation in photochemistry (see §1.3.2), 3) non-radiative (heat) decay directly into the ground state and 4) decay via intersystem crossing to a Chl triplet state, $^3$Chl $a^*$ (Fig 1.12).

Chl fluorescence emission is a minor competing process for Chl deexcitation. The fluorescence yield ($\Phi_F$) of free Chl in solution is about 33% (Brody and Rabinowitch, 1957; Latimer et al., 1956), with the remainder of the excitation energy lost as heat. *In vivo*, if the reaction centres are closed, meaning that there is no pathway for photochemistry, the Chl fluorescence signal is about 3 % (Krause and Weis, 1991), if the reaction centres are open, $\Phi_F$ drops about five times to roughly 0.6 %, mainly due to competition with photochemistry (Bowers and Porter, 1967).

Despite the low yield, the chlorophyll fluorescence signal of photosynthetic organisms is a rich source of information regarding the photochemical and non-photochemical pathways that quench it. Variation in the fluorescence signal was first observed by Kautsky and Hirsch (1931) after they applied light to a dark adapted photosynthetic sample. Since then, as a highly informative, non-invasive

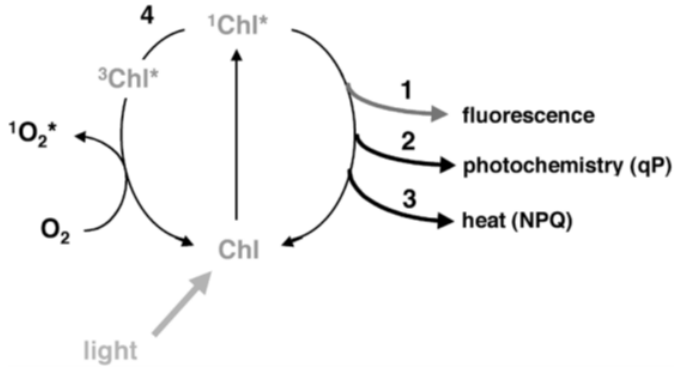


**Figure 1.12:** Mechanisms of deexcitation of Chl*. The four pathways of relaxation for Chl after the absorption of light excited the molecule from its ground state to its excited state. Figure taken from Müller et al. (2001).

and rapid method, chlorophyll fluorescence measurement has become indispensable for photosynthesis investigation. Chlorophyll fluorescence measurement is further discussed in §2.9.1.

The other $^1$Chl* deexcitation pathways shown in Fig 1.12, (4) formation of triplet state Chl ($^3$Chl*), a potentially damaging process, due to the formation of $^1O_2$*, and (3) heat dissipation, which includes a protective mechanism to avoid that damage, are discussed in §1.4.2.1 (photoinhibition) and §1.4.2.2 (photoprotection), respectively.

### 1.3.2 Charge separation, primary electron transfer and water splitting

In PSII, following the transfer of an exciton to the reaction centre, the energy is channelled to the site of the primary electron donor, Chl *a* P680, and a series of extremely rapid redox reactions follow which can be summarised by the following equation series (Krause and Weis, 1991):

$$\begin{aligned}
&(Tyr_z + P680 + Pheo + Q_A + Q_B) && \\
&\textbf{photon/exciton} \quad \downarrow && (1.2)\\
&(Tyr_z + P680^* + Pheo + Q_A + Q_B) && \\
&\downarrow && (1.3)\\
&(Tyr_z + P680^+ + Pheo^- + Q_A + Q_B) && \\
&\downarrow && (1.4)\\
&(Tyr_z + P680^+ + Pheo + Q_A^- + Q_B) && \\
&\downarrow && (1.5)\\
&(Tyr_z^+ + P680 + Pheo + Q_A^- + Q_B) && \\
&\mathbf{e}^- \quad \downarrow && (1.6)\\
&(Tyr_z + P680 + Pheo + Q_A^- + Q_B) && \\
&\downarrow && (1.7)\\
&(Tyr_z + P680 + Pheo + Q_A + Q_B^-) &&
\end{aligned}$$

where Tyr$_z$ is a redox-active tyrosine residue (D1Tyr$_z$161) of the D1 protein and is located between P680 and the OEC (Debus et al., 1988). Charge separation is initiated when P680, located on the lumenal side of the thylakoid, is excited to P680* by the absorption of a photon or exciton (Eq. 1.2). This results in the rapid (3 ps) transfer of an electron from P680 to the primary electron acceptor Pheo *a* (Eq. 1.3). Within the next 250-300 ps, an electron is transferred from Pheo $a^-$

to $Q_A$ which is bound to the D2 protein and located on the stromal side of the thylakoid (Eq. 1.4) (Krause and Weis, 1991).

A strong charge separation is created across the membrane by the formation of $P680^+PheoQ_A^-$ (Eq. 1.4), at this moment $P680^+$ is the strongest known biological oxidising agent (McDonald, 2003). On a nano-second timescale, $P680^+$ is restored to its uncharged state by the donation of an electron from the $Tyr_z$ residue of the D1 protein (Eq. 1.5), in turn an electron from the $Mn_4$ cluster of the OEC reduces $Tyr_z^+$ (Eq. 1.6) creating a positive charge in the OEC. $Q_A^-$, on the stromal side, transfers an electron via an intermediate non-haem Fe to a second, D1-bound, quinone, $Q_B$ (Eq. 1.7) transforming it into a semiquinone (Barber, 2014).

During the time that $Q_A$ is reduced (Eq.s 1.4-1.6), the reaction centre is said to be 'closed', meaning that it cannot accept another excitation transfer. The transfer of a second electron from $Q_A^-$, creating $Q_B^{2-}$, and the addition of two $H^+$ drawn from the stroma, results in the fully reduced plastoquinol ($PQH_2$), this species is then able to leave PSII and merge with the mobile PQ pool located within the thylakoid membrane lipid bilayer.

### Water splitting, oxygen evolution

Light induced charge separation at PSII leads to a positive charge in the Mn cluster of the OEC. For the full oxidisation of $H_2O$, two water molecules and

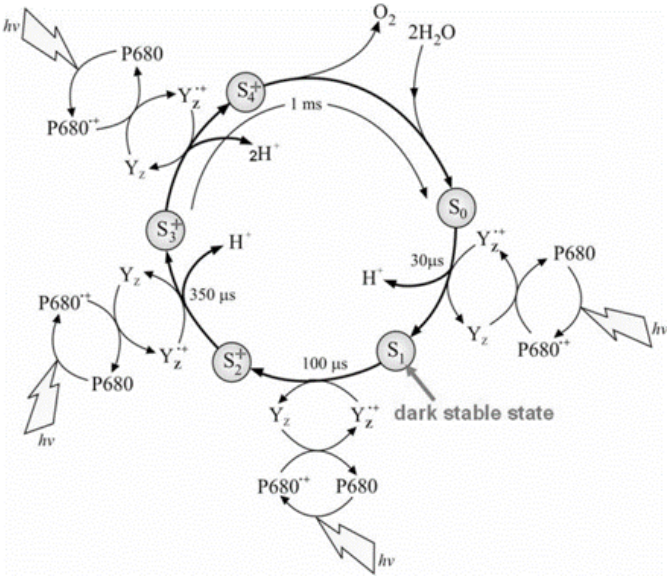


**Figure 1.13:** The S-state cycle describing $O_2$ evolution by the OEC. $Y_z$ is an abbreviation for the $D1Tyr_Z161$ residue that passes the electrons from the manganese cluster to $P680^+$. See main text for discussion. The figure was taken from Barber (2006).

the accumulation of four positive charges are required, resulting in the release of molecular oxygen and four $H^+$:

$$4\ photons + 2\,H_2O \longrightarrow 4\,e^- + 4\,H^+ + O_2 \tag{1.8}$$

The four-turnover cycle is called the S-state cycle, and is represented in Fig 1.13. The water molecules are bound in the Mn cluster where four electrons are stripped sequentially in light-driven reactions ($S_0 \rightarrow S_4$), two from each $H_2O$. During each transition after $S_1$, $H^+$ are released into the lumen, adding to its acidification. In the light independent recovery step ($S_4 \rightarrow S_0$), $O_2$ is released and two more $H_2O$ are bound. The full cycle is thought to take roughly 10 ms (Barber, 2006).

### 1.3.3 The photosynthetic production of NADPH and ATP by light-driven electron and proton transfer

The stabilisation of the captured energy into chemical bonds by the formation of ATP and NADPH occurs via i) linear electron flow (LEF) and ii) cyclic electron flow (CEF). LEF begins with charge separation in the PSII reaction centre which initiates electron transfer to PSI via Cyt $b_6f$. LEF ends at PSI with the reduction of $NADP^+$ to NADPH. Coupled to the electron flow, is the transfer of $H^+$ across the membrane into the lumen, where $H^+$ build-up drives ATP-synthase activity. CEF occurs between PSI and Cyt $b_6f$, and is driven only by light absorption at PSI. The cycle transfers $H^+$ into the lumen, but does not include net formation of NADPH or $O_2$ formation (Nobel, 2009). Fig 1.14, describes the pathways of LEF and CEF. It also indicates the concomitant drive of $H^+$ across the membrane into the lumen for the development of the electrochemical proton gradient ($\Delta$ pH) to power the phosphorylation of adenisine diphosphate (ADP) to ATP by the membrane-bound ATP-synthase. NADPH and ATP are two energy storage compounds, that can readily diffuse around within a cell, carrying energy in the form of reducing power (NADPH) and Gibbs free energy (ATP) (Nobel, 2009). Fig 1.14, describes the pathways of LEF and CEF. It also indicates the concomitant drive of $H^+$ across the membrane into the lumen.

#### 1.3.3.1 The linear electron pathway

As already described (§1.3.2), linear electron flow (LEF) begins with the primary charge separation at P680 resulting in the reduction of $Q_A$. $Q_A^-$ reduces $Q_B$, transforming it into a semiquinone (Barber, 2014). Once doubly reduced and protonated, the resultant $PQH_2$ has a low affinity for the $Q_B$ binding site and leaves PSII to merge with the mobile PQ pool located in the lipid bilayer of the

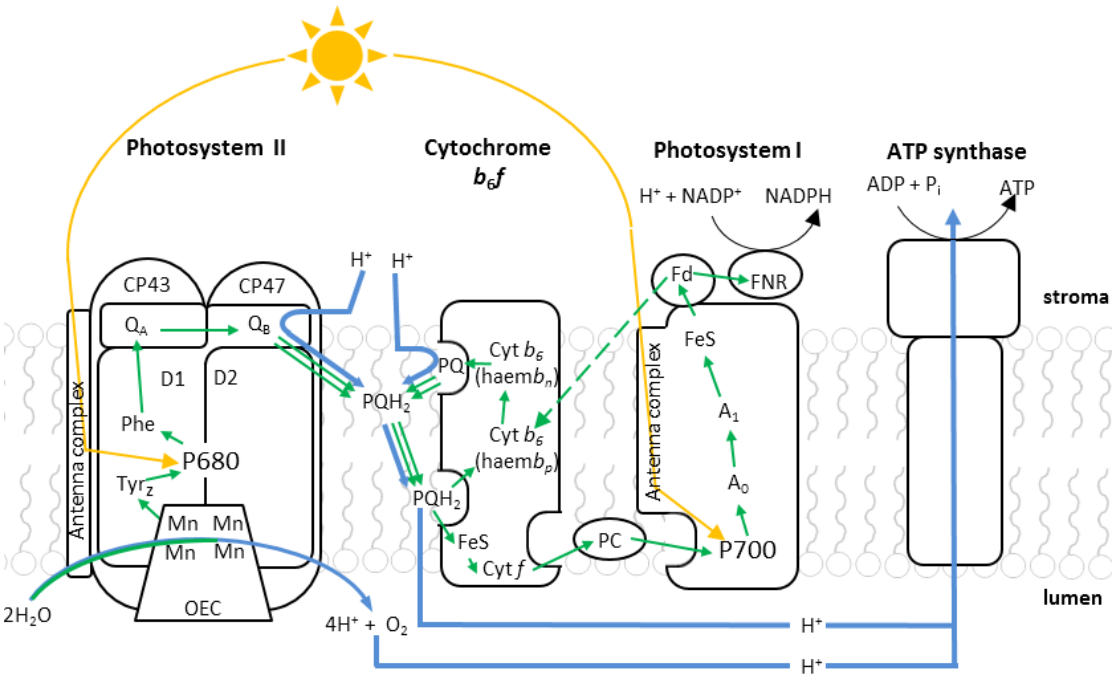


**Figure 1.14:** Schematic diagram of the solar-powered electron and proton transport pathways in the thylakoid membrane. The four complexes: PSII, Cyt $b_6f$, PSI and ATP-synthase are shown. In addition, the redox active cofactors involved in electron transport are indicated (see main text for definitions). The passage of photons/excitons is shown in *yellow*, electrons in *green* and protons in *blue*. The steps in the pathway that proceed with two electrons are described by double arrows. The *dashed green* line indicates the transfer from Fd to Cyt $b_6f$ forming the cyclic electron flow. See §1.3.3.1 and §1.3.3.2 for further discussion of linear and cyclic electron flow respectively. The figure is redrawn with modifications from Blankenship (2002).

thylakoid membrane (Kyle, 1985; Ferreira et al., 2004; Fig 1.14).

A $PQH_2$ species from the PQ pool binds to Cyt $b_6f$ at the lumenal side of the complex and enters what is known as the Q-cycle, where two-electron oxidation takes place. The first electron is passed to the $Fe_2S_2$ cluster of the Rieske protein, then to cytochrome $f$ followed by transfer to a bound plastocyanin (Pc) (Fig 1.14). The second electron is translocated across the membrane via haem$b_p$ and haem$b_n$ of the Cyt$b_6$ protein (Fig 1.14). Here, at the stromal side, the transferred charge is used to reduce a bound quinone. The addition of a second electron and two protons, drawn from the stroma creates $PQH_2$ which is ejected into the PQ pool. During the oxidation of $PQH_2$ by Cyt $b_6f$, protons are liberated into the thylakoid lumen contributing to the proton motive force (pmf).

The reduction of plastocyanin causes it to dissociate from Cyt $b_6f$ and diffuse though the lipid bilayer towards PSI in the stroma lamellae where it functions

as the primary electron donor of this complex. Electron transfer through PSI is initiated by photoexcitation of the reaction centre. The exact mode of action of the electron pathway in PSI has, until recently, remained obscure due to the uncertainty of the precise function of Branch-A and Branch-B (Busch and Hippler, 2011; Nelson and Yocum, 2006). In Fig 1.15, the electron transport chain (ETC) through the redox-active components of the PSI ETC is shown.

Recent findings contradict the previously held belief that initial charge separation occurs in P700* (or $ec1_{A/B}$), and instead found that the primary charge separation occurs between the $ec2_{A/B}/ec3_{A/B}$ (or $A/A_1$) pair, so in fact initiation of primary electron transfer can occur independently in each branch (Müller et al., 2010; Busch and Hippler, 2011). The theory suggests that after radical pair formation ($ec2^{+}_{A/B}/ec3^{-}_{A/B}$ ), P700 rapidly transfers an electron to $ec2^{+}_{A/B}$ and $ec3^{-}_{A/B}$ passes an electron to the $Fe_4S_4$ clusters, bound by the stomally-located PsaC polyeptide, and which provide an electron pathway, $F_X \rightarrow F_A \rightarrow F_B$, away from the reaction centre (Fig 1.15). $P700^+$ is re-reduced by the electron from Pc (Busch and Hippler, 2011; Golbeck, 2003; Müller et al., 2010).

The final electron acceptor of LEF is the soluble $Fe_4S_4$ protein, ferredoxin (Fd), which picks up the electron from the final PSI $Fe_4S_4$ cluster ($F_B$). Once reduced, Fd can form a complex with the membrane-associated ferredoxin-$NADP^+$ reductase (FNR) where the electron is used to reduce $NADP^+$ to NADPH.

The full reduction of one molecule of $NADP^+$ requires two electrons from one water molecule. Each electron transfer from $H_2O$ to $NADP^+$ requires two photons, one for each reaction centre, thus a minimum of four photons are required to generate one NADPH (Nelson et al., 2008). The reaction can be summarised with the following equation:

$$4\ photons + H_2O + NADP^+ \longrightarrow NADPH + H^+ + \tfrac{1}{2}\,O_2 \tag{1.9}$$

#### 1.3.3.2 Cyclic electron transport

In cyclic electron flow, first described by Arnon et al. (1954), an electron is passed from the PSI reaction centre to ferredoxin. From there, the negative charge is passed to Cyt $b_6f$ along a pathway that is not yet understood. Electron transfer to FNR, and the subsequent reduction of NADPH, is thus avoided. The electron is returned back to P700 via plastocyanin. The energy of one photon is needed to convey one electron around the cycle. One cycle drives one $H^+$ across the membrane via Cyt $b_6f$ (Fig 1.14) contributing to the pmf needed for ATP generation (Nelson et al., 2008).

The dual operation of the linear and cyclic electron flow is proposed to be a regulatory mechanism that allows the plant to adjust the ratio of ATP:NADPH

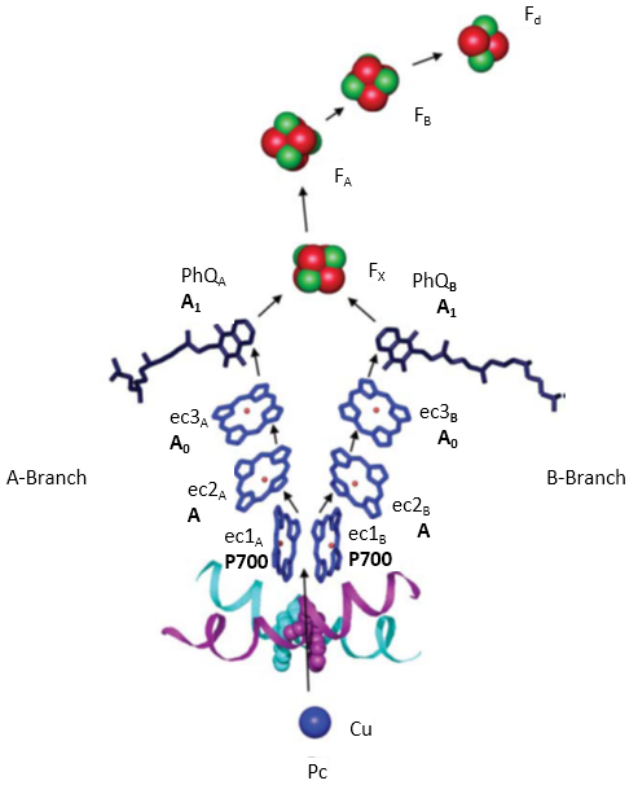


**Figure 1.15:** ETC redox-active components of the PSI reaction centre. The six Chls (*blue*) of the reaction centre and the phylloquinines (*black*) are shown comprising Branch A and Branch B. They are labelled according to both the older (P700, A, $A_0$ and $A_1$, in bold) and to the newer ($ec1_{A/B}$, $ec2_{A/B}$, $ec3_{A/B}$, $PhQ_{A/B}$) nomenclature according to Müller et al. (2010). Also shown are the $Fe_4S_4$ clusters (*red/green*) and the Cu-containing plastocyanin (Pc *blue*). Electron transfer is indicated by arrows. The turquoise and purple structures are tryptophan residues that might be involved in electron transfer from Pc to P700. The figure is reproduced with modifications from Nelson and Yocum (2006).

to match the 3:2 ratio needed for carbon-assimilation (Nelson et al., 2008). However, CEF is a poorly understood mechanism and its requirement for balanced ATP/NADPH adjustment under normal conditions is debated (Allen, 2003; Iwai et al., 2010; Schöttler et al., 2011), with some research suggesting that it is perhaps more likely to be a photoprotective mechanism under stressful circumstances (Munekage et al., 2002, 2004).

#### 1.3.3.3 Photophosphroylation

The transfer of $H^+$ into the lumen during LEF and CEF forms a transmembrane pH gradient ($\Delta$ pH) which subsequently powers the ATP-synthase enzyme, often

called the 'coupling-factor' in the phosphorylation of ADP to ATP:

$$\mathrm{ADP^{3-}} + \mathrm{P_i^{2-}} + \mathrm{H^+} \xrightarrow{\Delta pH} \mathrm{ATP^{4-}} + \mathrm{H_2O} \tag{1.10}$$

where $P_i$ is an inorganic phosphate ion. The ATP-synthase operates as a proton-driven rotary system powered by the pmf generated by the lumen acidification. By translocating $H^+$ ions across the membrane from the lumen to the stroma, the ATP-synthase can perform up to 700 rotations per second (von Ballmoos et al., 2009). Although not fully established, it is thought that the 'c' proteins of subunit III, each bind a $H^+$ ion, the ions are then each translocated across the membrane during one rotation (Blankenship, 2002). There are 14 c-subunits in chloroplast ATP-synthase, therefore theoretically, in one rotation 14 $H^+$ ions could be used to generate 3 ATP (Nelson and Ben-Shem, 2004), giving a $H^+$/ATP stoichiometry of 4.67, however this figure has not been demonstrated experimentally (Blankenship, 2002).

### 1.3.4 Carbon fixation

Carbon fixation is the second of the two sequences that characterise photosynthesis. Here, the high energy products of the 'light reactions' are used for the construction of carbohydrate from ambient $CO_2$ in a complex series of reactions known as the light-independent (or dark) reactions. The reactions were first described by Melvin Calvin, Andrew Benson and James Bassham in a series of publications in the mid-1900s and which were summarised in the nobel prize award lecture by Calvin (1962). The reactions are now collectively known as the Calvin-Benson-Bassham cycle. The overall reaction can be summarised with the following equation:

$$\begin{aligned} \mathrm{CO_2} + 2\,\mathrm{NADPH} + 3\,\mathrm{ATP} + 2\,\mathrm{H_2O} \longrightarrow \\ (-\mathrm{CH_2O}-) + 2\,\mathrm{NADP^+} + 3\,\mathrm{ADP} + 3\,\mathrm{Pi} + \mathrm{H^+} \end{aligned} \tag{1.11}$$

where $-CH_2O-$ represents a unit of carbohydrate. For complete carbohydrate ($C_6H_{12}O_6$) production, six turnovers of the cycle are required. In plants, carbon sequestration occurs in the stroma of the chloroplast. The stroma is an aqueous phase and so contrasts with the location of the 'light-dependent' reactions in the solid state of the thylakoid membrane.

## 1.4 Light fluctuations and plant responses

Natural light differs from all other abiotic resources in terms of amplitude and rate of variation (Long et al., 1994). Change in the quantity and spectral quality

of the sunlight that falls on photosynthetic pigments is constant, and occurs both periodically and stochastically. Periodic light change is due to the perpetual repositioning of the photosynthetic organism in relation to the sun. The Earth's rotation causes diurnal cycles in which light intensity changes over two to three orders of magnitude every 24-hours, while the Earth's orbit around the sun mediates the diurnal light changes by year-long seasonal cycles.

Superimposed over the periodic cycles, are stochastic fluctuations with frequencies ranging from seconds to centuries. Changes in solar output, for example, can cause shifting averages of light intensity that are only detectable over years, decades or longer, while gradual overshadowing from a tree growing nearby might take months. In mid-day sun the light intensity can reach 2000 $\mu$mol photons $m^{-2}$ $s^{-1}$, at the same time on the following day, if overcast, there might be as little as 100 $\mu$mol photons $m^{-2}$ $s^{-1}$. In addition, highly unpredictable, high frequency light fluctuation, on a time scale of seconds to minutes, caused by sunflecks and dappling might form from movements in overhead clouds or a canopy. A light-meter recording by Adams III et al. (1999), shown in Fig 1.16, demonstrates the irregular flux in light availability, during ten hours of daylight, in the understory of a forest.

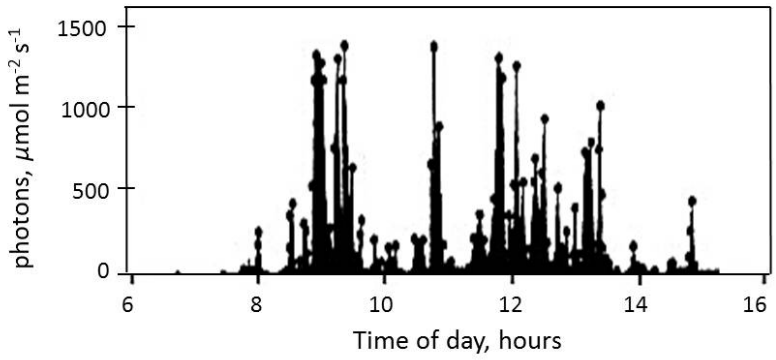


**Figure 1.16:** Short-term fluctuation in the quantity of light incident upon a leaf in a forest understory. Image adapted from Adams III et al. (1999).

As well as the intensity, the spectral quality of light changes across time and space due to filtering by intercepting objects (Casal, 2012; Murchie and Niyogi, 2011; Ruban, 2009, 2012). For example, the amount of red light is diminished under a canopy due to the absorption of photosynthetically active radiation (PAR) by the overhead vegetation (Anderson et al., 1988). The red:far-red light ratio (R:FR) is also reduced in low lying sun and under shallow soil (Batlla et al., 2000;

McDonald, 2003).

Safe and efficient harvesting of natural light by photosynthetic organisms requires plants to light-adjust on multiple scales, from changes to the genome, brought about through adaptive evolutionary processes over generations (Raven and Geider, 2003), to phenotypic responses in individuals at the level of the whole organism through to transient, molecular mechanisms in the thylakoid membrane. The predictability of light cycles allows plants to adjust to them using circadian systems whereby biological rhythms are endogenously synchronised to the light periodicity (Dunlap, 1999; Lumsden and Millar, 1998; McWatters et al., 2000). In contrast, stochastic fluctuations demand non-endogenous adjustment through constant light-sensing which must integrate plant regulation across all levels.

Photosynthetic organisms acclimate to their long-term light environments with regulated gene expression and protein degradation, often involving hormone signalling pathways, while rapid light changes, over seconds and minutes, are mediated by transient, reversible, molecular mechanisms in the thylakoid membrane. The processes of light acclimation to the prevailing environment, and of molecular mechanisation against rapid light fluctuations are discussed below in §1.4.1 and §1.4.2, respectively.

### 1.4.1 Plant acclimation to the long-term light environment

Plants acclimate to their average long-term environmental conditions through regulated protein synthesis and degradation. Light acclimation manifests in the phenotype, at the resolution of the whole plant, leaf, cell, chloroplast, thylakoid and pigment-protein complexes of the photosynthetic apparatus (Walters, 2005; Schöttler and Toth, 2014). Studies in plant acclimation usually distinguish between sun or high light (HL) grown plants and shade or low light (LL) grown plants, and the associated characteristics have been extensively documented for various species (Boardman, 1977; Kendrick and Kronenberg, 1994; Lichtenthaler et al., 1981; Oguchi et al., 2003; Pyke, 2009; Terashima et al., 2001).

Put broadly, the leaves of HL plants are typically relatively small, to reduce water loss, and are thicker in cross-section. The palisade mesophyll cells form a deep, packed layer above a thick layer of spongy mesophyll, where there are relatively few intercellular air spaces. In contrast, it is typical for shade leaves to have a relatively large surface area for increased light interception. They also tend to be thinner in cross-section with a less well developed mesophyll layer and more extensive intercellular spaces (Kendrick and Kronenberg, 1994; Lichtenthaler et al., 1981; Sundberg, 1992; Terashima et al., 2001).

Acclimation to HL or LL can produce significant compositional and structural

differences in the thylakoid membrane (Ruban, 2012). Under LL, plants tend to have a higher ratio of stacked to unstacked thylakoids, grana tend to have increased diameter and more layers whereas in HL plants, grana diameter and the number of grana layers are reduced (Walters, 2005).

The membrane complexes of the thylakoids are also subject to acclimative development. Photosystem reaction centres, light harvesting complexes, ATP-synthase and other members of the electron transport chain are quantitatively and stoichiometrically regulated. For example, far red enriched environments favour PSI, requiring the plant to develop an increased quantity of PSII antennas. An increase in LHCII, can be observed in the pigment complement as a concomitant decrease in the Chl $a$:$b$ ratio. With more LHCII associated with PSII, the energy capture rates of the photosystem remain relatively high (Bailey et al., 2001). The thylakoid membrane complexes are composites of nuclear-encoded and chloroplast-encoded protein subunits, therefore acclimative stoichiometric regulation, must involve strict cooperative expression of the chloroplast subgenome (plastome) and nuclear subgenome, which is discussed further in §1.5.

### 1.4.2 Molecular mechanisation against rapid light change

Short-term (seconds to minutes) fluctuations in light are mediated by molecular mechanisms within the thylakoid membrane. Two short-term light environments can be distinguished relative to the optimal conditions to which the organism has

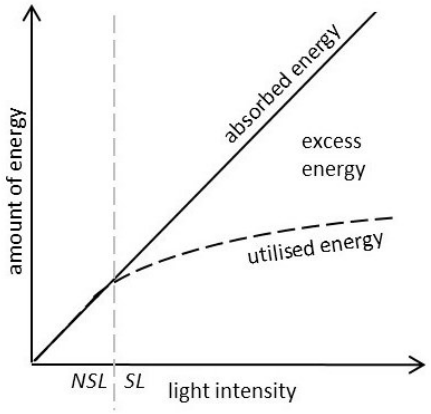


**Figure 1.17:** A hypothetical plot of the amount of light absorbed by the photosynthetic apparatus (*solid line*) and the amount utilised in photochemistry (*dashed black line*) as a function of increasing light intensity. The optimal light intensity is indicated *dashed grey line* below which is non-saturating light (NSL) and above which is saturating light (SL). Reproduced from Ruban (2012).

acclimated. These are non-saturating light (NSL) and saturating light (SL). NSL and SL are described in Fig 1.17 which shows a hypothetical plot of the amount of the total amount of absorbed energy and the amount of absorbed energy that is used in photochemistry, as light intensity increases.

The initial slope at low light intensity describes NSL, where light limits photochemical rates (Fig 1.17). NSL, otherwise known as photolimitation or light starvation, manifests as an imbalance in energy transfer to the reaction centres of PSII and PSI, as the photosystems are connected in series, this causes suboptimal electron flow through the ETC. In order to optimise electron transport under NSL, a process known as state transitions occurs during which the relative antenna size of the photosystems is adjusted through redistribution of the LHCII trimer. State transitions are discussed more fully in §1.4.2.3.

As light intensity increases (Fig 1.17), the energy demand for photochemistry is saturated and the amount of absorbed energy that is utilised in photochemistry plateaus as photosynthesis becomes limited by electron transport rates. However, light energy is still absorbed by the system. Unused energy in the photosystem can cause significant, potentially fatal, damage in a process called photoinhibition (see §1.4.2.1). Because light harvesting antenna systems are highly specialised to first, capture energy, and then reduce the risk of escaped energy, in the case that the system needs to release energy to avoid photoinhibition, it must be contrived in a regulated, inbuilt mechanism. This photoprotective mechanism is observed as a non-photochemical quenching of chlorophyll fluorescence (NPQ) mechanism, and is discussed further in §1.4.2.2.

#### 1.4.2.1 Photoinhibition

The strong electro-chemical potential of the reactants in oxygenic photosynthesis inevitably cause oxidative damage to the photosynthetic apparatus (Niyogi, 1999; Walters, 2005). This is an inherent process that occurs at all light intensities, at a low quantum yield (Aro et al., 2005). However, under high, saturating light, excess energy accumulates in the system, and the repair mechanisms of PSII cannot keep pace with the increase in oxidative damage, and a decrease in the overall photosynthetic rate occurs (Aro et al., 2005). This is known as photoinhibition (Niyogi, 1999).

In PSII, the major site for the generation of harmful oxidising species are the Chl molecules of the LHC antenna (Niyogi, 1999). As described in §1.3.1.1, one of the pathways for $^1$Chl$^*$ deexcitation is via intersystem crossing into triplet state Chl ($^3$Chl$^*$), a relatively long-lived species, which can react with $O_2$:

$$^3Chla/b^* \ + \ ^3O_2 \longrightarrow \ ^1Chla/b \ + \ ^1{O_2}^* \tag{1.12}$$

the reaction yields Chl in a singlet ground state ($^1$Chl $a/b$) and oxygen in a singlet excited state ($^1O_2{}^*$). The reason $^3$Chl $a/b^*$ can react with $O_2$ is because, unusually for a molecule, $O_2$ has a triplet ground state ($^3O_2$) and as such is able to react with $^3$Chl $a/$b$^*$ (Duffy, 2009). The product, $^1O_2{}^*$, is a highly reactive oxygen species (ROS) because as well as being a metastable (long-lived) species, it is able to react with singlet ground state molecules and is thus capable of causing extensive, long-term damage in the form of pigment bleaching and lipid and protein degradation.

$^3$Chl $a/b^*$, can also be brought to singlet ground state in a process called triplet quenching which involves chlorophyll-carotenoid interaction in which the triplet excitation is transferred from a Chl to a neighbouring carotenoid:

$$^3Chl\,a/b^* \; + \; ^1Car \longrightarrow \; ^1Chl\,a/b \; + \; ^3Car^* \tag{1.13}$$

the triplet state energy of the carotenoid is dissipated relatively rapidly and harmlessly as heat through the protein scaffold. The linear structure of the carotenoid provides a faster quenching of the triplet state than the Chl because the 'open' structure allows for vibrational motion over a much larger frequency, compared to the smaller vibrational frequency of the Chl molecule's rigid, cyclic head (Duffy, 2009). Under normal light intensities, generation of $^3$Chl $a/b^*$ is minimal and efficiently dealt with through triplet-quenching. However, under higher, saturating light intensities, the yield of $^3$Chl$^*$ increases, the capacity for triplet quenching is exceeded and the potential for ROS production significantly increases.

A second major site for the generation of ROS is the PSII reaction centre, P680, where two separate pathways, based on electron transfer at either the acceptor side or donor side of P680, can lead to photoinhibition (Barber, 1995; Niyogi, 1999). Acceptor-side inhibition may occur when electron transfer from Pheo$^-$ to $Q_A$ during charge separation (see §1.3.2) is inhibited by a build up of reduced plastoquinone at PSII. In this case, charge recombination of the P680$^+$/Pheo$^-$ radical pair can occur, which may generate triplet P680 ($^3$P680$^*$; Vass et al., 1992). Like the Chl molecules in the antenna, $^3$P680$^*$ can now react with $O_2$ to form $^1O_2{}^*$.

Donor-side photoinhibition occurs if the efficiency of electron donation to P680$^+$ from $H_2O$ via $Tyr_z$, falls below the rate of P680 oxidation (Barber, 1995; Krieger-Liszkay, 2005). When this happens, the average lifetime of P680$^+$ increases and inevitably, P680$^+$ itself starts to oxidise the surrounding pigment and protein molecules, particularly the D1 protein (Barber, 1995).

The risk of photoinhibition increases significantly under high, saturating light (SL). This is because under SL, the plastoquinone pool can be significantly reduced,

which prohibits forward electron transfer from $Pheo^{-}$, and increases the risk of acceptor-side inhibition (Krieger-Liszkay, 2005). And secondly, SL results in the development of low lumen pH which has been linked to the inhibition of the OEC and the consequent reduced efficiency in electron donation to PSII (Keren and Krieger-Liszkay, 2011; Krieger et al., 1998), increasing the potential for to donor-side inhibition.

#### 1.4.2.2 Photoprotection: NPQ

ROS result from $^{3}Chl^{*}$ formation in the antenna and reaction centre (Krieger-Liszkay, 2005). Photoinhibition occurs under strong light intensity when the rate of $^{3}Chl^{*}$ formation increases. Photosynthetic organisms have evolved a regulatory molecular mechanism that serves to protect the system against photoinhibition by increasing the rate of $^{1}Chl^{*}$ deexcitation by non-radiative (heat) decay pathways (Müller et al., 2001; Ruban and Horton, 1994). In Fig 1.12, this process of heat dissipation is depicted as a pathway in competition with the photochemical and Chl fluorescence pathways, for the deexcitation of $^{1}Chl^{*}$.

Indeed, that there are competing pathways, was first realised when Kautsky and Hirsch (1931) observed complicated kinetics in the Chl *a* fluorescence signal when they treated dark-adapted photosynthetic samples with light (Govindjee, 1995). Further work linked fluorescence decline to increased photosynthetic rates (Kautsky et al., 1959; McAlister and Myers, 1940), and then more specifically, to electron transfer from P680 to $Q_A$ (Duysens and Sweers, 1963), in a process that was termed photochemical quenching of fluorescence (qP). Another quenching pathway, that was not photochemical and that was competitively active in the deexcitation of $^{1}Chl^{*}$ was also apparent. This pathway was depicted in a model developed by Butler (1978) as a heat loss pathway and became known as non-photochemical quenching of chlorophyll fluorescence (NPQ).

An increase in NPQ manifests as a decrease in the fluorescence yield. A measure of NPQ can be taken from the chlorophyll fluorescence signal by briefly closing the photochemical pathway (see §2.9.1 for a description of the method). NPQ measurement from the Chl fluorescence signal is now standard practice for the indirect determination of heat dissipation pathway activity. However, the heterogeneity of heat dissipation, involving multiple mechanisms, produces complicated kinetics, the interpretation of which is often still debated (Müller et al., 2001).

Damage to PSII (photoinhibition), or detachment of the LHCII antenna (measured as qT, see next paragraph), may also cause a drop in fluorescence that appears as a non-photochemical quenching of fluorescence. These processes however

should be considered as causing a fluorescence decline rather than true fluorescence quenching (Ruban and Johnson, 2009), although their effect can be difficult to separate from the effect of protective NPQ. Extensive research has been carried with the aim of deconvoluting the kinetics of NPQ formation and relaxation, and of uncovering the molecular mechanisms responsible for the different NPQ components, particularly those that form the photoprotective ($^1$Chl$^*$ quenching) mechanism(s) (pNPQ).

Based on the formation and relaxation kinetics, several components of NPQ have be identified: i) qI, a slow forming, slow relaxing component, that can persist for several hours and is associated with photo**i**nhibition; ii) qT, which results from the transfer of the LHCII trimer between PSII and PSI in a process known as state **t**ransitions, a mechanism that saturates at low light intensities and has not been found to significantly effect NPQ (Horton, 1996; see §1.4.2.3); iii) qZ, a recently identified **z**eaxanthin-dependent NPQ mechanism (Brooks et al., 2013; Nilkens et al., 2010) and iv) qE, a fast forming and fast relaxing component (over seconds and minutes), that correlates with the '**e**nergisation' of the membrane ($\Delta$pH formation).

The major component of pNPQ is thought to be qE, due to its obligate dependency on the formation of $\Delta$pH (Ruban et al., 2012; Ruban and Murchie, 2012). When increased light absorption leads to saturation of the ETC, the lumenal pH decreases, this results in a decrease of the fluorescence yield and down-regulation of the photosynthetic electron transport due to thermal dissipation. $\Delta$pH is thus recognised as the trigger for the activation of pNPQ (Duffy et al., 2012; Krüger et al., 2014; Ruban et al., 2012).

However, despite a clear link between the development of $\Delta$pH and qE, both the formation and, particularly, the relaxation kinetics of $\Delta$pH are faster than those of qE (Oxborough and Horton, 1988; Wraight and Crofts, 1970; Krause, 1974). This lack of a tight correlation in the kinetics of $\Delta$pH and qE, led to the suggestion of a less direct action, whereby protons act upon an unknown site in PSII to induce a conformational change into a protective state (Horton, 1996; Krause and Weis, 1991; Ruban et al., 2012). Continued work to resolve the qE mechanism has discovered the involvement of the xanthophyll pigment cycle, LHCII aggregation and the PSII PsbS protein, each of which are discussed below.

**Xanthophyll cycle** One of the four carotenoid binding sites of the LHCII monomer is occupied by a xanthophyll molecule which, by the enzymatic addition and removal of epoxy groups, is interconvertible between violaxanthin and zeaxanthin via the intermediary pigment antheraxanthin (the molecule is represented as violaxanthin in Fig 1.6). The process, known as the xanthophyll cycle,

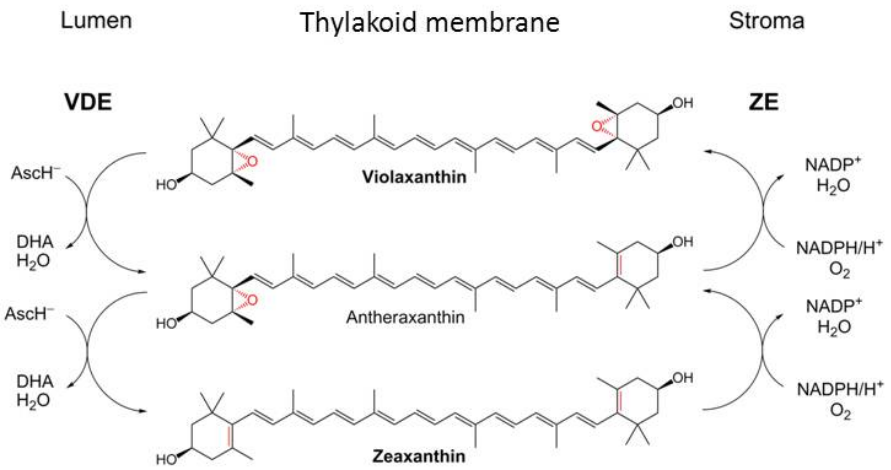


**Figure 1.18:** Xanthophyll deepoxidation cycle. As light levels increase, an epoxy group is removed from violaxanthin by violaxanthin deepoxidase (VDE), transforming it into antheraxanthin. The removal of a second epoxy group transforms antheraxanthin to zeaxanthin. Under light limiting conditions, zeaxanthin is transformed back to antheraxanthin and then to violaxanthin by the successive addition of epoxy groups by zeaxanthin epoxidase (ZE)

.

was first discovered by Sapozhnikov et al. (1957) and was later characterised by (Yamamoto et al., 1972: Fig. 1.18). The 'forward' reaction involves the removal of an epoxy group from violaxanthin by the enzyme violaxanthin de-epoxidase (VDE), transforming it into antheraxanthin, from which a second epoxy group is removed which converts the molecule into zeaxanthin. In the 'backward' reaction, the process is reversed by zeaxanthin epoxidase (ZE; Fig. 1.18).

The VDE enzyme is located within the thylakoid lumen (Hager and Holocher, 1994) and its activity is strictly coupled to the lumen pH (Hager, 1969). At neutral pH values, VDE is mobile in the lumen (Hager and Holocher, 1994), under high light illumination the proton content of the lumen increases and when pH reaches $\leq 6.5$, VDE binds to the thylakoid membrane where it gains access to its substrate violaxanthin (Hager and Holocher, 1994; Jahns et al., 2009). The epoxidation of zeaxanthin is mediated by ZE which is located in the stroma (Hager and Holocher, 1994) and although its regulation is not well understood, it has been shown that ZE activity is not affected by the transmembrane pH gradient (Jahns et al., 2009), nor by the stromal pH (Siefermann and Yamamoto, 1975).

Thirty years after its discovery, Demmig et al. (1987) connected the function of the xanthophyll cycle to the dissipation of excess light when they showed a correlation between zeaxanthin build up and the enhancement of NPQ. The finding led to the suggestion that zeaxanthin was the direct quencher of $^1Chl^*$ (Demmig et al., 1987). However, contrary to this proposal, Rees et al. (1989, 1992) and

Noctor et al. (1991) demonstrated that qE formation was possible in the absence of zeaxanthin, as long as the lumen pH was lower than 4.5-5.0.

In the work by Rees et al. (1992), thylakoids with no zeaxanthin content or with high zeaxanthin content, were isolated from dark and light adapted plants respectively. Chlorophyll fluorescence quenching was measured in the presence of 3-(3,4-dichlorophenyl)-1,1-dimethylurea (DCMU), which inhibits electron transfer from $Q_A$ to $Q_B$ and thus halts $^1Chl^*$ deexcitation by photochemistry (Krause and Weis, 1984), and nigericin, an uncoupler that dissociates the production of ATP from electron transport by dissipating $\Delta$pH (Huot and Babin, 2010). They found that by acidifying the buffer they were able to induce fluorescence quenching in thylakoids both with and without zeaxanthin, although in the absence of zeaxanthin, quenching was dependent on a lower pH. The same findings were reported in similar work by Noctor et al. (1991), using isolated chloroplasts.

The accumulation of zeaxanthin in the thylakoid membrane was thus shown to simply alter the relationship between $\Delta$pH and qE formation, so that the qE mechanism was activated at higher lumen pH (5.7-6.2) in the presence of zeaxanthin (Ruban et al., 2012). Furthermore, Ruban and Horton (1999) showed that the rate of qE formation kinetics also increased with the accumulation of zeaxanthin. These results, all support the proposal that zeaxanthin is a 'quenching amplifier', allosterically modulating the formation of qE (Demmig-Adams, 1990; Noctor et al., 1991; Rees et al., 1992; Ruban and Horton, 1999).

**The LHCII aggregation model** A model for qE was proposed by Horton et al. (1991), in which qE was suggested to result from the aggregation of the major LHCII complex in the thylakoid membrane. The proposal was based on the noted similarities between the spectroscopic changes associated with qE formation in the PSII band, observed in 77 K fluorescence emission spectra of isolated thylakoids (Ruban et al., 1991), and those measured upon aggregation of isolated LHCII (Horton et al., 1991; Mullet and Arntzen, 1980). The similarities pointed to a common origin, located in LHCII and activated under aggregation. Aggregation of LHCII in the thylakoid membrane was suggested to result from a conformational transition in the LHCII complex caused by the protonation of the complex at the lumenal side. The presence of zeaxanthin, was suggested to promote aggregation rather than have direct involvement in energy quenching. Violaxanthin on the other hand was shown to inhibit aggregation (Horton et al., 1991).

Four scenarios were envisaged, where either violaxanthin or zeaxanthin were bound to LHCII that was either protonated or not protonated. In the original hypothesis (Horton et al., 1991), these states were presented as models of various degrees of LHCII aggregation which were directly proportional to the various

degrees of heat dissipation. However, further investigation of the thylakoid membrane using electron microscopy (Dekker and Boekema, 2005) and CD spectrocopy (Garab and Mustárdy, 2000) revealed greater complexity in structure and protein interaction, forcing the conclusion that the aggregation states observed in isolated LHCII were not possible *in vivo* (Horton and Ruban, 2005). The model was therefore updated (Horton and Ruban, 2005) to suggest that the four functional/structural LHCII states (I-IV), instead represent various conformational states of individual antenna complexes.

The LHCII aggregation model (Horton et al., 2005; Ruban et al., 2012) is depicted in Fig 1.19. State (I) describes a dark or low light adapted system, where little or no difference in the pH between the lumen and the stroma means that the system is unenergised, proton binding is minimal and violaxanthin is present in LHCII. Under several minutes of saturating light, the lumen pH decreases sufficiently to produce maximal proton binding and zeaxanthin content, driving the system into a fully quenched state (IV).

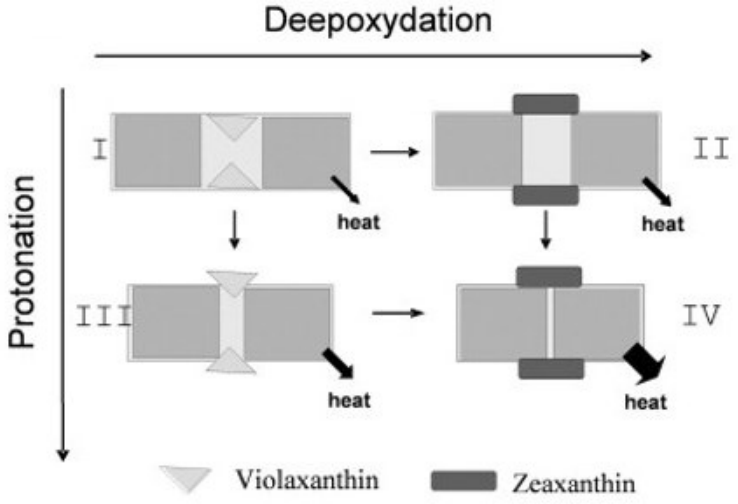


**Figure 1.19:** LHCII aggregation model for NPQ. The model as proposed by Horton and Ruban (2005), see main text for details of states (I)-(IV). Figure taken from Ruban et al. (2012).

State (III), in which the system is protonated but still binds violaxanthin, is proposed to be a possible transitional state between (I) and (IV). Full LHCII aggregation is inhibited by the presence of violaxanthin and so is only partially aggregated due to protonation. State (III) also serves to explain the partial quenching state brought about, for example, in dark adapted thylakoids (binding violaxanthin) suspended in low pH buffer (protonated). State (II) is referred to as a 'memory' state which occurs after light removal, when the system is no longer

protonated due to the relaxation of ΔpH, but still binds zeaxanthin, for which the epoxidation back to violaxanthin is relatively slow. State (II) may also offer some explanation for the NPQ component, qI, that remains after qE has relaxed.

The LHCII aggregation model was able to account for many of the NPQ related phenomena that had been observed, however it lacked clarity regarding key structural details. Advances in the understanding of the composition, structure and organisation *in vivo* and *in vitro*, of the various LHCII antenna (Bassi and Dainese, 1992; Bassi et al., 1993; Butler and Kühlbrandt, 1988), as well as discoveries in proton binding sites and proton translocation (Jahns and Junge, 1990) fuelled a new debate over whether the site of qE was based in the major or minor antenna of LHCII (Bassi and Dainese, 1992; Bassi et al., 1993) which was not addressed by the LHCII aggregation model.

**PsbS involvement in qE** Work to resolve the PSII protein complement, revealed a new subunit, PsbS (Ghanotakis and Yocum, 1986). Sequencing of the encoding gene (*psbS*), revealed that the protein was a member of the LHC family (Kim et al., 1992; Wedell et al., 1992). However, unlike other members of the antenna family, PsbS was found to be stable in the absence of pigments and was therefore determined to not be involved in light harvesting (Funk et al., 1995). Mutants lacking PsbS have revealed that instead, the subunit has an important role in photoprotection (Li et al., 2000, 2002).

However, later work by Johnson and Ruban (2010), found that qE was still demonstrable to wildtype levels in the absence of PsbS, and as such PsbS is not essential for qE formation. More recent suggestions are that PsbS is a part of a proton signal cascade that triggers NPQ, whereby protonation of PsbS glutamates 122 and 226 (Li et al., 2004) trigger reorganisation in the thylakoid membrane that lead to the protonation of LHCII and a consequent change in LHCII conformation (Belgio et al., 2013; Petrou et al., 2013). Neither the mechanism, nor the location of PsbS in PSII has yet been resolved and there is ongoing work to clarify how PsbS is involved in qE.

#### 1.4.2.3 Optimising the light harvest in short-term limiting light: state transitions

State transitions are a short-term light adaptation mechanism that occurs when an imbalance of excitation transfers to P680 and P700 manifests as a redox change of the plastoquinone (PQ) pool. Imbalance occurs because the reaction centre chlorophylls of photosystem I and II, have different excited state energies, absorbing maximally at 700 nm and 680 nm respectively (Walker, 1992). In correspondence, the antenna systems associated with each photosystem have different spectral

designs in order to efficiently meet the reaction centre requirements (Ruban and Johnson, 2009). Absorption by the PSII antenna, predominantly LHCII, is relatively blue shifted due to a low Chl $a$:$b$ ratio ($\sim$ 1.33 in LHCIIb; Liu et al., 2004). In contrast, the PSI antenna has an Chl $a$:$b$ ratio of about 8.5 (Wientjes et al., 2013) and furthermore, possesses a collection of red-shifted Chl $a$ forms that absorb in the 690-710 nm region (Liu et al., 2004; Melkozernov and Blankenship, 2005; Ruban and Johnson, 2009).

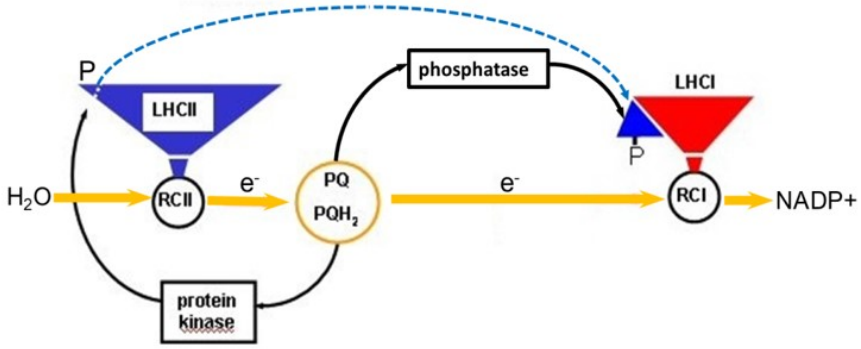


**Figure 1.20:** A diagram describing the state transitions phosphorylation model, see main text for information. PQ, plastoquinone; $PQH_2$, fully reduced plastoquinone (plastoquinol); P, phosphate group; RCI and RCII, reaction centre I and II respectively. Taken from Ruban and Johnson (2009)

The difference in the photosystem absorption profiles, creates the potential for asymmetrical absorption when the light spectral quality deviates from that to which the plant has acclimated and when light levels drop into light limiting conditions (see Fig 1.17; Ruban and Johnson, 2009; Wollman, 2001). The result is a heterogeneous rate of electron flow in the ETC causing suboptimal photosynthetic performance. In this situation, state transitions serve to re-equilibrate light absorption at PSI and PSII by adjusting their relative antenna size. This is done by the redistribution of a portion of peripheral LHCII between PSII and PSI, thus redressing the excitation bias by adjusting both the absorption cross-section and spectral profile of the respective antenna cross-sections (Niyogi, 1999).

Fig 1.20 presents the phosphorylation model of state transitions feedback regulation. LHCII migration is activated by phosphorylation and dephosphorylation of the LHCII N-terminus. The kinase and phosphatase activation has been shown to be controlled by the redox state of the plastoquinone pool (Allen, 2003; Ruban and Johnson, 2009; Puthiyaveetil et al., 2012). If light quality favours PSII over PSI, the plastoquinone pool (PQ pool) becomes reduced. This triggers a kinase to phosphorylate LHCII. P-LHCII decouples from PSII and migrates through the

membrane to couple with PSI. PSII and PSI cross-sections are thus reduced and increased, respectively. Electron flow through PSI increases, draining away the excess electrons in the PQ pool. Preferential excitation of PSI, manifests as PQ pool oxidation. This activates a phosphatase that dephosphorylates LHCII, ensuring its disassociation from PSI and migration back to PSII (Allen, 2003; Ruban and Johnson, 2009; Puthiyaveetil et al., 2012). The acclimated, or natural state of the LHCII antenna is considered to be in functional attachment to PSII, and is referred to as State I (STI) (Allen, 2003). PSI-LHCII is known as State II(STII).

## 1.5 The chloroplast endosymbiosis theory

The mechanisms described above, occur in the thylakoid membrane of the chloroplast. As already mentioned, the chloroplast is now widely accepted to be an ancestral remnant of a once free living organism of the ancient cyanobacterial lineage (de Alda et al., 2014). According to the theory, first put forward by Constantin Mereschkowsky in 1905 (Martin and Kowallik, 1999) and later developed by Margulis (1970), the transformation of a once free-living prokaryotic autotrophic cell into what is now recognised as the modern-day chloroplast in a eukaryotic cell, was realised by the gradual transfer of the genome of the endosymbiont to the nucleus of the host cell, transforming the captured organism into an obligate organelle (Margulis, 1970; Schmitz-Linneweber et al., 2002).

A small fraction of the endosymbiont genome, the plastome, still resides in the chloroplast as a circular genome of about 120-200 kbp, which encodes for roughly 100 - 170 proteins (Pyke, 2009; Zybailov et al., 2008), most importantly, these include the core subunits of the light-reaction supercomplexes of the thylakoid membrane (Allen et al., 2011; Blankenship, 2002). The other $> 98$ % of the chloroplast proteins, estimated to number over 3000 for a fully functioning chloroplast (Jarvis, 2008), are transcribed from nuclear DNA and synthesized on 80S ribosomes in the cytosol.

Table 1.1, lists the genes required for the construction of the principle thylakoid membrane protein complexes, PSII, Cyt $b_6f$, PSI and ATP-synthase and indicates in which subgenome, the nucleur or plastid, they are encoded. Fig 1.4, also indicates gene location in a colour-coded diagram of the thylakoid membrane complexes. The proximity Core components of PSII, PSI, Cyt $b_6f$, and ATPsynthase such as D1 (PsbA), D2 (PsbD) are chloroplast encoded.

Typically, nuclear encoded proteins have an amino-terminal targeting signal, the transit peptide, which is used to 'address' the precursor-form protein to the chloroplast, where it is imported through the chloroplast membrane via the Tic-Toc gateway (see §1.2.1) to the chloroplast stroma. Here, further the transit

**Table 1.1:** Genes encoding for polypeptide subunits of the protein complexes in the photosynthetic membrane. The location of the gene, in the nucleus (n) or the chloroplast (c), is given. Table reproduced with some changes, from Allen et al. (2011).

| *Gene* | Product | |
|---|---|---|
| **Photosystem II** | | |
| *psbA* | D1 | c |
| *psbB* | CP47 | c |
| *psbC* | CP43 | c |
| *psbD* | D2 | c |
| *psbE* | Cytochrome b559$\alpha$ | c |
| *psbF* | Cytochrome b559$\beta$ | c |
| *psbH* | PsbH | c |
| *psbI* | PsbI | c |
| *psbJ* | PsbJ | c |
| *psbK* | PsbK | c |
| *psbL* | PsbL | c |
| *psbM* | PsbM | c |
| *psbN* | PsbN | c |
| *psbO* | OEC33 | n |
| *psbP* | OEC23 | n |
| *psbQ* | OEC16 | n |
| *psbR* | PsbR | n |
| *psbS* | PsbS | n |
| *psbTc* | PsbTc (Ycf8) | c |
| *psbTn* | PsbTn | n |
| *psbW* | PsbW | n |
| *psbX* | PsbX | n |
| *psbY* | PsbY | n |
| *psbZ* | PsbZ (Ycf9) | c |
| *psb27* | Psb27 | n |
| *psb28* | Psb28 | n |
| *psb29* | Psb29 | n |
| *psb31* | Psb31 | n |
| *lhcb1-6* | Lhcb1-6 | n |
| **Ycf12* | Ycf | |
| **Cytochrome $b_6f$** | | |
| *petA* | Cytochrome f | c |
| *petB* | Cytochrome $b_6$ | c |
| *petC* | Rieske Fe-S | n |
| *petD* | Subunit IV | c |
| *petG* | Subunit G | c |
| *petL* | Subunit L | c |
| *petM* | Subunit M | n |
| *petN* | Subunit N | c |

*...continued...*

| *Gene* | Product | |
|---|---|---|
| **Photosystem I** | | |
| *psaA* | PsaA | c |
| *psaB* | PsaB | c |
| *psaC* | PsaC | c |
| *psaD* | PsaD | n |
| *psaE* | PsaE | n |
| *psaF* | PsaF | n |
| *psaG* | PsaG | n |
| *psaH* | PsaH | n |
| *psaI* | PsaI | c |
| *psaJ* | PsaJ | c |
| *psaK* | PsaK | n |
| *psaL* | PsaL | n |
| *psaM* | PsaM | n |
| *psaN* | PsaN | n |
| *psaO* | PsaO | n |
| *psaP* | PsaP | n |
| *lhca* | LHC I | n |
| ***psaR* | PsaR | - |
| **ATP-synthase** | | |
| *atpA* | $\alpha$-Subunit | c |
| *atpB* | $\beta$-Subunit | c |
| *atpC* | $\gamma$-Subunit | n |
| *atpD* | $\delta$-Subunit | n |
| *atpE* | $\varepsilon$-Subunit | c |
| *atpF* | Subunit I | c |
| *atpG* | Subunit II | n |
| *atpH* | Subunit III | c |
| *atpI* | Subunit IV | c |
| **Plastocyanin** | | |
| *petE* | Plastocyanin | n |
| **Cytochrome *c6*** | | |
| *petJ* | Cytochrome c6 | n |
| **Ferredoxin** | | |
| *petF* | Ferredoxin | n |
| ***FNR*** | | |
| *petH* | FNR | n |

**Note* The Ycf12 subunit was recently identified (Kashino et al., 2007; Umena et al., 2011). It is thought that it was formally designated as PsbN (Barber, 2014).
**PsaR was recently identified by Amunts et al. (2010).

peptide is cleaved away and the polypeptide is transferred to its target location. For the light-reaction complexes, this entails assemblage around the chloroplast encoded core complex and insertion in to the thylakoid membrane. Plastome gene products also function in the transcription and translation of the plastid itself, which characterises the chloroplast with a quasi-autonomy. However the expression of the chloroplast encoded genes is also dependent upon nucleus-encoded factors (Jarvis and López-Juez, 2013).

## 1.6 Cytoplasmic hybrid plants

Cytoplasmic hybrid (cybrid) plants are cell engineered somatic hybrids in which the subgenome complement (the nuclear genome, the chondriome and the plastome), is of specifically heterogeneous origin. Cybrids are created by chemically induced fusion of somatic protoplasts from two different plant species. This form of regenerative crossing avoids the process of nuclear recombination that is one of the basic, inherent mechanisms of genetic variation in sexual reproduction. Instead, the cell is an expression, of the cooperative government of the taxonomically distinct subgenomes.

Upon protoplast fusion, the elimination of chromosomes from one or other parent is often observed (Gernand et al., 2005; Liu et al., 2005). Similarly, the rapid segregation of plastids into like with like is typical, such that the population of chloroplasts in the recovered cybrid is usually of a single parental origin (Belliard et al., 1979; Morgan and Maliga, 1987; Sanchez-Puerta et al., 2014). This phenomenon reflects the observation that during plant growth and development, chloroplasts do not normally fuse (Sanchez-Puerta et al., 2014).

In contrast, mitochondria regularly fuse or, less frequently, undergo unequal fission (Arimura et al., 2004; Sanchez-Puerta et al., 2014) and widespread horizontal transfer of mitochondrial genes between flowering plants has also been reported Bergthorsson et al. (2003). Consequently, the assumption of uniparental mitochondrial inheritance, based predominantly on studies of animal mtDNA, has been brought into question (Barr et al., 2005; Bergthorsson et al., 2003). The natural tendency of the mitochondrial DNA (mtDNA) towards chimeric fusion, could explain the frequently observed mtDNA recombination of the cybrid plants (Belliard et al., 1979; Kuchuk et al., 2006; Kushnir et al., 1987; Peter et al., 1999; Zubko et al., 2003).

In cybrid creation, after protoplast fusion and then after full protein turnover, the components of the cell that have chloroplast parental origin, are now only the chloroplast DNA (cpDNA), and the about 100-160 products it encodes. With the exception of the mitochondria, the rest of the cell, including the vast proportion

of the chloroplast, is encoded by the nuclear parent.

Previous research in plant cytoplasmic hybridisation has been for the purpose of agricultural crop development (Bajaj, 1994; Nagata and Bajaj, 2001). The main drive being the possibility to overcome barriers that are inherent in sexual crossing between divergent genotypes, with the potential for greatly increasing the gene pool that is available for crop development. In addition, novel phenotypes such as cytoplasmic male sterilty (CMS), linked to recombination in the mitochondria (Babiychuk et al., 1995), are frequently observed in cybrids and are considered valuable traits in crop breeding programmes (Liu et al., 2005).

Only a handful of cybrid constructs have been investigated in other fields of plant research. Predominantly, these have been with the aim to elucidate the co-evolutionary relationship of the nucleus and the chloroplast, as a possible mechanism for speciation processes (Babiychuk et al., 1995; Kushnir et al., 1987; Kochevenko et al., 2000). Cybrid studies in nucleo-chloroplast compatibility, began in the 1970s with parasexual cybrid constructs between species of the *Nicotiana* genus (Carlson et al., 1972). Further work produced cybrids across increasingly distant taxonomic ranks which revealed that the so-called nuclear-organellar incompatibility was not closely correlated with the taxonomic proximity.

In a particularly interesting case, reciprocal-crosses of *N.tabacum* and *Atropa belladonna* were created (Kushnir et al., 1987, 1991). The resulting cybrid plants were $Nt(Ab)$ and $Ab(Nt)$, denominated, as described before, by the initials of the nuclear parent followed by those of the chloroplast parent in brackets. While the $Nt(Ab)$ cybrids were phenotypically much like *N.tabacum*, the $Ab(Nt)$ cybrid was entirely chlorophyll deficient with an albino phenotype, and were only able to grow heterotrophically *in vitro* (Kushnir et al., 1991) .

To rule out the possibility that the unusual phenotype was due to mutation during *in vitro* culturing, Kushnir et al. (1991) fused the *A. belladonna* nucleus and the *N.tabacum* plastome from the $Ab(Nt)$ cybrid with a freshly extracted *A. belladonna* plastome and a *N.tabacum* nucleus respectively. Normal, green plants were recovered in each line, indicating that the $Ab(Nt)$ phenotype occurred due to *N.tabacum* nuclear control over the *A. belladonna* chloroplast. This finding introduces the notion that the nucleo-cytoplasmic incompatibility derives from a deeper synergism than a straightforward correlation with evolutionary divergence times.

### 1.6.1 *N.tabacum*(*H.niger*) cybrid plants

Cytoplasmic hybridisation of *N.tabacum* with *H. niger*, was established by Zubko et al. (1996). The protocol used by Zubko et al. (1996) for cybrid construction,

is described in detail in the Materials and Methods (Chapter 2, §2.7.1). Zubko et al. (1996) recovered three *Nt*(*Hn*) plant lines (Rhn1-3) from protoplast fusion cultures of wildtype *H. niger* and albino *N.tabacum*. As with other cybrid plants with a *N.tabacum* nuclear parent, the general appearance was that of *N.tabacum*, although there was some difference between the three recovered lines, where one of the lines, Rhn3, developed *N.tabacum*-like leaves and corolla while Rhn1 and Rhn2 bore elongated leaves and the corollas were absent from the flowers.

In all Rhn lines, pollen production was evident, although when used in self-pollination, the plants failed to develop seeds. Pollination of wildtype *N.tabacum* however, did produce viable seeds. It was therefore concluded that, like previous cybrids, the *Nt*(*Hn*) phenotype had established cytoplasmic male sterility (CMS) but possessed female fertility (Zubko et al., 1996, 2003). The underdeveloped anthers and infertile pollen grains of *Nt*(*Hn*) persisted through repeated backcrossing with wildtype *N.tabacum*, demonstrating the maternal (cytoplasmic) inheritance of the male sterility.

# Aims of the project

The aim of the work presented in this thesis was to investigate light acclimation and photoregulation in the *Nt*(*Hn*) cybrid plant. As far as we are aware, cybrid plants have not yet been examined in their ability to plastically couple their structural and functional phenotype to changes in the light environment. These plants, however, offer an intriguing model for the investigation of light adaptation against the flux of natural light. This is firstly because light acclimation is dependent on the cooperative government of nuclear and chloroplast gene expression. Secondly, for short-term, non-genetic, molecular mechanisms of photoregulation, the rapid and precise interaction of nuclear and chloroplast encoded proteins is crucial, particularly at the level of the thylakoid membrane where these proteins are structurally and functionally bound to each other. In this investigation our intention was to analyse the *Nt*(*Hn*) cybrid in terms of:

(a) its general development and phenotype through monitoring plant growth and morphology.

(b) its acclimation to HL and LL growth environments, by investigation of:

i) leaf tissue and cell phenotype using light and confocal microscopy.

ii) chloroplast morphology and organisation within the cell using confocal and transmission electron microscopy.

iii) the organisation of thylakoid membranes within the chloroplast using thin section transmission electron microscopy.

iv) the composition and relative abundance of the thylakoid membrane polypeptides using FPLC gel filtration of detergent solubilised membranes followed by characterisation of fractions by SDS-PAGE and spectroscopic techniques, and pigment analysis using HPLC.

v) its functional response to short-term light change using rapid light curves constructed from chlorophyll fluorescence signal traces measured under increasing light intensity.

(c) the plant's ability for short-term (non-genetic) regulatory response in the thylakoid membrane, to rapid changes in the light environment by analysis of:

i) the capacity for high light management through photoprotective energy dissipation (NPQ) as monitored using PAM fluorescence induction.

ii) the investigation of the NPQ capacity through analysis of the PsbS protein, the xanthophyll cycle and the quenching capacity of the major light harvesting complex (LHCII).

iii) the ability to compensate for energy imbalance between the two photosystems that is experienced under low light intensity (state transitions), using PAM fluorescence induction and 77 K fluorescence measurements.

(d) any novel or interesting phenotype or response that became apparent during the above investigations.

# Materials and Methods

# Chapter 2

# Materials

## 2.1 Laboratory equipment

| **Equipment** | **Brand, model** |
|---|---|
| • Centrifuge, bench-top | Eppendorf AG, 5418 |
| • Centrifuge, swing bucket, refrigerated | Harrier 18/80R, MSE |
| • Dual-PAM 100 chlorophyll fluorescence photosynthesis analyzer | Heinz Walz |
| • FPLC, AKTA Purifier system | GE Healthcare |
| • Freeze Fracture Control Unit | Polaron Instruments, E6432 |
| • Gel-electrophoresis mini-gel system | BioRad |
| • HPLC System, Summit | Dionex |
| • Iso-electric Focusing System | GE Healthcare |
| • IEF tray (125 x 260 x 5 cm) | Amersham Sciences |
| • Leica confocal microscope | Leica Microsystems, Wetzlar, Germany |
| • Microtome | Leica, Reichert-Jung Ultracut E |
| • PAM-101 Fluorimeter | Heinz Walz, Germany |
| • pH meter | Hanna Instruments, 111pH/ORP meter |
| • pH micro-electrode | Mettler Toledo InLab micro |
| • Polytron blender | Kinematica, Lucerne, Switzerland |
| • Scanner | Epson Perfection 4490 photo |
| • SDS-PAGE apparatus | BioRad PROTEAN mini-gel, |
| • Spectrophotometer | Amersham, Ultrospec 2100 pro |
| • Spectrofluorimeter | Jobin Yvon |
| • Transmission electron microscope | JEOL, Tokyo, Japan, JEM 1230 |
| • Vortex | IKA, Genius 3 |

| | |
|---|---|
| • Weighing scales, precision | Fisherbrand PS-100 |
| • Western Blot apparatus | BioRad |

## 2.2 Software

| **Software name** | **Developer/Publisher** |
|---|---|
| • Chromeleon | Dionex Corporation |
| • DualPAM v. 1.19 | Heinz Walz |
| • ExPASy Compute pI | Swiss Institute of Bioinformatics, (www.expasy.org) |
| • ImageJ | National Inst. of Health (rsb.info.nih.gov/ij/) |
| • Jalview | Waterhouse et al. (2009), (www.jalview.org) |
| • Leica Application Suite | Leica Microsystems |
| • LAS Lite v. 2.6.0 | Leica Microsystems, (www.leica-microsystems.com) |
| • Mascot, v. 2.3.02 | Matrix Science Ltd |
| • OrgGenDRAW | (Lohse et al., 2013) (http://ogdraw.mpimp-golm.mpg.de) |
| • Olis | Olis, Inc. |
| • Origin v. 7.5 | Originlab Corporation |
| • PhotochemCAD v. 2.1 | Jonathan Lindsey (Du et al., 1998; www.photochemcad.com) |
| • Sigmaplot v. 12.5 | Systat Software |
| • Spekwin32 v. 1.71.6.1 | Spekwin32 Software (http://www.effemm2.de/spekwin) |
| • Unicorn v. 5.11 | GE Healthcare |
| • Volocity | Perkin Elmer |

## 2.3 Laboratory consumables

| **Equipment** | **Brand, product detail** |
|---|---|
| • Blotting paper | Sigma-Aldrich, Z613886 |
| • Desalting column, PD-10 | GE Healthcare, 52-1308-00 BB |
| • Elution columns, PEGG | GE Healthcare, 80-11061-75 |
| • Copper grids Hexagonal 300 thin bar | Agar Scientific, G2740C |
| • Photographic paper | Kodak |
| • Pigment standards | Serva, Heidelberg, Germany |
| • Nitrocellulose membrane | Amersham, Biosciences, Hybond-ECL |

| Chemical | Supplier |
|---|---|
| • Acetic acid 99 % | VWR |
| • Acetone | VWR |
| • Acetonitrile | VWR |
| • Acrylamide, 30 % solution | Sigma-Aldrich |
| • Agar, select | Sigma-Aldrich |
| • Ampholine carrier ampholytes, pH 2.5-5 | GE Healthcare |
| • APS | Sigma-Aldrich |
| • Araldite CY212 | Agar Scientific |
| • Benzyl dimethylamine | Sigma-Aldrich |
| • Bovine serum albumin (BSA) | Sigma-Aldrich |
| • Bromophenol blue | BDH |
| • Calcium chloride ($CaCl_2$) | VWR |
| • Cellulase "Onozuka" RS | Yakult Pharmaceuticals |
| • Coomassie brilliant blue R250 | BDH |
| • Developer (for photographic developing) | Kodak |
| • Dithiothreitol | Sigma-Aldrich |
| • $\alpha$-DM (n-Dodecyl-$\alpha$-D-Maltopyranoside), Anagrade | Affymetrix |
| • $\beta$-DM (n-Dodecyl-$\beta$-D-Maltopyranoside), Anagrade | Affymetrix |
| • Driselase, cellulase | Sigma-Aldrich |
| • Dodecenyl succinic anhydride | Sigma-Aldrich |
| • EDTA (Ethylenediaminetetraacetic acid) | Sigma-Aldrich |
| • Ethanol | VWR |
| • Fixer (for photographic developing) | Kodak |
| • Glutaraldehyde solution Grade I, 50 % in $H_2O$, for EM | Sigma-Aldrich |
| • Glycine | Melford |
| • HEPES (4-(2-hydroxyethyl)-1-piperazineethanesulfonic acid) 99.5 % (titration) | Sigma-Aldrich |
| • Hexane (n-Hexane) 95 % Chromanorm for HPLC | VWR |
| • Hydrochloric acid (HCl) | VWR |
| • Immersion oil for microscopy | Sigma-Aldrich |
| • Luminol | Fluka |
| • Macroenzyme R10 | Yakult Pharmaceuticals |
| • Methanol (MeOH) | VWR |
| • Methyl nadic anhydride | Sigma-Aldrich |
| • Paraformaldehyde | VWR |
| • Peroxide | Amersham |

| | |
|---|---|
| • Pharmalyte broad range pH 2.5-5 | VWR |
| • PBS (Phosphate buffered saline) | Sigma-Aldrich |
| • Ponceau S for electrophoresis | Sigma-Aldrich |
| • Potassium chloride (KCl) | Sigma-Aldrich |
| • Potassium dihydrogen ($KH_2PO_4$) | BHD |
| • Potassium hydroxide (KOH) | Sigma-Aldrich |
| • Reynold's Lead Citrate stain | TAAB |
| • Sephadex G-75 Superfine | GE Healthcare |
| • SDS, Sodium dodecyl sulfate (electrophoresis grade) | Sigma-Aldrich |
| • Sodium bicarbonate ($NaHCO_3$) | VWR |
| • Sodium chloride (NaCl) | Sigma-Aldrich |
| • Sodium phosphate dibasic dodecahydrate ($NaHPO_4 \cdot H_2O$) | Melford |
| • Sorbitol (D-Sorbitol) | Melford |
| • Tannic acid | Sigma-Aldrich |
| • TEMED (Tetramethylethylenediamine) | Sigma-Aldrich |
| • Toluidine blue | Sigma-Aldrich |
| • Tris (Tris(hydroxymethyl)aminomethane) | VWR |
| • Trizma base | Sigma-Aldrich |
| • TWEEN 20 - average Mn 1,228 | Sigma-Aldrich |
| • Uranyl acetate, aqueous | SPI-Chem |
| • Western Blotting Detection Reagents, ECL Plus | Amersham |

## 2.4 Solutions and buffers

Recipes are given within the description of the method.

## 2.5 Plant Material

Seeds of each plant type were procured once at the start of the project. From these stocks, plant lines for experimental use were generated and maintained in the growth rooms under controlled lighting or in the rooftop greenhouses at Queen Mary, University of London.

- Wildtype *Nicotiana tabacum* L. (*N.tabacum*; cv. Wisconsin 38), 2n = 4x = 48. Seeds were kindly donated by Dr Mikhajlo Zubko.

- Wildtype *Hyoscyamus niger* L. (henbane), 2n = 2x = 34. Seeds were kindly supplied by Oxford Botanical Gardens.

- Seeds of cytoplasmic hybrid (cybrid) plants with a *N.tabacum* nuclear parent and a *H. niger* plastome parent (*Nt*(*Hn*)) were kindly donated by Dr Mikhajlo Zubko. The *Nt*(*Hn*) line used in this study originated from a a single protoplast fusion event (*Nt*(*Hn*) line Rhn3; Zubko et al., 1996). The resulting plants had been back-crossed with wildtype *N.tabacum* (cultivar W38) for at least four generations before their donation to this project. For information about cybrid construction, see §2.7.1.

## 2.6 Materials for plant growth

All consumables for plant growth were, unless otherwise stated, purchased from Interhort, Cheshire, UK (http://www.interhort.com/).

**Equipment**

- Plant growth chamber from Sanyo (MLR-351H)
- Tailor-made open-front shelving fitted with under-shelf Polylux light fixtures

**Consumables**

- Compost, Westfield Multipurpose compost with John Innes
- Seed tray half size, vacapak
- 15.5 cm diameter plant pots
- 3 L plant pots
- Horticultural sand
- Perlite
- Polylux W38/840 bulbs from GE Lighting, Brackmills, UK

# Methods

## 2.7 Plant material

### 2.7.1 Cybrid construction

The method used for the construction of the *Nt*(*Hn*) cybrid plants, created in Dr Mikhajlo Zubko's lab (Zubko et al., 1996), is reported here (§2.7.1).

**Cybrid parental plant material** Albino plastome mutants of *N.tabacum* (R100a1, Zubko et al. (1991)) and wild–type *H. niger* (Marburg, Germany) were grown *in vitro* on agar with MS medium (Murashige and Skoog, 1962) supplemented with 30 g $L^{-1}$ and 20 g $L^{-1}$ sucrose for *N.tabacum* and *H. niger*, respectively.

**Isolation and fusion of protoplasts** Parental protoplasts were prepared from aseptic leaves using an enzyme mixture of 0.3 % (w/v) cellulase Onozuka R10, 0.2 % (w/v) Macerozyme R10 and 0.1 % (w/v) Driselase dissolved in W5 solution (154 mM NaCl; 125 mL $CaCl_2$; 5 mM KCl; 5 mM glucose; pH = 5.6; Menczel et al., 1981). For protoplast fusion, 400 $\mu$L of PEG solution (40 % (w/v) polyethylene glycol; 0.3 M glucose; 66 mM $CaCl_2$; pH 6) was pipetted into a flow centrifuge tube (1 cm diameter).

Protoplasts of *H. niger* and *N.tabacum* were mixed in a 1:1 ratio to a final quantity of approximately $2 \times 10^5$, washed and resuspended in 0.5 mL of W5 solution, then carefully plated on top of the PEG solution using a Pasteur pipette. The preparation was centrifuged at 600 rpm for 40 s during which a fraction of the protoplasts formed a compact interphase between the solutions. After standing for 15 min, 0.5 mL of a high pH buffer (0.3 M glycine - NaOH buffer pH 10.5 ; sterilised and filtered) was gently added on top of the W5 solution and left (15-20 min). To remove the PEG and buffer, the protoplast mix was washed with W5 solution (10 mL) while gently centrifuging.

**Regeneration of cytoplasmic hybrids** Protoplasts were resuspended in SW culture medium (Sidorov et al., 1987) and cultivated at a density of $10^4$ cells

$mL^{-1}$ at 26 °C in the dark for 1 week. Fresh medium was then added and the dishes transferred to dim light (9 $\mu$mol photons $m^{-2}$ $s^{-1}$). After two weeks, the microcolonies were diluted 3-fold with liquid C-medium (Shepard and Totten, 1977) then plated on the surface of C-medium solidified with 0.8 % (w/v) agar, under an increased light intensity (36 $\mu$mol photons $m^{-2}$ $s^{-1}$).

**Selection for *Nt(Hn)* cybrids** After 4 weeks, the colonies that showed greening, indicating the presence of *H. niger* chloroplasts, were transferred to MS medium mixed with 1 mg $L^{-1}$ kinetin and 10 g $L^{-1}$ sucrose. Shoots were rooted on hormone-free MS medium. To select for *N.tabacum* nuclei in the cybrids, plants with the outward phenotype of *N.tabacum* were selected by eye and then further verified by chromosome analysis (§2.7.1).

***Nt(Hn)* chromosome analysis** To arrest cells during cell division, root tips were treated with 0.02 % (w/v) colchicine solution for 3-4 h and then fixed overnight in ethanol : glacial acetic acid (1 : 3). The tips were stained with 1 % (w/v) aceto-orcein and squashed on a microscope slide for viewing.

### 2.7.2 Plant growth

Compost, sand and perlite were mixed in a ratio of 9 : 2 : 1 and autoclaved. *N.tabacum*, *H. niger* and *Nt(Hn)* seeds were sown in the compost mix in seed trays to a depth of 2-4 mm about 4 cm apart, watered then stored at 4 °C for vernalisation. After 3 days they were moved to growth cabinets fitted with 'Cool White' Polylux W38/840 bulbs with a 10 h photoperiod at a light intensity of about 70 $\mu$mol photons $m^{-2}$ $s^{-1}$ and a day/night temperature of 22/18 °C respectively. At 7, 7-8 and 11-12 weeks, *N.tabacum*, *H. niger* and *Nt(Hn)* plants respectively (see Results for more details) were transplanted into individual pots (15 cm diameter) and placed on shelves also fitted with Polylux 58/840 bulbs, at either high light (HL, 300-400 $\mu$mol photons $m^{-2}$ $s^{-1}$) or low light (LL, 80-100 $\mu$mol photons $m^{-2}$ $s^{-1}$). *N.tabacum* plants were used in experiments at 8-12 weeks old, *H. niger* 9-15 weeks and the *Nt(Hn)* cybrid from 14-17 weeks. Remaining plants were re-potted into 3 L pots and transferred to greenhouses for flowering and seed collection.

### 2.7.3 Pollination and seed collection

*N.tabacum* and *H. niger* flowers were pollinated by transferring pollen between flowers within the same plant or between plants of the same species using a clean paintbrush. *Nt(Hn)* plants were pollinated by transfer of wildtype *N.tabacum* pollen to the *Nt(Hn)* stigma. Only flowers showing typical wildtype characteristics,

were used for sedd production (see §3.3) Pollinated flowers were sealed in large paper bags to avoid cross-pollination and aid seed collection.

## 2.8 Biochemistry and molecular biology techniques

### 2.8.1 Isolation of thylakoids

The buffers described below are for the preparation of unstacked thylakoids. To prepare stacked thylakoids, 5 mM $MgCl_2$ was added to each buffer.

Plants were dark adapted for 1 h, then in dim background light, leaves were removed from plants and midribs cut out. The leaf material was roughly cut with scissors, weighed, then homogenized to 'pesto' consistency in ice-cold, slushy grinding buffer (300 mL; 330 mM Sorbitol, 10 mM $Na_4P_2O_7$; pH 6.5) using a Polytron blender (Kinematica). The homogenate was filtered through two layers of muslin, tightly squeezed to force out the suspension, then filtered again through $2 \times 2$ layers of muslin, between which was 1 layer of cotton wool for starch removal, care was taken not to squeeze the cotton wool. The filtrate was centrifuged (4000 $\times$ g; 10 min; 4 °C) and the pellet resuspended using a squirrel-tail paintbrush in a small quantity of washing medium (330 M Sorbitol, 10 mM MES; pH 6.5) and centrifuged again (4000 $\times$ g; 10 min; 4 °C). This next pellet was resuspended in 30 mL of resuspension medium (330 mM Sorbitol, 1 mM EDTA, 50 mM HEPES; pH 7.6) and transferred to a 250 mL beaker. 50 mL of break medium (10 mM HEPES; pH 7.6) was added to rupture the chloroplasts by osmotic shock for 30 sec with gentle agitation. The reaction was then stopped with the addition of osmoticum medium (50 mL; 660 mM Sorbitol, 40 mM MES; pH 6.5) to restore the sorbitol content. The suspension was centrifuged a final time (4000 $\times$ g; 10 min; 4 °C) and the pellet was resuspended in resuspension medium to a final Chl concentration of about 2 – 2.5 mg Chl $mL^{-1}$, frozen in liquid nitrogen ($LN_2$) and stored at -80 °C until needed.

The buffer volumes given above were appropriate for about 80 g of leaves (about 4 *N.tabacum* plants), for different quantities of plant material the volumes were roughly adjusted. Chl concentration was determined according to the method of Porra et al. (1989) described in §2.8.2.

**Isolation of thylakoids in State I and State II** Thylakoids were prepared as described above with the following modifications: i) NaFl (10 mM) was added to each of the buffers to inhibit phosphatase activity (Bellafiore et al., 2005) and ii) instead of dark adaptation, plants were treated for 1 h under growth lights (Osram L 18W/827 Lumillux) fitted with either a red filter (Lee 027 medium red

from Lee Filters; to induce ST I) or an orange filter (Lee 105 Orange, to induce ST II), thylakoid preparation was performed in the light. The thylakoids were then Western blotted to determine the amount of LHC-II phosphorylation (see §2.8.9).

### 2.8.2 Determination of chlorophyll concentration

Chl concentration in thylakoid and LHC preparations was determined following the procedure of Porra et al. (1989). The calculation is based on the linear relationship between Chl concentration and absorption (Beer-Lambert law) which attains for $OD_{663}$ between 0.2-0.8.

Samples were vortexed to ensure homogeneity, then a small, measured quantity (2-20 $\mu$L) was diluted in 80 % (v/v) acetone to a final volume of 1 mL, mixed well and centrifuged (5 min; 16 800 × g). The supernatant was transferred to a quartz cuvette and absorption was measured at 664 nm and 647 nm using an Ultrospec 2100 pro spectrophotometer. A reference baseline was acquired from 80 % (v/v) acetone and subtraction from sample measurements was automated in the spectrophotometer. A custom built programme was used to calculate Chl concentration (Chl *a*, Chl *b*, total Chl and Chl *a*:*b* ratio) using the following equations (Porra et al., 1989):

$$Chla\ (\mu g\ mL^{-1}) = 12.25 \cdot A_{663.6} - 2.55 \cdot A_{646.6} \quad (2.1)$$

$$Chlb\ (\mu g\ mL^{-1}) = 20.31 \cdot A_{646.6} - 4.91 \cdot A_{663.6} \quad (2.2)$$

$$total\ Chl\ (\mu g\ mL^{-1}) = Chla + Chlb \quad (2.3)$$

where $A_n$ is the absorbance at a given wavelength ($n$). Multiplication by the dilution factor gave the final Chl concentration ($\mu$g mL$^{-1}$) of the sample. In order to be in the absorption linearity range, thylakoids were 500-fold diluted in acetone, most accurately obtained by a short dilution series. At least three replicates were prepared per sample.

### 2.8.3 Preparation of intact chloroplasts

Leaves were taken from a single dark adapted (1 h) plant, midribs were removed and the leaf material roughly chopped with scissors and blended in ice-cold, slushy homogenisation buffer (100 mL; 0.45 M sorbitol, 20 mM Tricine, 10 mM EDTA, 10 mM $NaHCO_3$, 0.1 % (w/v) BSA; pH 8.4) using three 1 sec bursts of a Polytron blender (Kinematica) at 50 % power. The homogenate was filtered through 4 layers of muslin then again through 4 layers of muslin with a central layer of cotton wool. The filtrate was centrifuged (4000 × g; 20 s; 4 °C) and 2-3 drops of reaction buffer (0.45 M Sorbitol, 20 mM HEPES, 20 mM MES, 20 mM Sodium citrate, 10

mM EDTA, 10 mM $NaHCO_3$ 0.1 % (w/v) BSA, 5 mM $MgCl_2$; pH 8) was used to gently resuspend the chloroplasts. To verify chloroplast intactness, a dilute drop of chloroplast preparation was viewed under a light microscope. Chloroplast samples were used within one hour of preparation.

### 2.8.4 Protoplast preparation

Protoplast preparation followed the procedure of Pyke (2011). Tissue was cut from the leaf and torn laterally to expose the lower epidermis which was then removed with tweezers and discarded. The upper epidermis was cut into 1 $cm^2$ pieces and floated exposed side down, on pre-plasmolysis buffer (0.65 M sorbitol, 1 mM $CaCl_2$, 5 mM MES; pH 6) in a Petri dish for 15 min. Then the buffer was replaced with digestion medium (1 % (w/v) cellulose Onozuka R-10, 0.4 % (w/v) macroenzyme R-10, 0.2 % (w/v) BSA, 5 mM sodium ascorbate, 0.65 M sorbitol, 1 mM $CaCl_2$, 0.25 mM EDTA, 5 mM MES, pH 5.5) and placed on an plate shaker (30 shakes $min^{-1}$) at 25 °C for 40 min. This medium was then carefully replaced with washing solution (0.65 M sorbitol, 1 mM $CaCl_2$, 0.25 mM EDTA, 5 mM MES; pH 6). The Petri dish was tapped and swirled to release the protoplasts from the tissues. All further steps were performed at 4 °C. The protoplast suspension was filtered through a 60 $\mu$m nylon filter and the filtrate was centrifuged at 100 × g for 3 min. The pellet was resuspended in suspension medium (0.65 M sorbitol, 1 mM $CaCl_2$, 0.5 mM $MgCl_2$, 10 mM HEPES; pH 7).

### 2.8.5 Mesophyll cell preparation

Leaf discs were cut from fully expanded, mature leaves using a cork borer (diameter 5 mm, Usbeck) and transferred to individual eppendorfs with glutaraldehyde solution (3.5 % (v/v) in $H_2O$) for 1 h in the dark for fixation. Next, they were washed once in $H_2O$, then EDTA solution (0.1 M EDTA disodium salt dehydrate pH 9) was added to each eppendorf before transferring to a heat block (60 °C) for 3 h in the dark. Samples were then left to cool to room temperature before being stored at 4 °C overnight. They were used within 3 days.

### 2.8.6 Separation and analysis of membrane proteins by FPLC (gel filtration)

Membrane proteins were separated on the basis of their size after detergent based digestion of unstacked thylakoids (see §2.8.1 for thylakoid preparation) following the method developed by van Roon et al. (2000) with some modifications. An ÄKTA Purifier Fast Protein Liquid Chromatography (FPLC) system (GE Healthcare)

fitted with a Superdex 200 HR 10/30 column (GE Healthcare) was used for the purpose.

**Sample preparation** Unstacked thylakoid preparation (about 300 $\mu$L) was suspended to a final Chl concentration of 1 mg mL$^{-1}$. $\alpha$-DM was added to a final concentration of 1 % (w/v) Samples were vortexed (1 min) and incubated on ice (1-5 min), vortexed again (1 min) then centrifuged (1 min; 16 800 $\times$ g) for removal of unsolubilized material. The supernatant was passed through a 0.45 $\mu$m nylon filter and loaded onto the column using the appropriate loop.

**FPLC** After loading, the sample was subjected to gel filtration chromatography using a filtered running buffer (20 mM Bis Tris, 0.03 % (w/v) $\alpha$-DM; pH 6.5) at a flow rate of 1 mL min$^{-1}$. The elution profile, generated by the incorporated software (Unicorn), was transferred to scientific graphing software (SigmaPlot) for comparative analysis. Fractions (0.5 mL) were collected when needed for further use.

### 2.8.7 Isolation of light harvesting complexes by IEF

Isoelectric focusing (IEF) separates protein complexes based on their iso-electric point (pI). We used non-denaturing IEF to separate LHCII components from thylakoid preparations following the method of Bassi et al. (1991) with modifications by Ruban et al. (1994) and a few further modifications made here.

**Gel preparation** Eight 10.7 cm long IEF electrode strips (GE Healthcare) were prepared. Six strips were wetted through with electrode strip solution (2 % (v/v) Ampholine carrier ampholites, pH 2.5-5; GE Healthcare) and placed in two stacks of 3, one at each short end of a 24.4 $\times$ 10.8 cm gel tray (GE Healthcare) ensuring a precise fit. The tray was then placed on weighing scales and levelled. Next, a gel slurry (100 mL) containing 2.5 % (v/v) Ampholine, 1 % (w/v) glycine, 0.06 % (w/v) $\beta$-DM and 4.6 % (w/v) Sephadex G-75 Superfine was prepared on a stirrer with constant mixing for smoothness at a slow-medium speed to avoid bubbles. The slurry was carefully poured into the tray to form a homogeneous layer and left until 37 g had evaporated. To accelerate evaporation to about 3 h, a clamp-mounted fan was set about 60 cm above the gel.

The gel tray was transferred to the cooling plate (9 °C) of a Multiphor II Electrophoresis system (GE Healthcare), to maintain a low temperature. Good thermal contact was achieved by applying a thin layer of Triton solution (0.1 % (v/v) Triton X-100) to the plate beforehand and eliminating any bubbles between

the plate and the tray. The two remaining IEF strips were saturated, one in anode solution (5.3 % (v/v) $H_3PO_4$) and one in cathode solution (1 M NaOH) and carefully applied on top of the strips already in place at the anode and the cathode positions respectively. The electrode holder was positioned with good, even contact between the electrode wires and the IEF strips. A constant power (8 W) was applied for 2 h to mobilise the ampholytes into a pH gradient along the gel.

**Sample preparation** Unstacked thylakoids (2 mL) with a total Chl concentration of 2.5 mg $mL^{-1}$ were defrosted on ice and then incubated with 1 mL of 5 % (w/v) $\beta$-DM in water (final $\beta$-DM concentration 1.67 %, w/v) for 60 min during which time they were kept on ice and vortexed for 1 min every 10 min to allow complete protein solubilisation. To apply the sample to the prefocused gel, an applicator was used to isolate a 9.4 $\times$ 2 cm area of gel at a distance of 2 cm from the cathode. The gel was scraped out, added to the sample and vortexed to mix fully, it was then poured back into the gel applicator space and allowed to settle for 3 min before the applicator was removed.

**2-lane gel** To compare the IEF profile of two samples, the volume of each was reduced to 0.8 mL and digested in 0.4 mL of 5 % (w/v) $\beta$-DM (final $\beta$-DM concentration 1.67 %, w/v). Two equal areas of gel were scraped from the applicator space leaving a central 2 cm wide strip of gel to separate the samples. Samples were applied to the gel as above.

**Iso-electric focusing and sample elution** A constant power (8 W; 9 °C) was then applied to the gel tray for 17 h to draw the proteins to their iso-electric points. Upon completion, the gel was photographed and a micro pH meter (Mettler Toledo InLab) was used to determine the pH of the gel at 0.5 mm intervals along the central length of the sample lane.

For LHC collection, the gel was scraped away around the green banded region in 5 mm wide strips using a spatula, transferred to PEGG elution columns (GE Healthcare) and run through with elution buffer (25 mM HEPES, 0.01 % (w/v) $\beta$-DM; pH 7.6) according to the column instructions. The elute was then filtered through a PD-10 desalting column (GE Healthcare) according to instructions, in order to remove the ampholytes. The desalted elute was collected and concentrated when necessary. LHCs were either used directly (fresh) in SDS-PAGE or they were frozen in $LN_2$ and stored at -80 °C.

**LHC migration analysis within IEF gels** Densitometric analysis of in-gel LHC banding patterns after IEF, was performed from photographs of the gels using ImageJ. In the software, 'set scale' was used for size calibration of each individual photograph. Rectangular areas were defined along the gel lane in areas where deviation of the band from the perpendicular was minimal. Plot profiles were acquired and exported. The density plot was zeroed at the lowest y-axis coordinate (distance from cathode) and then normalised at the largest peak.

### 2.8.8 Separation of polypeptides by SDS-PAGE

Sodium dodecyl sulfate polyacrylamide gel electrophoresis (SDS-PAGE) was used to separate protein polypeptides. Negatively charged SDS detergent binds to amino acids (aa) at regular intervals, this denatures the protein and imparts a charge that is proportional to the polypeptide length so driving separation based on electrophoretic mobility as a function of mass.

**Gel preparation** Gels were made of two layers; at the top, a low percentage acrylamide gel (stacking gel) was used to align the polypeptides into a band for collective migration into the lower layer gel (running gel, 15 %, w/v Acrylamide mix) where they were selectively separated. The ingredients for each gel are listed in Table 2.7. Gels were hand-cast using a BioRad (Mini-PROTEAN II system) casting apparatus with 0.75 mm spacers, which was assembled according to the instructions and sealed around the bottom with melted agar (1 %, v/v) to avoid leaks. The gels were prepared in falcon tubes by adding the ingredients in the order stated in the ingredients list up to TEMED (the main polymerisation catalyst), which was only added to the mix directly before casting. Running gel was applied by pipette up to 2 cm from the plate tops. A layer of $H_2O$ was added to cover the running gel and reduce oxygen interference with the polymerisation process. When set (30 -60 min), the water was poured off and blotting paper was used to thoroughly dry between the plates while avoiding touching the running gel. A comb (10-12 teeth) was inserted half-way into the plates and stacking gel was applied, the comb was fully inserted avoiding air bubbles. Gels were left to set for at least 1 h or wrapped in damp paper towel and stored at 4 °C and used within two days.

**Protein preparation** To solubilise the proteins, 10 $\mu$L of sample was added to 10 $\mu$L of Laemmli buffer (50 mM Tris pH 6.8 titrated with HCl, 100 mM dithiothreitol, 2 % (w/v) SDS, 0.1 % (w/v) bromophenol blue dye, 10 % (w/v) glycerol) (Laemmli, 1970) and flicked to mix, put in a heat block (10 min; 90 °C)

**Table 2.7:** The solutions required to make 15 % ((w/v) Acrylamide mix) SDS-polyacrylamide gels. The quantities are for two BioRad mini-gels.

| | **stacking gel** (4 mL) | **running gel** (12 mL) |
|---|---|---|
| sterile $H_2O$ | 2.2 mL | 2.8 mL |
| Acrylamide mix* | 0.67 mL | 6.0 mL |
| 1 M Tris pH 6.8 | 1.0 mL | - |
| 1.5 M Tris pH 8.8 | - | 3.0 mL |
| 10 % (w/v) SDS | 0.04 mL | 0.12 mL |
| 10 % (w/v) APS | 0.04 mL | 0.12 mL |
| TEMED | 0.004 mL | 0.005 mL |

*30 % (w/v) acrylamide/bis-acrylamide, 29:1, SigmaAldrich

then centrifuged (16 800 × g; 5 min).

**Sample loading** Combs were removed and the wells were washed gently with running tap water to remove traces of unpolymerised acrylamide before being fitted into the BioRad electrophoresis tank according to instructions. Fresh running buffer (5 mM Tris-base, 50 mM glycine (electrophoresis grade), 0.02 % (w/v) SDS) was poured into the tank to fully submerge the gel plates. The samples (15-18 $\mu$L) and a Prestained Broad Range marker (New England Biolabs) were loaded.

Samples to be used in Western blotting (§2.8.9), were loaded twice within the same gel. Following SDS-PAGE, one well was subjected to Western blotting and the other was stained (see below) to be used as a reference.

**Electrophoresis** Gels were first run at 150 V for 15 min for full sample alignment in the stacking gel, after which power was increased to 180 V for about 1 h or until the dye had begun to run from the bottom of the gel.

**Staining** At the end of the run, gels were removed from the plates and either used for Western blotting (§2.8.9) or stained with Coomassie brilliant blue dye (45 % (v/v) methanol, 45 % (v/v) $H_2O$, 10 % (v/v) acetic acid, 0.25 % (w/v) Coomassie Brilliant Blue R250) for 1 h on a plate shaker or for 20 min at 50 °C. The gels were then washed in destaining solution (10 % (v/v) ethanol, 10 % (v/v) acetic acid, in ultrapure $H_2O$) for 1 h and then again in fresh destaining solution

overnight, they were finally stored in $H_2O$ at 4 °C. Gels were scanned (Epson) for digital records and analysis.

### 2.8.9 Protein detection by immunoblotting (Western blot)

**Protein transfer** Immediately after SDS-PAGE (§2.8.8) the gel and blotting equipment (BioRad) (sponges, transfer cassette, blotting paper ×3 (cut to size), nitrocellulose membrane (Amerhsam, cut to the same size as the gel) were soaked in transfer buffer (150 mM glycine, 20 mM Tris base). A sandwich was constructed in the buffer as follows: black cassette wing; sponge; blotting paper ×2; gel; membrane; blotting paper ×1; sponge; clear cassette wing. The sandwich was tightly squeezed to remove air bubbles and fitted in the electrode holder in the transfer tank with an ice block to avoid over-heating, submerged in transfer buffer and run at 400 mA for 60 min with constant mixing.

**Staining to verify protein transfer** After the run, the membrane was carefully removed from the sandwich and soaked in Ponceau stain (0.1 % (w/v) Ponceau S, 0.5 % (v/v) acetic acid in $H_2O$) for about 5 min. Then it was gently washed under running tap water with care taken not to wash away the bands. The bottom left corner was cut for orientation and the limits of each lane and the protein bands of the marker were marked using a pencil and the membrane was photographed. If testing against multiple antibodies, the membrane was cut into corresponding sections and corners were cut and lanes were marked on all pieces. The remainder of the Ponceau stain was then washed away. At this point the membrane could be dried and stored (RT; 1 year) for immunoblotting.

**Immunoblotting** PBS buffer (×10; 750 mM NaCl, 30 mM KCl, 545 mM $Na_2HPO_4$, 15 mM $KH_2PO_4$) was used to make Solution A (10 % (v/v) ×10 PBS buffer, 1 % (w/v) Tween 20, 5 % (w/v) skimmed milk powder). The membrane was washed in Solution A for 1 h on a shaker to prevent non-specific binding, then incubated in primary antibody (diluted in Solution A according to Agrisera's instructions) at 4 °C overnight (no agitation). The next day the primary antibody was collected and stored at -20 °C for further use (usable 2 - 3 times). The membrane was washed in Solution A, 4 × 10 min with agitation. The membrane and secondary antibody (ECL plus, 1:30,000 Solution A) were incubated together under foil for 1 h on a shaker. The membrane was then washed in Solution B (1 % (w/v) Tween 20, 10 % (v/v) × 10 PBS buffer, in ultrapure $H_2O$) 2 × 10 min on a shaker.

**Protein detection** At the end of the final wash, peroxide and luminol reagents (ECL plus) were mixed (40:1 ; 8 mL : 0.2 mL) in a small tupperware box. The final Solution B wash was discarded leaving enough buffer to keep the membrane moist. In the dark, the membrane was incubated in the reagent mix for 5 min, carefully drained off and arranged in the developing cassette under a plastic sheet. The photographic paper (Kodak) was cut to size with cut corners to correspond to the membrane the film pieces were then exposed to the membrane in the closed cassette for 1-3 min then incubated in developing solution (Kodak, 1 min), washed in water and incubated in fixer solution (Kodak). Once dry, films were scanned for digital analysis.

### 2.8.10 Pigment isolation and separation by HPLC

Pigments were separated according to hydrophobicity following the method of Farber et al. (1997) with some modifications (see below). A Dionex HPLC machine was used with integrated UCI-100 Universal Chromatography Interface, P680 Pump, ASI-100 Automated Sample Injector and a PDA-100 photodiode array detector (Dionex) in combination with a Merck Lichrospher 100 RP-18 column with a 5 $\mu$m particle size. All solvents were HPLC grade.

**Sample preparation** Leaf tissue (1 $cm^2$) was collected either 1) directly from plants in their normal growth light environment or 2) from leaves that had been dark adapted for 1 h under foil or 3) from leaf tissue that had been treated with AL at 600 $\mu$mol photons $m^{-2}$ $s^{-1}$from the Dual-PAM for 30 min, as in the NPQ protocol (see §2.9.3). The leaf tissue was ground completely in an eppendorf tube in 1 mL of ice-cold 100 % acetone using an electric pestle and mortar, vortexed and centrifuged (5 min; 16 800 × g). Filtered supernatants (0.2 $\mu$m nylon filter) were kept at RT and subjected to HPLC within 48 h of preparation. For processing, the sample was loaded into inserts within amber glass vials fitted with a PTFE septa in the lid.

**Liquid chromatography** A combination of two solvents was used to separate pigments: Solvent A composed of acetonitrile, methanol and 0.1 M Tris/NaOH pH 8, mixed in a ratio of (87:10:3) and Solvent B of methanol and hexane (80:20 mix). They were run with the following elution profile:

| | |
|---|---|
| 0 - 9 min | 100 % A |
| 9.1 - 12.5 min | 0 - 100 % B |
| 12.6 - 18 min | 100 % B |
| 18.1 - 19 min | 0 - 100 % A |

19.1 - 23 min  100 % A

By the $18^{th}$ min all pigments had eluted thus the final flush with Solvent A served to wash the column before running the next sample. The injection volume was 20 $\mu$L sample$^{-1}$ and the flow rate was 1 mL min$^{-1}$.

**Pigment analysis** Light absorption was detected from 280 - 750 nm by the PDA-100 detector. Each pigment species was identified by the retention time and absorption spectrum. Calculation of the pigment concentration from the peak areas was obtained by comparing the integrated areas with those corresponding to pure pigment standards of Chls and carotenoids of known concentration (Serva).

## 2.9 Function probing techniques

### 2.9.1 The Chlorophyll *a* fluorescence signal and the principle of pulse amplitude modulated fluorescence

Photosynthesis is a photobiological process and as such light absorption and fluorescence emission are inherent properties. Fluorescence emission by Chl pigments carries useful information about the structure and functions of the photosynthetic antennae and reaction centers (Ruban, 2012). Moreover, it is the only Chl deexcitation pathway which can be measured directly and although its yield is less than 3 % of the absorbed energy (Krause and Weis, 1991), the output is highly sensitive to internal changes in the photosynthetic apparatus.

The fluorometric investigation of photosynthetic function, first realised by Kautsky and Hirsch in 1931 (Govindjee, 1995), is now widespread. At physiological temperature, fluorescence emission between 680 - 740 nm from plants, algae and cyanobacteria is considered to be primarily from Chl *a* at PSII (Strasser et al., 2004). The reason that this fluorescence emission carries information about photosynthesis related function, is because its yield directly relates to the capacity of the photochemical and (other) non-photochemical deexcitation pathways (see Fig 1.12) at the time of measurement.

The summed yields of photochemistry, fluorescence and non-radiative decay (heat-loss) pathways, amount to unity, that is, together, in terms of energy content, they equal the energy of the light that was absorbed by the photosynthetic sample. Fluorescence yield ($\Phi_f$) therefore (not fluorescence intensity), carries information about photosynthetic function, and it is this that is measured during PAM fluorometry (Schreiber et al., 2012). In absolute terms, the quantum yield of fluorescence

is defined as:

$$\Phi_{f(absolute)} = \frac{total\ no\ of\ photons\ emitted}{total\ no\ of\ photons\ absorbed} \tag{2.4}$$

However, light absorption is not measured in absolute terms and is not measured at all in fluorometry. Instead, a relative measure can be taken provided that the incident light (or the measuring light (ML) in PAM fluorometry, see §2.9.1) is of constant intensity, and that we make the assumption that the Chl absorption cross-section does not change. Under these conditions, it can be assumed that the total yield of all deexcitation pathways is both constant and equal to the energy absorbed. Thus, $\Phi_f$ can be expressed in terms of the deexcitation pathway's rate constants (no. of transitions or events per second; k):

$$\Phi_f = \frac{k_f}{k_p+k_f+k_o} \tag{2.5}$$

where the subscripts denote the rate constants for the deexcitation pathways of fluorescence (f), photochemistry (p) and all others (o, comprised mainly of pathways of heat loss). In a time-resolved fluorescence measurement, the task is to differentiate which pathway is responsible for any observed quenching of the fluorescence yield; photochemical quenching (qP) or non-photochemical quenching of fluorescence (NPQ).

### Dark adaptation: maximal, minimal and variable fluorescence

For most fluorescence measurements, it is necessary to begin with a dark adapted sample. Dark adaptation (usually for about 1 h), ensures that the ETC is fully oxidised (RCs are 'open'); the trans-thylakoid pH gradient ($\Delta$ pH) is depleted; photoprotective mechanisms are relaxed (Ralph and Gademann, 2005) and mobile LHCII is functionally attached to PSII (State I). In this state a measure of 'minimal fluorescence' ($F_o$) can be taken as $k_p$ is maximal (approaching a value close to 1) and $k_o$ is minimal (Govindjee, 2004). The $F_o$ measurement is followed by a measurement of maximum florescence ($F_m$) whereby a SP of actinic light is issued to close all RCs, so that $k_p$ approaches zero whilst the SP is short enough (0.8 s) to ensure that heat loss pathways ($k_o$) are not activated and remain minimal, thus revealing maximal fluorescence yield ($F_m$). From these two measurements we may obtain a calculation of the variable fluorescence ($F_v$):

$$F_v = (F_m - F_o) \tag{2.6}$$

In healthy plants, the $F_m$:$F_o$ ratio is remarkably constant at ≈5. Using the $F_v$ value, a measure of PSII maximum operating efficiency can be made using the equation described by Genty et al. (1989):

$$(\Phi_{PSII})_{max} = F_v/F_m = (F_m - F_o)/F_m \quad (2.7)$$

where $(\Phi_{PSII})_{max}$ is the maximum PSII efficiency or quantum yield meaning that it is a proportional measure of the total light absorbed by PSII-associated Chl used in photochemistry (Maxwell and Johnson, 2000).

### Pulse amplitude modulated (PAM) chlorophyll fluorometry

In PAM Chl fluorometry, a low intensity light (1-10 $\mu$mol photons $m^{-2}$ $s^{-1}$) called the measuring light (ML), is applied in pulses of $\mu$s duration and rapid frequency to photosynthetic material in order to stimulate a pulsed fluorescence signal. Crucially, the ML intensity must be low enough so as not to allow the accumulation of reduced PSII (Schreiber et al., 2012), i.e. so that the application of the ML itself does not cause an increase in its own fluorescence signal.

The intensity of the pulsed fluorescence signal is the only measurement taken during PAM fluorometry. The signal is exclusively detected, even against a busy light environment which usually includes much stronger lights and other fluorescence emission. The highly sensitive and selective detection is achieved using a photo-diode detector that is fitted with a long-pass filter to protect from light with wavelength ($\lambda$) < 700 nm, and an AC-coupled pulse-amplifier set to correspond with the frequency of the ML, to protect from all remaining light that is not pulsed at the same frequency (Schreiber, 2004).

The intensity of the measured fluorescence signal changes only because changes occur in other energy dissipation pathways within the photosynthetic apparatus, namely the closing/opening of RCs in the photochemical pathway and the stimulation/relaxation of heat dissipation pathways, the main component of non-photochemical quenching. Changes in photochemical and non-photochemical de-excitation pathways are brought about by the application of various lights to the sample, in a usual set-up this includes actinic light (AL), far red light (FR) and a saturating light applied as a pulse (SP for saturating pulse). A simple PAM application is depicted schematically in Fig. 2.1. The Fig presents two basic measurements, $F_o$ and $F_m$ taken successively from one sample which is represented as a green surface containing doors to signify the PSII RCs.

In the first panel a dark adapted sample is treated with ML only (blue dashed line). The fluorescence yield (red dashed line) is minimal as nearly all of the energy is used photochemically (black dashed line) because the intensity and the

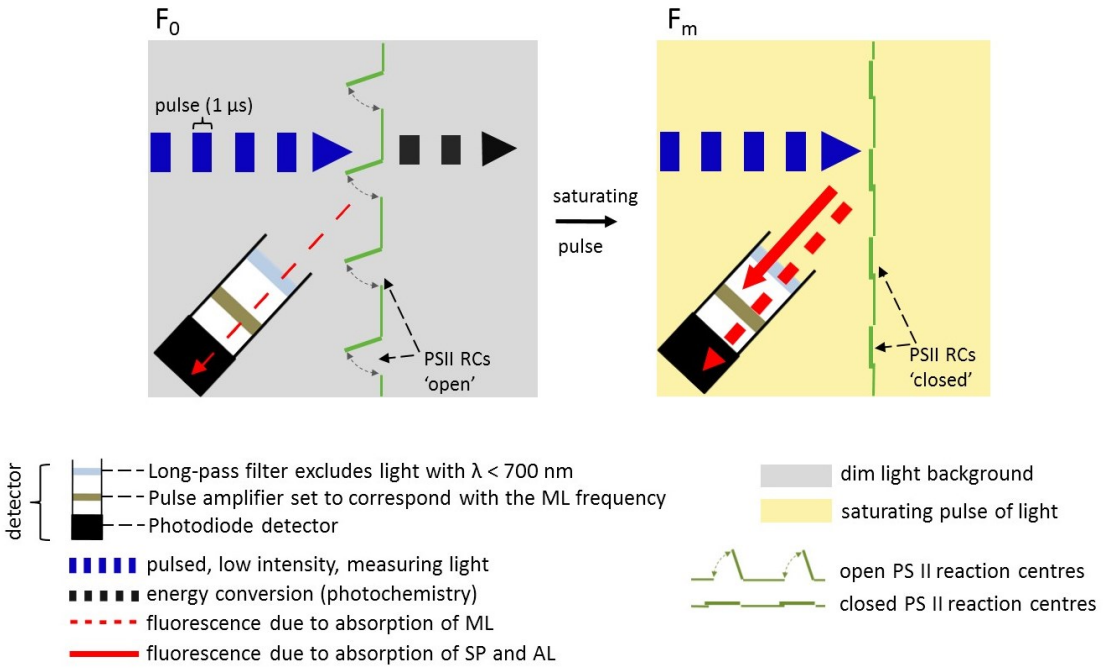


**Figure 2.1:** A scheme to illustrate the principle of PAM fluorometry and $F_o$ and $F_m$ determination. The figure is explained in the main text (§2.9.1)

frequency of the ML is low enough that a reduced (closed, see Eq. 1.2) RC is oxidised (opened) in time to accept the next energy transfer, meaning that reduced RCs do not accumulate and a measure of $F_o$ can be taken. Next, in panel 2, a SP is applied which transiently closes all RCs so that the fluorescence signal yield becomes maximal ($F_m$). The light of the SP (yellow background) and the fluorescence that is emitted as a result of excitation by the SP (continuous red arrow) are not measured due to exclusion by the detection system.

It should be mentioned that due to the scattered directions of fluorescence emission, it is unavoidable that fluorescence detection is of a relative yield to total fluorescence yield with an implicit assumption that the Chl fluorescence is scattered homogeneously and so the quantity recorded by the detector is proportionally constant to the total (absolute) Chl fluorescence emission (Govindjee, 2004). A second important consideration is that the fluorescence signal at room temperature is generally regarded to be derived mostly from Chl at PSII with a small, fraction of fluorescence originating from PSI (Govindjee, 2004; Pfündel et al., 2013). Until recently, the PSI contribution to the room temperature fluorescence signal has been regarded as non-variable and as such, possible to estimate and then system-

atically subtract the PSI fluorescence contribution in the Dual-PAM 100 software (Pfündel et al., 2013). However, recent work by Giovagnetti et al. (2015) brings this assumption into question.

**Dual-PAM 100 and experimental set-up** The principle florometer used in this study to monitor photosynthetic function was the Dual PAM 100 photosynthesis analyser (Walz, Germany). The instrument has a dual capacity for measuring, in parallel, activity at PSII by Chl *a* fluorescence measurement and activity at PSI through pulse amplitude modulation (PAM) of transmitted light at 830 nm and 875 nm. The PSI signal depends on small absorbance differences between P700 and P700* calculated in the software as $\Delta(I_{875}$ - $I_{830})$. When P700 is completely reduced (P700 open), the signal is minimal, when it is oxidised (P700 closed) or when the primary acceptor (A) is reduced (P700 closed), the signal increases (Klughammer and Schreiber, 2008). Inbuilt light emitting diode (LED) arrays comprised the following light sources for measurement and photosynthetic induction:

- pulse-modulated fluorescence measuring light (**F ML**, 460 nm) for excitation of Chl fluorescence
- actinic light (**AL**, 635 nm) to induce photosynthetic function
- a saturating pulse light (**SP**, 635 nm) to close all the reaction centres
- far red light (**FR**, 730 nm) to selectively drive PSI
- pulse modulated P700 ML of dual-wavelength, (**P ML**, 830 nm and 875 nm) for the measurement of P700 activity.

Detection of the modulated Chl fluorescence signal and the transmitted, modulated light at 830 nm and 875 nm was by a single photodiode system.

Dual-PAM measurements were conducted in dim light to avoid the confounding effects of unselected, background light on the photosynthetic system. For dark adaptation, samples were kept in darkness or dim light for 1 h prior to fluorescence measurement. Measurements were only performed on plants with $F_v/F_m \geq 0.8$.

### 2.9.2 Rapid light curves

A rapid light curve (RLC) plots a photosynthetic parameter (e.g. ETR or the effective photosynthetic yield of PSII, $\Phi_{PSII}$) against increasing irradiance (Ralph and Gademann, 2005) over a short time period of about 2-5 min (see Chapter 3, §4.5.1 for further discussion). As an exception to other fluorescent measurements,

RLCs were measured from light adapted plants that were subjected to only 20 s of darkness before measurement. Darkness was necessary to allow oxidation of the primary electron acceptor ($Q_A$), but was kept brief in order to i) avoid relaxation of the NPQ mechanisms so that the $\Phi_{PSII}$ measurement was indicative of a response in the field, and ii) to avoid the induction kinetics (Kautsky effect) associated with a fully oxidised ETC (Ralph and Gademann, 2005). The inbuilt 'light curve' routine of the Dual PAM 100, was used with default settings and 'fluo + P700' mode. The programme issued ten × 30 s steps of increasing light intensity (30, 37, 46, 77, 119, 150, 240, 363, 555 and 849 $\mu$mol photons $m^{-2}$ $s^{-1}$). Each step was begun with a saturating pulse (SP). A curve was fitted for $\Phi_{PSII}$ against PAR using 'EP fittings' (Eilers and Peeters, 1988) in the Dual PAM software.

### 2.9.3 Inducing chlorophyll fluorescence for NPQ measurement

Chl fluorescence was measured in attached, dark adapted leaves using a Dual PAM 100 fluorimeter. A custom made 'trig run' light routine was used, which ran as follows: to start, the ML (9 $\mu$mol photons $m^{-2}$ $s^{-1}$) was applied, at 30 s a SP (2000 $\mu$mol photons $m^{-2}$ $s^{-1}$) was made using the 'FoFm' key to determine minimal fluorescence ($F_o$) and maximum fluorescence ($F_m$). AL (700 $\mu$mol photons $m^{-2}$ $s^{-1}$) and FR (setting 7, Walz) were turned on at 2 min to induce NPQ and then turned off after 7 min of application to allow the NPQ mechanisms to relax in the dark for 5 min. The cycle was then repeated (AL + FR for 7 min; dark for 5 min). During the entire run, SPs (0.8 s; 2000 $\mu$mol photons $m^{-2}$ $s^{-1}$) were applied every one minute to determine maximum fluorescence ($F'_m$). NPQ was calculated by Dual-PAM software and defined as:

$$NPQ = (Fm - Fm')/Fm' \tag{2.8}$$

### 2.9.4 State transitions measurements at room temperature

State transitions were measured in dark adapted leaves at room temperature using a Dual-PAM 100 (Heinz Walz). Superimposition of FR light over a weak AL in 15 min intervals was used to induce LHC migration between PSI and PSII. The full light program is represented schematically in Fig. 2.2 and described here: first, the ML (9 $\mu$mol photons $m^{-2}$ $s^{-1}$) was applied, then at 30 s, a SP (2000 $\mu$mol photons $m^{-2}$ $s^{-1}$) was given using the FoFm key for determination of $F_o$ and $F_m$. At 2 min, low intensity AL (6 $\mu$mol photons $m^{-2}$ $s^{-1}$) and FR (setting

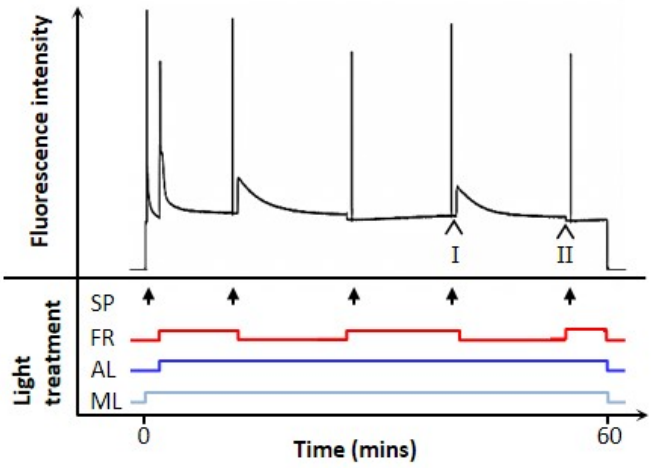


**Figure 2.2:** Measuring state transitions at room temperature. A typical light regime (bottom) and corresponding fluorescence trace (top) are shown. The light regime indicates when the light sources (measuring light (ML), actinic light (AL) and far red light (FR)) are on or off when the associated line is raised or lowered respectively. Closed arrow heads indicate when a saturating pulse (SP) is applied. Two open headed arrows (top panel) mark the moments at which the leaf is removed and the tissue excised for 77 K fluorescence measurements in STI and STII (see §2.9.5).

7; Walz) were activated. After 15 min, FR light was turned off to induce LHC migration to PSI (State II), 15 min later, FR was turned back on to induce a return to State I. The cycle was repeated a second time. SPs (open headed arrows, Fig. 2.2, bottom) were given 30 s after the start and before the end of the FR light application to reveal maximal fluorescence ($F'_m$). From the acquired traces, three parameters were calculated from several fluorescence transients in order to quantitatively compare the capacity for state transitions in each plant (Ruban and Johnson, 2009). Their equations are given in §5.2 and described schematically in Fig. 5.1.

### 2.9.5 State transitions measurements by 77K fluorescence emission spectroscopy

State transitions were induced at RT using the method described in §2.9.4 with the exception that a paper stencil was attached to the leaf prior to light application, to exactly demarcate the area of treatment. When the desired point pertaining to STI or STII (marked as 'I' or 'II' in Fig. 2.2) was reached, the leaf was removed and a leaf disc was cut out from the centre of the treatment area with a cork borer (5 mm diameter, Usbeck, see below for determining cork borer size) and frozen

in $LN_2$. The leaf disc was ground to homogenate with 1 mL of ice-cold buffer containing 10 mM HEPES at pH 7.6 (for STII the buffer also contained 10 mM of MgCl and 10 mM NaF to maintain the phosphorylation of LHCII). The sample was injected into a precooled custom-made sample holder and frozen in $LN_2$.

Low temperature (77 K) fluorescence emission spectra (600-800 nm) were recorded using a Jobin Yvon FluoroMax-3 spectrophotometer equipped with a $LN_2$ cooled cryostat. Excitation was defined at 435 nm with a 5 nm spectral bandwidth. The fluorescence spectral resolution was 1 nm. Spectra were normalized at 685 nm (PSII maximum) in order to observe relative changes in fluorescence from PSI (735 nm).

**Establishing the best size leaf sample for 77 K fluorescence measurement** Absorption at 77 K is most accurately measured at low Chl concentrations to avoid the effects of scattering and reabsorption. Furthermore, in order to be able to accurately compare low temperature excitation spectra, Chl concentration should be consistent as excitation spectra can have different shapes at different pigment concentrations (Ruban, 2012). To establish a suitable sample size, cork borers of various sizes (Usbeck) were used to cut leaf discs which were ground in 10 mM HEPES at pH 7.8 and absorption was measured at 680 nm, the results are shown in Table 2.9. Based on these calculations, cork borer no. 1 (5 mm diameter) was chosen for leaf sampling.

**Table 2.9:** Absorption (680 nm) in leaf homogenates of various concentrations at room temperature.

| **Cork borer no. (Usbeck)** | 1 | 2 | 3 |
|---|---|---|---|
| **Area cut ($mm^2$)** | 13.85 | 23.33 | 35.26 |
| **Absorption ($\sim$ 680 nm)** | 0.221 | 0.347 | 0.4917 |
| **SD** | $\pm$ 0.011 | $\pm$ 0.023 | $\pm$ 0.0045 |

### 2.9.6 Fluorescence quenching in isolated LHCII at various pH

The experimental set up was the same as the one given in Petrou et al. (2013) and is described again here. The procedure was performed in dim background light using LHCIIs isolated by IEF and diluted to $OD_{676} \sim 1$ in 1 cm in elution buffer (see §2.8.7). A quartz cuvette (2 mL) was set-up with a Dual-PAM liquid cell adapter and a micro-stirrer, the Dual PAM 100 was set in 'fluo' mode. RT

buffer (1940 $\mu$L; 10 mM HEPES, 10 mM Sodium Citrate, 0.004 % (w/v) $\beta$-DM (see below for determination of $\beta$-DM concentration); pH 7.8) was added to the cuvette. Next, the ML (4 $\mu$mol photons $m^{-2}$ $s^{-1}$) was turned on, then the measurement was started. After 4 s, 60 $\mu$L of LHCII sample was added with a single, smooth dispensing action.

At the 10th second, a small amount of HCl (1 M) was injected into the cuvette. The quantities of HCl are given in Table 2.10. They were determined to give a desired final pH. Fluorescence was measured for a further 5 min, until steady state had been reached. At the end of each run, samples were retained for verification of pH. Measurements for each pH were taken from the same LHCII preparation. Throughout the procedure, LHCIIs were kept on ice and buffers were kept at RT.

**Table 2.10:** Quantity of HCl added to LHCII preparations for a given pH during quenching analysis (see §2.9.6).

| **final pH** | **HCl ($\mu$L)** | ***continued...*** | |
|---|---|---|---|
| 7.8 | 0 | 5.6 | 24 |
| 7.0 | 7 | 5.1 | 31 |
| 6.5 | 13 | 4.5 | 40 |
| 6.0 | 16.5 | 4.0 | 46.5 |

To determine the concentration of $\beta$-DM that achieved LHCII solubilisation that both inhibited spontaneous aggregation of LHCII but allowed sufficient proton-sensing and consequent LHCII interaction (Petrou et al., 2013), the procedure was first conducted with *N. tabacum* LHCIIs in buffers with various concentrations of $\beta$-DM (0.001 %, 0.003 %, 0.004 %, 0.0045 % 0.005 % and 0.008 %). See §5.8 for the results.

## 2.10 Proteomic investigation of LHCII

### 2.10.1 Mass Spectrometry

**Sample preparation** Light harvesting complexes of *N.tabacum* and *Nt*(*Hn*) plants were isolated by IEF (see §2.8.7). LHC polypeptides were then separated by SDS-PAGE and visualised by Coomassie stain (as described in §2.8.8). Bands were selected for proteomic investigation, excised using a new scalpel blade, individually stored in eppendorfs with 50 $\mu$L of ultrapure $H_2O$ (to reduce the risk of contamination with extraneous protein) and sent to Cambridge Centre for

Proteomics (CPP; Department of Biochemistry, University of Cambridge, UK; http://proteomics.bio.cam.ac.uk/) for proteomic analysis.

**LC-MS/MS** Samples were treated according to CCP's protocol, described briefly here: gel bands were destained, reduced with dithiothreitol and alkylated with iodoacetamide then digested with trypsin overnight. The supernatant was subjected to automated analysis by liquid chromatography (LC) coupled with tandem mass spectrometry (MS/MS) performed using a nanoAcquity UPLC system (Waters Corp, MA, USA) and an LTQ Orbitrap Velos hybrid ion trap mass spectrometer (Thermo Scientific, Waltham, MA).

MS/MS data were converted to .mgf files then matched against NCBI and UniProt databases using the Mascot search engine (Matrix Science, London, UK) with the following parameters:

- Digestion enzyme = Trypsin
- Maximum missed cleavages = 2
- Fixed modifications = Carbamidomethyl (C)
- Variable modifications = Oxidation (M)
- Peptide Mass Tolerance = 25 ppm
- Fragment Mass Tolerance = 0.8 Da

Peptide identifications were accepted if they could be established at greater than 95.0 % probability.

### 2.10.2 Theoretical calculation of LHC pI and MW upon N-terminal amino acid removal

*N.tabacum* LHC sequences were copied from the UniProt database into the online ExPASy Compute pI tool (Swiss Institute of Bioinformatics, http://web.expasy.org/compute_pi/). Transit peptides, identified in UniProt, were deleted. Molecular weight (MW) and the theoretical isoelectric point (pI) of the peptides were calculated using the ExPASy software as the N-terminal amino acid (aa) residues were manually deleted one by one sequentially. Changes in MW ($\Delta$ MW) and in pI ($\Delta$ pI) were calculated from the MW and theoretical pI of the full, mature, peptide sequence.

## 2.11 Microscopic cell and tissue analysis

### 2.11.1 Cell and chloroplast measurements

**Slide preparations** Protoplasts were prepared in suspension medium as described in §2.8.4, and mounted on a microscope slide. For mesophyll cell analysis, prepared leaf tissue (see §2.8.5) was crushed on a microscope slide under a coverslip until no large tissue fragments were visible. The suspension was transferred to a fresh slide in a drop of EDTA solution (§2.8.5). Lastly, intact leaf tissue was cut from fresh, mature leaves, using a 5 mm diameter cork borer and floated on sucrose solution (0.9 M) for 2 h to inhibit chloroplast movement. Small plasticine scrapes were made at each corner of a coverslip for height so as to avoid compressing the sample. The coverslip was pressed into place and sealed with VALAP (vaseline, lanolin, paraffin, melted together in a 1:1:1 ratio, w/w/w). Slides were viewed under the microscope within two days and kept at 4 °C in between observations.

**Microscopy** Preliminary protoplast and mesophyll cell analyses were performed using a Leica DM 2000 compound microscope (Leica Microsystems, Germany) with an eye-lens mounted hand-held camera (Sony, Cyber-shot, DSC-W530). Data collection was carried out using a Leica TCS SP5 laser-scanning confocal microscope with integrated Leica Application Suite (LAS) software. Chl was excited using the 488 nm line of a 100 mW argon laser. Chl fluorescence was detected between $670 - 720$ nm. A $10 \times$ objective was used for widefield imaging of the overall sample composition. Palisade mesophyll cells were identified by their typical rod-like shape and viewed under a $40 \times$ oil immersion objective. Z-stacks were performed with 2.8 $\mu$m steps, for single cells.

**Image analysis** Confocal images were analysed in LAS Lite (Leica). Using the inbuilt measurement tool, cells were measured at their longest length and central width, and chloroplasts were measured across their diameter. Total chloroplast counts within single cells were made during z-stack analysis.

### 2.11.2 Thin section for tissue analysis by light and electron microscopy

**Embedding** Tissue was taken from mature, green leaves (unless otherwise stated in the Results) using a cork borer (5 mm diameter, Usbeck). The leaf disc was submerged in fixative medium (glutaraldehyde 3 % (v/v), paraformaldehyde 1 % (w/v), tannic acid 0.5 % (w/v) in Na-phosphate solution 0.05 M; pH 7), cut into

pieces (0.5-1 $mm^2$) and incubated for 3 h on an orbital rotator. Samples were then 3 × washed with Na-phosphate buffer (0.1 M; pH 7) and left overnight in the same buffer on a rotator. The next day leaf tissue was stained by incubation with Osmium tetroxide solution (1 : 1 (v/v), $OsO_4$ : Na-phosphate solution 0.2 M; pH 7) for 2 h on a rotator. This was followed by washing in sterile $H_2O$ × 2 and then an acetone−dehydration series in which samples were washed 2 × 15 min at each of the following acetone concentrations (v/v): 30 %, 50 %, 70 %, 90 %, 100 %. Samples were transferred to araldite (araldite CY212 (40 % (w/v), dodecenyl succinic anhydride 60 % (w/v), methyl nadic anhydride (2 % (w/v), benzyl dimethylamine (1 % (w/v)) at a concentration of 50 % (v/v) in acetone on a rotator, after 1 h, this was replaced with 100 % araldite, then after another 1 h replaced again with fresh araldite (100 %) and left on a rotator overnight. The next day tissue pieces were positioned in embedding moulds with araldite (100 %) and baked at 60 °C for 2-3 days.

**Semi-thin sectioning** Araldite blocks were trimmed on a hand microtome (Reichert-Jung Ultracut E, Leica) to reveal a clear leaf cross-section. For histological analysis, semi-thin sections (2.8 $\mu$m) were cut by glass knife, mounted and dried using a heat block on a microscope slide then incubated in a drop toluidine blue (toluidine blue 1 % (w/v) dissolved in 1 % (w/v) borax solution) for 30 s. The stain was rinsed away with $H_2O$. Sections were examined using a Leica SP5 confocal microscope under optical transmission with 20 × and 40 × (immersion oil) objectives. Images were obtained using a camera (Sony, Cyber-shot, DSC-W530), mounted at the eye-lens. Sections were also viewed using a Leica DMRA2 upright bright field microscope coupled with a Retiga Exi Fast 1394 camera and Volocity software which was used for imaging and measuring leaf thickness using × 10 and × 20. For EM, trimmed blocks were used to cut ultra-thin sections (see below).

**Ultrathin sectioning** Ultra-thin sections (50-70 nm) were cut by glass and diamond knife. Sections were mounted on 400-mesh copper grids (Agar Scientific) and post stained with Aqueus Uranyl acetate (SPI-Chem) and Reynold's Lead Citrate stain (TAAB). All ultra thin sectioning was done by Dr Giulia Mastroianni.

### 2.11.3 Freeze fracture replication technique with chloroplasts

A suspension of intact chloroplasts (see §2.8.3) was pressed into a thin film between double replica copper plates (Bal-Tec, now Leica), rapidly frozen in slushy $LN_2$ (-175 °C) and loaded in a specimen carrier sandwich (Bal-Tec). The film

was fractured in a $LN_2$ cooled Polaron E6432 freeze fracture (FF) unit (Polaron Instruments). Using the same instrument, replicas were produced by shadowing with platinum and then carbon. The replicas were floated from the copper plates by water immersion then transferred to 30 % (v/v) bleach for cleaning (1 h). FF replicas were floated on water a second time to remove the bleach. Shadow replicas were mounted on copper grids (Hexagonal 300 thin bar, Agar Scientific) for examination by EM (see §2.11.4). FF was done in collaboration with Dr Petra Ungerer.

### 2.11.4 Transmission electron microscopy

FF replicas (§2.11.3) and thin sections (§2.11.2) were examined using a JEOL 1230 electron microscope (JEOL instruments, Tokyo, Japan). Transmission electron microscopy (TEM) was performed by Dr Giulia Mastroianni and Dr Petra Ungerer. TEM images were analysed in ImageJ.

# Results and Discussion

Chapter 3

# A general characterisation of the *Nt*(*Hn*) cybrid

## 3.1 Introduction

In this chapter we introduce the general aspect of the *Nt*(*Hn*) cybrid plant in terms of seed germination rates, plant growth and general phenotype including flower morphology. We discuss the findings in terms of the results reported by Dr Mikhajlo Zubko and co-workers, regarding the construction of *Nt*(*Hn*) (Zubko et al., 1996), the analysis of the plant's nuclear, plastid and mitochondrial sub-genomes (Zubko et al., 1996, 2001) and flower morphology (Zubko et al., 2003).

## 3.2 Germination and plant development

After sowing, seeds were kept at 4 °C for 3 days, to simulate the vernalisation period. They were then transferred to controlled environment, Sanyo growth cabinets (GC), under a light intensity of 60-80 $\mu$mol photons $m^{-2}$ $s^{-1}$. After 7-8 weeks (*N.tabacum* and *H. niger*) or 12-13 weeks (*Nt*(*Hn*)) the plants were transferred to LL (80-100 $\mu$mol photons $m^{-2}$ $s^{-1}$) or HL (300-400 $\mu$mol photons $m^{-2}$ $s^{-1}$) shelves for acclimation.

Seeds were sown in batches, usually 8-12 seeds per plant type, and the number that germinated and developed to cotyledon stage was recorded. At cotyledon stage, excess seedlings or those that showed obvious abnormalities were disposed of or kept for observation without experimental use. From the plants that were maintained for experimental work, we monitored the number that reached maturity. Table 3.1 presents the results. From the total number of *Nt*(*Hn*) seeds sown, only 34.3 % reached the cotyledon stage compared to *N.tabacum* at 82.7 % and *H. niger* with a somewhat lower yield at 58.7 %.

Between-batch plant growth was very unpredictable in *Nt(Hn)* cybrids, with differences in germination success ranging from 0 - 63.6 %. *H. niger* also had a fairly large range in germination rates from 12.5 - 75.0 %, while *N.tabacum* gave a higher and more consistent germination yield (62.5 - 100 %) (Table 3.1).

Of the seeds that did develop to cotyledon and were maintained for experimental use, the percentage that reached maturity was high in *N.tabacum* at 94 %, fairly high in *Nt(Hn)* at 70.4 % but low in *H. niger* at 58.6 % (Table 3.1). The number of days between sowing and reaching cotyledon stage for *N.tabacum* was 16.0 ± 3 days, *H. niger* 18.8 ± 4 days, while development of the *Nt(Hn)* cybrid was extremely delayed, with cotyledons appearing on average, after 37.7 ± 9.2 days, although, again the variation, indicated by the large SD, was notable.

**Table 3.1:** Seed viability and germination rates in *N.tabacum*, *Nt(Hn)* and *H. niger* plants. For each species, data were collected from 12 batches totalling approximately 130 seeds.

| | ***N.tabacum*** | ***Nt(Hn)*** | ***H. niger*** |
|---|---|---|---|
| **germination to cotyledon, %** | 82.7 | 34.3 | 58.7 |
| **min - max viability of batches, %** | 62.5 - 100 | 0 - 63.6 | 12.5 - 75.0 |
| **cotyledons to reach maturity, %** | 94.0 | 70.4 | 58.6 |
| **no. of days until cotyledon*** | 16.0 ± 3.0 | 37.7 ± 9.2 | 18.8 ± 4.8 |

*data are mean average of batch averages ± SD

Plant development was monitored from photographs such as those shown in Fig 3.1a. The plant size was approximated by calculating the total area of the plant in the photograph, using ImageJ. For this general assessment of the *Nt(Hn)* plant, only the results for the growth period within the GC are presented in Fig 3.1b. Plant development after transfer to LL or HL is presented in Chapter 4. In Fig 3.1b, the difference in development rate between *N.tabacum* and *Nt(Hn)* is clear, the first sign of germination occurring in the *Nt(Hn)* cybrid about two weeks after *N.tabacum*, although seedling development while in the GC is delayed by about three weeks.

Examples of plants at the time of transfer from the GC to the LL/HL GEs, 56 days (8 weeks) for *N.tabacum* and *H. niger* and 84 days (12 weeks) for *Nt(Hn)*, are shown in Fig 3.1a. Mature plants after 4 weeks incubation in the GEs, at 84 days and 112 days for wildtype plants and *Nt(Hn)* respectively, are also presented. The reduced size of *Nt(Hn)* was evident throughout and was suggestive of dwarfism

rather than developmental delay as, although not quantified here, the number of leaves was greater than expected for the plant size, although approximately representative of the plant's age. This is most clearly observed by comparing the photographs of *Nt(Hn)* at 84 days with *N.tabacum* at 84 days in Fig 3.1a. The predominant leaves number six in each case, despite the much reduced size of the

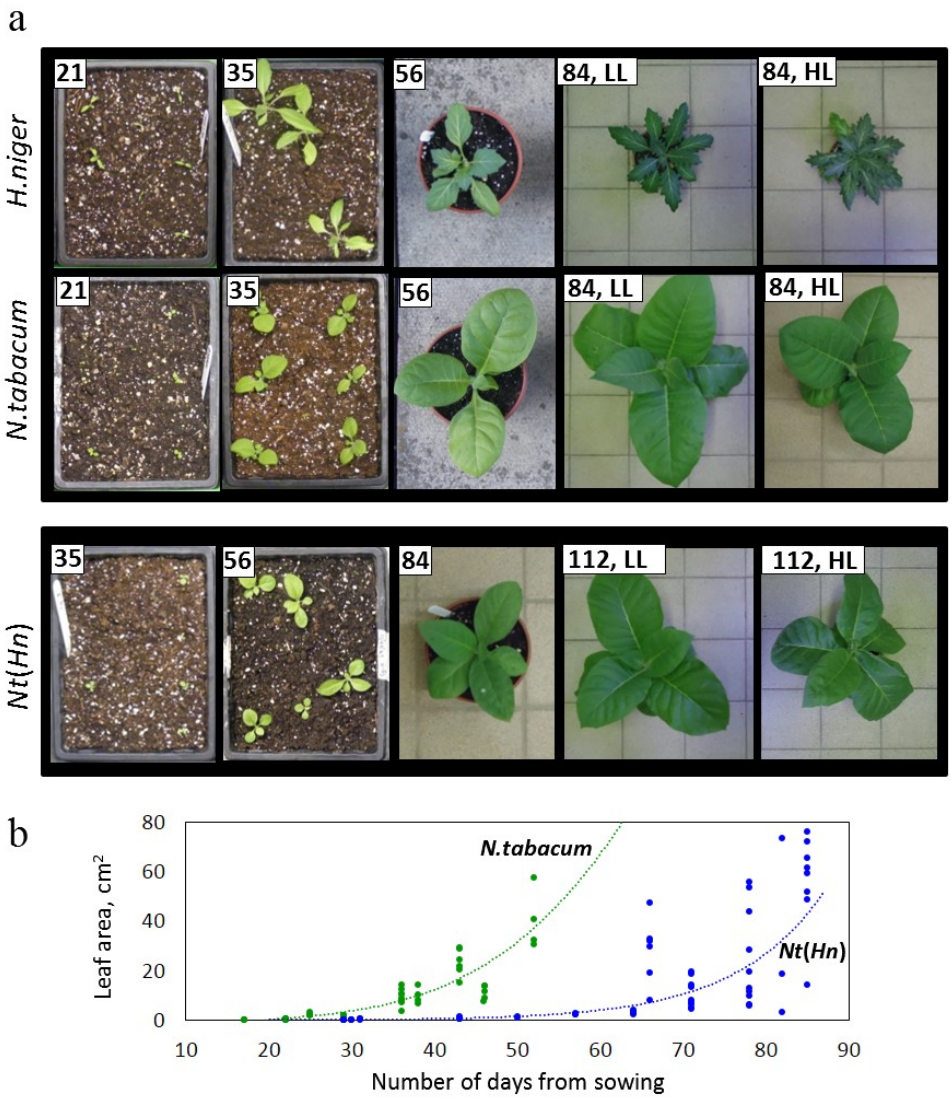


**Figure 3.1:** Plant growth. **a)** Photographs are presented for plants typical in size for their age, i.e. the number of days from sowing (given with each photograph). Note that *Nt(Hn)* development was delayed by about 3 weeks. Mature plants grown in LL and HL are shown at 12 weeks for *N.tabacum* and *H. niger*, and 16 weeks for *Nt(Hn)*. **b)** Graph plotting the change in plant size over time, measured as total leaf area ($cm^2$) from photographs as in a).

*Nt*(*Hn*) plant. The 84 day old *Nt*(*Hn*) cybrid is more similar in size to the 56 day old *N.tabacum* plant, which is clearly still immature with only three developed leaves.

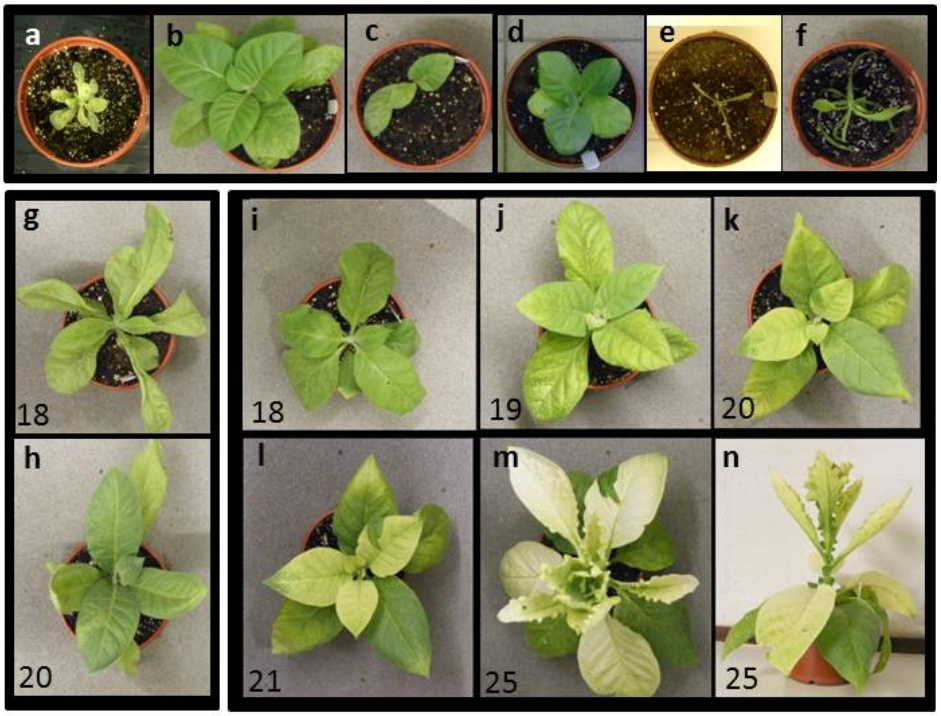


**Figure 3.2:** Unusual plant development and morphologies in *Nt*(*Hn*). Numbers in the bottom left corners show plant age in weeks. **a-f)** Plants are at least 20 weeks old and have extremely stunted growth. **g-h)** An individual plant at 18 and 19 weeks respectively to show that in some cases *Nt*(*Hn*) developed a more typical phenotype with maturation. **i-n)** A chronologically ordered series of photos of one plant in which the plant's morphology became particularly remarkable with age. The plant exhibited extensive mosaic bleaching and crenelation of the upper leaves. Note that *e,f* and *g* are examples of *Nt*(*Hn*) with elongated leaves.

From the *Nt*(*Hn*) seeds that germinated during this study, a few ($\sim$ 8 %) exhibited highly unusual phenotypes and a couple of cases were particularly remarkable, these plants were either discarded or kept for observation without experimental use. Some examples are shown in Fig 3.2. All atypical *Nt*(*Hn*) plants grew at a much slower rate than the results already reported, and apart from a couple of cases discussed below, showed extremely stunted growth with either thin thread-like leaves, that usually curled at the edges as in Fig 3.2e,f or rounded and clustered leaves as in Fig 3.2a,b,c,d.

Two of the remarkably unusual phenotypes are presented in Fig 3.2g-n. In Fig 3.2g-h an individual plant is shown where it can be observed that at 18 weeks the leaves showed elongation and slight curling at the edges (Fig 3.2g) which, two weeks later (Fig 3.2h) had changed into rounded leaves that exhibited isolated pale patches. Fig 3.2i-n presents a second example which occurred in a single case, where at 18 weeks (Fig 3.2i), the plant was smaller than average but with normal greenness. At 19 weeks (Fig 3.2j), the same plant showed signs of bleaching and gradually, until 25 weeks old, it developed intense bleaching with variegated patches in the upper half (Fig 3.2k-n). The upper leaves also became crenelated and up-wards reaching, similar to those of *H. niger* while the lower leaves remained predominantly green, rounded and flatter as in *N.tabacum*.

## 3.3 Flower morphology

At 12 weeks old for *N.tabacum* and *H. niger*, and 14-17 weeks for *Nt*(*Hn*), plants were transferred to the greenhouse to flower for seed production. There was significant variation in flower morphology between *Nt*(*Hn*) plants and occasionally also between flowers of an individual plant (see Fig 3.3a-f). Petal number was


**Figure 3.3:** Flower morphology. **a-f)** *Nt*(*Hn*) flowers with various corolla morphology. Four petal corollas (*a,d*); five petals, (*b*); six petals, (*c*); fused petals (*e*) and a deformed flower (*f*). **g-k)** *N.tabacum* flowers with four petals (**h**); five petals (*g,i*) and with extreme abnormalities as in (*j,k*). **l)** *H. niger* flowers are shown for comparison.

usually five (Fig 3.3b), although 4 (Fig 3.3a,d), and 6 (Fig 3.3c) petalled or fused petal (Fig 3.3e) flowers were not uncommon. Strong developmental disturbance was apparent in a small number of cases as represented in Fig 3.3f.

Most *N.tabacum* flowers developed typical wildtype *N.tabacum* 5-petal flowers, although petal shape was variable from rounded (Fig 3.3g) to pointed (Fig 3.3i). Unexpectedly however, non-typical phenotypes were also occasionally apparent in *N.tabacum*. Typical *N.tabacum* flowers are trumpet-shaped and white/pink with five lobes, the shade and pattern of the pink colour and the exact shape of the petals is known to vary between cultivars. However, of the *N.tabacum* plants that we grew, even on the same inflorescence of an individual plant, we observed flowers with different numbers of petals (Fig 3.3g,h). In two separate cases, extreme phenotypic disturbance was apparent (Fig 3.3j,k). It should be noted that, cross-pollination of *N.tabacum* flowers and pollination of *Nt*(*Hn*) flowers with *N.tabacum* pollen for the production of seeds, was conducted between 5-petal flowers only.

## 3.4 Discussion

*Nt*(*Hn*) cybrids broadly resembled *N.tabacum* in appearance. However, differences were apparent in germination rates, growth rates, plant size, seed viability, flower morphology and the extent of between plant variability. Unexpectedly, the wildtype *N.tabacum* plant also showed unusual flower morphology. To discuss these results we first describe the chloroplast DNA (cpDNA) and mitochondrial DNA (mtDNA) analyses conducted by Zubko et al. (1996, 2001).

### 3.4.1 Organelle DNA analysis

A *N.tabacum* nuclear DNA was confirmed in the *Nt*(*Hn*) by Zubko et al. (1996, 2001) using total DNA hybridisation probed with citrus ribosomal DNA fragments. The results showed identical banding patterns between *N.tabacum* and *Nt*(*Hn*) nuclear DNA. Chromosome counts were also found to be identical between the *Nt*(*Hn*) plants and wildtype *N.tabacum* with a diploid number of 48 chromosomes (2n = 48) (Zubko et al., 1996). *H. niger*, for comparison, has 2n = 38 chromosomes. As described in §1.6, the inheritance of one set of parental chromosomes, and elimination of the other, is often observed in cybrid generation (Gernand et al., 2005; Liu et al., 2005).

The results of the cpDNA and mtDNA analysis by Zubko et al. (1996), are presented in Fig 3.4. The methods used to test the DNA are described briefly here. After *Nt*(*Hn*) construction, cpDNA and mtDNA were isolated for restriction fragment length polymorphism (RFLP). Restriction enzymes *Hin*d III and *Bam*HI

were used for digestion of the cpDNA (Fig 3.4a) and mtDNA respectively. Digests were then separated by gel electrophoresis, the cpDNA banding patterns are shown in Fig 3.4a. For mtDNA analysis, samples were then subjected to Southern Blot hybridisation using probes of the mitochondrial genes for cytochrome oxidase, subunits I, II and III from *Oenothera* (Fig 3.4c).

In a second experiment by Zubko et al. (1996), total DNA extracts were digested with *Bam*HI (for mtDNA) or *Pst*I + *Sal*I (for cpDNA) and separated by electrophoresis. cpDNA digests were probed with a fragment of *rbcL* (RuBisCo large subunit) plastid gene from spinach (Fig 3.4b). mtDNA digests were probed with a fragment of the mitochondrial *atpα* gene (Fig 3.4d) or a fragment of mitochondrial *nad3/rps12* gene cluster from *Arabidopsis* (Fig 3.4e).

Chloroplast DNA (cpDNA) digests always showed identical banding patterns between *H. niger* and *Nt*(*Hn*), with differences to *N.tabacum* (Fig 3.4a,b), indicating that the plastid genomes in the *Nt*(*Hn*) were of *H. niger* origin (Zubko et al., 1996, 2001). As with the nuclear genome, it is typical to find chloroplasts of a single parental origin in cybrid plants du to their natural segregation into like with like (Belliard et al., 1979; Morgan and Maliga, 1987; Sanchez-Puerta et al.,

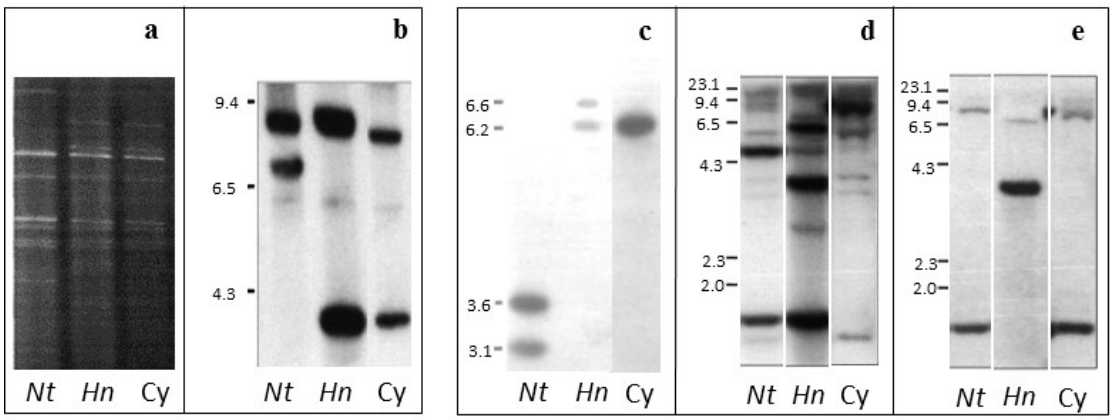


**Figure 3.4:** Analysis of cpDNA (a-b) and mtDNA (c-e) by Zubko et al. (1996, 2001). **a)** RFLP of cpDNA digested with *Hin*dIII (Zubko et al., 1996); **b)** Southern blot hybridisation of plastomes that were digested with *Pst*I + *Sal*I restriction enzymes and then hybridised with $^{32}$P-labelled *rbc*L probe (Zubko et al., 2001). **(c-e)** in all cases, mtDNA was digested with *Bam*HI followed by **c)** Southern blot hybridisation with *cox*I probe (Zubko et al., 1996); **d)** hybridisation with *atpα* probe and **e)** hybridisation with the *nad3/rps12* probe (Zubko et al., 2001). Figure is adapted from Zubko et al. (1996) and Zubko et al. (2001). C, *Nt*(*Hn*); T, *N.tabacum* W38; H, *H. niger*

2014) (see §1.6).

In contrast to cpDNA, *Nt(Hn)* mtDNA showed extensive recombination. Hybridisation with the *rbsL* (ribosomal large subunit) probe, found that although pertaining to the *H. niger* band pattern in general, the major band at 6.6 kb was missing (Fig 3.4c). Digests that were probed with the mitochondrial *atpα* gene (Fig 3.4d) revealed novel bands that did not clearly pertain to either the *N.tabacum* or the *H. niger* banding patterns. The final probe (mitochondrial *nad3/rps12*), shown in Fig 3.4e, showed *Nt(Hn)* mtDNA banding pattern to be similar to *N.tabacum*.

### 3.4.2 Germination delay and dwarfism in *Nt(Hn)* cybrids

The proportion of *Nt(Hn)* seeds that developed to cotyledon (34.3 %) was comparable to that reported by Zubko et al. (1996) at 31 %, however the time delay between sowing and cotyledon stage in the *Nt(Hn)* was quite different between studies. We found that cotyledons, on average, appeared at 37.7 ± 9.2 days after sowing, whereas Zubko et al. (2001), reports that *Nt(Hn)* development was only delayed by about 3-5 days compared to *N.tabacum*. In addition, they found that the delay was reduced when the seeds were grown in soil rather than *in vitro* and when they were grown under a low light intensity (10-20 $\mu$mol photons $m^{-2}$ $s^{-1}$). They ascribe these results to an increased photosensitivity in germinating leaves (Zubko et al., 2001).

Light intensity in our growth chambers was, on average 70 $\mu$mol photons $m^{-2}$ $s^{-1}$, significantly higher than that used by Zubko et al. (2001). The theory that *Nt(Hn)* exhibited increased light sensitivity could therefore explain the extended delay in germination that was observed here. A more general environmental sensitivity might explain between batch variability in germination rates and development patterns. Sensitivity to small changes in the amount of water, soil condition, pollutants in the water, air condition and temperature may have had an impact on *Nt(Hn)* growth rates. As well as possibly explaining between batch variability, environmental impact might also offer some explanation for the reduced size of *Nt(Hn)*.

In §3.2, we suggested that the *Nt(Hn)* plant phenotype was suggestive of disproportionate growth, that resembled dwarfism rather than a uniform developmental delay. The observation was based upon the fact that the number of leaves was greater than expected for the plant size, although approximately representative of plant age with comparison to *N.tabacum*. The severity of the 'dwarfism' attenuated with age, so that mature *Nt(Hn)* plants were similar in size to *N.tabacum*, suggesting that this particular nuclear-organellar incompatibility was transient, perhaps

due to inhibition of regulatory factors during plant development. Dwarfism has been reported in previous work using different cybrid plants (Babiychuk et al., 1995; Pelletier et al., 1983) and is described as a persistent nuclear–organellar incompatibility (Pental et al., 1986; Schmitz-Linneweber et al., 2002).

### 3.4.3 Reduced development and growth rates could be linked to altered plant hormone response systems

The *Nt*(*Hn*) plant's small stature during development was, at least in part, due to reduced leaf size and height. Leaf number, seemed to be relatively unaffected by cybridisation. These differences suggest that there were separate systems governing the different aspects of growth, and only some were changed in *Nt*(*Hn*). A possible explanation for disproportionate growth might be that some plant hormone (phytohormone) regulation and/or signalling pathways were affected due to cybridisation.

Phytohormones are secondary metabolites comprising small signal molecules that are present in low concentrations (Davies, 2010). They are key components in shaping plant growth regulation and architecture (Santner and Estelle, 2009). Currently about ten phytohormones have been identified in plants (Santner and Estelle, 2009). They are perceived by a variety of receptors that ultimately lead to the changes in expression of hundreds of genes. Phytohormone signalling pathways are integrated at multiple levels during plant growth and development (Santner and Estelle, 2009), although evidence so-far shows that, on the whole, there is very little over-lap in the target genes (Jaillais and Chory, 2010).

Different phytohormones have been identified as regulating different aspects of plant growth. For example, growth involving cell division and differentiation has been associated with cytokinins, while organ size and expansion along the longitudinal axes have been associated with gibberellins, auxins and brassinosteroids (Jaillais and Chory, 2010). Dwarfism is usually found to occur if the function of even just one of these hormone pathways is lost (Jaillais and Chory, 2010). Jasmonates have also been identified as active in plant dwarfing by reducing the rate of leaf expansion through decreasing cell number by inhibiting mitosis (Zhang and Turner, 2008).

Jasmonates are oxylipin signalling molecules that are involved in a broad range of developmental and stress related signalling pathways (Kombrink, 2012). Jasmonic acid (JA) is synthesised in the chloroplast (Svyatyna and Riemann, 2012) by oxidisation of chloroplast-membrane derived galactolipids by a lipoxygenase (LOX) enzyme (Wasternack and Hause, 2013). The LOX enzymes, are nuclear-encoded and targeted to the chloroplast where they are mostly associated with

the thylakoid membrane (Farmaki et al., 2007). The synthesis of JA is regulated by pathways that involve chloroplast-nucleus signalling to regulate LOX gene expression, and by interaction with other hormone and hormone related-proteins (Santner and Estelle, 2009).

The dwarf-like phenotype of *Nt(Hn)* could be linked to a disruptive alteration of the proteins that are involved in phytohormone regulation. Of these, the jasmonate hormone system is suggested to be a likely candidate given that its production and regulation is dependent on nuclear-chloroplast interaction, as well as its previous association with stunted growth. If the nuclear-encoded LOX genes that are involved in JA synthesis and regulation are different between wildtype *N. tabacum* and *H. niger*, then it seems reasonable to propose that *N. tabacum* LOX activity in the context of *H. niger*-chloroplast-encoded proteins could be affected, causing altered growth and developmental patterns in *Nt(Hn)*.

An alternative, or additional explanation, for phytohormone-related dwarfism in *Nt(Hn)* cybrid, could be that there was an increase in the production of some phytohormone(s) due to stress, caused for example, by heightened sensitivity to abiotic factors such as light.

### 3.4.4 Alterations in the mtDNA could explain unusual flower morphology

The mtDNA of the *Nt(Hn)* plants used in this study had undergone recombination and was different from both *N.tabacum* and *H. niger*. Mitochondrial recombination in somatic hybrids is common (Boeshore et al., 1983; Belliard et al., 1979) and is closely associated with cytoplasmic male sterilty (Makaroff and Palmer, 1988; Hanson and Bentolila, 2004; Hanson, 1991), a valuable trait in agricultural practice (Pelletier and Budar, 2007), and which was also a feature of *Nt(Hn)* (Zubko et al., 2003).

Flower morphology is known to be strongly linked to the mitochondrial genome (Linke et al., 2003; Linke and Börner, 2005). Flower morphology in *Nt(Hn)* has already been investigated by Zubko et al. (2003). In their report, the Rhn3 line that was used in this study was found to have stable flower morphology consistent with the tobacoo wildtype. During *Nt(Hn)* creation (Zubko et al., 1996), two other *Nt(Hn)* cybrid lines (Rhn1 and Rhn2) were established which showed extensive flower modifications, often without corolla and with branched filamentous stamens, these variations are attributed to altered nucleo-mitochondrial interactions (Zubko et al., 2003).

On the whole, the flower morphology of *Nt(Hn)* conformed to typical *N.tabacum* flower morphology, although, in contrast to Zubko et al. (2003), we also observed

some heterogeneity between *Nt*(*Hn*) flowers, often on the same inflorescence of the same plant, although modifications were not as extensive as those reported for Rhn1 and Rhn2 *Nt*(*Hn*) cybrid lines (Zubko et al., 2003). We suggest that heterogeneity in flower morphology could indicate a heterogeneous population of mitochondria within *Nt*(*Hn*), perhaps due to recombination between *H. niger* and *N.tabacum* mtDNAs, originating in the protoplast fusion event, or in subsequent natural, recombination. Differences between local mitochondrial sub-populations within a plant could explain the various flower morphologies that we observed within one plant. When mtDNA is extracted from plant tissue, it is pooled meaning that local differences would evade detection, and the analysed content would represent a total mtDNA that was not necessarily representative of any single mitochondrial genome in the organism.

In a personal communication, Professor Andrew Leitch (plant geneticist, QMUL) suggested that the mix of typical and atypical flower morphology observed in the *N.tabacum* plants, might be due to genetic mosaicism in the *N.tabacum* W38 cultivar, as a result of genetic manipulation of the lineage at sometime previously. Given the emerging evidence for the occurrence of mitochondrial horizontal gene transfer and mtDNA recombination, fission and fusion in natural plant populations (Arimura et al., 2004; Sanchez-Puerta et al., 2014; Bergthorsson et al., 2003; Barr et al., 2005; Bergthorsson et al., 2003), a mosaic content of mtDNAs in the plant tissue, seems a likely candidate to explain the morphologically heterogeneous *N.tabacum* flowers. Furthermore, *N.tabacum* is a popular model in plant genetics which heavily utilises *in vitro in vitro* culturing, a technique which is known to stimulate mtDNA recombination and mutation (Kushnir et al., 1991). There is thus a strong possibility that the *N.tabacum* line used in this work also presents recombined mitochondria.

Chapter 4

# Acclimation to the long-term light environment

## 4.1 Introduction

The potential for acclimation differs between species depending on their capacity for phenotypic plasticity, a trait that arises from non-reversible, evolutionary pressure on the genome in response to the organism's environment. As demonstrated in previous cybrid work, plant genome evolution entails a co-evolutionary relationship between the nucleus and the chloroplast subgenomes (see §1.6).

The aim of the work presented in this chapter was to assess the characters of plants grown in high light intensity (HL) and low light intensity (LL) growth environments (GE). By investigating the acclimative phenotypes of the *N.tabacum*, *H. niger* and *Nt*(*Hn*) plants to LL and HL growing environments, we are addressing the question of how well the regulated gene expression of the *N.tabacum* nuclear and *H. niger* chloroplast subgenomes has been coordinated.

Acclimation was characterised according to changes in the photosynthetic organs and organelles. Leaves, chloroplasts and thylakoids, were assessed microscopically; biochemical analyses were performed on proteins and pigments, while Chl fluorescence measurements were used to assess photosynthetic function. For the discussion, the results were collected and comparatively summarised in Table 4.2 which compares LL with HL characteristics in each plant line according to expected trends from the literature, and in Table 4.3, which compares the acclimative response of *Nt*(*Hn*) to that of *N.tabacum* and *H. niger* in each GE.

## 4.2 Plant growth under LL and HL intensities

*N.tabacum* and *H. niger* plants were transferred to LL (80-100 $\mu$mol photons $m^{-2}$ $s^{-1}$) and HL (300-400 $\mu$mol photons $m^{-2}$ $s^{-1}$) growth environments at 8 weeks after sowing. Due to the slower germination time and development of *Nt*(*Hn*) (see §3.2), their transfer was delayed until 12 weeks after sowing. The plants than spent 4-5 weeks at either LL or HL, before being transferred to the greenhouse for flowering. During LL/HL incubation, plant growth was monitored using photographs such as those shown in Fig 3.1a, and from which plant size was approximated by measuring the total green area ($cm^2$) using ImageJ. The results are presented in Fig 4.1.

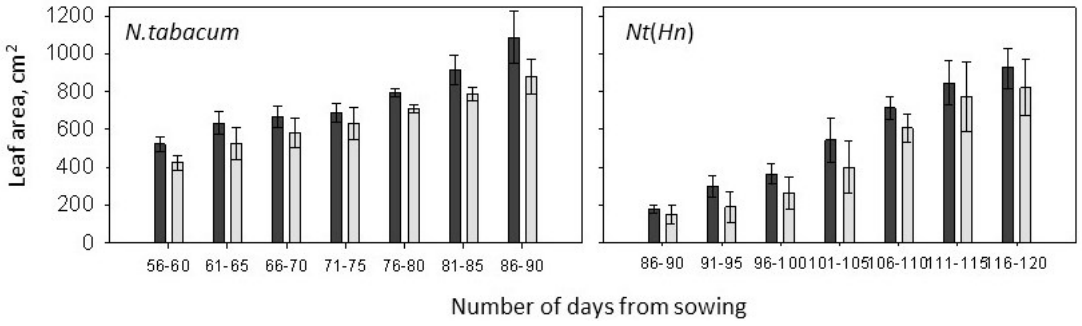


**Figure 4.1:** Sizes of *N.tabacum* (*left*) and *Nt*(*Hn*) (*right*) grown under LL (*dark grey bars*) and HL (*light grey bars*). Data are mean average ± SD from 3-4 plants.

Examples of plants at the time of transfer from the GC to LL/HL growth environments, and just before transfer to the greenhouse after 4 weeks under LL/HL intensity, are shown in Fig 3.1a. As already mentioned in Chapter 3, *Nt*(*Hn*)'s reduced size, compared to *N.tabacum*, was evident throughout. *N.tabacum* and *Nt*(*Hn*) LL grown plants bore larger leaves and were paler compared to HL plants (Fig 4.1). Notably however, the size difference between the LL and HL *Nt*(*Hn*) plants was less pronounced than in *N.tabacum*, particularly in the older plants (106-120 days, Fig 4.1). Indeed, LL and HL grown *N.tabacum* plants were easy to distinguish from each other in a visual screening, LL and HL *H. niger* similarly, could be easily separated by eye, due to the paleness, thinner leaf tissue and longer petioles of the LL plants. In contrast, although on average *Nt*(*Hn*) LL plants were smaller, their identification as LL or HL grown was not usually certain by eye alone. The inter-variability between the LL and HL *Nt*(*Hn*) plants is demonstrated by the large error bars in Fig 4.1.

## 4.3 Analysis of microscopic parameters

In order to gain information regarding cell, chloroplast and thylakoid phenotype after acclimation to LL and HL GEs, we prepared leaf tissue and isolated cells from mature plants for observation in electron transmission and confocal microscopy, respectively.

### 4.3.1 Leaf cross-section analysis

To compare the general profile of the leaf cell layers, leaf tissue was fixed in glutaraldehyde and embedded in araldite blocks, sectioned by microtome (2.8 nm thick slices) and viewed with a light microscope. Images of typical samples are shown in Fig 4.2. In general, the *Nt*(*Hn*) leaf sections were comparable to *N.tabacum* rather than *H. niger* which were easily distinguishable by their longer pallisade mesophyll cells, particularly in the HL plants. We could find no remarkable alteration in the leaf cell-layer profile of *Nt*(*Hn*) as compared to *N.tabacum*.

There were differences however in the alignment of the chloroplasts against the cell wall. Compared to those in HL, in wildtype LL plants, chloroplasts were distributed more sparsely around the cell perimeter, creating open spaces along the mesophyll cell walls indicated by arrows in Fig 4.2, these spaces were absent in LL *Nt*(*Hn*) and in all the HL grown plants.

Surprisingly, only the *H. niger* plants showed the typical HL trait of thicker leaves (203.8 ± 10.5 $\mu$m) compared with those from a LL GE (125.9 ± 3.0 $\mu$m). Indeed, image analysis, using ImageJ, revealed that the mean average thickness of HL grown wildtype *N.tabacum* was slightly less than LL plants at 106.5 ± 3.3 $\mu$m and 110.9 ± 8.9 $\mu$m respectively (Fig 4.2g). The same pattern was found in *Nt*(*Hn*) plants where leaf thickness was 110.0 ± 11.1 $\mu$m in HL plants and 118.4 ± 5.1 $\mu$m in LL grown plants, although in both cases the difference was not significant. LL and HL *Nt*(*Hn*) plants both yielded a leaf that on average, was slightly thicker than *N.tabacum*, although again, the difference was not significant (Fig 4.2g).

### 4.3.2 Confocal microscopy of cells in intact leaves

For initial observation, cell and chloroplast arrangement and aspect were examined *in vivo*. Leaf discs were cut and floated in 0.9 M aqueous sucrose solution for 1 hour in the dark to inhibit chloroplast movement, they were then mounted on microscope slides and pressed gently under a cover-slip to remove air bubbles. Samples were viewed using an oil immersion ×40 and ×63 lenses (Fig 4.3).

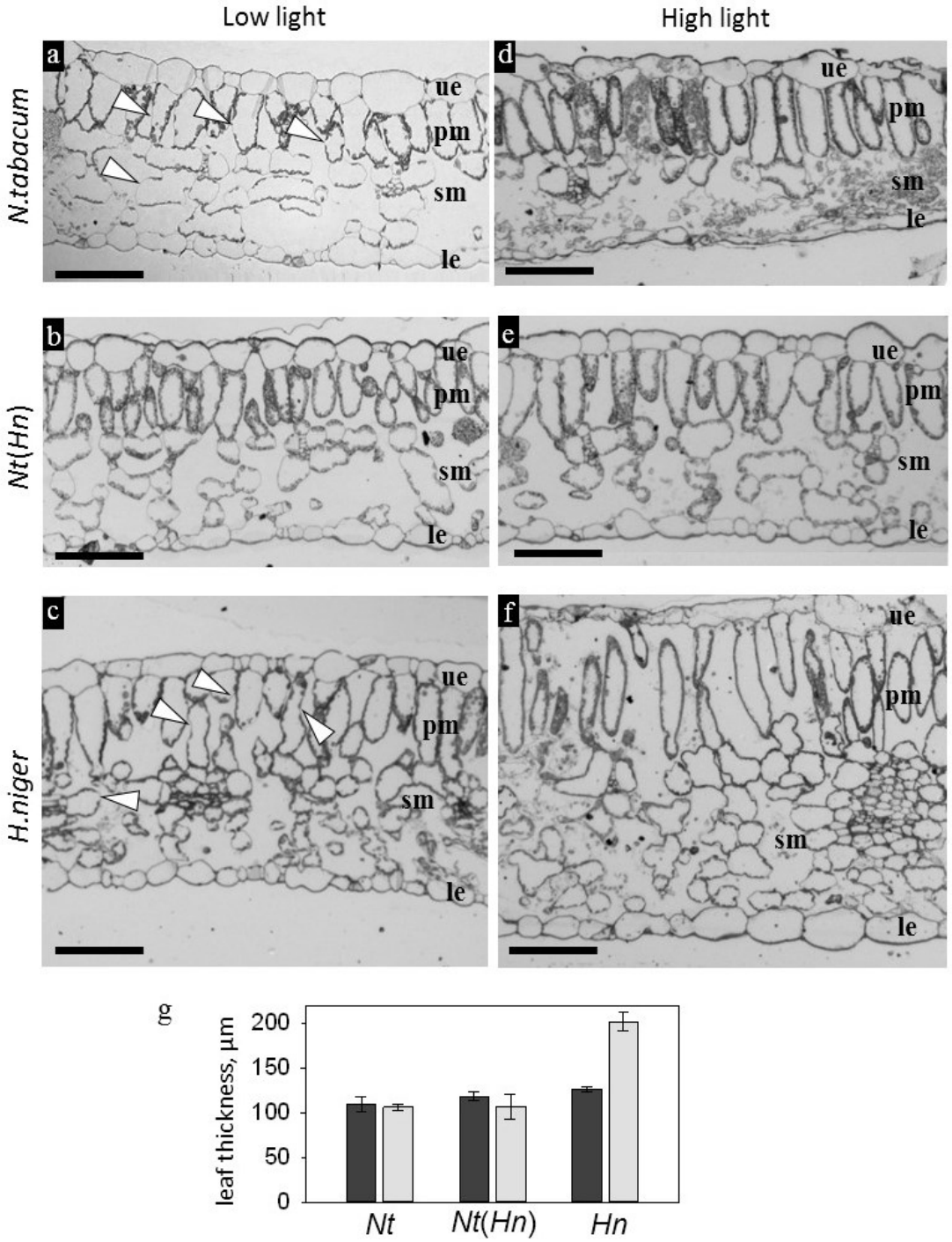


**Figure 4.2:** Leaf cross-section analysis **a-f)** Representative light micrographs of leaf cross-sections from LL (*a-c*), and HL (*d-f*) grown plants of *N.tabacum* (*a,d*), *Nt(Hn)* (*b,e*) and *H. niger* (*c,f*). Arrowheads indicate open spaces between chloroplasts along the cell wall. The upper epidermis (ue), pallisade mesophyll (pm), spongy mesophyll (sm) and lower epidermis (le) are labelled in each figure. Scale bars are $\sim 50$ $\mu$m. **g)** Mean average leaf thickness of LL (*darker bars*) and HL (*lighter bars*) grown plants.

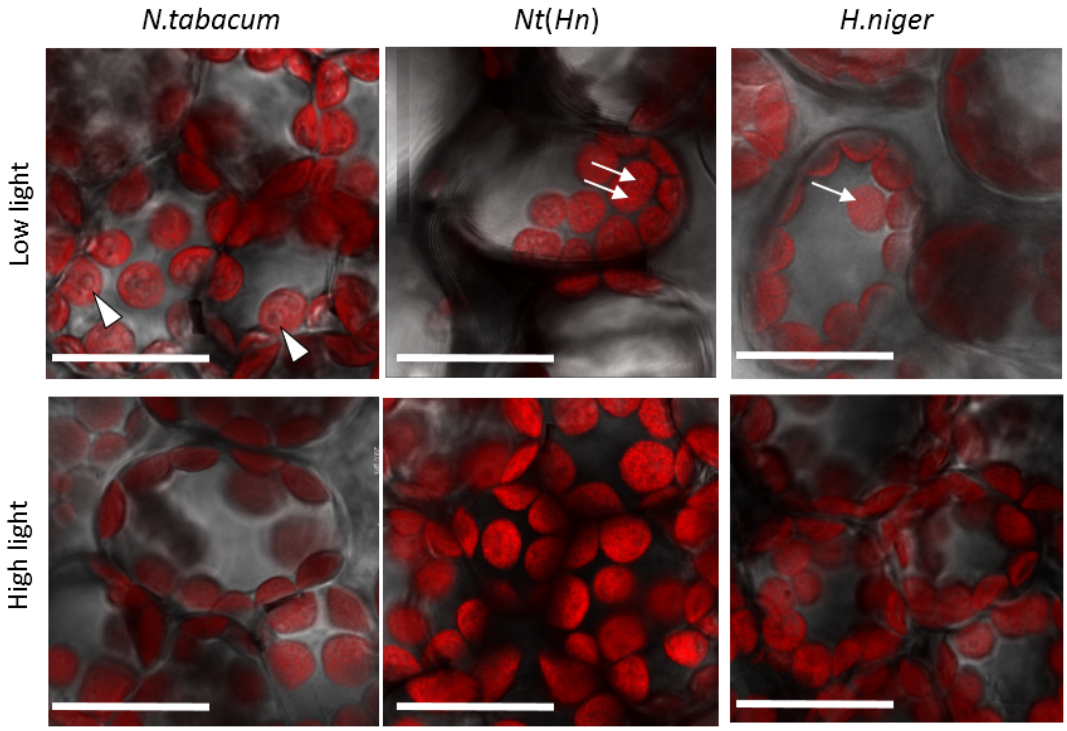


**Figure 4.3:** Confocal fluorescence microscopy of cells and chloroplasts in intact leaf tissue. Examples are shown from LL (*top row*), and HL (*bottom row*) *N.tabacum* (*left*), *Nt*(*Hn*) (*middle*) and *H. niger* (*right*). Individual cells are apparent in which chloroplasts are visualised through the detection of the chlorophyll fluorescence and visualised as red spots. The red grains within the chloroplasts are individual grana. The most clearly observable grana are marked (*white arrow*). Visible starch grains (*arrowhead*) are also indicated. Scale bars are $\sim$ 20 $\mu$m.

We did not find any obvious observable differences between the plant types when using this technique. However, due to the heterogeneity within the leaves, cells and chloroplasts, combined with a small depth of focus, it was difficult and timely to collect data with consistency in order to measure cell parameters to test for small differences, it was therefore decided to isolate cells for full analysis.

### 4.3.3 Confocal microscopy of isolated cells

Two protocols, described by Pyke (2011), were tested for the purpose of cell separation. Firstly, protoplasts were prepared and viewed by light microscope, however, with the removal of the cell wall, the cells became fragile and were short lived, furthermore, they lost their shape, becoming spherical, so that it was impossible to distinguish between cell types. Examples are shown in Fig 4.4a-c.

In the second method, leaf samples were fixed in glutaraldehyde then boiled in

EDTA to disintegrate the tissue and gently squashed on a microscope slide. This was found to be the most suitable approach, as individual cells and types could be easily identified, as shown in Fig 4.4d, samples could also be stored for 2-3 days. For measurement, the cells were viewed using a confocal florescence microscope. All analyses were done on pallisade mesophyll cells, as they primarily enlarge along one axis, whereas spongy mesophyll cells are irregularly shaped, making cell size and chloroplast number difficult to ascertain (Boasson et al., 1972).

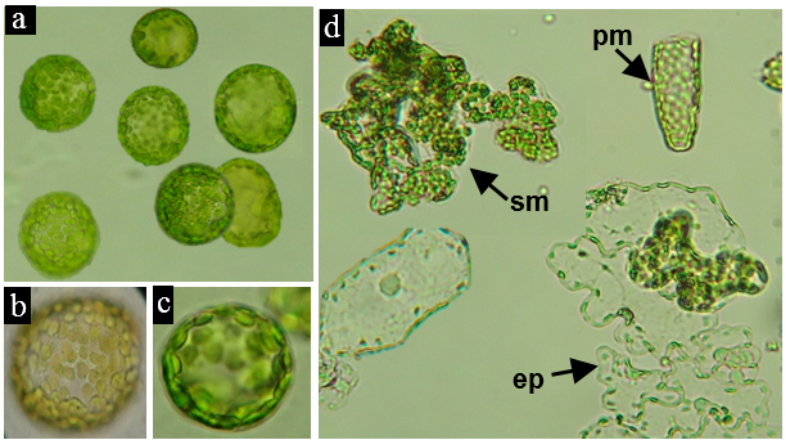


**Figure 4.4:** Protoplast and cell preparations for preliminary investigation into the best method for comparatively analysing cell and chloroplast phenotype, as seen using a light microscope. **a-c)** Protoplasts of *Nt(Hn)* (*a*), *N.tabacum* (*b*) and *H. niger* (*c*). **d)** Cell separations after fixation. Palisade mesophyll cell, pm; spongy mesophyll cell, sm; epithelial cells, ep. Images not to scale as scale bars were not recorded in the initial tests.

Samples were prepared from 1-3 immature plants from the growth cabinet (GC), at 8 weeks (*N.tabacum* and *H. niger*) and 12 weeks (*Nt(Hn)*). However pallisade mesophyll cells were only found in the *H. niger* samples and these appeared somewhat distorted (Fig 4.5c). In samples of *N.tabacum* and *Nt(Hn)*, only chloroplast clusters were present (Fig 4.5a,b), presumably because the cells had not yet fully formed at the time of sample preparation and consequently, were easily damaged during the preparation procedure, maybe due to incomplete cell wall formation.

Three mature plants for each of *N.tabacum*, *H. niger* (both at 12 weeks) and *Nt(Hn)* (at 17 weeks) grown in LL and HL were also sampled. The pallisade mesophyll cells were identified by their typical rod-like shape, as shown in the

confocal images presented in Fig 4.5d-i. From each sample, between 3-20 cells were measured at their central width and length and the volume was calculated with the assumption that the cell shape was cylindrical.

In general, *Nt*(*Hn*) cells more closely resembled cells of *N. tabacum* than *H. niger*, although there were some differences to both. In height, width and volume, *N.tabacum* and *Nt*(*Hn*) cybrid cells were larger in LL grown plants than in HL grown plants, for *H.niger* cells, the reverse was true, where cell height, width and volume was greater in HL grown plants as compared to those from LL (Fig 4.5j,k,l). Cell width was similar between *N. tabacum* and *Nt*(*Hn*) in both LL and HL plants, although length was slightly increased in the *Nt*(*Hn*) cells in both cases, as compared to *N. tabacum* (Fig 4.5j), resulting in slightly greater volume for the *Nt*(*Hn*) (Fig 4.5l).

The number of chloroplasts in each cell was determined either by a full count through a z-stack of an individual cell or by counting the chloroplasts over one half of the cell and doubling the number to account for those located on the other side. The two methods were found to give comparable results. Chloroplast number per cell and per unit volume, are presented in bar charts in Fig 4.5m,n, respectively.

Despite the large difference in cell volume between LL grown wildtypes, the numbers of chloroplasts per cell were similar between *N. tabacum* (86.9 ± 14.3) and *H. niger* (93.7 ± 31.4). Interestingly, cells of the LL grown *Nt*(*Hn*) cybrid, on average, contained 161.8 ± 33.9 chloroplasts per cell, almost double the number of *N.tabacum*, even though cell volume was only slightly increased as compared to *N. tabacum*. Under HL, the number of chloroplasts per cell increased slightly by 9 % in *N. tabacum* to 94.9 ± 19.6, even given the smaller volume of the HL cells, and by 68 % in *H. niger*, to 157.7 ± 27.9 chloroplasts per cell, an increase which closely matched the increase in cell volume of the *H. niger* HL plants. However, in the HL cybrid the number of chloroplasts per cell dropped by 22 % compared to LL plants, to 126.1 ± 18.2 (Fig 4.5m), a figure approximately mid-way between the values for HL *N.tabacum* and *H. niger*.

Nevertheless, when expressed as number of chloroplasts per unit volume (Fig 4.5n), in all cases, the value was greater in the HL plants. Notably, in the LL *Nt*(*Hn*) plants the number of chloroplasts per unit volume (3.3 ± 1.3) more closely resembled the numbers in LL *H. niger* cells (3.5 ± 1.1) than LL *N.tabacum*, which contained about 60 % that number (2.1 ± 0.6). In contrast, the HL *Nt*(*Hn*) cells were more similar in chloroplast number per unit area, to *N.tabacum* HL cells than to *H. niger* (Fig 4.5n).

To further analyse the trend, we plotted chloroplast number against cell volume (Fig 4.6). Trendlines describing the relationship in LL and HL *H. niger* cells, are almost exactly in-line suggesting a strong causal relationship between cell size and

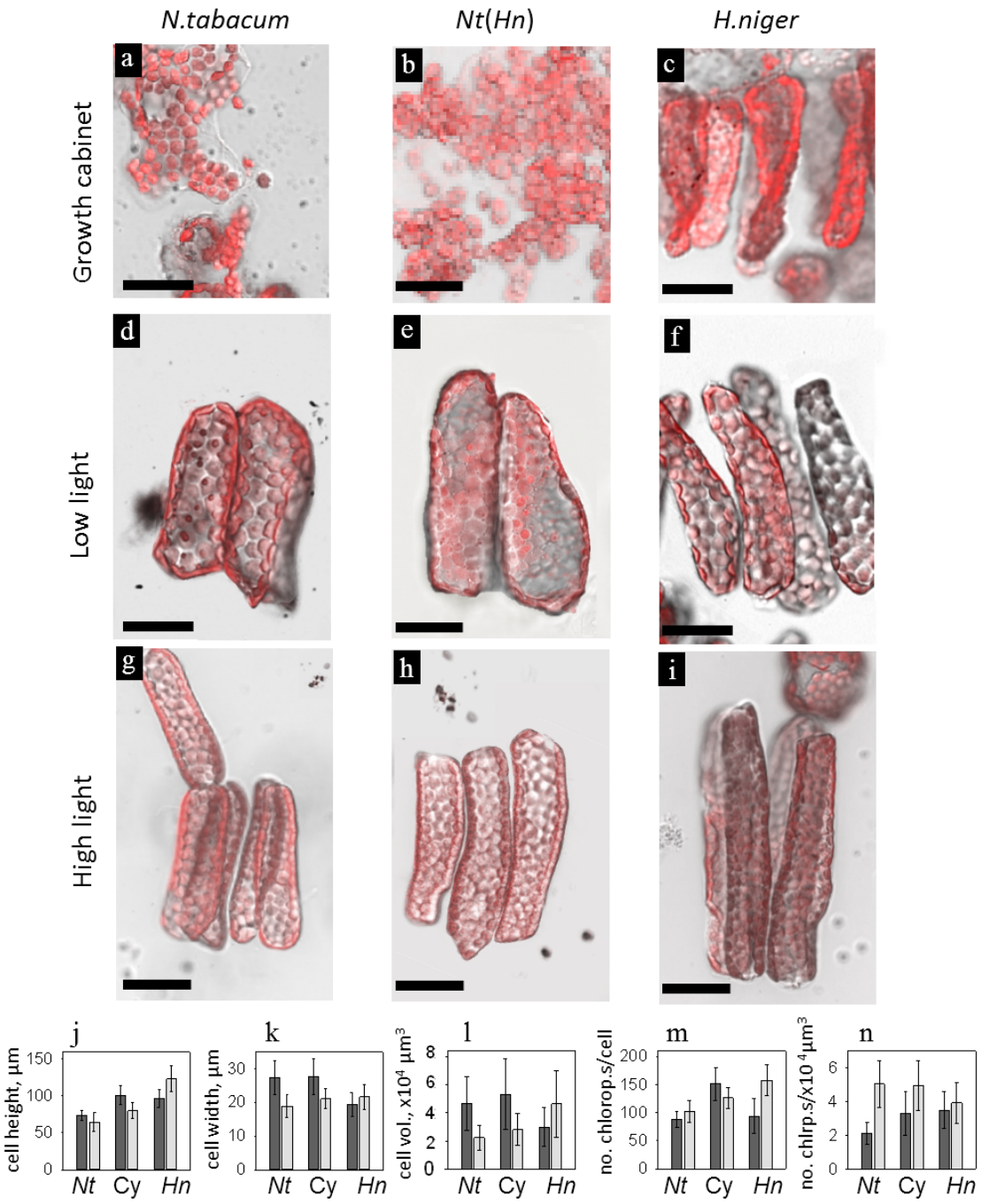


**Figure 4.5:** Pallisade mesophyll cell analysis. **a-i)** Confocal fluorescence microscopy of typical pallisade mesophyll cells from *N.tabacum*, *Nt(Hn)* and *H. niger*. **a-c)** cell preparations from immature plants taken from the growth cabinet (GC). *N.tabacum* (*a*) and *H. niger* (*c*) were 8 weeks and *Nt(Hn)* (*b*), 12-14 weeks old. **d-i)** Cells from mature *N.tabacum* (*d,g*) and *H. niger* (*f,i*) at 11-12 weeks old and from *Nt(Hn)* plants (*e,h*) at 14-17 weeks, grown in LL (*d-f*) and in HL (*g-i*). Scale bar = 50 $\mu$m. **j-n)** Measured and calculated cell parameters, from LL (*darker bars*) and HL plants (*lighter bars*). Data are mean average ± SD, n $\geqslant$ 20. **j)** Cell height. **k)** Cell width **l)** Cell volume. **m)** Number of chloroplasts per cell. **n)** Number of chloroplasts per unit volume of cell.

chloroplast number. In contrast, the HL and LL trendlines were different in both *N. tabacum* and *Nt(Hn)*, suggesting that at least one of the parameters, cell volume or chloroplast number was more strongly correlated with another variable associated with the different light intensities. Furthermore, the large cells containing high numbers of chloroplasts from the *Nt(Hn)* LL grown plants, had a wide spread around the trendline, indicating that under LL the correlation between cell volume and number of chloroplasts was relatively weak (Fig 4.6).

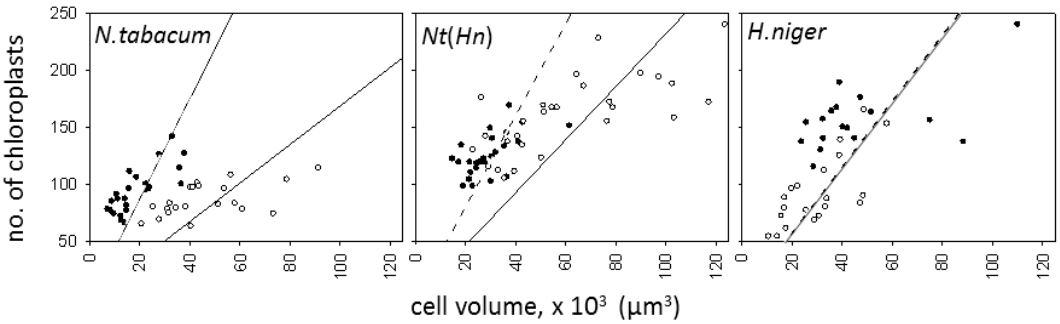


**Figure 4.6:** Number of chloroplasts per cell expressed as a function of cell volume. Measurements were taken from pallisade mesophyll cells of LL (○) and HL (●) grown *N.tabacum* (*left*), *Nt(Hn)* (*middle*) and *H. niger* (*right*). Trendlines for LL (——) and HL (- - - -) were fitted in Excel. Each data point is representative of an individual cell from a pooled data collection from 2-4 mature plants.

### 4.3.4 Chloroplast and thylakoid ultrastructure by TEM

Chloroplast and thylakoid ultrastructure, was investigated using transmission electron microscopy (TEM) micrographs of ultra-thin sections prepared from the same resin blocks as those used for leaf histological analysis. Low magnification images are presented in Fig 4.7a-f, to show chloroplast organisation, and general aspect, within the cell. Notably both LL and HL *Nt(Hn)* chloroplasts had a greater starch content than the parent wildtype plants. Starch content was quantified from the images as a percentage of the chloroplast area using ImageJ software. Starch content in LL (35 ± 16 %) and HL (55 % ± 14) *Nt(Hn)* plants was about double that of the *N.tabacum* controls for LL (14 ± 7 %) and HL (32.7 ± 19.8 %). *H. niger* starch content remained relatively low (Fig 4.7g). In all cases starch content was higher in the HL plants compared to LL plants.

Plastoglobulin content (%) was also quantified (Fig 4.7h) and found to be similar between *N.tabacum* and *Nt(Hn)*, with a marked increase in HL plants, although in both cases this was fairly variable as demonstrated in the large error bars. The other notable feature of these images was that in some places there was

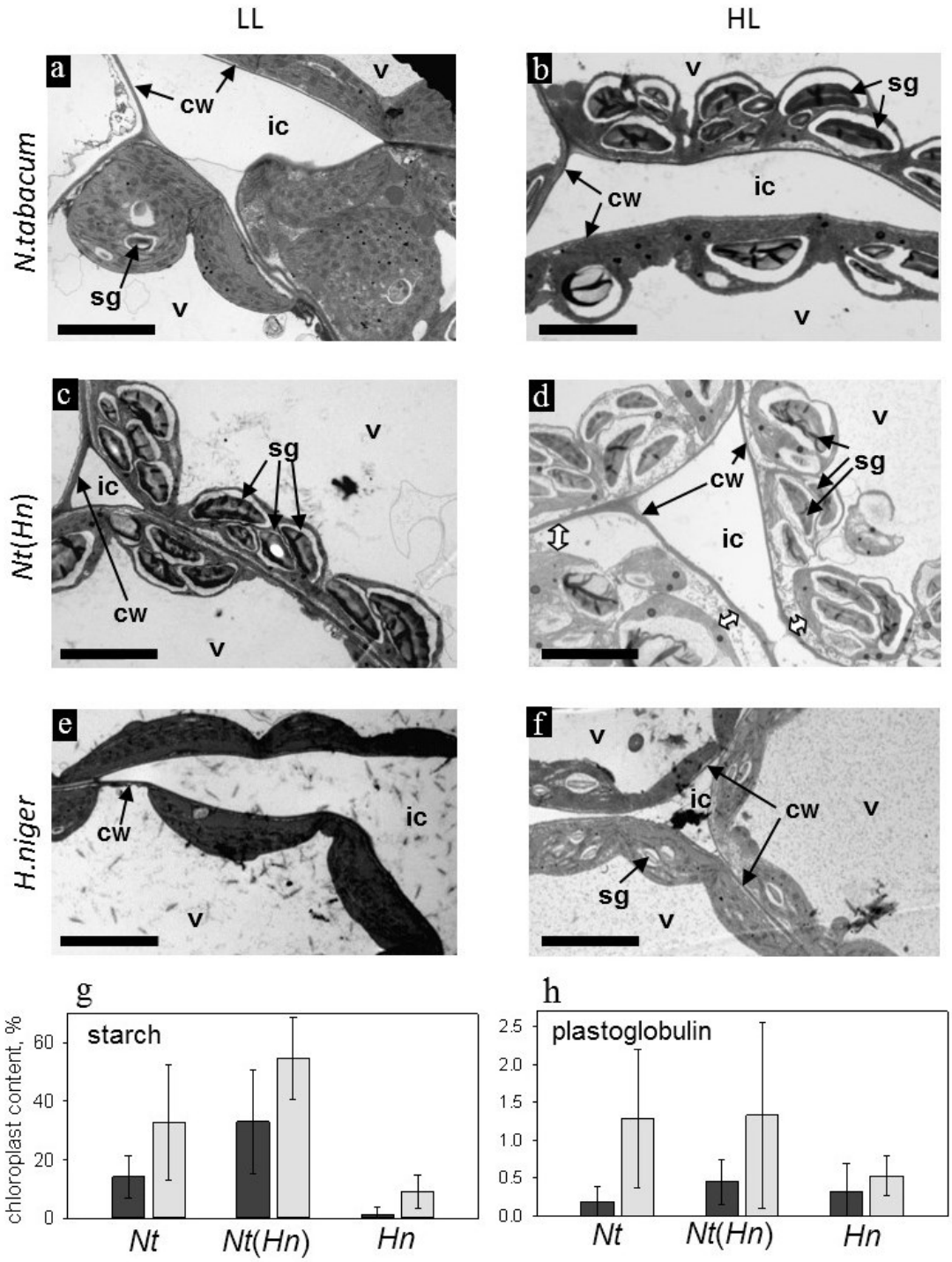


**Figure 4.7:** Chloroplast content analysis. **a-f)** Transmission electron micrographs of plants from LL (*left*) and HL (*right*), *N.tabacum* (*a,b*), *Nt*(*Hn*) (*c,d*) and *H. niger* (*e,f*) to show the general chloroplast aspect and arrangement along the cell wall. Abbreviations are: cw, cell wall; sg, starch grain; ic, intercellular space; v, vacuole. Scale bars represent 5 $\mu$m. **g)** Percentage starch content of the chloroplast. **h)** Percentage plastoglobulin content of the chloroplast. For g and h, data are mean average measurement from 15 chloroplasts from two plant samples ± SD from LL (*darker bars*) and HL (*lighter bars*).

a large gap between the chloroplast and the cell wall of the *Nt(Hn)* HL plants, indicated by the double headed arrows in Fig 4.7d, and shown in a detail in Fig 4.8k. In all other cases, the chloroplasts showed the usual position close against the cell wall.

Fig 4.8 presents a closer analysis of the chloroplasts to reveal the organisation of the thylakoids. In the LL plants the tylakoid organisation was typical (Fig 4.8a-c). In HL *N.tabacum* and *Nt(Hn)* chloroplasts, we found examples of densely packed thylakoids (Fig 4.8d,e). Grana were distinguisable with close inspection and examples are outlined in the figures. There were also cases where the large starch grains seemed to impact on thylakoid organisation as in Fig 4.8 g and h for *N.tabacum* and *Nt(Hn)* HL plants respectively.

Measurements of chloroplast diameter and the number of grana per chloroplast are presented in Fig 4.8j and k. The chloroplast diameter measurements were made from the fluorescence confocal images of isolated cells (see Fig 4.5). From each cell measured, the diameter of at least 10 chloroplasts were also recorded. Chloroplasts of the two wildtype plants were similar in diameter at 6.33 ± 0.41 $\mu$m and 6.05 ± 0.48 $\mu$m for *N.tabacum* and *H. niger* LL grown plants respectively and in both cases there was a slight reduction in chloroplast diameter in the HL plants to 5.46 ± 0.52 $\mu$m for *N.tabacum*, and to 5.62 ± 0.53 $\mu$m for *H. niger*. Interestingly, despite the large starch content, *Nt(Hn)* chloroplast diameter was diminished, with little difference in size between chloroplasts from LL at 5.22 ± 0.59 $\mu$m or HL at 5.09 ± 0.45 $\mu$m (Fig 4.8i).

Grana were quantified per $\mu m^2$ of stroma for each chloroplast by first subtracting the area of starch and plastoglobulin from the total chloroplast area and then dividing by the number of grana (Fig 4.8j). There was a notable reduction in the number of grana in the *Nt(Hn)* chloroplasts at 4.51 ± 1.06 in the LL plants with even lower number in the HL plants at 3.07 ± 1.06. In comparison, *N.tabacum* LL chloroplasts on average contained 5.03 ± 1.04 grana per $\mu m^2$ of stroma with this value increasing to 5.72 ± 2.12 in HL plants. Similar wildtype values were found in *H. niger* at 4.91 ± 1.25 in LL plants, again, with an increase to 5.89 ± 1.53 grana per $\mu m^3$ stroma in the HL plants. The trend in both wildtype species was to, on average, increase the number of grana per unit area under HL conditions by 14-19 % compared to LL plants, whereas the *Nt(Hn)* showed a decrease by about 32 %.

Analysis of the thylakoid membrane ultrastructure is presented in Fig 4.9. Micrographs of granal stacks are presented in Fig 4.9A-F, and details from these figures are presented at a higher magnification in Fig 4.9a-f. From these sections, we determined the diameter of the grana stacks, the no of repeat layers in each grana and the distance between repeated stacks. Grana diameter were determined

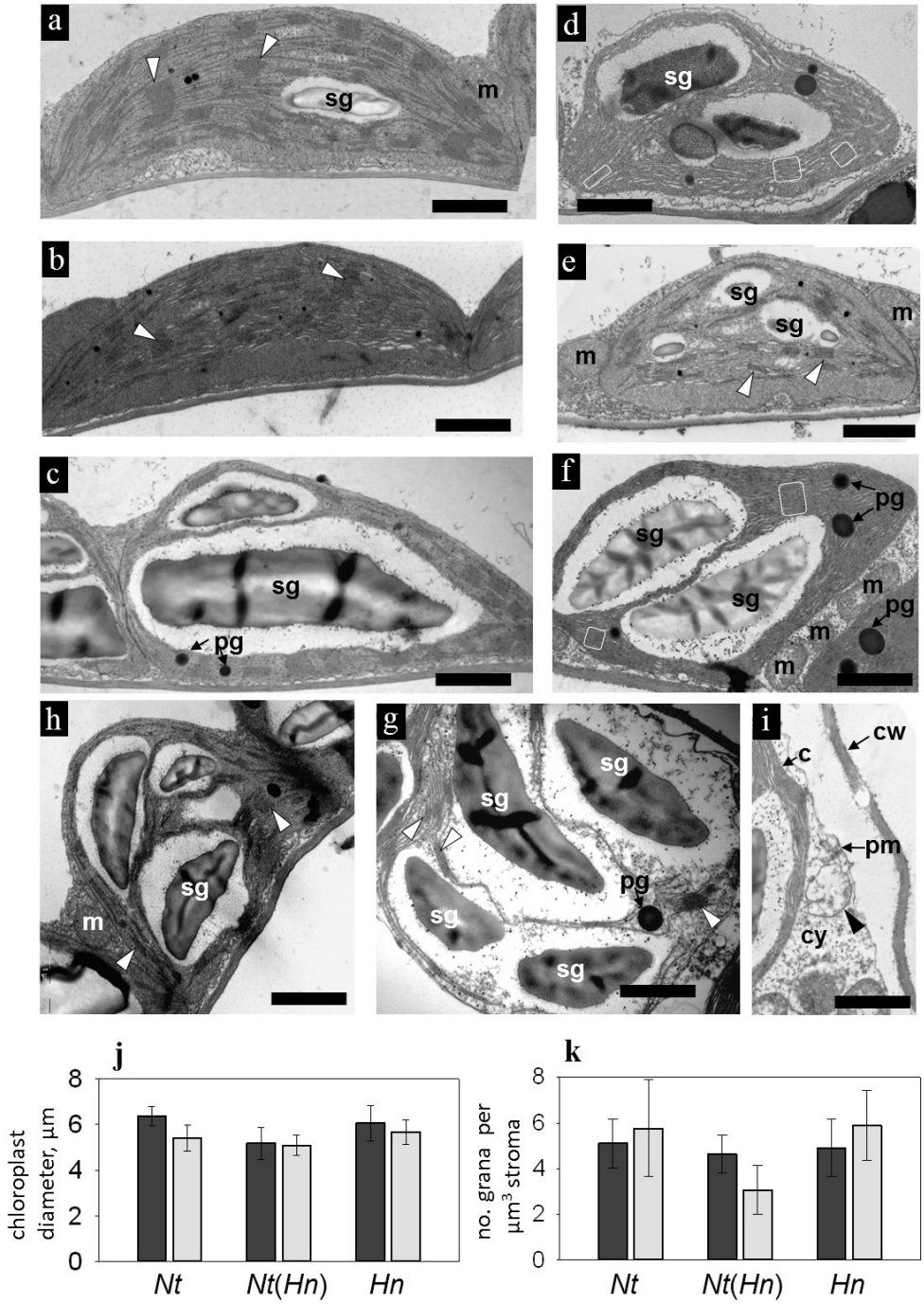


**Figure 4.8: a-i)** Transmission electron microscopy of chloroplasts from LL *N.tabacum* (*a*), *H. niger* (*b*) and *Nt*(*Hn*) (*c*), and HL *N.tabacum* (*d,h*), *Nt*(*Hn*) (*f,g,i*) and *H. niger* (*e*). Grana are indicated by *white arrowheads* or, in *d* and *f*, white boxes. sg, starch grain; pg, plastoglobulin; m, mitochondria; cw, cell wall; cy, cytoplasm; pm, plasma membrane; c, chloroplast. Scale bars represent 1 $\mu$m. **j)** Chloroplast diameter of pallisade mesophyll cells, measured during confocal microscopy. Data are mean average ± SD. In each case cell preparations were viewed from three mature plants. From each plant, 10 chloroplasts were measured from 3-10 cells, so that between 180-290 chloroplasts were measured for each data set. **k)** no. of grana per unit ares of stroma. LL plants (*darker bars*); HL plants (*lighter bars*)

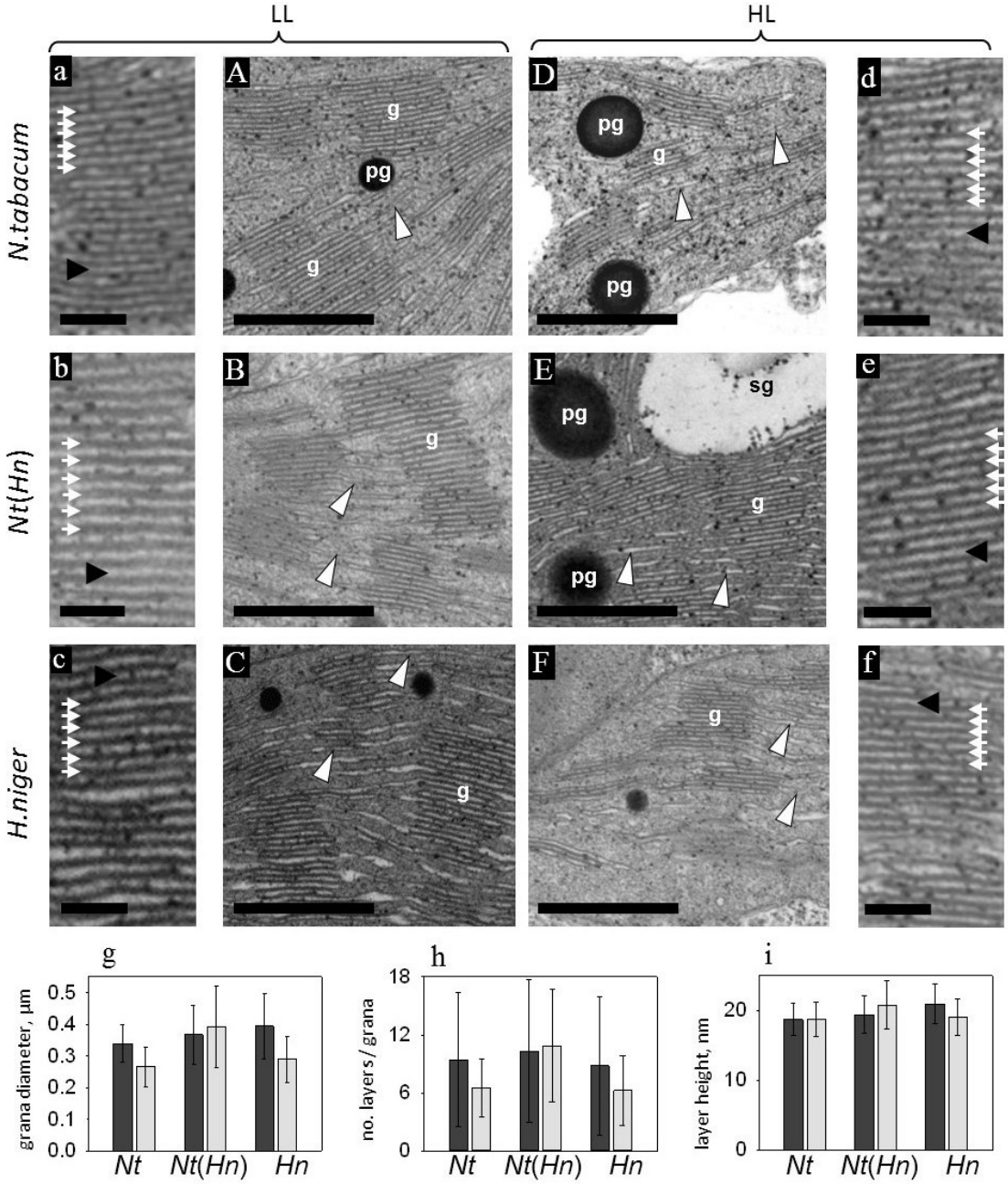


**Figure 4.9:** Ultrasructural analysis of thylakoid membranes. **A-F)** Low magnification TEM-images of LL (*A-C*) and HL (*D-E*) grown *N.tabacum* (*top row, A,D*), *Nt*(*Hn*) (*middle row, B,E*) and *H. niger* (*bottom row, C,F*) plants. Grana (*g*), stroma lamellae (*white arrowheads*) and plastoglobulin (*pg*) are indicated. **a-f)** High magnification detail from images A-F respectively. The thylakoid lumen is marked by a *black arrow*, granal layers (defined as one granal disc sandwiched by two half partition gaps, not distinguishable here) are demarked from each other with *white arrows*. **g)** Grana diameter ($\mu$m). Data are mean average ± SD. **h)** Mean average number of layers per grana. **i)** Average height of repeating layer. For *g-i*, LL data are *darker* bars and HL data are *lighter* bars. Scale bars in A-F represent 500 nm, and in a-f represent 100 nm.

by measuring the width at the middle distance between the top and the bottom of the stack. The grana diameter of the LL plants was fairly similar between plant types at 359 ± 73 nm, 366 ± 92 and 395 ± 99 nm for *N.tabacum*, *Nt*(*Hn*) and *H. niger* plants respectively. In HL GEs, the wildtype plants both decreased their granal diameter by roughly 35 % to 278 ± 61 in *N.tabacum* and 290 ± 73 nm in *H. niger*. Grana diameter in the *Nt*(*Hn*) cybrids was on average, slightly increased in HL grown *Nt*(*Hn*) cybrids by 6 % to 388 ± 123 nm, although variability between samples was large as noted in the error bars and the difference between LL and HL grana diameter was negligible (Fig 4.9g).

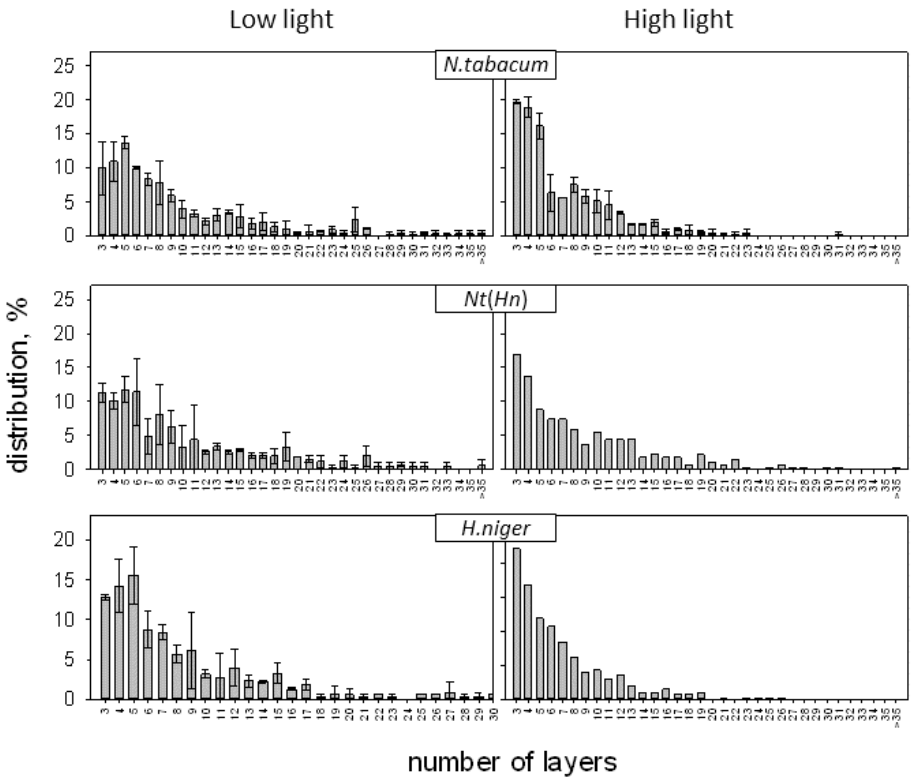


**Figure 4.10:** Percentage distribution of the number of layers per granum in *N.tabacum* (*top)*, *Nt*(*Hn*) (*middle*) and *H. niger* (*bottom*) plants from LL (*left*) and HL (*right*), counted from TEM micrographs as in Fig 4.9. Data for *N.tabacum*, *Nt*(*Hn*) LL and *H. niger* LL are mean average percentage ± SD, from two plant samples in which the number of layers were counted in 170-370 grana per plant. For *Nt*(*Hn*) HL and *H. niger* HL, data were from one plant in which the number of layers were counted in 271 and 393 grana respectively.

Grana are multiple layers of flattened discs that comprise an upper and a lower

membrane bilayer separated by the lumen. We considered each disc to be one 'layer', which were counted using the Cell Counter plugin in ImageJ, the mean average values that we obtained are presented in Fig 4.9h, which show a drop in the no of layers in the wildtype HL plants compared to LL grown plants. *Nt*(*Hn*) again, showed little variation in the mean average difference between GEs. However the error bars were particularly large in all groups so to extrapolate the differences into more detail, we plotted the percentage distribution of the number of layers between the grana stacks (Fig 4.10).

We can observe from Fig 4.10 that the distribution of the grana differed between HL and LL plants in similar ways in all plant types, with the modal average number of layers being 5 in LL plants and slightly less at 3 in HL plants, in all cases. There were notably more grana with a greater number of layers in *Nt*(*Hn*) HL grown plants (maximum 47 layers) than in the HL wildtypes, in which the maximum number of layers was 31 and 27 for *N.tabacum* and *H. niger* respectively. This explains the skew in the mean average number of grana of the cybrid HL plants away from the modal average, shown in Fig 4.9h.

In between each granal disc is a region of aqueous stromal phase called the partition gap. We measured the height of each repeating layer which we defined as one grana disc (two membrane bilayers and lumen) plus one partition gap following the method of Kirchhoff et al. (2013). In Fig 4.9a-f, white arrows indicate the assumed interface between each layer that defined the measured distance. Measurements were only taken from grana that showed regular layering, for each plant type we measured the height of between 350-900 layers.

'Layer height' was remarkably similar with minimum values 12.48 - 12.75 and maximum values between 29.27 - 29.93 in LL grown plants. The HL plants were slightly more variable with values ranging in *N.tabacum* from 11.82 - 28.6 nm, for *Nt*(*Hn*) from 9.90 - 33.46 nm and for *H. niger* from 12.22 - 29.40 nm. Some slight differences in mean averages were observed such as an increased distance between repeat layers in LL *H. niger* and in HL *Nt*(*Hn*), but all the differences fell well within the size of the error bars and were not significant.

## 4.4 Pigment and protein analysis

Acclimation of the photosynthetic apparatus to long-term growth under HL and LL was assessed through analysis of pigment and protein composition.

### 4.4.1 Acclimative regulation of chlorophyll and carotenoid content

Pigments were extracted from mature leaf tissue by grinding in acetone, promptly upon removal from their GE, without dark adaptation. Chl absorbance is more accurately measured at lower concentrations ($OD_{663}$ = 0.2-0.8) than those needed for carotenoids ($OD_{470} \sim 3$), therefore, the Chl *a*:*b* ratio was determined from absorbance at 663 nm and 647 nm in dilute samples using a bench-top spectrophotometer (Fig 4.11). For the determination of carotenoid content concentrated samples were processed by HPLC (Fig 4.11b).

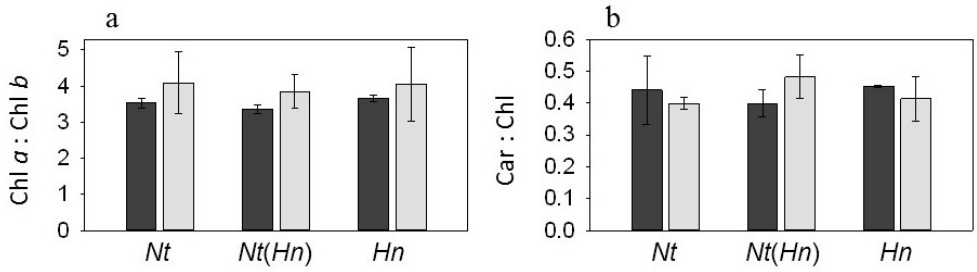


**Figure 4.11:** Pigment ratios of LL (*dark grey bars*) and HL plants (*light grey bars*). **a)** Chl *a*:*b* molar ratio, determined from spectrophotometer readings. **b)** Car:Chl ratios as determined by HPLC analysis. Data are mean average ± SD, n ≥ 3.

There was no significant difference in the Chl *a*:*b* molar ratios between LL plants at 3.54 ± 0.12 in *N.tabacum*, 3.38 ± 0.14 in *Nt*(*Hn*) and 3.68 ± 0.17 in *H. niger*, nor was there between the *N.tabacum* and *Nt*(*Hn*) HL plants at 3.96 ± 0.61 and 3.85 ± 0.47 respectively ($p > 0.05$). The slightly greater difference in the mean Chl *a*:*b* ratios between HL plants of *H. niger* (4.14 ± 0.87) and *Nt*(*Hn*) HL plants was found to be significant (p=0.010). All the plant types showed a typical increase in the Chl *a*:*b* ratio when grown under HL compared LL (Fig 4.11a).

Pigments were identified during separation by HPLC, by their UV/visible absorption spectra and retention time compared to standards, with separation based upon hydrophobicity. Quantification was calculated using published extinction coefficients. Wildtype Car:Chl ratios were similar at 0.44 ± 0.09 and 0.43 ± 0.04, for LL *N.tabacum* and *H. niger*, with slight decreases to 0.40 ± 0.02 and 0.41 ± 0.07, in HL plants respectively. *Nt*(*Hn*) LL plants had a comparatively reduced Car:Chl ratio compared to wildtype, at 0.37 ± 0.08, furthermore, the trend seen in wildtype was reversed in *Nt*(*Hn*) with an increase in Car:Chl content under HL to 0.48 ± 0.07 (Fig 4.11b). Statistical analysis (t-test) however, found that the difference between *N.tabacum* and *Nt*(*Hn*) Car:Chl ratios in HL plants was not

significant (t=11, p=0.057).

In Fig 4.12, the carotenoid pigment composition, expressed as carotenoid (mmols) per total Chl (mol), of LL and HL grown plants is summarised. Data revealed a 20 % reduction in lutein content in HL to LL plants of both wildtype species, from 238.9 ± 52.1 to 190.0 ± 18.5 in *N.tabacum* and from 246.8 ± 66.7 to

**a**

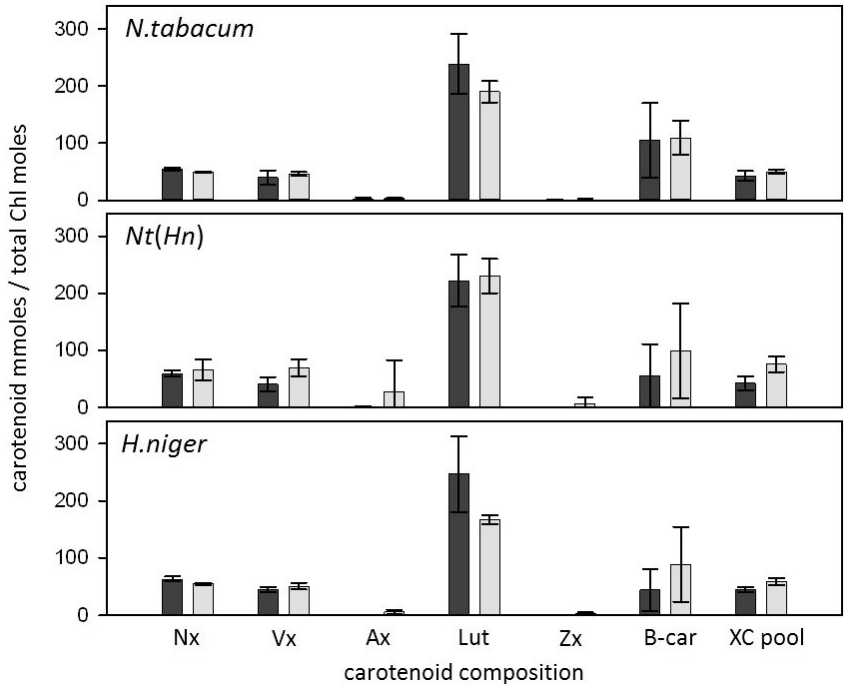


**b**

| | *N.tabacum* | | *Nt(Hn)* | | *H. niger* | |
|---|---|---|---|---|---|---|
| | **LL** | **HL** | **LL** | **HL** | **LL** | **HL** |
| **Nx** | 54.5 ± 2.2 | 48.9 ± 1.0 | 59.4 ± 5.2 | 76.8 ± 33.2 | 63.0 ± 4.3 | 59.0± 10.0 |
| **Vx** | 39.7 ± 12.8 | 46.2 ± 3.7 | 41.0 ± 12.3 | 73.6 ± 17.3 | 44.7 ± 4.2 | 57.9 ± 16.7 |
| **Ax** | 2.0 ± 3.0 | 2.9 ± 1.0 | 1.3 ± 1.5 | 23.9 ± 51.3 | 0.0 ± 0.0 | 5.2 ± 3.3 |
| **Lut** | 238.9 ± 52.1 | 190.0 ± 18.5 | 222.1 ± 45.9 | 243.2 ± 44.4 | 246.8 ± 66.7 | 196.7 ± 67.8 |
| **Zx** | 0.68 ± 1.2 | 1.1 ± 2.3 | 0.0 ± 0.0 | 5.9 ± 10.4 | 0.0 ± 0.0 | 2.2 ± 2.1 |
| **$\beta$-car** | 104.8 ± 65.3 | 109.5 ± 29.6 | 55.3 ± 55.4 | 85.0 ± 83.8 | 44.0 ± 36.5 | 71.7 ± 68.4 |
| **XC** | 42.4 ± 8.6 | 50.2 ± 4.1 | 42.3 ± 12.1 | 78.8 ± 14.7 | 44.7 ± 4.2 | 65.3 ± 14.9 |
| **XC % ratio** | 93.7:4.7:1.6 | 92.0:5.8:2.2 | 97.0:1.2:1.0 | 66.7:26.7:6.6 | 100:0:0 | 85.9:9.6:4.6 |

**Figure 4.12:** Carotenoid composition of LL and HL grown plants. **a)** The carotenoid composition (expressed as mmoles mole$^{-1}$ of total chlorophyll) of *N.tabacum* (*top*), *Nt*(*Hn*) (*middle*) and *H. niger* (*bottom*). **b)** Tabulation of the results presented in *a*. The final row gives the percentage content of the XC pigments to the XC pool in the order Vx:Ax:Zx. Abbreviations are: Nx, neoxanthin; Vx violaxanthin; Ax, antheraxanthin; Lut, Lutein; Zx, seaxanthin; $\beta$-car, $\beta$-carotene; XC pool, xanthophyll pool (Vx + Ax + Zx). Data are mean average ± SD, n ≥ 3.

196.7 ± 67.8 in *H. niger*. Interestingly, mean average lutein content in the *Nt*(*Hn*), increased slightly by 9 % from 222.1 ± 45.9 in LL plants to 243.2 ± 44.4 in HL plants, although there was large variability between samples.

A second notable observation was the difference in the xanthophyll pool (Vx + Ax + Zx) size. LL grown plant types had XC pools of similar size between 42 - 44 mmoles mole$^{-1}$ Chl. All the plants acclimated to HL by increasing their XC pool size, although the increase relative to the LL plants, was largest in *Nt*(*Hn*) at 86 %, while the wildtype plants by comparison increased their XC pool size by 18 % in *N.tabacum* and 39 % in *H. niger*.

The percentage content of each XC pigment (%Vx:%Ax:%Zx) in the XC pool is given in the final row of the table in Fig 4.12b. In all cases the % content of Vx is decreased in the HL plants compared to LL, due to the increase of the deepoxidised pigments, Ax and Zx. Under LL, Ax + Zx content was 2.2 % for *Nt*(*Hn*) and 0 % for *H. niger*, in tobacco the value was slightly higher at 6.3 %. Under HL the value increased to 8 % in *N.tabacum* and 14 % in *H. niger*, interestingly there is a much greater increase of 33 % in *Nt*(*Hn*). These results suggest that the *Nt*(*Hn*) used the short-term adaptive strategy of XC pool deepoxidation to cope with long-term HL exposure to a relatively high degree. Some acclimative stress might also be apparent in the LL *N.tabacum* as indicated by the relatively high Ax + Zx content.

### 4.4.2 Thylakoid protein stoichiometry

Unstacked thylakoid preparations, with a Chl concentration of 1 mg mL$^1$, were rapidly solubilised by the addition of $\alpha$-DM detergent to a final concentration of 1 % (w/v) for 5 min. Pigment-protein complexes were separated by FPLC on a gel filtration column, according to a method developed by van Roon et al. (2000). This type of gel filtration gently separates the membrane components on the basis of size, the largest particles eluting first. Protein absorbance was measured at 280 nm, chlorophyll at 680 nm and carotenoid at 470 nm, the elution profiles are presented in Fig 4.13a,b, unfortunately we were unable to collect data for LL grown *Nt*(*Hn*) and *H. niger* due to technical problems with the FPLC machinery.

Elution profiles resemble those published by Belgio et al. (2012). Six bands (I-VI) were identified, five of these were distinguishable as peaks, or shoulders, we also differentiated a sixth band (IV) between the third and forth peaks (Fig 4.13a,b), as this is commonly found to contain the PSII core (Belgio et al., 2012). With the understanding that particle elution is based on size, and with reference to published results (Belgio et al., 2012; Pagliano et al., 2012; van Roon et al., 2000), the protein composition of each band was predicted to be as follows: I, fragments of unsolubilised membrane; II, PSII supercomplexes; III, PSI core; IV PSII core;

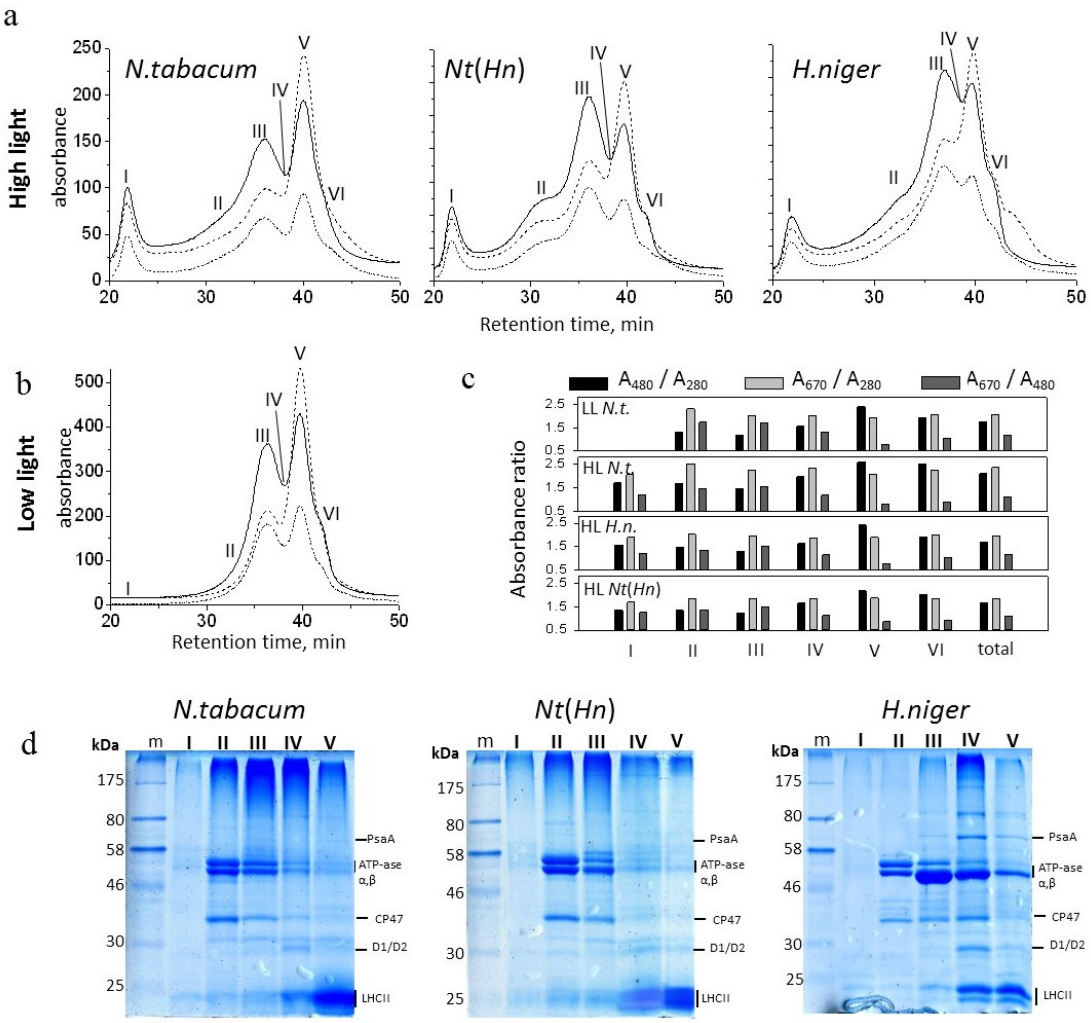


**e**

| | | I | II | III | IV | V | VI |
|---|---|---|---|---|---|---|---|
| **LL** | ***N.tabacum*, %** | 0.8 | 5.7 | 25.8 | 22.6 | 31.8 | 14.1 |
| **HL** | ***N.tabacum*, %** | 14.5 | 9.7 | 20.2 | 14.7 | 27.8 | 13.1 |
| | ***Nt(Hn)*, %** | 10.9 | 12.2 | 26.1 | 17.4 | 23.1 | 10.4 |
| | ***H. niger*, %** | 8.3 | 10.3 | 25.1 | 21.0 | 23.3 | 11.9 |

**Figure 4.13:** Thylakoid protein composition. **a,b)** Gel filtration (FPLC) elution profiles of $\alpha$-DM solubilised thylakoids from HL (*a*) *N.tabacum* (*left*), *Nt*(*Hn*) (*middle*) and *H. niger* (*right*) and from LL *N.tabacum* (*a*), unfortunately we were unable to collect data for *Nt*(*Hn*) and *H. niger* LL plants. Absorption was measured at 670 nm (*solid line*), 280 nm (*dash-dot line*) and 470 nm (*dashed line*) for detection of chlorophyll, protein and carotenoids respectively. **c)** Absorption ratios measured from the elution profiles for *N.tabacum* (T), *Nt*(*Hn*) (C) and *H. niger* (H) grown in high light (HL) and *N.tabacum* grown in low light(LL). **d)** SDS-PAGE gels showing the separation of proteins from the elute of bands I-V. **e)** The relative protein content of each band (I-VI), calculated as a percentage of the sum of the peaks based on the 280 nm absorption profile.

V, LHCII trimers and VI, monomeric antenna complexes.

To aid characterisation of the six bands, absorbance ratios were plotted in bar charts, shown in Fig 4.13c. The relatively high $A_{480}/A_{280}$ and low $A_{670}/A_{480}$ ratios of band V, supports its identification as the carotenoid containing LHCII trimer, in all plant types. The high chlorophyll and low carotenoid content of the proteins in band III, indicated by the $A_{670}/A_{280}$ and $A_{480}/A_{280}$ ratios respectively, suggests that it is the most likely to contain PSI core, as predicted.

Further characterisation and comparative analysis of the HL samples, was performed on the eluted fractions using SDS-PAGE gel separation (Fig 4.13d), room temperature absorption spectroscopy (Fig 4.14a,b), and 77 K fluorescence emission spectroscopy (Fig 4.14c). In general, the SDS-PAGE gel separations of *N.tabacum* and *Nt*(*Hn*) fractions appeared similar with the notable exception that the band at about 58 kDa in fraction III was somewhat stronger and more pronounced in *Nt*(*Hn*), and secondly, that the 25 kDa band in lanes IV and V, appeared broader and comprised of more bands than in the *N.tabacum* gel (Fig 4.13d). These bands are highly characteristic of the components of the PSII major antenna, supporting our predicted identity of fraction V to be LHCII trimers.

Through comparison with similar work by Belgio et al. (2012) and Pagliano et al. (2012), and according to their position and MW, we tentatively labelled the other major bands with their estimated identities. Using these identities. Fraction IV was estimated to contain the PSII core, and although not conclusive, the expected D1/D2 bands are strongest, in the fraction IV SDS-PAGE lane, in all plants (Fig 4.13d). Band III was presumed to be PSI core, usually most identifiable by the large PsaA protein at about 83 kDa (Pagliano et al., 2012). Unfortunately, the band is difficult to locate in our gels, except for a possible appearance in lane IV of *H. niger* (Fig 4.13d).

Fig 4.13e shows the relative protein content of each FPLC band (I-VI), calculated as a percentage of the sum of the peaks based on the 280 nm absorption profile. By comparing LL and HL *N.tabacum* samples, we see that fraction V from *N.tabacum* LL, contained 31.8 % of the total protein content while from *N.tabacum* HL, this quantity was 27.8 %, again, given that it is typical for LL grown plants to have relatively high quantities of LHCII, these results support the identification of peak V as LHCII trimers. However, we would also expect a comparative decrease in the PSI:PSII ratio from LL to HL plants whereas a comparison between peaks III and IV, reveals that the peak III:IV ratio increases from 1.14 in LL to 1.37 in HL, which either contradicts our predicted identification of peaks III and IV being PSI and PSII respectively, or most likely, is an inaccurate measure due to contamination by other components.

Indeed, the strong bands that are characteristic of ATP synthase $\alpha$ and $\beta$

subunits at about 50 kDa, are heavily present in fraction III but relatively much less so in fraction IV. Furthermore, the HL *N.tabacum* sample was not as fully solubilised as the LL sample, evident in the larger peaks I and II. Given that solubilisation does not proceed uniformly with each complex, we might presume that the unsolubilised material could contain quantities of PSI and/or PSII that were disproportionately representative of the sample, biasing the calculations made from the more solubilised peaks (Fig 4.13).

The PSII supercomplex content of fraction II, is uncertain as although, in the gel, the band that is suggested to be CP47, the core antenna of PSII, had highest concentration in lane II for both *N.tabacum* and *Nt*(*Hn*), other PSII supercomplex proteins are missing, an again, there is a strong presence of higher MW bands considered to be ATP synthase, indicating contamination of membrane fragments. The estimated location of the D1/D2 proteins at about 30 kDa do present bands most strongly in lane IV, consistent with the theory that this fraction contained PSII core complexes. However, in general the protein resolution was low, and contamination between fractions high, with many of the bands appearing in several

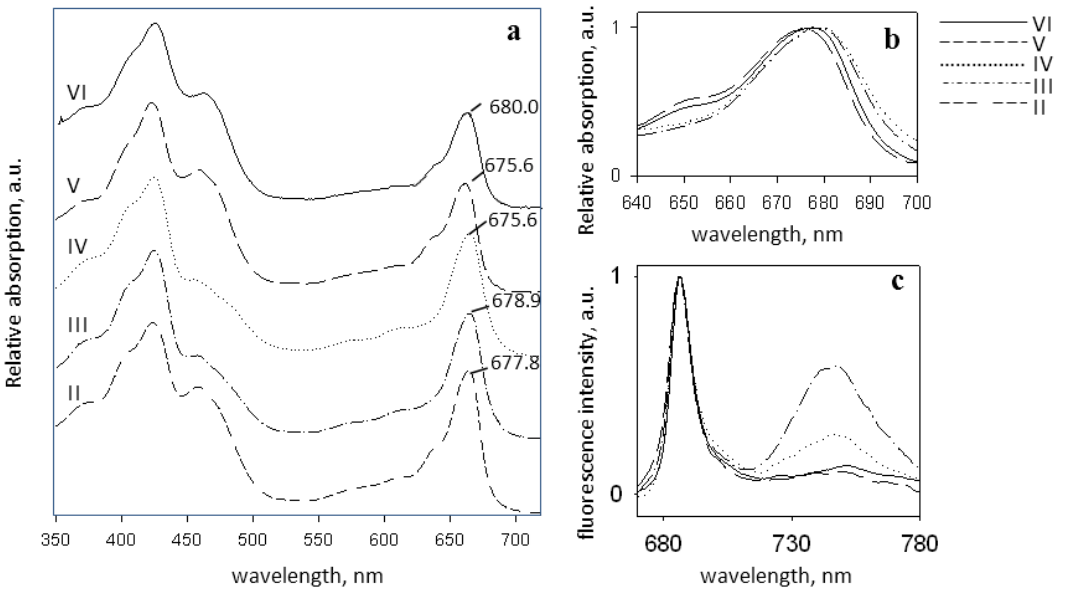


**Figure 4.14:** Spectroscopic analysis of thylakoid protein fractions isolated by FPLC (Fig 4.13). **a)** Absorption spectra of *N.tabacum* fractions containing peaks II-IV, the spectra are staggered for clarity. **b)** A detail from the $Q_y$ region of the spectra in *a* for closer analysis of the changes in the maxima around 650 and 680 nm of peaks III-VI. **c)** Fluorescence emission spectra at 77 K of *N.tabacum* FPLC fractions containing peaks (III-VI).

lanes.

Finally, spectroscopic analysis of the fractions from HL *N.tabacum*, were performed. Room temperature absorption and 77 K fluorescence emission spectra are presented in Fig 4.14. From the absorption spectra (Fig 4.14a), the LHCII content of band V is clearly identifiable by the characteristic broad shoulder at 470 nm and relatively large shoulder at 650 nm (van Roon et al., 2000). The absence of both these shoulders in fraction III, together with the red-shifted absorption peak at 678.9 nm and the red-tail at around 700 nm, that can be observed in the detail shown in Fig 4.14b, indicate the fraction as enriched in PSI. This is further corroborated by the 77K emission spectra of peak III in Fig 4.14c, where the relatively large 735 nm emission band is derived from PSI.

The location of PSII core, predicted to be in band IV of the FPLC elute according to van Roon et al. (2000), is difficult to detect and is likely to overlap considerably with PSI. In the detail of the peak IV absorption spectra of Fig 4.13b, the slight broadening of the spectra around the peak could indicate PSII content (van Roon et al., 2000). The absorption spectrum of peak VI, reveals it to contain monomeric LHCII as while showing a large shoulder at 470 nm, the 650 nm shoulder, a feature of trimeric LHCII (Peter and Thornber, 1991), is reduced as compared to peak V.

Interestingly, according to the table in Fig 4.13e, peak V, which the evidence suggests to be LHCII trimers, is relatively more abundant in the HL samples of *N.tabacum* compared to *Nt*(*Hn*) and *H. niger*. The content of peak II, supposedly PSII supercomplexes, was also more pronounced in the *Nt*(*Hn*) with a relative content of 12.2 %, compared to *N.tabacum* at 9.7 % and *H. niger* at 10.3 %. The peak III:IV:V stoichiometry of the *Nt*(*Hn*) was notably more resemblant of *H. niger* while *N.tabacum* differs by being dominated by peak V.

## 4.5 Photosynthetic function

### 4.5.1 Rapid light curves

A light curve assesses photosynthetic capacity as a function of increasing photosynthetically active radiation (PAR). In traditional light curve measurements, long illumination steps (about 10 min each) are used to allow the plant to adapt to each light intensity so that photosynthetic performance is measured in steady state. Here, we measured rapid light curves (RLCs) which, by comparison, use short illumination steps (30 s) and begin measurement from a light adapted plant. The RLC method provides an assessment of the plant's function that is more indicative of a plant's response to rapid light changes in the field (Ralph and Gademann,

2005).

RLCs were measured using an in-built program of the DUAL PAM fluorometer, we used the dual mode to simultaneously record Chl fluorescence from PSII and absorption changes at P700 enabling us to measure RLCs for both PSII and PSI. The program ran ten × 30 s steps of increasing light intensity. Each step was preceded by a saturating pulse of light to obtain a measure of maximum fluorescence ($F_m$'), from this, a value for effective quantum yield ($\Phi_{PSII}$) was calculated using:

$$\Phi_{PSII} \;=\; \Delta F/F'_m \;=\; (F'_m - F')/F'_m \tag{4.1}$$

where F' is fluorescence emission from a light adapted sample. As demonstrated by Genty et al. (1989), $\Phi_{PSII}$ gives an accurate indication of how much energy is used in photochemistry, with this parameter, relative electron transport rate (rETR) was calculated at each light intensity using:

$$rETR = \Phi_{PSII} \times PAR \times 0.5 \times 0.84 \tag{4.2}$$

where 0.5 is a multiplication factor to correct for absorption at two photosystems and 0.84 is the assumed PSII absorption coefficient (Ralph and Gademann, 2005; White and Critchley, 1999). These data were plotted against PAR and the RLC was produced by fitting a curve using the software-incorporated 'EP model' (Eilers and Peeters, 1988).

The classic rectangular hyperbola of the curve is formed by the initial slope under lower light intensities where light limits photosynthetic rates. Under increased light intensity the curve plateaus as the photosynthetic rate becomes limited by the photosynthetic pathway. In traditional light curves, the plot may begin to curve downwards again as a result of photoinhibition, although this is avoided during RLCs due to the short exposure time to high light intensity (Ralph and Gademann, 2005).

*N.tabacum*, *Nt*(*Hn*) and *H. niger* RLCs from PSI and PSII, are presented in Fig 4.15a-f. In all cases the rETR of PSII and PSI in HL plants was greater at higher light intensities than rETR in LL plants, as expected. LL plants were grown at 80-100 $\mu$mol photons $m^{-2}$ $s^{-1}$, whereas HL plants were grown at 300-400 $\mu$mol photons $m^{-2}$ $s^{-1}$. The 3-4 fold increase in GE light intensity is closely reflected in the *N.tabacum* RLCs, where HL rETR plateaus at roughly three times the amplitude of LL (Fig 4.15a). *H. niger* revealed a greater efficiency for rETR in both light environments, compared to *N.tabacum*, but the HL plants only increased rETR by about 50 % compared to LL (Fig 4.15c). rETR in LL *Nt*(*Hn*) was very similar to *N.tabacum* although acclimation of *Nt*(*Hn*) cybrids to HL was less

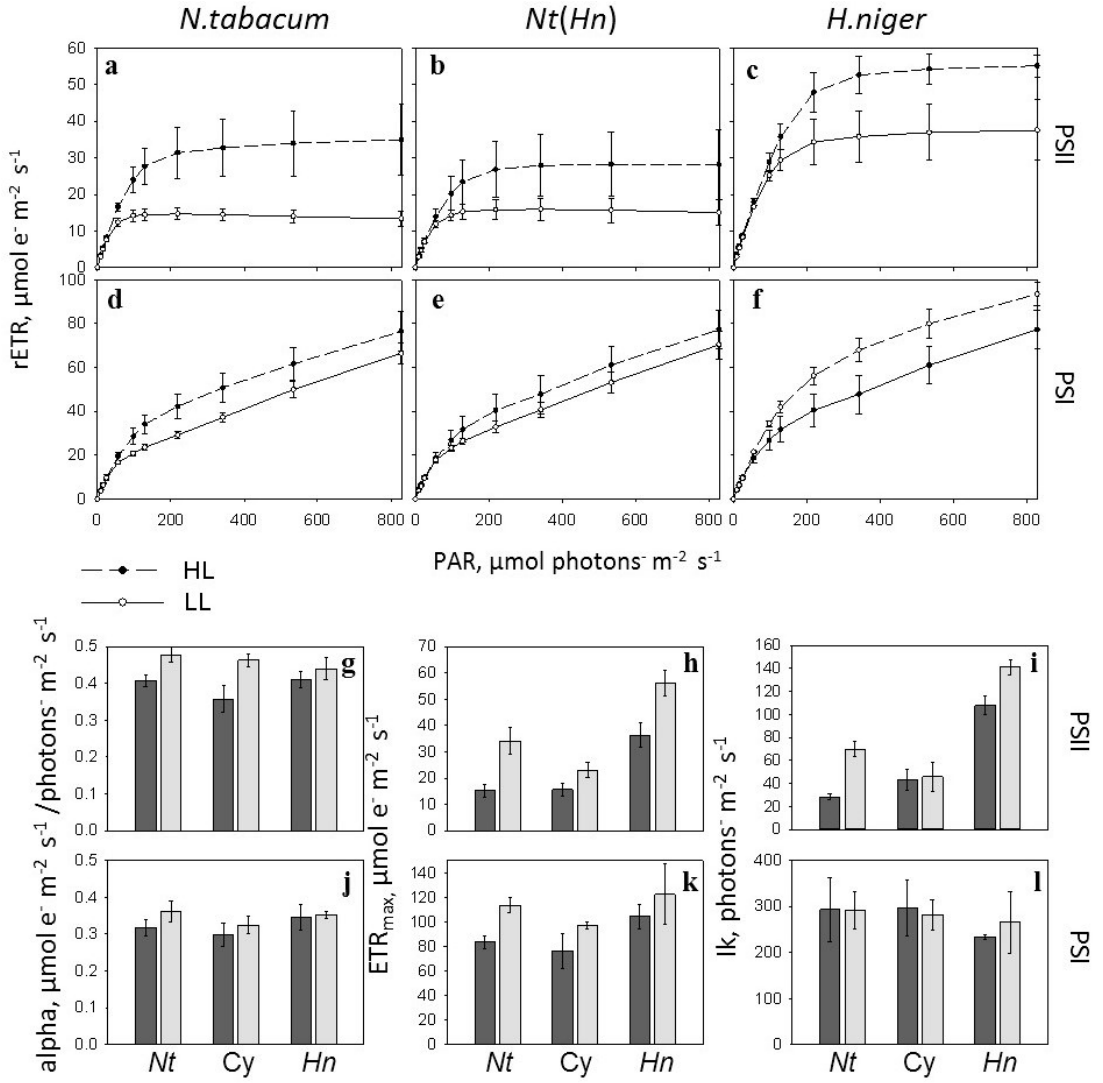


**Figure 4.15:** Rapid light curve analysis. **a-f)** RLCs measured from LL (○ *solid line*) and HL plants (● *dashed line*). Plots are rETR ($\mu$mol electrons $m^{-2}$ $s^{-1}$) against PAR ($\mu$mol photons $m^{-2}$ $s^{-1}$) in PSII (*a-c*) and PSI (*d-f*). **g-l)** RLC parameters of PSII (*top row*) and PSI (*bottom row*). $\alpha$, ETR in limiting light (*g,j*), $rETR_{max}$, limited by the photosynthetic pathway (*h,k*) and Ik, minimum saturating irradiance (*i,l*), calculated from the RLCs shown in *a-f* for LL (*dark grey bars*) and HL plants (*light grey bars*). Data are mean average ± SD from 3-4 measurements.

.

effective than *N. tabacum*, increasing by only about double that of LL (Fig 4.15b). rETR in PSI, also increased under HL although only marginally, indicating that PSII acclimation to GE light intensity was stronger than PSI (Fig 4.15d-f).

For a quantitative assessment, three parameters were measured from the RLCs. The first, $\alpha$, is a measure of the slope at the initial, linear portion of the RLC, calculated using:

$$\alpha = rETR \ / \ PAR \tag{4.3}$$

$\alpha$ is an indication of the ETR under non-saturating light, more specifically it indicates the electron turnover rate at PSII ($Q_A$), per photon absorbed ($\mu$mol $e^{-}m^{-2}s^{-1}/\mu$mol photons $m^{-2}$ $s^{-1}$). The second parameter, rETRmax, is a maximum ETR value, calculated at saturating actinic irradiance (White and Critchley, 1999), and is calculated using:

$$rETRmax = P_s(\alpha/\alpha + \beta)(\beta/\alpha + \beta)^{\beta/\alpha} \tag{4.4}$$

where $\beta$ is the slope of the light curve beyond the onset on photoinhibition. In the absence of photoinhibition, $\beta = 1$ (White and Critchley, 1999). The last parameter is Ik, calculated using the equation:

$$Ik = rETRmax \ / \ \alpha \tag{4.5}$$

Ik is a measure of the minimum saturating irradiance, when light is no longer a limiting factor, but is also not intense enough to cause photoinhibition.

Calculated parameter values are presented in Fig 4.15g-l. Usually, due to a larger LHCII antenna in LL grown plants, photon absorption is greater under non-saturating light conditions, than in HL plants, reflected in a high $\alpha$ value (Ralph and Gademann, 2005). However, here we found the opposite trend, where rETR in limiting light ($\alpha$), was slightly greater in HL plants, at both PSI and PSII (Fig 4.15g,j), suggesting that HL plant photosystems were able to absorb more light, presumably due to greater energy capture by the antenna systems.

Typically, plants grown in low light invest in antennas rather than reaction centres, in order to increase energy capture. This then means that if light intensity increases, the PSII turnover rate is quickly saturated and a low $rETR_{max}$ is established at relatively low minimum saturating irradience (Ik). This trend was reflected in our observations from the RLCs, and in calculated values for Ik and $rETR_{max}$. In *N.tabacum*, $rETR_{max}$ at PSII increased from 15 to 34 $\mu mole^{-}m^{-2}s^{-1}$ in HL, compared to LL, with the limitations of the photosynthetic pathway (Ik) becoming apparent from 63 $\mu$mol photons $m^{-2}$ $s^{-1}$and 28 $\mu$mol photons $m^{-2}$

$s^{-1}$respectively. As already explained these increases roughly reflect the difference in GE light intensity. Lowered PSII capacity of the HL grown *Nt*(*Hn*), as seen in the RLC, was quantified as a 32 % decrease in $rETR_{max}$ compared to HL *N.tabacum*, Ik was also reduced to 0.65 times the saturation point of *N.tabacum* HL.

In contrast, $rETR_{max}$ of PSII in LL *H. niger* was 2.4 times greater than LL *N.tabacum*, with the onset of electron pathway saturation at nearly 4 times greater at 107 $\mu$mol photons $m^{-2}$ $s^{-1}$. HL *H. niger* PSII $rETR_{max}$ was also increased, but less so to 1.64 times larger than *N.tabacum* at 59 $e^{-}m^{-2}s^{-1}$, with minimum saturation at 142 $\mu$mol photons $m^{-2}$ $s^{-1}$, a 64 % increase on *N.tabacum* HL.

The ETR of PSI in limiting light ($\alpha$) was relatively similar between all plant types indicating that the absorption capacity of PSI was comparable. In *H. niger*, PSI $\alpha$ was slightly larger in LL grown plants. PSI ETR of the HL grown *Nt*(*Hn*) was, in non-limiting light, larger than the LL grown plants in the RLCs, the difference was reduced at higher PAR (Fig 4.15e) and the maximum ETR was only slightly larger at 104.9 ± 3.9, compared to LL at 92.1 ± 16.0 (Fig 4.15k).

### 4.5.2 PSII quantum yield

**Table 4.1:** PSII quantum yields ($F_v/F_m$) calculated from dark adapted plants. Data are mean average ± SD, $\geqslant 5$.

| | $\Phi_{PSII}$ **LL** | $\Phi_{PSII}$ **HL** |
|---|---|---|
| ***N.tabacum*** | 0.822 ± 0.010 | 0.826 ± 0.013 |
| ***Nt*(*Hn*)** | 0.815 ± 0.017 | 0.827 ± 0.014 |
| ***H. niger*** | 0.832 ± 0.019 | 0.833 ± 0.012 |

In separate experiments, PSII quantum yields ($\Phi_{PSII}$) were calculated from dark adapted plants to obtain values for maximal $\Phi_{PSII}$. The results are shown in Table 4.1. *H. niger* $\Phi_{PSII}$, was highest at about 0.83 in both LL and HL grown plants. *N.tabacum* and *Nt*(*Hn*) both showed a slight increase in PSII efficiency in HL plants, with the larger difference in *Nt*(*Hn*) cybrids which had a similar HL $\Phi_{PSII}$ to *N.tabacum*, but a slightly decreased value in LL plants, however the differences were particularly small and all the values fell within the range expected for 'normally' functioning plants.

**Table 4.2:** A comparative summary of *N. tabacum*, *H. niger* and *Nt(Hn)* acclimative trends to LL and HL GEs. Expected LL/HL trends (from the literature) are shown using ↑ and ↓ to indicate relative increase and decrease respectively. Our findings are presented when they differed from expectation. '=' indicates no difference between LL and HL; 'x' = no data.

| **Level of** | **Feature** | ***N.tabacum*** | ***Nt(Hn)*** | ***H. niger*** | **Expected** | **Reference** |
|---|---|---|---|---|---|---|
| **Resolution** | | **LL HL** | **LL HL** | **LL HL** | **LL HL** | |
| *Leaf* | size | | | | ↑ ↓ | Nobel (2009) |
| | thickness | = | = | | ↓ ↑ | Terashima et al. (2001) |
| *Cell* | volume | ↑ ↓ | ↑ ↓ | | ↓ ↑ | Boardman (1977) |
| | inter-chloroplast space | | = | | ↑ ↓ | Oguchi et al. (2003) |
| *Chloroplast* | no. chloroplasts unit cell vol.$^{-1}$ | | | | ↓ ↑ | Wild and Wolf (1980) |
| | diameter | | = | | ↑ ↓ | Anderson et al. (1988); Givnish (1988) |
| | starch content | | | | ↓ ↑ | |
| | plastoglobulin | | | | ↓ ↑ | |
| *Grana* | grana per $\mu$m$^{-2}$ stroma | ↓ ↑ | | ↓ ↑ | ↑ ↓ | Anderson and Aro (1994) |
| | no. of layers stack$^{-1}$ | | = | | ↑ ↓ | Walters (2005) |
| | stack diameter | | ↓ ↑ | | ↑ ↓ | Lichtenthaler et al. (1981) |
| *Proteins* | Chl a:b | | | | ↓ ↑ | Anderson et al. (1995) |
| *pigments* | Car:Chl | | ↑ ↓ | | ↓ ↑ | Zivcak et al. (2014) |
| | Lutein:Chl | ↑ ↓ | | ↑ ↓ | ↓ ↑ | Demmig-Adams et al. (1996) |
| | $\beta$-car:Chl | | | | ↓ ↑ | Matsubara et al. (2009) |
| | XC pool size | | | | ↓ ↑ | Valladares and Niinemets (2008) |
| *Physiological* | $\Phi_{PSII}$ (Fv/Fm) | | ↓ ↑ | | = | Walters (2005) |
| *response** | PSII $\alpha$ | ↓ ↑ | ↓ ↑ | ↓ ↑ | ↑ ↓ | Ralph and Gademann (2005) |
| | PSII ETR$_{max}$ | | | | ↓ ↑ | Ralph and Gademann (2005) |
| | PSII Ik | | = | | ↓ ↑ | Ralph and Gademann (2005) |
| | PSI $\alpha$ | ↓ ↑ | ↓ ↑ | = | ↑ ↓ | Ralph and Gademann (2005) |
| | PSI ETR$_{max}$ | | | | ↓ ↑ | Ralph and Gademann (2005) |
| | PSI Ik | = | = | | ↓ ↑ | Ralph and Gademann (2005) |

*apart from $\Phi_{PSII}$, expected physiological response trends are compared to data from *Zostera marina*, (Ralph and Gademann, 2005)

**Table 4.3:** A results summary that compares *N.tabacum* (T) and *H. niger* (H) phenotypes in LL and HL GEs. The response of the *Nt*(*Hn*) is indicated as either resembling T or H, or as differing from both parent species using arrows. Double arrows indicate significant difference; '=' indicates no difference between the plant types.

| **Level of** | **Feature** | **Low light** | | | | **High light** | | | |
|---|---|---|---|---|---|---|---|---|---|
| **Resolution** | | ***Nt*** | ***Hn*** | **Cy** | **notes on *Nt*(*Hn*)** | ***Nt*** | ***Hn*** | **Cy** | **notes on Cy** |
| *Leaf* | thickness | ↓ | ↑ | T | slightly larger | ↓ | ↑ | T | |
| | size | n | nc | T | slightly smaller | n | nc | T | slightly smaller |
| *Cell* | volume | ↑ | ↓ | T | slight increase | ↓ | ↑ | T | slightly larger |
| | inter-chloroplast space | ↑ | ↓ | ↓↓ | no space | = | = | = | no space |
| *Chloroplast* | no. chloroplasts unit cell vol.$^{-1}$ | ↓ | ↑ | H | | ↑ | ↓ | T | |
| | diameter | = | = | ↓ | significantly less | = | = | = | slightly less |
| | starch content | ↑ | ↓ | ↑↑ | significantly more | ↑ | ↓ | ↑↑ | significantly more |
| | plastoglobulin | = | = | ↑ | slightly more | ↑ | ↓ | T | slight increase |
| *Thylakoids* | no. grana per $\mu$m$^{-2}$ stroma | = | = | ↓ | slight reduction | = | = | ↓↓ | significant decrease |
| | grana diameter | ↓ | ↑ | T | | = | = | ↑↑ | significant increase |
| | average no. layers grana$^{-1}$ | = | = | = | slightly more | = | = | ↑↑ | large increase |
| *Proteins* | PS:LHCII$^{\bullet}$ | x | x | x | | ↓ | ↑ | H | |
| *pigments* | Chl a:b | = | = | = | slight reduction | = | = | = | slight reduction |
| | Carotenoid:Chl | = | = | ↓ | slight reduction | = | = | ↑ | slight increase (9 %) |
| | Lutein:Chl | = | = | ↓ | slight reduction | = | = | ↑↑ | large increase |
| | XC pool size | = | = | = | | ↓ | ↑ | ↑↑ | large increase |
| *Physiological* | $\Phi_{PSII}$ (Fv/Fm) | ↓ | ↑ | T | slightly lower | ↓ | ↑ | T | |
| *response* | PSII $\alpha$ | = | = | ↓ | | = | = | = | |
| | PSII ETR$_{max}$ | ↓ | ↑ | T | | ↓ | ↑ | ↓↓ | |
| | PSII Ik | ↓ | ↑ | T | slightly larger | ↓ | ↑ | T | slight increase |
| | PSI $\alpha$ | = | = | = | slight reduction | = | = | = | slight reduction |
| | PSI ETR$_{max}$ | ↓ | ↑ | T | slight reduction | = | = | = | slight reduction |
| | PSI Ik | ↑ | ↓ | T | | ↑ | ↓ | T | |

nc = not comparable; n = normal

$^{\bullet}$PS:LHCII ratios are estimated based on the % content of peaks III and V of the FPLC elution profiles.

## 4.6 Discussion

The aim of the work presented in this chapter was to investigate the *Nt*(*Hn*) cybrid's capacity for acclimation to LL and HL intensity environments. To collate the results for a comparative overview of acclimation in *Nt*(*Hn*), we have produced two tables. In the first, Table 4.2, we have summarised the results to compare LL grown plants with HL grown plants in order to indicate the acclimative trends to the light environment in each plant line. We do this by comparing our findings to those that were expected according to the literature, our result is entered in the table when it differed from the 'expected'.

In Table 4.3, the data has been rearranged to compare *Nt*(*Hn*) with *N.tabacum* and *H. niger* phenotypes from each GE. To do this, we first compare *N.tabacum* and *H. niger*, then indicate whether the *Nt*(*Hn*) result was similar to the nuclear or chloroplast parent, or whether it differed from both. Significant differences are represented by a double arrow. Twenty-five parameters were summarised, ranging from trends in leaf size to electron transport rates (Tables 4.2 and 4.3).

In general, the wildtype plants conformed to the expected trends in relative LL/HL acclimation, although there were some exceptions. In four cases both wildtype species deviated from what was expected as according to the literature, and *N.tabacum* was different in a further three (Tables 4.2). The *Nt*(*Hn*) cybrid's acclimative response to LL/HL, on the whole resembled *N.tabacum* as might be expected under *N.tabacum* nuclear control (Table 4.3). In six instances *Nt*(*Hn*) deviated from the acclimative trend found in *N.tabacum* (Table 4.2).

A comparison between LL plants, found that in nine parameters, *Nt*(*Hn*) deviated from the measured *N.tabacum* parameter, in four of these, the deviation was strong, one of which, number of chloroplasts per unit area of cell, was found to be more similar to *H. niger* (Table 4.3). In comparing the HL plants we found that there were ten cases in which *Nt*(*Hn*) results were notably different from *N.tabacum*. Most differences were the same deviations as seen in LL *Nt*(*Hn*) plants with the exception that, grana diameter and XC pool size were more altered under HL.

It was also interesting to note that under HL, the number of chloroplasts per unit cell area in *Nt*(*Hn*) was more similar to the nuclear parent, in contrast to the *Nt*(*Hn*) plant grown under LL, in which chloroplast number resembled the chloroplast parent *H. niger*. Of the results that were similar to *N.tabacum*, most of them also showed some slight difference (Table 4.3). These responses and others are further discussed below. It should be emphasised that the observed similarities of the *Nt*(*Hn*) to one or other parent plant were correlative and do not necessarily imply causality based on nuclear or chloroplast influence.

### 4.6.1 Leaf and cell phenotypes under LL/HL

Although *Nt(Hn)*, like *N.tabacum*, was found to be smaller under HL, the correlation between light intensity and plant size was weaker in *Nt(Hn)* plants, which, unlike *N.tabacum*, were difficult to distinguish by eye as LL or HL grown. This indicated that a stronger variable than light intensity determined the plant's size. Investment in a larger leaf area, as seen in LL or shade plants, is usually at the cost of leaf thickness (Valladares and Niinemets, 2008). Surprisingly, here, leaf thickness was even slightly less in the HL *N.tabacum* and *Nt(Hn)* compared to LL.

The increased leaf thickness in HL *H. niger* was at least partly due to the increased length of the pallisade mesophyll cells (Fig 4.5i). Elongation along the axis perpendicular to the leaf surface, allows cell expansion while maintaining relatively high density packing in the mesophyll layer, at the same time, the arrangement also promotes light penetration further into the leaf through internal reflections (Nobel, 2009). Indeed, in the HL *H. niger* plants, large intercellular spaces are present between the pallisade mesophyll cells (Fig 4.2f), presumably to increase $CO_2$ movement amongst them. In fact, the slightly larger leaf cross-section of the *N.tabacum* and *Nt(Hn)* LL plants may also be due to the increased size of the LL pallisade mesophyll cells, which showed some increase in length compared to HL cells, although unusually, a greater increase was in width (Fig 4.5).

Some further evidence of an unusual phenotype at the cellular level in the LL *N.tabacum* cells, was found in the plots between cell volume and number of chloroplasts (Fig 4.6). Close correlations between cell size and chloroplast number have been reported consistently across plant species in the literature (Pyke and Leech, 1987), and was observed here as a strong trend in *H. niger*. However, the increased volume of the LL *N.tabacum* cells skewed this trend. Environmental factors affecting cell size are temperature and water stress, although these are normally accompanied by smaller cells (Nobel, 2009). The same pattern was seen to be inherited by *Nt(Hn)* although, interestingly, chloroplast numbers were higher in *Nt(Hn)* than *N. tabacum*, particularly when grown in LL.

Another feature associated with $CO_2$ diffusion was apparent in *N. tabacum* and *H. niger*, but was absent in *Nt(Hn)*. Open spaces between chloroplasts aligned along the cell wall, were found in leaf cross-sections in the LL wildtype plants only (Fig 4.2). A decrease in the area of chloroplast surface facing the intercellular spaces indicates a reduced demand for $CO_2$ under LL (Oguchi et al., 2003) as the amount of $CO_2$ diffusion $CO_2$, to sites of carboxylation in the chloroplast(Nobel, 2009) is reduced. The spaces were absent in the LL *Nt(Hn)* and instead chloroplasts were fairly densely packed along the cell periphery. This is also reflected in the high numbers of chloroplasts seen in the LL *Nt(Hn)* cells. The increased area

of chloroplast surface facing the intercellular space in *Nt*(*Hn*) could indicate an increased diffusion of $CO_2$ into the cells, compared to the wildtype species.

Increased $CO_2$ uptake is usually associated with an increased activity of ribulose-1,5-bisphosphate carboxylase/oxygenase (Rubisco) (Evans et al., 1994), which can lead to an accumulation of starch. A large starch content was certainly evident in LL grown *Nt*(*Hn*) from the TEM micrographs, and as a deposit in tube after centrifugation during the preparation of thylakoids. The expression of Rubisco was not measured during this study, but Rubisco's subunits, rubisco large subunit (rbcL) and rubisco small subunit (rbcS), are encoded in the chloroplast and nucleus respectively. In cybridised plants there is thus the potential for alteration of the Rubisco complex, through mis-assembly, inefficient co-regulation of the subunits or mis-processing.

In a study by Wang et al. (2010), Rubisco and Rubisco activase were reported to be significantly upregulated in a cybrid combination of *Citrus unshiu*(*Citrus grandis*). However, for cpDNA analysis of the *Nt*(*Hn*) cybrids, Zubko et al. (2001) hybridised cpDNA with *rbc*L. In the Southern blots shown in Fig 3.4, the banding patterns are the same as in *H.niger*, however, DNA content is reduced which might indicate a smaller amount of *rbc*L gene in *Nt*(*Hn*), with the consequence of reduced protein expression. It is also possible that it could instead be due to unequal amounts of DNA loaded in the wells as the methods state '3-5 $\mu$g per lane'. Furthermore, the finding of Wang et al. (2010) has not been reported in the numerous other cybrid plants of *Nicotiana* species. However, research aiming to improve the turnover rate of Rubisco, as the rate limiting step for photosynthetic efficiency, is extensive (Ellis, 2010; Lin et al., 2014), and the cybrid plant shows potential as an interesting model for Rubisco research.

### 4.6.2 Light acclimation of the chloroplast and thylakoids

The typical trend for reduced chloroplast size in a HL environment (Givnish, 1988), was observed here in *N.tabacum* and *H.niger*, based on measurements of chloroplast diameter. *N.tabacum* and *H.niger* chloroplast size was also remarkably similar in both GEs. *Nt*(*Hn*) chloroplast size however was not changed in response to its light environment, and in fact the size was even marginally smaller in HL compared to LL *N.tabacum* and *H.niger*. Furthermore, the unusually large starch content of the *Nt*(*Hn*) cybrid chloroplasts, even in LL, greatly impeded on the % stromal content, and seemed, from TEM analysis (Fig 4.7), to impact the organisation of the thylakoid membrane.

Cave et al. (1981) found that the build up of large starch grains in plants under high $CO_2$ concentrations was likely to have directly disrupted chloroplast

structure and function in clover plants, resulting in a decrease in Chl content. Starch is synthesised in the chloroplast as a product of photosynthesis where it accumulates during the day. At night it is degraded and then exported from the chloroplast. The study by Cave et al. (1981), does not indicate whether the effect on Chl content was lessened after starch depletion during the night, but if this is the case, the amplitude of the starch impact might also follow a diurnal pattern. We did not measure changes in starch content over a diurnal period but it would be interesting to see if the quantity of starch that was accumulated during the day, was fully diminished after night, or whether night-time starch degradation pathways were somehow disrupted in *Nt*(*Hn*).

The chloroplast proteins involved in starch degradation are the nuclear-encoded, glucan water dikinases (GWDs; Hejazi et al., 2012; Edner et al., 2007; Ritte et al., 2002). When the night-time supply of starch-derived carbohydrate is reduced, either because of reduced starch synthesis in the day or inhibited degradation at night, plant growth rates can be severely affected (Smith et al., 2005). A reduction in starch degradation could provide an explanation for the starch accumulation observed in the *Nt*(*Hn*) as well as for the reduced growth rates of *Nt*(*Hn*). The comparison of starch content between mature wildtype plants and *Nt*(*Hn*) must also take into consideration that the *Nt*(*Hn*) plant was several weeks older and increased starch content is known to be a feature of older leaves.

Anderson and Aro (1994) describes an acclimative trend for increased number of grana and more extensive stacking in low light or shade plants. In agreement with these results we found a increased stacking in grana of LL *N.tabacum* and *H.niger*, although we found, the number of grana per unit area of stroma was higher in HL plants. *Nt*(*Hn*) did show lower grana number in the HL plants although this may be related to an impact of the greatly increased starch content of the HL plants on grana formation, rather than direct inhibition of acclimative pathways. Anderson and Aro (1994) point out that even within the cell, a gradient of stacking and grana number can occur between chloroplasts lying along the light gradient that naturally occurs in the cell from light attenuation due to photosynthetically active interceptors. It might be then, that our sample size was not sufficient to account for these differences and the LL/HL grana ratio is not representative of the average.

### 4.6.3 Acclimation of the thylakoid membrane complexes

Although not quantified here, due to only partial resolution of the contents of the FPLC fractions, we observed that *Nt*(*Hn*) more closely resembled *H. niger* than *N. tabacum* in the shape of the FPLC elution profiles. A rough calculation of

the peak (III+IV):V protein ratios (measured from absorbance at 280 nm), where peak V fairly certainly contained the LHCII trimers and the content of peaks III and IV were estimated from MW based separating gels, absorption and emission spectra to be predominantly PSI and PSII, gave an indication of the PS:LHCII ratio. This data indicates that PS:LHCII ratios in the *Nt(Hn)* were more similar to *H. niger* than *N. tabacum*. This could suggest that the amount of LHCII was stoichiometrically determined by the quantity of chloroplast-encoded reaction centre proteins.

### 4.6.4 Pigment content under HL/LL

The increased lutein content of LL *N.tabacum* and *H.niger* was in disagreement with the trends described by Demmig-Adams et al. (1996), who found that, in respect to Chl content, lutein decreased in shade grown *Smilax australis* compared to sun-grown plants. $\beta$-carotene content, in the same plants was, conversely enhanced. Our results showed the opposite trends in both cases. However a report by (Matsubara et al., 2009) found that lutein content, calculated on a Chl basis was highly variable between sun and shade species of 86 forest plants, with mean average values showing no significant difference. Furthermore their finding that $\beta$-carotene content was strongly enhanced in sun plants supported our findings (Table 4.2).

### 4.6.5 Electron transport rates

From the rapid light curves (Fig 4.15), it was interesting to find that $\alpha$, which gives an indication of the ETR under limiting light, was larger in HL plants than LL plants at both PSI and PSII in *N. tabacum*, *H. niger* and *Nt(Hn)*, suggesting greater energy capture by HL photosystem complexes in all cases. Typically, the reverse trend is found due to an increased antenna size in LL grown plants. LHCII antenna size can be roughly approximated from the Chl*a:b* ratios. We found that *N. tabacum*, *H. niger* and *Nt(Hn)*, all had a greater Chl*a:b* ratio under HL (Fig 4.11), which indicates a typical decrease in the Chl *b*-containing LHCII, relative to LL grown plants. Further evidence for an increased quantity of LHCII under LL, was found in comparing the FPLC data for LL and HL grown *N. tabacum*.

The slight reduction in $ETR_{max}$ in *Nt(Hn)*, might indicate a reduced electron sink capacity. $CO_2$ fixation in the Calvin-Benson cycle is the primary electron sink in photosynthesis. Rates of $CO_2$ fixation are limited by the slow enzyme activity of Rubisco and research aiming to improve photosynthetic efficiency by increasing the turnover rate of Rubisco is extensive (Ellis, 2010; Lin et al., 2014). Rubisco's subunits, rubisco large subunit (rbcL) and rubisco small subunit (rbcS), are encoded

in the chloroplast and nucleus subgenomes respectively. In cybridised plants there is thus the potential for novelty in the Rubisco complex, through mis-assembly, inefficient co-regulation of the subunits or post-translational misprocessing. Such an effect in the *Nt*(*Hn*) cybrid could explain the decreased ETRmax in the HL plants, furthermore it might suggest that such alteration was dependent on the prevailing light environment, as the effect was not observed in LL grown *Nt*(*Hn*) cybrids, where instead ETRmax was comparable to that of *N. tabacum*.

Chapter 5

# Molecular mechanisation against short-term changes in light

## 5.1 Introduction

Plant fitness depends upon rapid self-regulatory adjustments to the shot-term fluxes of natural light. This is most crucial, at the site of membrane-bound light harvesting and photochemical processes. Regulatory molecular mechanisms have evolved in plants to minimise the limitations imposed on the electron transport rate, caused by imbalanced excitation of PSII and PSI complexes, that occur under light-limiting or non-saturating light (NSL). Protective mechanisms have also evolved to rapidly switch the LHCII complex between the roles of harvesting energy into the system and expelling energy away from it to defend against the dangerous risk caused by trapped excess energy.

The associations of the interspecifically encoded LHCII and photosystem complexes of a cybrid plant have, as far as we are aware, never been investigated in terms of state transitions or non-photochemical quenching. These mechanisms however are based precisely upon the close associations and rapid, cooperative interactions of the chloroplast encoded PSII and PSI cores with the nuclear-encoded antennas. In this chapter we investigate these mechanisms as well as some of the components involved in their mechanism.

## 5.2 An assessment of state transitions

### 5.2.1 Room temperature fluorescence measurements

Chlorophyll fluorescence was traced during application of a standard light regime for inducing state transitions, details of which are given in §2.9.4, Fig 2.2. The main

principle behind the established protocol for RT state transition measurements using the Chl *a* fluorescence signal, is the selective drive or slow-down of PSI by the addition or removal of far red light (FR; 730 nm) respectively, while PSII is driven continuously by a weak actinic light (AL; 635 nm) (see Fig. 2.2). In theory, superimposing FR over weak AL preferentially drives PSI compared to PSII, producing an oxidised PQ pool. In turn, the removal of FR inhibits PSI resulting in PQ pool reduction.

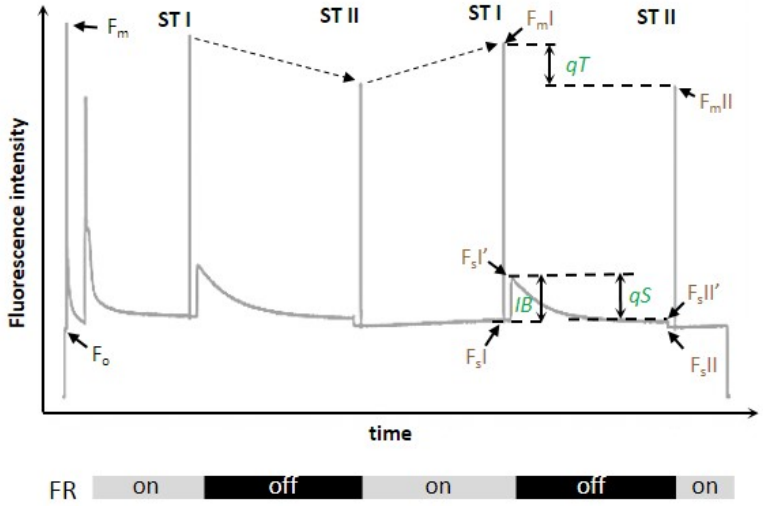


**Figure 5.1:** Schematic diagram describing the quantification of state transitions from RT fluorescence measurements. Measured (brown) and derived (green) parameters are indicated on a typical fluorescence trace, dashed arrows indicate the recovery of F'$_m$ from STII to STI . The derived parameters, IB, qT and qS are not precisely depicted as the final calculations also include division by Fo, Fm and (F$_s$I' – F$_s$II) respectively (Ruban and Johnson, 2009). (See main text of §5.2 for full explanation).

State transition measurements are quantified using parameters calculated from measured fluorescence transients. To describe these parameters a typical Chl fluorescence measurement made during the standard light regime is presented in Fig. 5.1. The fluorescence transients and the three parameters that describe state transitions, qS, qT and IB, are indicated. Maximal (F$_m$) and minimal (F$_o$) fluorescence are first measured from dark adapted leaves, then, after 15 min of light induction (AL + FR), two 15 min FR on/off cycles are applied. Measurements are made from the second cycle to avoid the confounding effects of induction kinetics after dark adaptation that may be present in the first. After 15 min of treatment with FR, the fluorescence yield reaches a steady state in state I (F$_s$I), a saturating

pulse is then applied to measure the PSII antenna size ($F_mI$). FR is then removed, and the subsequent reduction of the ETC is observed as an immediate increase in fluorescence to $F_sI$'. We can then obtain a calculation of imbalance (IB) using the equation:

$$IB = (F_sI'–F_sI)/F_o \tag{5.1}$$

IB indicates the relative extent of the reduction of the PQ pool and thus indicates the signal strength for activation of the kinase involved in phosphorylation of LHCII. Typically, IB falls within the range of 50 - 70 % (Ruban and Johnson, 2009).

The fluorescence rise to $F_sI$' after FR removal is followed by a gradual decrease over about 15 min (Fig 5.1). This is firstly because the PSII antenna size is reduced, so fewer photons are absorbed and the fluorescence signal correspondingly decreases and secondly, because the photochemical pathway at PSII opens as electron flow at PSI increases. When fluorescence reaches a steady state without FR ($F_sII$'), FR light is re-applied to reveal $F_sII$. A calculation called qS can then be made using:

$$qS = (F_sI' - F_sII')/(F_sI'–F_sII) \tag{5.2}$$

qS indicates how fully state transitions have managed to rebalance energy flow between the photosystems and is typically above 50 %, with 100 % indicating that the ETR is fully restored by transition to STII (Ruban and Johnson, 2009).

The third calculation, qT, is considered as a fluorescence decline rather than true quenching as it is an assessment of the difference in PSII antenna size in STI ($F_mI$) and STII ($F_mII$) and is obtained by the application of a saturating pulse (SP) during steady state conditions with and without FR (Fig 5.1). qT is defined as:

$$qT = (F_mI - F_mII)/F_mI \tag{5.3}$$

qT is normally variable between 0-25 % (Ruban and Johnson, 2009).

Representative RT state transition measurements from mature *N.tabacum*, *H.niger* and *Nt*(*Hn*) plants grown in HL and LL, are presented in Fig 5.2a. Wild-type plants were typical in their response to the changes in FR light. After FR removal, the sharp increase in fluorescence can be seen in all the traces, although in HL plants to a somewhat lesser degree. The subsequent fluorescence signal of *Nt*(*Hn*) plants was markedly different from the parental wildtypes. After the initial fluorescence increase, in *N.tabacum* and *H.niger*, the fluorescence signal decreased quickly, then more slowly until a steady state was reached near $F_sI$ levels. In

contrast, the drop in the florescence signal from *Nt*(*Hn*) was minimal with levels remaining closer to $F_s$I', even after 15 min without FR.

There were also differences in the PSII antenna size changes. In both wildtype species, the SP yielded a smaller signal 15 min after FR removal ($F_m$II) compared to the signal after 15 min with FR light ($F_m$I), indicating that the adsorption capacity at PSII had been reduced. In *Nt*(*Hn*) however, the signal during SPs was relatively similar when adapted to light with or without FR. Importantly, the drop in $F_m$ from STI to STII was shown to be reversible in the wildtype plants between with full recovery of $F_m$I from $F_m$II in the first FR on/off cycle (Fig 5.2 and Fig 5.1, dashed arrows), indicating that the fluorescence reduction was not due to photoinhibition.

The values for IB, qT and qS, that were calculated from these traces are presented in Fig 5.2b. The fluorescence increase after removal of FR, observed in all plant types, was lower in HL plants compared to those from LL, as shown in the comparatively low IB values of the HL plants. Mean average IB values from the LL plants, all fell within the normal range (Ruban and Johnson, 2009) at 57.5 % ± 15, 52.3 % ± 12.3 and 47.8 % ± 5.0, for *N.tabacum*, *Nt*(*Hn*) and *H.niger*, respectively (Fig 5.2b). An analysis of variance (ANOVA) found that the difference in IB between LL grown plants was not statistically significant ($p = 0.498$). The result indicated that the experimental light set-up effectively reduced the PQ pool to proportionally comparable levels in each LL grown plant type.

Despite the comparable IB values, the size of the PSII antenna in *Nt*(*Hn*), as already noted, showed little difference before or after FR removal compared to wildtype. The calculated mean averages of the corresponding state transition parameter, qT, demonstrated the observation quantitatively with values at 11.6 % ± 1.5 and 7.7 % ± 2.0 in *N.tabacum* and *H.niger* LL grown plants respectively with about half the level at 5.7 % ± 0.8 for *N.tabacum* and 3.4 % ± 2.3 for *H.niger* in HL grown plants, these values are comparable with those of wildtype plants reported in other studies (Bellafiore et al., 2005; Damkjaer et al., 2009). In contrast, qT in *Nt*(*Hn*) was much smaller at 2.0 % ± 0.7 and 1.7 % ± 0.8 for LL and HL grown plants respectively (5.2).

The restoration of balanced electron transport in LL plants after 15 min of FR removal (qS) was nearly complete in *N.tabacum* at 90.3 % ± 6.9 and was high in *H.niger* at 63.2 % ± 15.4. qS was significantly reduced in LL *Nt*(*Hn*) plants at 22.0 % ± 8.3. In the HL plants, qS was unchanged in *N.tabacum* at 89.6 % ± 5.5 and increased somewhat in *H.niger* to 89.8 % ± 5.6. In *Nt*(*Hn*) qS was also increased to 41.2 % ± 9.0 (Fig 5.2b). At first sight, an increase in qS in the HL plants, seems to contradict the decrease in qT, however qS enhancement can be explained in consideration of the low IB values, as the qS parameter is calculated

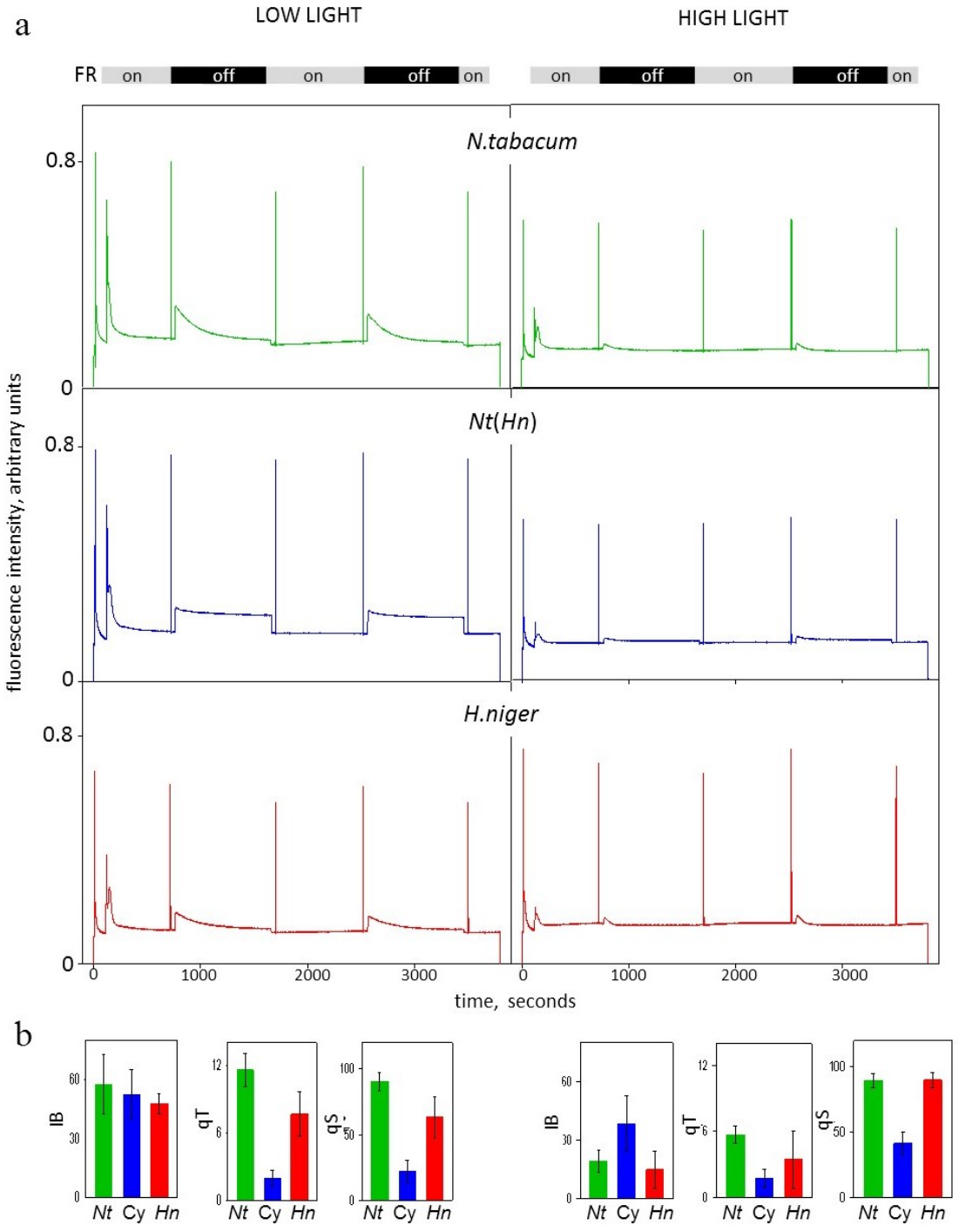


**Figure 5.2:** State transitions in *N.tabacum* (*green*), *Nt*(*Hn*) (*blue*) and *H.niger* (*red*), grown in LL (*left*) and HL (*right*). **a)** Fluorescence traces measured from leaves during subjection to a typical light regime, to induce transitions between STI and STII at room temperature. The grey and black bars at the top of the figure indicate when far red light (FR) is on/off. **b)** Parameters qT, qS and IB calculated from the traces in *a*. Data are mean average ± standard deviation, n ⩾ 3.

proportionally to the change in fluorescence after FR light removal (see Eq. 5.1).

### 5.2.2 77K fluorescence emission spectra

RT fluorescence measurements assess fluorescence changes at PSII and although they can indicate transfer of the LHCII antenna away from PSII, they are not conclusive as to whether the antenna has transferred and functionally attached to PSI. In order to ascertain antenna size change at PSI, measurements were made at liquid nitrogen ($LN_2$) temperatures (77 K) at which the effects from whole chain electron transport and the Calvin-Benson cycle on the PSI fluorescence signal are reduced (Krause et al., 1989). As IB was greatest in the LL grown plants, pertaining to normal wildtype values, further investigation of state transitions was performed on LL grown plants only.

77 K measurements were taken from leaf tissue collected from samples that had been brought to $F_s$I and $F_s$II' during RT light treatment, the points at which samples were collected are indicated in Fig 2.2 as 'I' and 'II', respectively. Upon removal from the DUAL-PAM equipment, the leaf tissue was quickly ground in buffer and frozen in $LN_2$. For fluorescence emission spectra, excitation was defined at 435 nm and fluorescence emission was measured from 660 -780 nm. The traces were normalised at 685 nm, the PSII maximum, in order to detect changes in fluorescence from PSI (735 nm maximum). The results are presented in Fig 5.3a.

The emission peak at 735 nm originates from Chl *a* molecules of LHCI in the PSI-LHCI complex (Morosinotto and Bassi, 2007). If LHCII is functionally attached, the fluorescence signal from LHCI increases due to energy transfer from LHCII. In Fig 5.3a, there is a clear increase in the fluorescence signal from PSI (735 nm) in $F_s$II samples compared to the $F_s$I samples, and relative to the signal from PSII at 685 nm, in both *N.tabacum* and *H.niger*. This indicates that the samples are truly in STII and STI respectively. In stark contrast there is no difference in the PSI emission spectra after FR removal in *Nt*(*Hn*), indicating that the mobile portion of LHCII did not change position either by detachment from PSII nor by attachment to PSI.

From Fig 5.3a, we also noted an apparent reduction in the shoulder at 680 nm in *Nt*(*Hn*) emission spectra, compared to *N.tabacum* and *H.niger*. Emission at this wavelength is characteristic of trimeric LHCII (Andreeva et al., 2010; Johnson and Ruban, 2009). A closer analysis comparing *N.tabacum*, *H.niger* and *Nt*(*Hn*) samples at $F_s$I and $F_s$II is presented in Fig 5.3b. Here we see that the differences between wildtype and *Nt*(*Hn*) plants is greater in STII compared to STI. In order to determine how the size of the shoulder changes relatively between each plant type, the fluorescence intensity at this peak is tabulated in Fig 5.3c. From the

table we can see that the 680 nm shoulder increases in STII compared to STI by about 9 % in *N.tabacum* and 6 % in *H.niger*, relative to the PSII maximum (685 nm). In *Nt*(*Hn*) there is no notable change in 680 nm florescence between samples and in fact, is relatively smaller by at least 7 % of *N.tabacum* (Fig 5.3c). It is not possible to tell whether this shoulder is emitted from LHCII trimers that are functionally attached to PSI, PSII or uncoupled.

Lastly, in the emission spectra we also observed a slight variation in emission at 695 nm, the main difference was observed between STI and STII in *H.niger* in Fig 5.3a. Interestingly, from parts b) and c) of Fig 5.3, we can see that changes in the size of the 695 nm shoulder occur only in *H.niger* in which emission increases by about 8 % from STI to STII, relative to the 685 nm peak. In *N.tabacum*, by contrast there is a negligible, decrease of 2 % while *Nt*(*Hn*) remained constant. The 695 nm shoulder revealed at low temperature fluorescence has been characterised as emission from a red-shifted Chl *a* of CP47 (Andrizhiyevskaya et al., 2005).

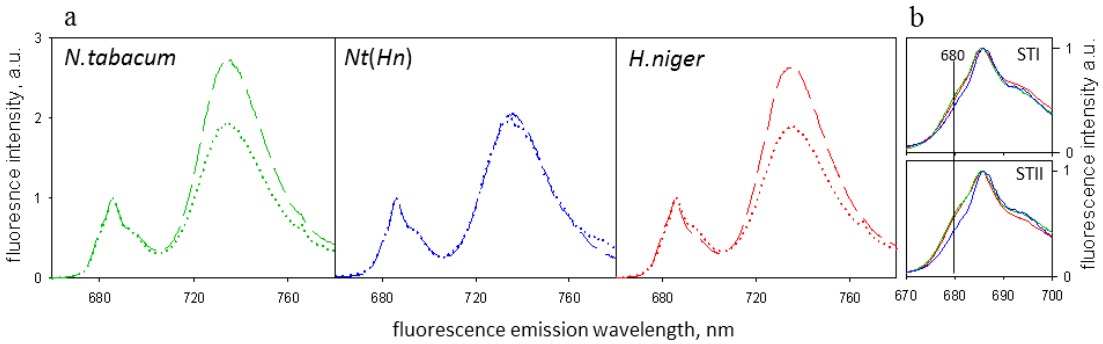


**c**

| **Fluo.** $\lambda$ | **680 nm** | | **695 nm** | |
|---|---|---|---|---|
| **State** | **I** | **II** | **I** | **II** |
| *N.tabacum* | 0.53 | 0.62 | 0.58 | 0.56 |
| *Nt*(*Hn*) | 0.46 | 0.45 | 0.57 | 0.57 |
| *H.niger* | 0.52 | 0.58 | 0.53 | 0.61 |

**Figure 5.3:** The 77 K fluorescence emission spectra from leaf homogenates. Excitation was defined at 435 nm and spectra were normalized at 685 nm (the PSII maximum) in order to observe the relative changes in fluorescence from PSI (735 nm) **a)** measurements taken from leaf tissue treated with FR light for the induction of STI (LHCII-PSII) (*dotted line*) or without FR light for the induction of STII (LHCII-PSI) (*dashed line*). **b)** detail of emission from PSII in STI and STII. The vertical line highlights the shoulder at 680 nm **c)** Fluorescence intensity at 680 nm and 695 nm relative to fluorescence at 685 nm, at which the spectra were normalised.

### 5.2.3 77K fluorescence excitation spectra

Attempts were made to record 77 K excitation (or action) spectra from the same samples as those in the fluorescence emission spectra. These results were desirable because we cannot rule out the possibility that the increase in fluorescence observed at PSI in Fig 5.3 is actually only a decrease in fluorescence at PSII which has been obscured through normalisation at the PSII maxima. Furthermore, although the findings show that *Nt*(*Hn*) emission spectra showed no difference after treatment with or without FR light, it is not possible to detect from these results whether the photosynthetic apparatus of *Nt*(*Hn*) was in STI or STII, i.e. there is the possibility that LHCII was invariably and functionally attached to PSI.

In excitation spectroscopy, the excitation monochromator issues a spectrum of wavelengths while fluorescence emission detection is fixed. By exciting each sample with light from 400 - 550 nm and detecting fluorescence at 680 nm (F680) or at 735 nm (F735), we obtain the action spectra of PSII or PSI respectively. However, because the amplitude of absorption is not a linear function of pigment concentration, meaning that as pigment concentration increases, the excitation spectrum changes shape through broadening (Ruban, 2012).

Controlling sample concentration is inherently difficult in this method. We found that although measures were taken to prepare leaf homogenates with the same OD, the inherent problems involved with homogenising leaf tissue at 77 K in buffer, followed by transfer to the sample holder, caused inconsistency between the concentrations of the measured samples. Between sample comparisons were therefore not possible as we could not be sure that differences between the excitation spectra were not due to differences in sample concentration causing qualitative alteration in the spectra.

## 5.3 An investigation of photoprotection: pNPQ

The chlorophyll fluorescence signal, was traced at room temperature from dark-adapted, mature leaves, during the application of a typical light regime for NPQ induction. Minimal ($F_o$) and maximal ($F_m$) fluorescence were measured from the dark-adapted plants prior to application of high intensity (700 $\mu$mol photons $m^{-2}$ $s^{-1}$) actinic light (AL) for 5 min. AL was then removed for 5 min. During the entire period, a saturating pulse (SP) was applied every 1 min to measure changes in maximal fluorescence $F_m$'. From these fluorescence traces, non-photochemical quenching (NPQ) was calculated using the following equation:

$$NPQ = (F_m - F'_m)/F'_m \tag{5.4}$$

where $F_m$ is the fluorescence maximum from the dark adapted sample and $F_m$' is the florescence maximum from the light adapted sample, measured during the SP. During a SP of light, RCs are saturated, meaning that they are reduced and are referred to as 'closed'. In this way, Chl fluorescence can be measured in the absence of photochemistry. The quenching of the fluorescence signal, during the SP is thus attributed to NPQ, which is quantified in respect to maximal fluorescence ($F_m$).

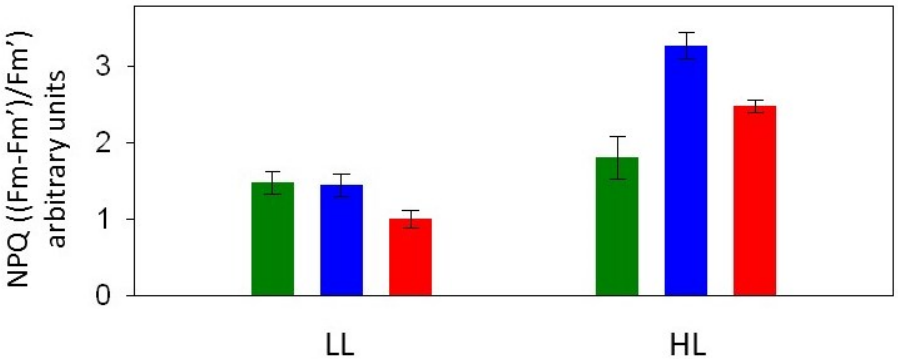


**Figure 5.4:** NPQ maximum amplitude in LL and HL plants of *N.tabacum* (*green*), *Nt*(*Hn*) (*blue*) and *H.niger* (*red*). Data are mean averages ± SD from at least 3 replicates.

Maximum NPQ amplitude measured during the 5 min exposure to high intensity AL, is shown in Fig 5.4. LL *N.tabacum* and *Nt*(*Hn*) plants yielded similar results at 1.48 ± 0.37 and 1.443 ± 0.26, while LL *H.niger* was somewhat decreased at 1.00 ± 0.20. All the HL grown plants showed a greater amplitude for NPQ than their LL counterparts. *N.tabacum* had the smallest increase of 22 % to 1.81 ± 0.70, *H.niger* had the largest increase by 147 % to 2.48 ± 0.13 while the *Nt*(*Hn*) HL plants increased their amplitude for NPQ by 123 % to 3.28 ± 0.31, a value that was 1.8 times larger than in HL *N.tabacum* and 1.32 times larger than *H.niger*.

To compare the kinetics of NPQ formation, changes in the NPQ amplitude were plotted during the 5 min exposure to high intensity AL (700 $\mu$mol photons $m^{-2}$ $s^{-1}$) and its subsequent removal. Plots derived from typical fluorescence traces are shown in Fig 5.5a,b. Details of the plots are also shown to reveal qE formation (Fig 5.5c,d) and relaxation kinetics (Fig 5.5e,f). LL grown *N.tabacum* and *Nt*(*Hn*) were matched in the rate of NPQ formation (Fig 5.5c), upon the application of AL, and the maximum amplitude was the same. Relaxation upon AL removal however was faster in *Nt*(*Hn*) cybrids, indicating a faster response to turn off the quenching mechanism (Fig 5.5e).

In contrast to LL grown plants, HL *N.tabacum* and *Nt*(*Hn*) were somewhat different to each other with faster NPQ formation and relaxation in *Nt*(*Hn*) cybrids (Fig 5.5d,f) with, as seen in Fig 5.4, a much greater amplitude for maximum NPQ.

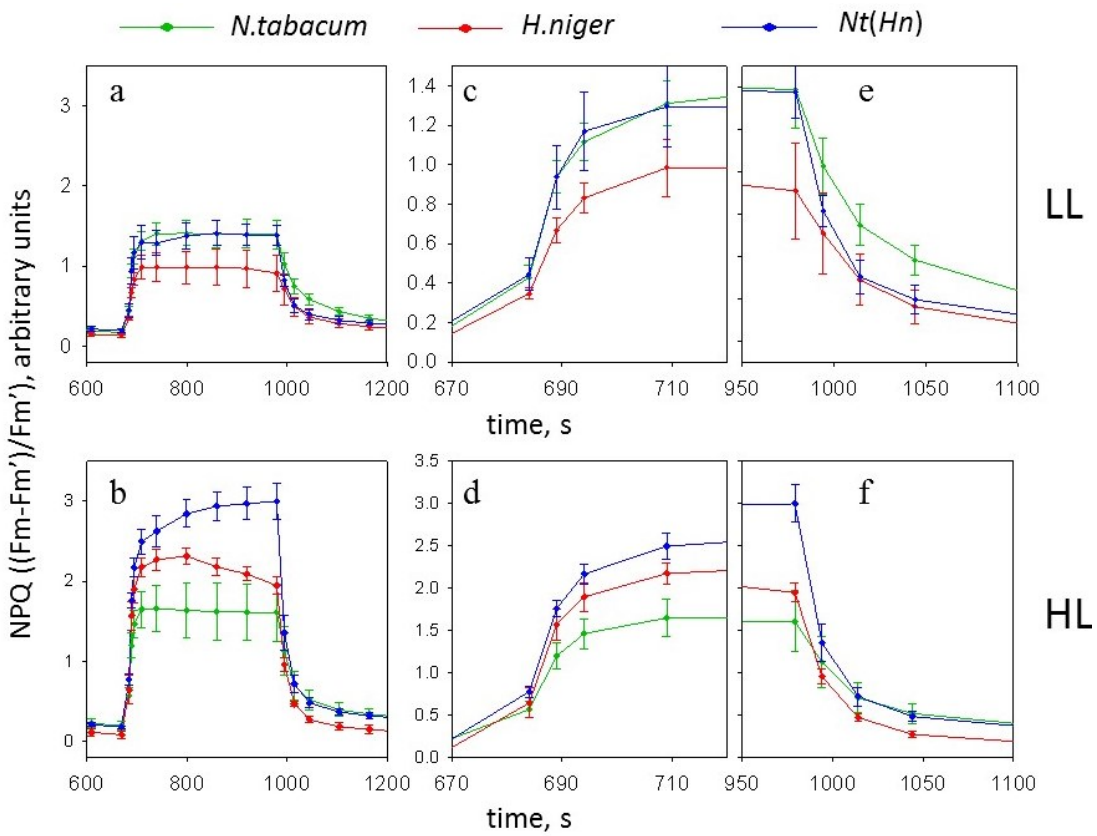


**Figure 5.5:** Kinetics of NPQ formation in LL (*top row, a,c,e*) and HL (*bottom row, b,d,f*) plants of *N.tabacum* (*green*) *Nt*(*Hn*) (*blue*) and *H.niger* (*red*). **a,b)** NPQ kinetics during 5 min of high light treatment. **c-f)** details from *a* and *b*, to show NPQ formation *c,d* and NPQ relaxation *e,f* kinetics. Data are mean averages ± SD from at least 3 replicates.

Interestingly, and in contrast to the LL plants, NPQ formation and relaxation kinetics, and maximum NPQ amplitude, in HL *Nt*(*Hn*), were more similar to the chloroplast parent, *H.niger*, than to *N.tabacum*. Although, in HL *H.niger* and to a lesser extent in LL *H.niger*, signs of photoinhibition, the qI component of NPQ, can be observed as a slight reduction in qE amplitude before the completion of 5 min AL exposure. In HL *N.tabacum* there is also a slight decrease in qE (Fig 5.5a,b). In strong contrast, at the end of the 5 min exposure to AL, NPQ formation does not reach steady state in the HL *Nt*(*Hn*) cybrids, suggesting that maximum NPQ formation might be even greater than 3.28 (Fig 5.5b).

### 5.3.1 Testing for contributory factors to increased NPQ

As discussed in §1.4.2.2, several factors have been identified as playing a role in the rapidly reversible qE component of NPQ. The build up of a proton gradient

($\Delta$pH) across the thylakoid membrane when treated with saturating light, has been identified as the trigger for NPQ formation. Regulation of the de/epoxidation state of the xanthophyll cycle carotenoids and of the PsbS protein are both known to contribute to the dynamic control of NPQ. Aggregation of isolated LHCII also leads to fluorescence quenching that resembles qE. To identify the mechanism that contributed to the elevated NPQ levels seen in *Nt*(*Hn*), we investigated PsbS, xanthophyll cycle pigment de/epoxidation state and LHCII aggregation under different pH.

### The PsbS protein is not altered in *Nt*(*Hn*)

PsbS is a nuclear encoded protein, whose involvement in qE has been demonstrated (Li et al., 2000; Zia et al., 2011). Increases in the amount of PsbS content are associated with an increased capacity for thermal dissipation (Demmig-Adams et al., 2006), although the presence of PsbS is not essential for the NPQ mechansim (Ruban et al., 2012). To check for possible involvement of PsbS in the enhanced capacity for NPQ in HL *Nt*(*Hn*) cybrids, solubilised thylakoids were subjected to SDS-PAGE and then Western blotted against PsbS anti-bodies. Fig 5.6 presents the Western blot of the PsbS proteins from HL grown *N.tabacum*, *Nt*(*Hn*) and *H.niger* plants.

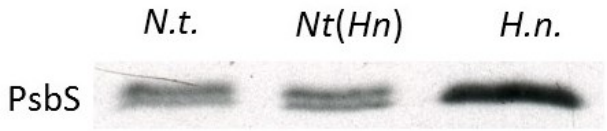


**Figure 5.6:** Western blot of PsbS from plants in HL

There was no difference, either in MW or protein concentration between PsbS banding patterns of *Nt*(*Hn*) and *N.tabacum*, furthermore they were different from *H.niger*, indicating that PsbS was not altered in *Nt*(*Hn*) and cannot be responsible for the increase in *Nt*(*Hn*) NPQ.

### Deepoxidation state of the xanthophyll cycle pigments

For the assessment of the deepoxidation state (DEPS) of the xanthophyll cycle pigments, mature leaves were harvested from LL and HL grown plants that were dark adapted or treated with 30 min of high intensity (700 $\mu$mol photons $m^{-2}$ $s^{-1}$) light. The light treatment was issued using the AL source of the DUAL-PAM in order to simulate the same light conditions under which we observed high NPQ. The treated leaf tissue was ground in acetone and subjected to analysis by HPLC.

The results are presented in Fig 5.7. Xanthophyll cycle pool (XC pool) size (Vx + Ax + Zx/total carotenoid content) was, in all cases, without significant change between dark and light treated samples (Fig 5.7c,f). Compared to plants grown in LL, HL grown plants increased their XC pool size by 49 %, 52 % and 69% in *N.tabacum*, *Nt*(*Hn*) and *H.niger* respectively. However, despite the large increase in XC pool size, the DEPS under HL only increased by 4 % in *N.tabacum*, 17 % in *Nt*(*Hn*) and 38 % in *H.niger*.

XC pool size was lowest in *N.tabacum* at 9.51 % ± 0.75 in LL and 14.23 ± 2.03 in HL gown plants. In *Nt*(*Hn*) these values were slightly larger at 11.12 % ± 3.11 in LL and 16.96 % ± 3.16 in HL and *H.niger* XC pool size was the largest

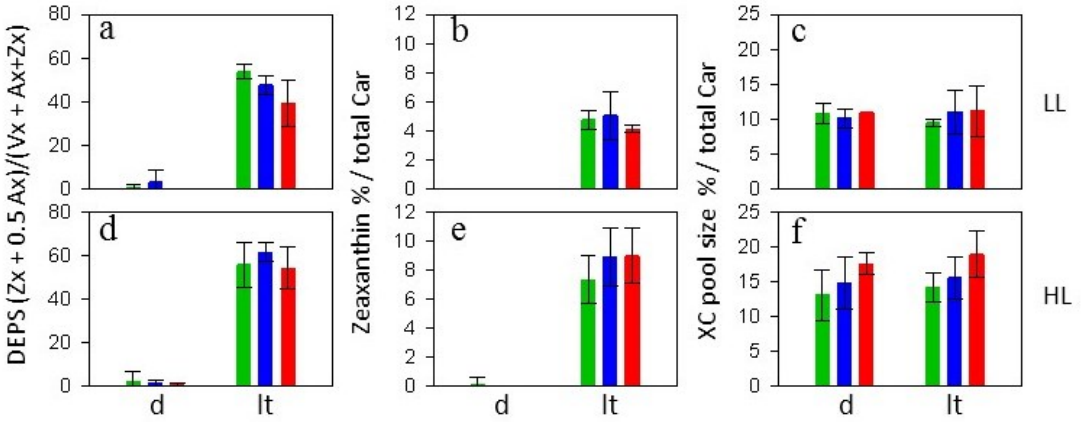


**g**

| GE | Plant | DEPS (%) | Zx (%) | V+A+Z (%) |
|---|---|---|---|---|
| LL | *N.t.* | 53.65 ± 4.28 | 4.76 ± 0.86 | 9.51 ± 0.75 |
| | *Nt*(*Hn*) | 47.68 ± 4.15 | 5.07 ± 1.63 | 11.12 ± 3.11 |
| | *H.n.* | 39.30 ± 10.42 | 4.14 ± 0.25 | 11.21 ± 3.60 |
| HL | *N.t.* | 55.77 ± 10.33 | 7.36 ± 1.61 | 14.23 ± 2.03 |
| | *Nt*(*Hn*) | 55.58 ± 10.02 | 8.36 ± 1.87 | 16.96 ± 3.16 |
| | *H.n.* | 54.39 ± 9.50 | 8.97 ± 1.89 | 18.93 ± 3.35 |

**Figure 5.7:** Deepoxidation state of the xanthophyll cycle carotenoids in dark adapted (d) and light treated (lt), LL (*top row*) and HL (*bottom row*) growth environment (GE) plants. **a,d)** Deepoxidised state of the XC pool calculated from (Zx + 0.5Ax)/(Vx + Ax + Zx). **b,e)** Zeaxanthin (Zx) % content. **c,f)** Xanthophyll pool size %. Carotenoid composition is expressed as % of total carotenoid content. *N.tabacum* is shown in *green*, *Nt*(*Hn*) in *blue* and *H.niger* in *red*. **g)** Values taken from *a-f* for light treated plants. Data are mean average ± SD, n ≥ 3.

increasing from 11.21 ± 3.60 to 18.93 ± 3.35 in HL (Fig 5.7c,f,g).

The deepoxidation state (DEPS) of the xanthophyll cycle increased after light treatment to comparable levels in all plants (Fig 5.7a,d). There was a slight increase in the DEPS of the HL grown *Nt*(*Hn*), compared to *N.tabacum* and *H.niger*, although the difference was not significant with large variation around the mean. From these data we could find no explanation for the increased capacity for NPQ that was observed in the HL *Nt*(*Hn*) cybrids.

#### 5.3.1.1 pH dependent quenching in LHCII trimers *in vitro*

To assess whether the increased NPQ capacity found in *Nt*(*Hn*) was due to an increased sensitivity of the LHCII to pH, LHCII was separated from thylakoid preparations by non-denaturing isoelectric focusing (IEF), collected and desalted. In this state, it is possible to measure the effect of pH on LHCII quenching capacity, in the absence of xanthophyll cycle activity.

The LHCII-quenching method measures Chl *a* fluorescence from isolated LHCII suspended in buffer with detergent ($\beta$-DM), at various acidities. Like all trans-

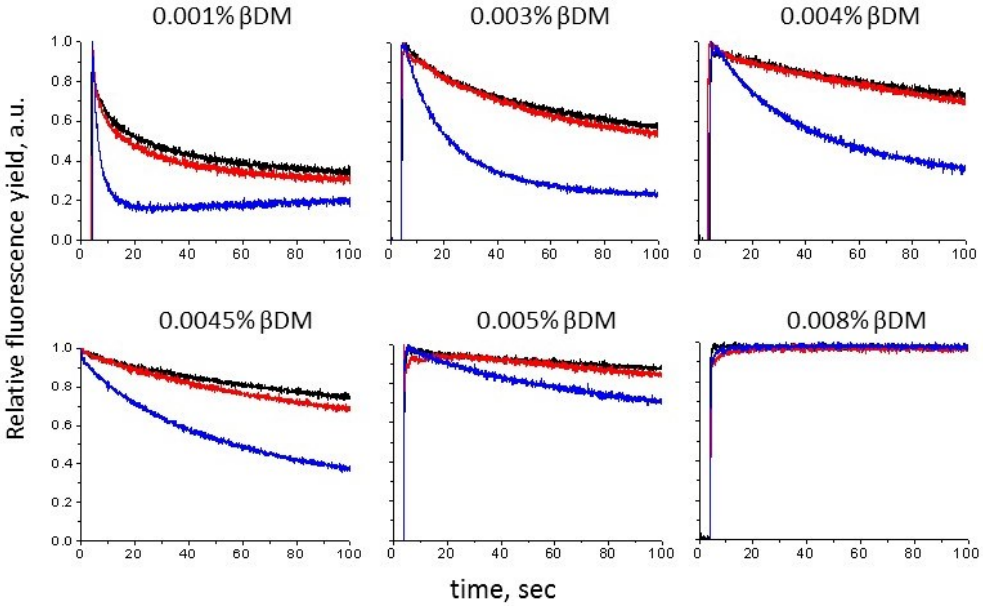


**Figure 5.8:** Determining detergent concentration to test the effect of protons on LHCII quenching. *N.tabacum* LHCII was added to buffer with various concentrations of $\beta$-DM (% (w/v)). Chl fluorescence quenching was measured at pH 7.5 (*black*), pH 6.0 (*red*) and pH 4.5 (*blue*) to determine which detergent concentration was most conducive with cmf.

membrane proteins, LHCII naturally aggregates in aqueous solutions. As already discussed (§1.4.2.2), for LHCII, this aggregation is associated with strong fluorescence quenching through formation of heat dissipation pathways. It is therefore important in LHCII-quenching experiments to first establish the detergent concentration in which LHCII is sufficiently solubilised in micelles to avoid spontaneous aggregation, while still allowing proton-sensing of the LHCII complexes (Petrou et al., 2013).

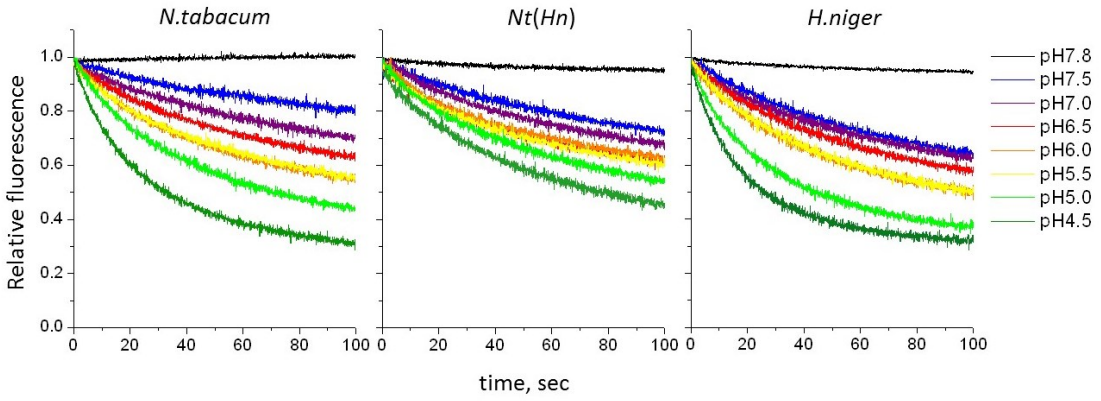


**Figure 5.9:** Fluorescence signal traces from Chl *a* of isolated LHCII from HL grown *N.tabacum*, *Nt*(*Hn*) and *H.niger*, at various pH. Samples were diluted in buffer containing 0.004 % $\beta$-DM, and, during Chl *a* fluorescence measurement, the sample was acidified by the addition of HCl to one of eight different pHs, as indicated. See main text for further details.

To determine a suitable detergent concentration, isolated LHCII from *N. tabacum* was suspended in a series of buffers with various concentrations of $\beta$-DM (0.001 %-0.008 %). PAM chlorophyll fluorescence was measured in each suspension at three different pHs (7.5, 6.0 and 4.5). A small amount of spontaneous quenching upon the application of light to the sample is unavoidable, therefore to separate the quenching due to acidification, HCl was added 10 s after light application, and the measurements were normalised to this point. The results are shown in Fig 5.8. $\beta$-DM concentration at 0.004 % was judged to give the greatest quenching range, from strong fluorescence quenching at pH 4.5, indicating good proton sensitivity, to relatively reduced quenching at pH 7.5, indicating that, in the absence of protons, LHCII did not quench significantly due to spontaneous aggregation.

Quenching data was thus collected using LHCII suspended in 0.004 % $\beta$-DM. Fluorescence was measured continuously until steady state. Eight measurements

at different pHs (7.8-4.5) were obtained. The results are presented in Fig 5.9. Measurements are shown from the moment of acid injection to which point they were also normalised.

Surprisingly, given the high NPQ capacity already observed in HL grown *Nt*(*Hn*) *in vivo*, fluorescence quenching in isolated LHCII was found to be reduced at low pH, relative to both wildtype parent species. *N.tabacum* and *H.niger* both responded to low pH much more readily than *Nt*(*Hn*), with both wildtypes quenching about 70 % at pH 4.5, while at the same pH, quenching in *Nt*(*Hn*) was about 50 % (Fig 5.9). *H. niger* showed a greater sensitivity to higher pHs, with fluorescence quenched by up to about 40 % at pH 7.5, compared to *N. tabacum*, at just under 20 % and *Nt*(*Hn*) at about 25 % quenching at pH 7.5.

In other experiments, using *Arabidopsis thaliana* (Petrou et al., 2013), a concentration of 0.003 % was determined to achieve best quenching results due to protonation. This suggests the interesting possibility that, between plant species, there is a difference in LHCII aggregation response in a given detergent concentration, which could explain differences between *N.tabacum* and *H.niger*.

### 5.3.2 Repeated NPQ measurements show reduced capacity for NPQ in HL grown *Nt*(*Hn*) plants

Given that no explanation could be found for the increased levels of NPQ that were observed in HL grown *Nt*(*Hn*) during measurements taken in 2011, NPQ measurements were repeated following the same procedure. Fig 5.10 shows the results already presented in Fig 5.5, with those taken two years later, in 2013. NPQ in LL grown plants is consistent over time whereby *Nt*(*Hn*) and *N.tabacum* measurements are similar to each other and different from *H.niger* which shows slightly less NPQ. The main difference is a slight, but statistically non-significant increase in *Nt*(*Hn*) NPQ in 2013 as compared to 2011. Fluorescence measurements taken from HL *N.tabacum* and *H.niger* also remain similar to the results obtained in 2011, with maximum NPQ at 1.8 and 2.1 respectively.

HL grown *Nt*(*Hn*) on the other hand shows major reduction in the capacity for NPQ, dropping to 1.1, compared to the findings made in 2011 at 3.28. In fact, HL grown *Nt*(*Hn*) NPQ capacity dropped to below that of *N.tabacum* and *H.niger* grown in HL. Moreover, the NPQ yield was even less than that of *Nt*(*Hn*) LL grown plants (Fig 5.10).

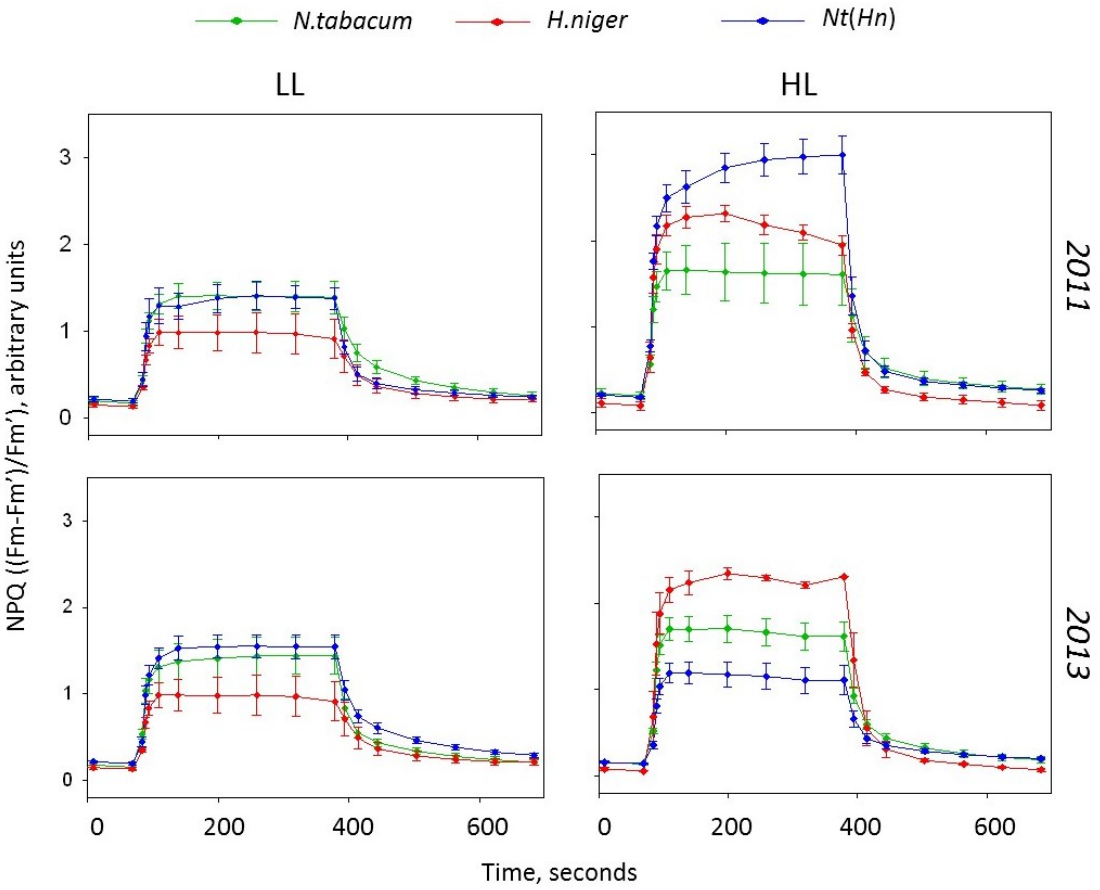


**Figure 5.10:** Repeated NPQ measurements. The original experiments, measured in 2011, are shown for comparison in the *top row*. Repeated measurements, in 2013, are presented in the *bottom row*.

### 5.3.3 State transitions remain inhibited in *Nt(Hn)*

Although a change in the NPQ response was observed only in HL *Nt(Hn)* plants, we were prompted to reassess state transitions at room temperature to verify whether the inhibited antenna redistribution was still present in *Nt(Hn)*. Five mature LL grown *Nt(Hn)* plants were tested using the same procedure as for the original measurements. All results were comparable to the original results with a strongly inhibited response in *Nt(Hn)* to FR removal or application.

## 5.4 Discussion

In this chapter we present the investigation aimed to test the *Nt(Hn)* cybrid capacity for regulating against short-term fluctuations in light. We found significant reduction in the capacity for state transitions in *Nt(Hn)* plants. In all the plant types, the effect of FR light removal was greater on the LL plants compared to HL

plants, as shown in the IB values. This result is typical and is usually explained with regards to greater quantities of LHCII in the LL plant. Therefore further investigation of state transitions were conducted on the LL plants only.

Early measurements also revealed a greater capacity for NPQ in *Nt*(*Hn*) from HL environments. This led to an analysis of the PSII PsbS protein, xanthophyll cycle activity and proton-related quenching in LHCII. However, none of these factors revealed an alteration that could explain the increased capacity for NPQ in *Nt*(*Hn*). Indeed, proton-dependent aggregation of isolated LHCII in fact showed reduced quenching capacity. Further NPQ measurements were made and, surprisingly, in contrast to the early measurements, on average, NPQ in *Nt*(*Hn*) was reduced, relative to the wildtype parent species. These findings are discussed below.

### 5.4.1 Strong state transition inhibition may be due to LHC modification

State transitions were measured from room temperature Chl *a* fluorescence traces, recorded during FR on/off light cycles that were superimposed over a weak AL, for the selective drive and slow-down of PSI, respectively. Upon FR light removal the typical reduction in the fluorescence signal at $F_s$ was not observed in *Nt*(*Hn*), nor was there a significant difference in qT before and after FR light removal. The possibility that the light set-up was not sufficiently strong to affect the redox state of the PQ pool by the preferential drive of PSII (in the absence of FR) or PSI (in the presence of FR), is ruled out on account of the large IB value which indicates adequate levels of PQ pool reduction (Ruban and Johnson, 2009). Our results suggest not only that LHCII in *Nt*(*Hn*) did not dock to PSI, but that it did not leave PSII, suggesting that the action necessary for dissociation of LHCII from PSII was impeded.

State transitions are triggered by phosphorylation and dephosphorylation of the threonine residue located at the N-terminus in lhcb1 and lhcb2 of the LHCII trimer (Forsberg and Allen, 2001). Assuming that LHCII was attached to PSII, the lack of state transitions in *Nt*(*Hn*) could be explained by either i) a failure of the kinase to phosphorylate LHCII, ii) an inability of LHCII to respond to phosphorylation or iii) a failure to phosphorylate LHCII due to the absence of the phosphorylation site.

In previous cybrid research, reports of LHC alterations are frequent. Kushnir et al. (1987) and Peter et al. (1999) found that cybrid plants of *N. tabacum* nuclear background and *Atropa belladonna* (deadly nightshade) plastome (*Nt*(*Ab*)) had altered expression of membrane proteins in the 27-25 kDa weight range and that the content of at least one of the major polypeptides, presumed to be a Chl *a/b*

binding protein, was significantly reduced (Kushnir et al., 1987). Later work by Babiychuk et al. (1995) showed similar results in five new cybrid combinations, all of which combined a *N. tabacum* nucleus with the plastome of a different species from the Solanaceae family.

Immunoblots of polypeptides of novel 26, 24.5 and 24 kDa bands in *Nt*(*Ab*) cybrids, were successful against anti-LHCII polyclonal antibodies showing that the polypeptides were in fact derived from LHCII nucleus-encoded genes (Babiychuk et al., 1995). A novel 26 kDa polypeptide band found in a *Nicotiana plumbaginifolia*(*Ab*) cybrid, was sequenced and matched to the wildtype lhcb1 polypeptide of the nuclear parent plant, although 11-12 amino acids were absent at the N-terminus (Babiychuk et al., 1995). LHCII polypeptide composition showed no difference however, in a cybrid with a *Solanum peruvianum* L. (previously *Lycopersicon*) var. *dentatum* Dun. (Peruvian nightshade) nuclear parent and *Solanum lycopersicum* L. (previously *Lycopersicon esculentum* Mill.) (tomato) plastome parent (Kochevenko et al., 2000).

Given these reports of LHC alteration in various cybrid plants, and furthermore that the reports of alterations are all based on cybrids with a *N. tabacum* nuclear parent, it seems reasonable to suggest that a similar alteration occurred for LHCII proteins of *Nt*(*Hn*). Provided that the N-terminus were cleaved downstream from the site of phosphorylation, LHCII misprocessing would provide a good explanation for state transition inhibition.

### 5.4.2 The HL grown *Nt*(*Hn*) plant is highly variable in its NPQ response to saturating light

NPQ measurements taken at the beginning of the project showed interesting differences between the wildtype and *Nt*(*Hn*) plants, in terms of increased NPQ, however measurements taken later gave different, even contradictory results, where NPQ capacity was in fact lower in *Nt*(*Hn*) than the parent species. The large difference in NPQ capacity in HL *Nt*(*Hn*) plants at the start of the project and at the end, is difficult to explain. As far as we are aware, the experimental set-up was the same, and the close similarity between the 2011 and 2013 measurements taken from the wildtype plants, and from LL grown *Nt*(*Hn*), supports this claim.

The implication then is that the difference in response was due to a change in the function/structure of HL grown *Nt*(*Hn*). We suggested in Chapter 3 that the inter-batch, and indeed the intra-batch, variability, observed during the growth of *Nt*(*Hn*) seedlings, might be explained by an increased environmental sensitivity to, for example, small differences in soil content, water pollutants, air condition and/or temperature. Perhaps some photosensitivity persisted in mature *Nt*(*Hn*)

plants. If so, growth under HL would be expected to cause stress, and perhaps a hypersensitivity to the surroundings. As such, if the environment of *Nt*(*Hn*) differed in some capacity that was not detected, or controlled by us, at the different times of NPQ measurement, it could possibly explain the instability and irregularity in the *Nt*(*Hn*) cybrid NPQ response.

Our analysis of PsbS, the deepoxidation state of the xanthophyll cycle pigments and quenching in isolated LHCII, did not support our early findings that NPQ was increased in *Nt*(*Hn*). These analyses were all performed around the same period as the later NPQ measurements in which *Nt*(*Hn*) NPQ was reduced, and rather supported those later results. It is interesting to note that in the later measurements we find a reduced NPQ capacity as compared to the parent species, while from an analysis of the PsbS, xanthophyll pigments and LHCII quenching, an explanation for altered (reduced) quenching capacity is found only in the isolated LHCII, which also show reduced quenching at low pH, as compared to *N. tabacum* and *H. niger*.

The finding suggests that the reduced NPQ in the 2013 *Nt*(*Hn*) plants was associated with the LHC proteins, and raises the question as to whether the LHCs were somehow different in *Nt*(*Hn*) at the beginning of the study compared to those grown later? It might be that had we investigated the PsbS protein, xanthophyll deepoxidation state and LHCII quenching in the 2011 *Nt*(*Hn*) plants, that did show high levels of NPQ, some altered phenotype of one of the NPQ 'candidates' may have been detected. However, the seeming instability of the *Nt*(*Hn*) NPQ phenotype under HL means that results from one plant cannot necessarily be used corroboratively with results from another.

Chapter 6

# An investigation of the LHC pigment-protein complexes

## 6.1 Introduction

For LHC quenching experiments, we isolated LHC antennas from thylakoid preparations, using non-denaturing isoelectric focusing (Chapter 5 §5.3.1.1). During the procedure, *Nt*(*Hn*) LHCs showed novel migration patterns in the IEF gel with comparison to the wildtype plants. IEF separates complexes based on their isoelectric point, the novel migration thus indicated that the LHC complexes had been altered as a consequence of *N.tabacum-H.niger* cybridisation.

As an integral component in state transitions and NPQ, the LHCII proteins, if altered, could provide a possible explanation for the observed reduction in state transitions in *Nt*(*Hn*) and might shed some light on the nature of the variability in the NPQ mechanism that was observed. To address this possibility, we began an investigation of the novel migration patterns of *Nt*(*Hn*) LHCs in the IEF gels. Non-denaturing IEF is a technique that is normally used for the preparation of LHCs (Walters et al., 1994). Here, we used the gels to more closely analyse changes in LHC pI due to cybridisation.

## 6.2 Isoelectric points of LHCII are different in *Nt*(*Hn*)

IEF separates protein complexes based on their iso-electric point (pI). We used mild detergent and a non-denaturing, flat bed IEF technique to separate LHCII complexes from thylakoid preparations. To do this, a soft gel bed with a pH gradient (pH >6-2.5) was established. Samples were loaded near the cathode and

a current was applied to draw the complexes through the pH gradient to their pI point, in effect, to where the protein complex had no charge.

Fig 6.1a shows examples of typical separation patterns of *N.tabacum*, *H.niger* and *Nt(Hn)* thylakoid proteins. The green bands are the Chl-binding antenna complexes that have migrated from the loading site (indicated near the cathode) to a low pH near the anode. Wildtype samples separated into a main green band with low pI and several weaker bands with slightly higher pIs. A strong green band was also present in the *Nt(Hn)* separation, although the weaker bands were not distinct, instead a fairly homogeneous green spread filled the gel at higher pHs.

Migration distance of the strong green band, most likely LHCII, of *N.tabacum* and *H.niger* were similar. In contrast, this band in the *Nt(Hn)* migrated considerably further to a lower pH, revealing that the *N.tabacum*-encoded LHCs of *Nt(Hn)*

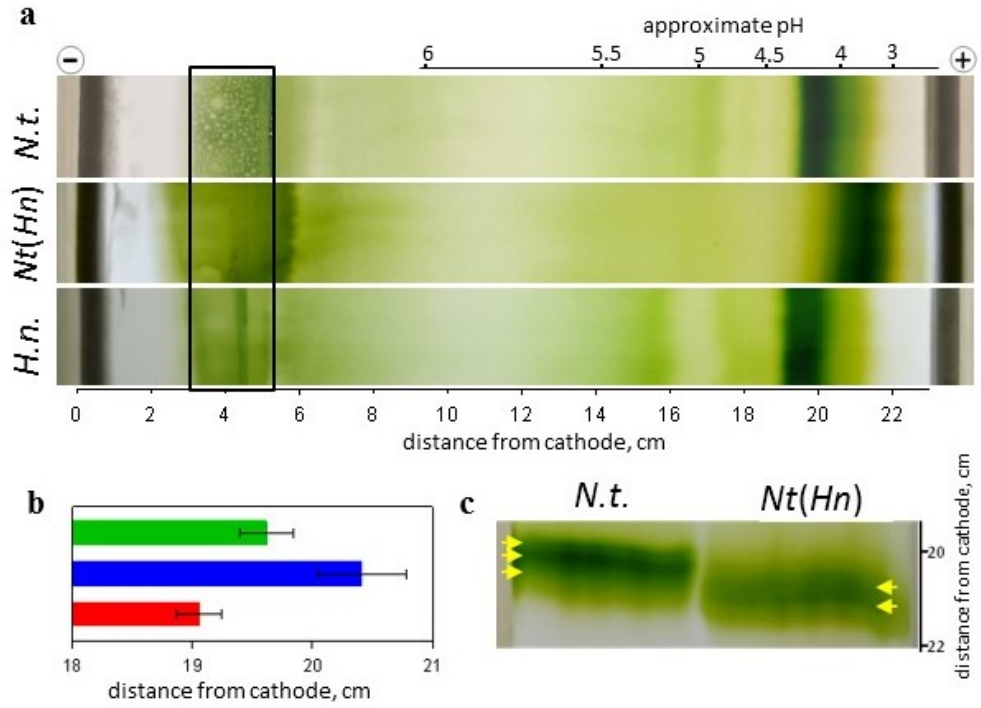


**Figure 6.1:** LHC separation on the basis of pI. **a)** Photographs of typical IEF gels after LHC focusing. The boxed area near the cathode defines the site of sample application. The pH scale is approximate as pH gradients varied slightly between gels. Images have been cropped to show the central aspect of the gel tray for easy comparison. **b)** Graphical comparison of LHC migration distance in IEF. Distance was measured from the position of the cathode to the first edge of the strong green LHC band. Data are mean average ± SD, for *N.tabacum* and *Nt(Hn)* n=7, for *H.niger*, n=4. **c)** Two-lane IEF comparing LHC separation in *N.tabacum* and *Nt(Hn)*, yellow arrows mark components of the main band.

had been altered resulting in a lower pI, as a consequence of the coalition government of the *N.tabacum* and *H.niger* genomes. When the procedure was replicated, a significant difference in the green band migration distance was calculated (Fig 6.1b). Measured from the cathode, mean average migration distances were 19.61 ± 0.226 cm (pH ∼ 4.04), 20.41 ± 0.37 cm (pH ∼ 3.69) and 19.06 ± 0.19 cm (pH ∼ 4.15) for *N.tabacum*, *Nt(Hn)* and *H.niger* respectively (Fig 6.1a,b).

For a more direct comparison between migration patterns and to avoid the

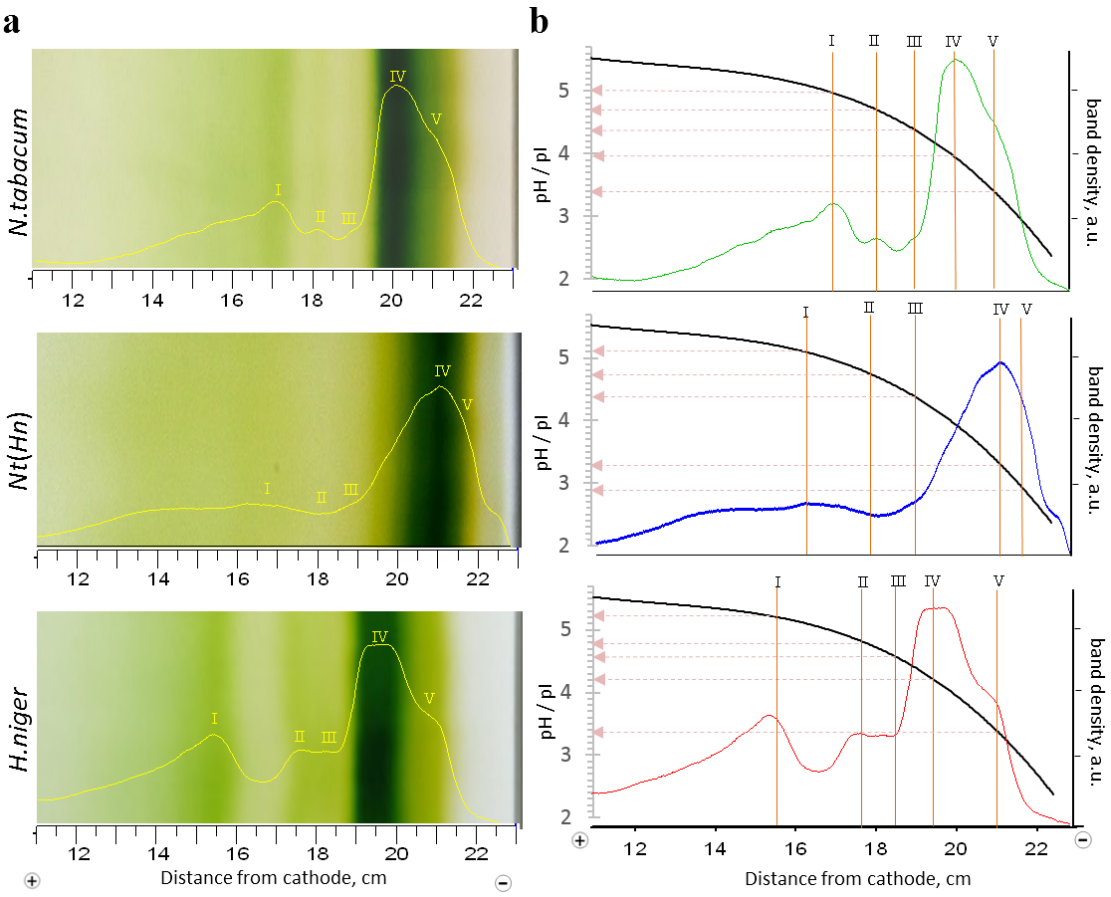


**c**

| Peak | I | II | III | IV | V |
|---|---|---|---|---|---|
| ***N.tabacum*** | 5.10 ± 0.10 | 4.75 ± 0.10 | 4.46 ± 0.07 | 3.99 ± 0.08 | 3.41 ± 0.21 |
| ***Nt(Hn)*** | 5.13 ± 0.11 | 4.53 ± 0.07 | 4.39 ± 0.08 | 3.48 ± 0.10 | 2.97 ± 0.10 |
| ***H.niger*** | 5.20 ± 0.06 | 4.79 ± 0.01 | 4.50 ± 0.08 | 4.21 ± 0.07 | 3.38 ± 0.08 |

**Figure 6.2:** Characterisation of LHCs by pI and MW. **a)** Density plots of banding in IEF gels are shown superimposed over the gel images. The peaks are labelled (I-V). **b)** The same density plots are shown for *N.tabacum* (*green*), *Nt(Hn)* (*blue*) and *H.niger* (*red*). Gel pH is also plotted (*black line*). Peaks are marked by orange drop lines and their respective pI points are indicated on the y-axis. **c)** Tabulation of band pIs (I-V). Data are mean average ± SD, n = 4

effect of possible differences in pH gradients between gels, *N.tabacum* and *Nt*(*Hn*) samples were focused simultaneously in two-lane IEF gels (Fig 6.1c). The reduced sample volume allowed some internal details of the main LHC band to be revealed, indicated by yellow arrows (Fig. 6.1c). However, the low sample concentration also meant that collection of LHCs for further analysis was limited and the weaker bands that were seen in the single lane gels at higher pHs, were absent.

To analyse the migration and banding patterns more closely, and to investigate the nature of the alterations that were evident in *Nt*(*Hn*) LHCs, densitometric analysis was performed on photographs of single-lane gels using ImageJ software (Fig 6.2a). In general, *N.tabacum* and *H.niger* density profiles were comparable and five bands (I-V) were identified in each (Fig 6.2a). We also differentiated five bands in *Nt*(*Hn*) at equivalent positions, although the designations were tentative. Gel pH, measured at 0.5 mm intervals, was plotted with the densitograms (Fig 6.2b) and from these alignments, peak pI points were discovered and are presented in Fig 6.2c.

The migration distance of band I was somewhat different between *N.tabacum* and *H.niger* although the pH gradient at their gel location was shallow and the pI points were similar at 5.10 ± 0.10 and 5.20 ± 0.01. A broad band was present in *Nt*(*Hn*) gel at a similar position, with maximum density at pH 5.13 ± 0.11. (Fig 6.2a). Band II was distinct in the wildtypes, again with similar pI points at 4.75 ± 0.10 and 4.79 ± 0.01 in *N.tabacum* and *H.niger* respectively. The peak was not identifiable in *Nt*(*Hn*) separation, and the designated position corresponds only to the position of band II in *N.tabacum*. Band III was identifiable in all the density plots on close inspection although its definition was obscured by the higher concentrations of the bands either side.

Band IV, the strongest band, was well delimited in both parental wildtypes, with a clear, steep rise from peak III to IV in the densitogram. Peak maxima were at pI 3.99 ± 0.08 in *N.tabacum* and with a slightly higher pI in *H.niger* at 4.11 ± 0.07. Band V was present as a shoulder to band IV at lower pIs of 3.41 ± 0.21 in *N.tabacum* and 3.38 ± 0.08 in *H.niger* (Fig 6.2b). By comparison, the densest band of *Nt*(*Hn*), also designated IV, was broad with a narrow peak with a relatively low pI at 3.48 ± 0.10. This main band lay skewed towards the right of the broader, gradated green region in which, at lower pI, a fifth band, tentatively assigned to be band V appeared as a shoulder.

To characterise the IEF bands, fractions were collected in 5 mm wide strips from 17.5 - 22 cm. The pigment-protein complexes were eluted and separated by MW in denaturing SDS-PAGE (Fig 6.3). The separation of LHCs by MW after separation based on pI, is indicative of the 2-dimensional gel technique, the difference here is that the second dimension is performed on discrete fractions

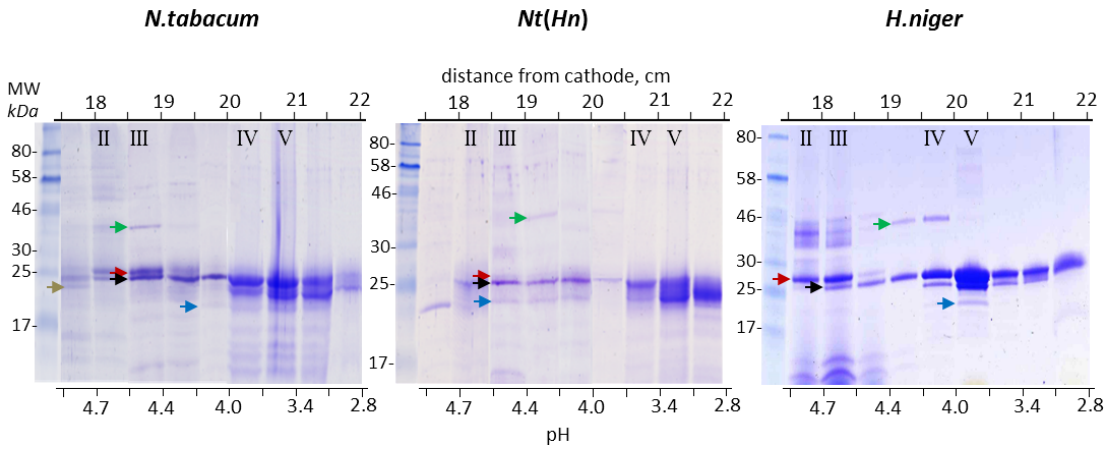


**Figure 6.3:** Characterisation of IEF fractions by MW based separation in SDS-PAGE 12 % acrylamide gels. Fractions were collected from the IEF gel in 5 mm wide bands from 17.5 - 22 cm. Gels were stained with Coomassie Brilliant Blue. Fractions containing IEF peaks (II-V) are identified at the tops of the wells. Distance from cathode, and pH are given above and below the gel respectively.

of the IEF gel rather than a continuous strip. To aid the identification of the fractions and their components, calculations of theoretical pI and MW, of mature *N.tabacum* minor and major PSII extrinsic antennas, were made from published sequences, available in UniProt, using ExPASy software (SIB; Artimo et al. (2012)). Calculations and UniProt accession numbers are presented in Table 6.1.

The most easily recognisable banding profile revealed in the SDS-PAGE gels was from IEF bands IV and V. MW based separation clearly revealed LHCII content, with the characteristic dual band at about 25 kDa, containing lhcb1, lhcb2 and lhcb3, the latter predicted to be in the lower band (Fig 6.3). The predicted MWs support this identification (Table 6.1). However, the predicted pI points for the lhcb1-3 polypeptides were quite different, ranging from 5.4 - 5.01 in lhcb1 isoforms (lhcb1.1 - 1.5), 5.02 for lhcb2 and 4.8 for lhcb3. IEF bands IV and V had pIs in the range of 3.2-4.0. The inconsistency might be explained by the difference in estimating pI from apoprotein sequences, compared with measurements taken from native pigment-protein complexes. In addition, LHC aggregation state and trimerisation, a likely occurrence in the IEF gels, is known to strongly influence pI (Bassi et al., 1991). Furthermore, Bassi et al. (1991), also using the non-denaturing IEF technique, found the pI point of *Zea mays* LHCII was 3.9-4.1, and Ruban et al. (1994) reported spinach LHCII with pI 4.05-4.25, values that are more indicative of our results.

The dimeric character of the LHCII bands was typical in the wildtype species, with a prominent upper band and weaker lower band. The *Nt(Hn)* line however,

showed differences. Blurring of the *Nt*(*Hn*) dimer was strong and the lower band, in contrast to the wildtype parents, was broader and more concentrated than the upper band. In wildtype gels, there were also bands of which the relative position and MW was consistent with identification as the minor antennas, CP29 and CP26 (Ruban et al., 1994) and are indicated with red and black arrows respectively (Fig 6.3). In *N.tabacum* and *H.niger*, these bands appeared together in the elute from IEF peaks II and III, corresponding to a pI of about 4.5-4.7 in *N.tabacum* and pI $\sim$ 4.5 - 5.2 in *H.niger*. *Nt*(*Hn*) polypeptide separations also revealed two bands in fraction III, although both bands were weaker than in wildtype, particularly the higher MW band, predicted to be CP29.

Faint bands at about 21 kDa were also observed in the wildtype protein separations, indicated with blue arrows in Fig 6.3, and conform to the characterisation of CP24 (Ruban et al., 1994; Ruban, 2012). Our suggested identifications of the minor antenna proteins give a pI separation profile in the order of CP29, CP26 and CP24. This differs from the separation profile reported by Ruban et al. (1994) and Bassi et al. (1991), who both found described pI separation in the order of CP29 (pI $\sim$ 4.7), CP24 (pI $\sim$ 4.5) and CP26 (pI $\sim$ 4.3). However, our results reflect the order of separation as predicted by the *N.tabacum* minor antenna theoretical pI points (Table 6.1).

**Table 6.1:** Theoretical pI and MW of LHC antenna proteins of *Nicotiana tabacum*. Calculations were made using the sequences available in UniProt database together with the ExPaSy compute pI/MW tool.

| **protein** | **UniProt acc no.** | **MW** (*kDa*) | **pI** |
|---|---|---|---|
| lhcb 1.1 | P27496 | 24.926 | 5.40 |
| lhcb 1.2 | P27493.1 | 24.707 | 5.01 |
| lhcb 1.3 | P27495.1 | 24.870 | 5.13 |
| lhcb 1.4 | P27491 | 24.908 | 5.10 |
| lhcb 1.5 | P27492 | 24.882 | 5.13 |
| lhcb 2.1 | P27494.1 | 24.784 | 5.02 |
| lhcb 3.1• | A0A076L1Y1 | 24.216 | 4.84 |
| CP29 (lhcb 4) | Q0PWS7 | 28.469 | 5.46 |
| CP26 (lhcb 5) | Q0PWS5 | 23.962 | 5.00 |
| CP24 (lhcb 6) | Q0PWS6 | 22.880 | 4.96 |
| PsbS | Q9SMB4 | 21.929 | 4.70 |

• for pI/MW calculation from mature peptide, the transit peptide indicated by Babiychuk et al. (1995), was removed manually from the available sequence.

Lastly, lane II of *N.tabacum* and *Nt(Hn)* and lane III of *H.niger*, contained a band at about 43 kDa, indicated by the green arrow in Fig 6.3. Similar bands were reported by Ruban et al. (1994) to be CP43, a core antenna protein of PSII. This protein is encoded by the chloroplast and notably, in the gels, its location in the *Nt(Hn)* SDS profile in lane 4 (pH 4.3-4-4.3) compares with *H.niger*, while in *N.tabacum*, the same band appears in lane 3 (IEF fraction III) with a slightly higher pI of 4.5-4.4. Surprisingly then, the theoretical pI and MW of CP43 in *H.niger* and *N.tabacum*, calculated in ExPASy using published sequences of mature proteins (Uniprot accession numbers are A0A059Q5U7 and P06413 respectively), was identical at 50.4 kDa and a pI of 6.34. It is possible that the apparent difference in CP43 pI points may be explained by slight differences in the local environment of the IEF gel caused by other chloroplast encoded proteins that distinguish *Nt(Hn)* and *H.niger* from *N.tabacum*.

## 6.3 Molecular weight based separation reveals novel LHC bands in *Nt(Hn)*

To better resolve the LHC content of IEF band IV, the fraction was run on higher percentage acrylamide gels (15 %), presented in Fig 6.4b. In the region of 25 to 20 kDa, a total of seven bands were counted in the *N.tabacum* sample and five in the *H.niger* sample. *Nt(Hn)* LHC separation revealed eight bands, demonstrating the presence of at least one novel band as compared to *N.tabacum*, suggested to be the band indicated by the pink arrow (Fig 6.4b). Other differences in band MWs and stoichiometry between *Nt(Hn)* and its nuclear parent, were also apparent.

Density plots of each lane were created to aid comparative analysis (Fig 6.4c), the peaks of the seven *N.tabacum* bands are defined by lines labelled 1-7. These fitted fairly well with the main peaks in the *H.niger* density profile with a few exceptions. *N.tabacum* peaks 1,2 are replaced by one large band in *H.niger* and peak 3 is absent. *H.niger* peaks 6 and 7 fall at slightly higher MW than in *N.tabacum*, and are indicated separately (Fig 6.4c). According to the literature (Aro et al., 2005; Caffarri et al., 2009), and to predicted MWs (Table 6.1), other than the major (lhcb1-3) and minor (CP24, CP26 and CP29) antenna proteins (polypeptides), the proteins comprising other bands, particularly at low MW are likely to be PsbP (OEC23), PsbQ (OEC16) and PsbS.

The dimeric band that was noted in the SDS-PAGE gels of peak IV-V IEF fractions (Fig 6.3), resolved in Fig 6.4b,c, as peaks 1 + 2 (or the single large band in *H.niger*) comprising the first of the dimeric band and peak 4 comprising the second. The weaker intermediate band, peak 3, was obscured in the previous gels

by the strong presence of bands 1, 2 and 4, and its comparatively low yield at 9.4 % (calculated from the total area of all seven *N.tabacum* bands). Interestingly, peak 3, was not detected in *H.niger* but had a relatively large percentage content (25.4 %) in the *Nt*(*Hn*) profiles.

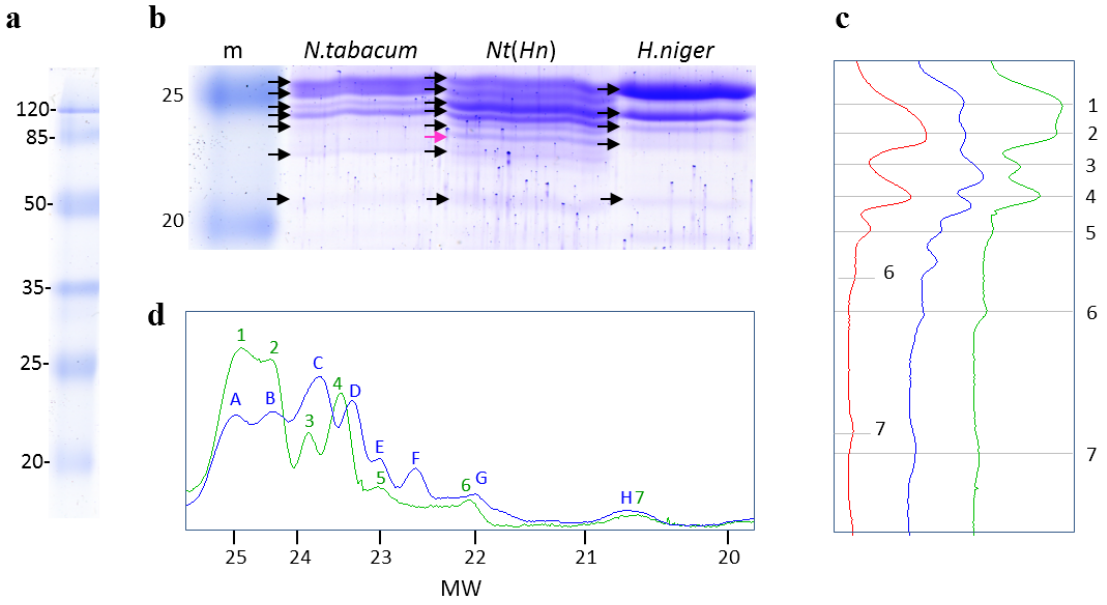


**e**

| ***N.t.*** | **1** | **2** | **3** | **4** | **5** | | **6** | **7** |
|---|---|---|---|---|---|---|---|---|
| **MW** | 25.1±0.30 | 24.6±0.03 | 23.9±0.04 | 23.6±0.10 | 23.1±0.10 | | 22.2±0.21 | 20.7±0.63 |
| **%** | 35.1 | 20.6 | 9.4 | 17.8 | 7.3 | | 4.5 | 5.2 |
| ***Nt*(*Hn*)** | **A** | **B** | **C** | **D** | **E** | **F** | **G** | **H** |
| **MW** | 25.0±0.14 | 24.7±0.21 | 23.7±0.12 | 23.3±0.15 | 22.9±0.11 | 22.6±0.23 | 21.9±0.22 | 20.6±0.31 |
| **%** | 20.4 | 17.2 | 25.4 | 13.7 | 6.1 | 6.7 | 7.5 | 3.0 |
| **ΔMW** | 2.4 | 2.1 | 1.1 | 0.7 | 0.3 | - | - | - |

**Figure 6.4:** Molecular weight analysis of SDS-PAGE separated LHCs. **a)** The protein standard marker used to determine MW on the x-axis of the plot shown in *d*. **b)** Separation of LHCII polypeptides from IEF band IV (see Fig 6.1) in a 15 % acrylamide gel. The protein marker is shown in the first lane (m) the standard weights are indicated. **c)** Density plots of the MW profiles shown in a), of *N.tabacum* (*green*), *Nt*(*Hn*) (*blue*) and *H.niger* (*red*). Peaks were numbered 1-7 in *N.tabacum* with equivalent peaks in *H.niger* being indicated if MW differed from *N.tabacum*. **d)** Closer comparison of *N.tabacum* and *Nt*(*Hn*) density plots, the *N.tabacum* peaks are labelled as in b) and in *Nt*(*Hn*), peaks were assigned letters (A-H). **e)** MW (kDa) and percentage content of total protein area of the LHC bands. The bottom row shows the difference (Δ) in MW (kDa) with band F. Data are mean average ± SD, n = 3.

For close comparison of *Nt(Hn)* and *N.tabacum* LHC bands, the density plots were overlayed (Fig 6.4d). *N.tabacum* peaks (1-7) are indicated and *Nt(Hn)* peaks were differentiated from A-H. The banding in *Nt(Hn)* differed from *N.tabacum* in two ways. Firstly, in the number and alignment of the bands and secondly, in protein stoichiometry. In the first case, *Nt(Hn)* peaks A, B, E, G and H aligned well to the wildtype bands 1, 2, 5, 6 and 7 respectively. Bands, C and D, were shifted to slightly lower MW respective to the equivalent bands, 3 and 4 in *N.tabacum*. However the apparent MW change, may be an artefact of relatively high protein content of C and D, causing the bands to spread into a lower MW region.

Band F in *Nt(Hn)* was novel, without an equivalent in the *N.tabacum* or *H.niger* polypeptide separations (Fig 6.4d). It had a fairly large relative protein content at 6.7 % of the total protein content (Fig 6.4e) and was clearly defined. A possible hypothesis to explain both the appearance of the novel band F and the reduced protein content of band A and B relative to *N. tabacum*, is that band F proteins might be a subset of truncated forms of A/B band proteins.

## 6.4 Proteomic investigation of LHCII

To test for N-terminal truncation, the most definitive approach would be to sequence the N-terminus. However, all N-terminal sequencing techniques require protein purity, which is considered unobtainable in natural samples of LHCII due to the similarity of the closely related monomers of lhcb1, lhcb2 and lhcb3. Moreover, lhcb1 is known to have at least five isoforms (lhcb 1.1 - 1.5) with some estimates of more (see Table 6.1). We therefore decided to conduct proteomic analysis of the LHCs by tandem mass spectrometry (MS/MS). This method would not be able to confirm an absence of the N-terminus in the *Nt(Hn)* cybrid because an absence in the data might only be the result of a failure to recover the peptide sequence during MS/MS. However, if the N-terminus was detected, this would confirm its presence.

For mass spectrometry, we made a further collection of band IV from IEF separations of *N.tabacum* and *Nt(Hn)* thylakoids. *Nt(Hn)* band IV was collected in 0.5 mm wide strips, differentiated from cathode to anode as $IV_i$-$IV_{iv}$, pIs were 4.1-3.8 ($IV_i$), 3.8-3.5 ($IV_{ii}$), 3.5-3.2 ($IV_{iii}$) and 3.2-2.9 ($IV_{iv}$). Each fraction was subjected to SDS-PAGE on a 15 % acrylamide gel (Fig 6.5). The reason for fractionating IEF band IV, was firstly, to gain a better resolution of the protein pI based distribution within the main LHCII band and secondly, to enable selection of perhaps purer proteins after separation by SDS-PAGE (Fig 6.5).

Bands were identified as before (Fig 6.4). The extrapolation of the C-IV band into four fractions, across four lanes, revealed a general trend for lower MW bands

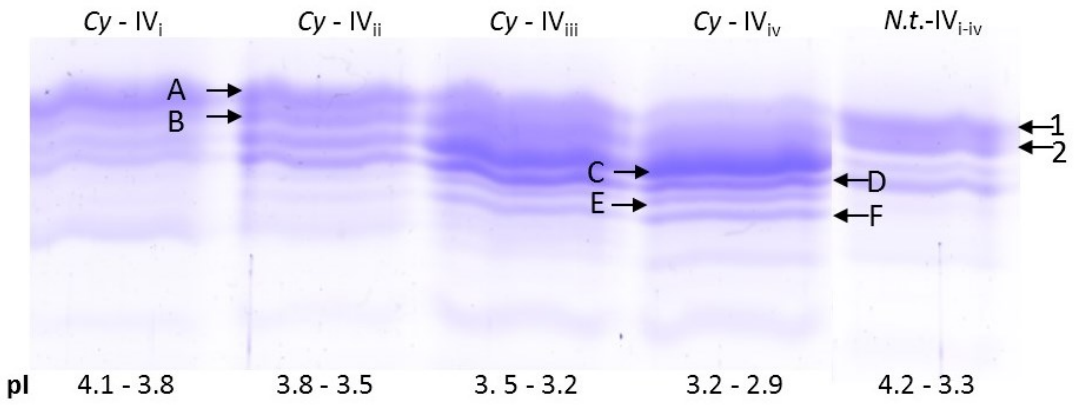


**Figure 6.5:** LHCs separated by SDS-PAGE. To prepare samples for proteomic investigation, LHCs from *N.tabacum* and *Nt*(*Hn*) were first isolated by IEF. The main green band (band IV, see Fig 6.2) was divided into four 5 mm strips (IV$_i$-IV$_{iv}$), collected and eluted. The four *Nt*(*Hn*) fractions (Cy-IV$_i$ - Cy-IV$_{iv}$) and the pooled *N.tabacum* fractions (*N.t.*-IV$_{i-iv}$) were then subjected to SDS-PAGE followed by Coomassie staining. *Nt*(*Hn*) bands (A-F), and *N.tabacum* bands (1-2), indicated in the figure, were excised from the gel and sent for proteomic analysis.

to appear in more acidic IEF fractions. The bands selected for proteomic work were 1 and 2 for *N.tabacum*, estimated to contain the LHCII proteins, and A-F for *Nt*(*Hn*), from which the principle bands of interest were C and D, due to their increased protein content, and the novel band F. The selection of the bands, indicated in Fig 6.5, was based on high concentration and clear definition in the gel. A total of eight bands for *Nt*(*Hn*) (labelled A-F) and two bands for *N.tabacum* (labelled 1-2) were excised, and sent to Cambridge Centre for Proteomics (CCP) for analysis by tandem-mass spectrometry with liquid chromatography (LC-MS/MS). Peptide sequences obtained from LC-MS/MS, were searched against UniProt and NCBI databases for protein matches, using the Mascot search engine.

The results of the Mascot search are summarised in Table 6.2. The top 5 hits are given for each band. Where alignments were found against *Nicotiana sylvestris* proteins, we BLAST searched the *N. sylvestris* sequence against *N.tabacum* in the Solgenomics database (http://solgenomics.net) which has a more up to date and comprehensive genomic dataset for the Solanaceae family. In all cases, we obtained 98 - 100 % sequence alignment with *N.tabacum*, therefore, *N. sylvestris* alignments may be considered equivalent to alignments against *N.tabacum*. The sequence similarity is because *N. sylvestris* is the maternal progenitor of *N.tabacum* the

cultivar (the male progenitor is *N. tomentosiformis*, Hasegawa et al., 2002; Yukawa et al., 2006).

Strong sequence similarity (%) was found between the MS-determined peptide sequences and the matched database sequences in all cases, for at least the top five hits (Table 6.2). This suggests that there was contamination of proteins across the excised bands. At least two isoforms of lhcb1 were found in every sample. Lhcb2.1 was also matched to peptides from several bands. The minor antennas, CP26 and CP29 were present in both *N.tabacum* bands and in band B of *Nt*(*Hn*).

**Table 6.2:** Identification, and N-terminal analysis, of *Nt*(*Hn*) LHC proteins by mass spectrometry. The top five hits from the database search, are shown for each band (Bd), 1 and 2 in *N.tabacum* and A-F in *Nt*(*Hn*). The sequence similarity of the aligned peptides to the mature protein sequence is given as a percentage. We also indicate whether the alignment was to *N.tabacum* (*N.t*) or *N.sylvestris* (*N.s.*).

| ***N.tabacum*** | | | | ***Nt*(*Hn*)** | | | | ***...continued..Nt(Hn)*** | | | |
|---|---|---|---|---|---|---|---|---|---|---|---|
| **Bd** | **Protein** | ***Sp.*** | **%** | **Bd** | **Protein** | ***Sp.*** | **%** | **Bd** | **Protein** | ***Sp.*** | **%** |
| 1 | CP26 | *N.t.* | 78 | A | Lhcb 1.2 | *N.t.* | 64 | D | Lhcb 2.1 | *N.t.* | 73 |
| | Lhcb 1.3 | *N.s.* | 74 | | Lhcb 1.5 | *N.s.* | 64 | | Lhcb ? | *N.t.* | 73 |
| | Lhcb 1.2 | *N.t.* | 74 | | Lhcb 1.3 | *N.t.* | 63 | | Lhcb 1.6 | *N.s.* | 72 |
| | Lhcb 2.1 | *N.t.* | 73 | | Lhcb 1.6 | *N.s.* | 63 | | Lhcb 1.5 | *N.t.* | 72 |
| | CP29 | *N.t.* | 68 | | Lhcb 1.7 | *N.s.* | 47 | | Lhcb 1.3 | *N.t.* | 71 |
| 2 | CP29 | *N.t.* | 73 | B | Lhcb 1.3 | *N.t.* | 73 | E | Lhcb 1.3 | *N.t.* | 82 |
| | Lhcb 1.4 | *N.s.* | 73 | | Lhcb 2.1 | *N.t* | 73 | | Lhcb 2.1 | *N.t.* | 72 |
| | Lhcb 1.7 | *N.s.* | 73 | | Lhcb 1.4 | *N.t.* | 72 | | Lhcb 1.4 | *N.s.* | 72 |
| | Lhcb 1.8 | *N.s.* | 71 | | CP26 | *N.t.* | 60 | | Lhcb 1.6 | *N.s.* | 71 |
| | CP26 | *N.t.* | 64 | | CP29 | *N.t.* | 57 | | CP24 | *N.t.* | 49 |
| | | | | C | Lhcb 1.3 | *N.t.* | 74 | F | Lhcb 1.2 | *N.t.* | 74 |
| | | | | | Lhcb 1.7 | *N.s.* | 74 | | Lhcb 2.1 | *N.t.* | 73 |
| | | | | | Lhcb 1.8 | *N.s.* | 74 | | Lhcb 1.6 | *N.s.* | 72 |
| | | | | | Lhcb 2.1 | *N.t.* | 74 | | Lhcb 1.3 | *N.t.* | 71 |
| | | | | | Lhcb 1.6 | *N.s.* | 73 | | CP24 | *N.t.* | 57 |

Matched protein sequences are presented in Table 6.6. We show 90 amino acids starting from the $27^{th}$ residue of the transit peptide at the N-terminus. Although alignments were made only from mature proteins, the transit peptide sequence is included for reference and is highlighted on a black background. The start of the mature polypeptide, usually begins one residue downstream from the leading methionine (Michel et al., 1991). Peptide alignment with the sequence is

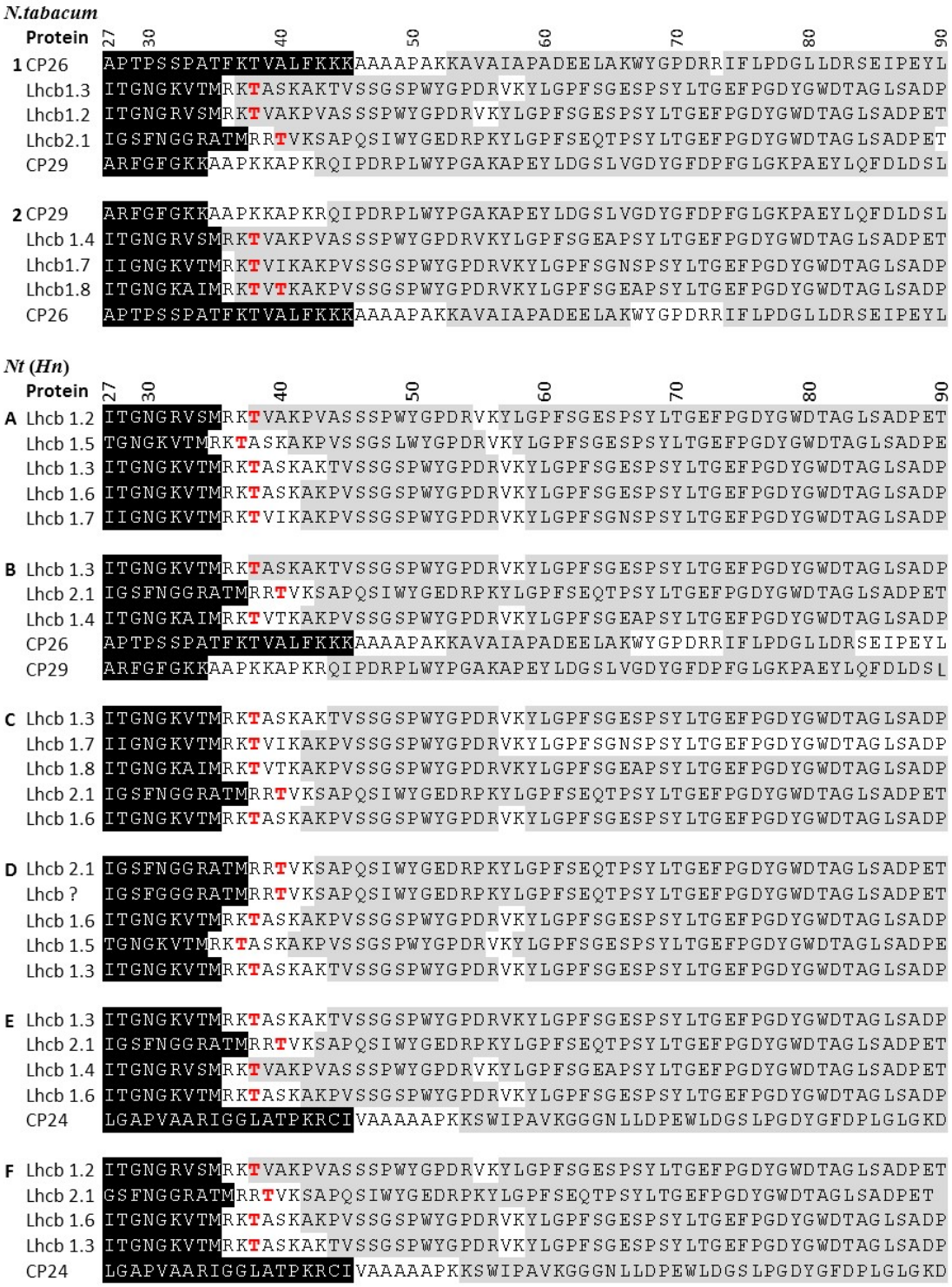


**Figure 6.6:** Summary of Mascot search results. MS/MS data were searched against NCBI and Uniprot databases for protein identification, using the Mascot search engine. The top five 'hits' are listed for *N. tabacum* samples 1-2, and *Nt*(*Hn*) samples A-F (identified on the left). N-terminal sequences are shown from residues 27-90. The first 26 residues are removed for clarity, the remaining transit peptide is shown on a black background. A grey background indicates where peptides identified from MS/MS, matched the protein sequence. Phosphorylation sites that are involved in state transitions are shown in red.

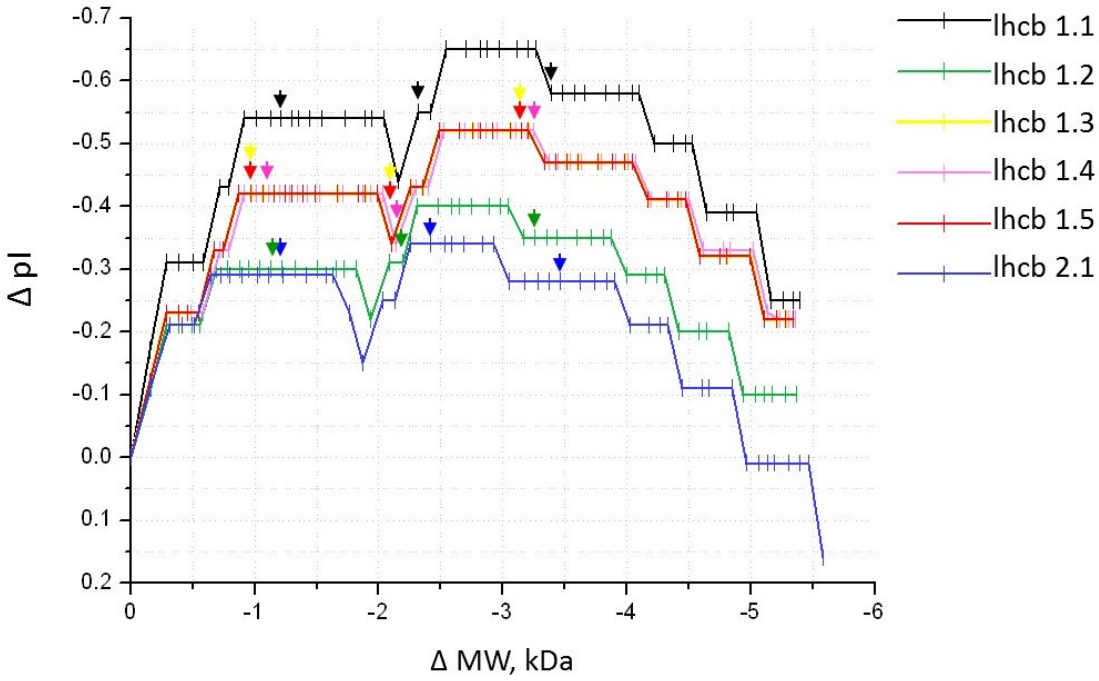


**Figure 6.7:** Theoretical changes in pI as N-terminal amino acids are removed. Using ExPAsY MW/pI calculation software, we calculated the pI point and MW of each of the lhcb1 isoforms (lhcb1.1 - lhcb 1.6), and of lhcb2.1 as amino acid residues were removed one by one. From this data we calculated ΔpI and ΔpH in respect to the full length sequence of the mature protein. Each small vertical line in the plot represents the amino acid removal, arrows indicate the 10th, 20th and 30th residue in each polypeptide.

highlighted in grey. N-terminal threonine residues of the lhcb1 and lhcb2 proteins are highlighted in red. These are the sites of phosphorylation that triggers the detachment of LHCII from PSII for migration to PSI in state transitions.

In order to gauge how the removal of N-terminal amino acids affects the pI point and MW of LHC proteins, mature peptide sequences of lhcb1 isoforms and lhcb2 (UniProt accession numbers in Table 6.1), were loaded into ExPAsY MW/pI calculation software and MW and pI were determined after sequential removal of individual N-terminal amino acid residues. The change in MW (ΔMW) and pI (ΔpI) was determined according to the difference with the full-length mature protein. Fig 6.7, shows the plots of ΔpI against ΔMW, calculated for lhcb1 and lhcb2 monomers. The plots show that even the removal of one amino acid, in all cases an arginine, causes a large ΔpI from $^{-}$0.21 - $^{-}$0.31. The removal of 4-6 amino acids causes a ΔpI of $^{-}$0.28 - $^{-}$0.43 depending on which lhcb protein has

been altered. In lhcb1.1,1.4 and 1.5, the removal of a further three residues again further reduces the protein pI.

The threonine phosphorylation site that is involved in state transitions is the third residue of the mature peptide. In Table 6.6, peptide alignments at the N-terminus are missing for between 6-8 residues in all the matched sequences, with the exception of lhcb1.2 in band A and lhcb1.3 in band B. By comparison in the peptide alignments for the proteins in bands 1 and 2 of *N.tabacum*, there are six hits against lhcb1/lhcb2 proteins, all of which include a peptide alignment at the N-terminus, including the threonine residue at position three. We need to emphasise that an unaligned region in mass spectrometry data does not confirm an absence, however the consistent non-alignment at the N-terminus, seen in all bands of the *Nt*(*Hn*) LHCs, except in bands A and B, where MW was the same as wildtype *N.tabacum*, strongly suggests that the N-terminus of the lhcb1 and 2 proteins was truncated. This is most likely due to misidentification of the transit peptide during cleavage.

## 6.5 Discussion

Based on the discovery during IEF, that *Nt*(*Hn*) LHCs had novel, lower pIs (Chapter 5), we investigated *Nt*(*Hn*) LHCII proteins for modification, with the expectation that the analysis might provide an explanation for state transitions inhibition and altered NPQ response in *Nt*(*Hn*). MW-based separation of *N. tabacum* LHCs collected from IEF gels, showed seven bands. Seven bands following the same basic migration pattern were also found in the *Nt*(*Hn*) cybrid. An additional eighth band (band F; Fig 6.4d) in *Nt*(*Hn*) was novel in that it was not present in either of the parent species.

Proteomic analysis was performed on each band. The LHC proteins from each *Nt*(*Hn*) sample were identified as, mostly, various isoforms of lhcb1/2 proteins from *N. tabacum*. From each of bands A,B,E and F, a single match was made against an lhcb1 isoform with almost complete N-terminal sequence coverage, in all other matches against lhcb1/2 isoforms, the sequence coverage did not include the first 5-8 N-terminal residues. In contrast, all *N. tabacum* peptide sequences retrieved from MS/MS and matched with lhcb1/2 isoforms, showed coverage at the N-terminus with the exception of only the first 1-2 amino acids. The results suggest that the N-terminus had been lost from a significant subset of the *Nt*(*Hn*) lhcb polypeptides.

The findings were somewhat surprising in that although, based on previous cybrid research, we expected that N-terminal removal might be the cause of novel pI and MW, we expected to find the truncated polypeptides in the novel MW

band, namely Band F, and perhaps as additional co-migratory proteins, in the other relatively low MW bands (e.g. bands C-E). However, peptide coverage of the N-terminus was absent to a comparable degree throughout the results for all the bands, including the relatively high MW bands A and B.

The fact that the five proteins with highest sequence coverage that were identified in each of the six *Nt*(*Hn*) samples were mostly of the same few types, namely, lhcb1/2 isoforms (Fig 6.6), which have almost identical MW (Table 6.1), and furthermore, from the proteomic data, were found to have similar sequence coverage throughout (Table 6.2), contradicts the notion that they migrated to six different, distinct positions in the gel. The results instead support the hypothesis that the excised gel bands were all subject to contamination from the same source(s), probably just one or two of the high protein concentration bands. It is most likely that contamination occurred during gel band excision.

If the results presented in Fig 6.6 represent contaminant proteins, then they are not indicative of the bulk protein content of the bands, and the real identity of the proteins in the bands remains unknown. Nevertheless, the data do indicate that a subset of lhcb1/2 proteins in which the N-terminus was truncated, was present in the *Nt*(*Hn*) cybrid and furthermore that the cleaved terminus included the threonine that is the site of phosphorylation in state transitions.

### 6.5.1 Possible mechanisms for LHC N-terminal mis-processing in the *Nt*(*Hn*) cybrid

Based on our isolation of LHCII from thylakoid preparations, as well as on measurements of photosynthetic function, protein quantification and grana stacking, we know that the truncated lhcb proteins were present in the thylakoid membranes of the *Nt*(*Hn*) cybrid, furthermore we know that the LHCII antenna was present in comparable quantities to that of the wildtype parent species. The N-terminal cleavage therefore occurred either after the LHC protein (LHCP) arrived at its final destination in the thylakoid membrane or, if it occurred at sometime prior to delivery, the truncation of the LHCP did not notably affect the delivery pathway.

#### 6.5.1.1 LHCP transport to the thylakoid membrane

The transport of nuclear-encoded chloroplast proteins to their final location within the chloroplast involves passage across several compartments and membranes. Firstly, the protein is synthesised in the cytosol as a precursor protein with an amino-terminal extension called a chloroplast transit peptide (cTP), which addresses the precursor LHCP (pLHCP) to the chloroplast stroma (Jarvis, 2008; Soll and Schleiff, 2004). pLHCP is imported into the chloroplast through the TOC-TIC

membrane gateway (see §1.2.1; Cline and Henry, 1996; Fuks and Schnell, 1997; Paila et al., 2015; Soll and Schleiff, 2004).

The necessity of the N-terminal cTP for the arrival of nuclear-encoded proteins into the stroma has been demonstrated (Buvinger et al., 1989; Gómez et al., 2003; Bruce, 2001; Forsberg et al., 2005). In addition, outside of the chloroplast, in the cytosol, the precursor LHCP of the *Nt*(*Hn*) cybrid is in a 'native' *N. tabacum* encoded environment, and so N-terminal removal in this compartment, due to cybridisation, would seem unlikely. We may assume then that *Nt*(*Hn*) LHCP N-terminal removal occurred within the chloroplast.

**SPP cleaves the pLHCP cTP.**

Once in the stroma, the cTP is cleaved from pLHCP by a nuclear-encoded, general stromal processing peptidase (SPP; Oblong and Lamppa, 1992; Richter et al., 2005), yielding the mature LHCP (mLHCP). The SPP enzyme recognises and binds to the cTP without interacting with the mature protein sequence (Richter et al., 2008), it then cleaves the polypeptide at the junction between the cTP and the mature protein in a single step, this releases the mature protein into the stroma, while the cTP is still bound. The cTP is only liberated after SPP cleaves again, forming two cTP fragments (Teixeira and Glaser, 2013), these are released and then enzymatically degraded in the stroma (Moberg et al., 2003).

As an N-terminal cleaving enzyme, SPP would seem a likely candidate for mis-processing the N-terminus of the *Nt*(*Hn*) LHCs. However, the SPP enzyme is nuclear encoded, and so poses the question: why would a *N. tabacum* nuclear-encoded SPP misprocess a *N. tabacum* nuclear-encoded LHCP? A possible explanation might be that the SPP has somehow been affected by a chloroplast encoded factor. However, no chloroplast-encoded component has been identified in the SPP pathway. Furthermore, one of the remarkable characteristics of SPP is that it is responsible for the removal of the cTP from most, if not all nuclear-encoded precursor proteins, that have entered the chloroplast via the TOC-TIC gateway (Richter et al., 2005). Not only are the proteins of a broad range, but the cTPs themselves are highly divergent, varying in length from 31-142 amino acids, without recognisable consensus sequences or secondary structure motifs (Richter et al., 2008).

Indeed, the conserved function of the cTPs seems to be somewhat at odds with the high levels of heterogeneity of their primary structures (Bruce, 2001). With this in mind, together with the understanding that SPP has been shown to not interact with the mature protein during cTP removal, it would perhaps seem unlikely that a possible interaction between the *N. tabacum* SPP and a *H. niger*

factor would cause the SPP enzyme to cleave the mature side of the cTP-mature protein junction. However, we cannot rule out that contained within the mature sequence domain is some structural component that enables the SPP to identify the cleavage site (Bruce, 2001), and could present a possible point of difference in the *Nt*(*Hn*) cybrid that leads to miscleavage if a *H. niger*-encoded factor is involved in cTP cleavage of *N. tabacum* LHCP.

### LHCP in the SRP pathway

Following cTP removal by SPP, nuclear-encoded chloroplast proteins enter one of four pathways for transportation to their final compartment or membrane (Jarvis and López-Juez, 2013). Two of the pathways, the chloroplast secretion (cpSEC) and the chloroplast twin arginine translocase (cpTAT) pathways, are dedicated to the transfer of proteins bound for the lumen. The transit peptide of lumen-targeted proteins is bipartite, whereon the removal of the cTP, exposes a second sequence, that forms the lumen transit peptide (lTP), which 'addresses' the precursor protein to the lumen. Here, thylakoidal processing peptidase (TPP) removes the lTP (see Jarvis and López-Juez (2013), for a review).

Nuclear-encoded proteins that are destined for insertion into the thylakoid membrane, translocate to the thylakoid either spontaneously, or via the chloroplast signal recognition particle (cpSRP) pathway. The transfer of nuclear-encoded proteins by the cpSRP pathway, so far, is found to be exclusive to LHCP (Gao et al., 2015), and does not involve a second transit peptide (Schünemann, 2004). This pathway is also remarkable in that it has uniquely evolved, in several ways, from an otherwise extremely conserved membrane-targeting SRP system that is retained in both the prokaryotes and eukaryotes (Akopian et al., 2013).

In the conserved pathway, the SRP is a ribonucleo-protein, and the protein delivery system that it mediates, is expressly co-translational (Schünemann, 2004). As mRNA translation proceeds in the ribosome, the nascent polypeptide N-terminus emerges and SRP recognises and engages with it via a signal sequence within the N-terminus. Through interaction with an SRP receptor (SR) associated with the target membrane, the ribosome-nascent chain (RNC)-SRP complex is delivered to a translocon within the membrane (Akopian et al., 2013). Here, SRP and SR dissociate and the nascent polypeptide is inserted into, or through, the membrane (Akopian et al., 2013; Groves et al., 2001).

The co-translational SRP-mediated pathway is also used in chloroplasts to deliver chloroplast-encoded nascent polypeptides to the thylakoid membrane. The separate, specialist cpSRP pathway that has evolved for the seemingly exclusive transfer of nuclear-encoded LHCP to the thylakoid membrane, is unique in that it

occurs post-translationally and does not include SRP-RNA (Schünemann, 2004). Furthermore, a 43 kDa SRP subunit (cpSRP43) is found only in cpSRP, and is responsible for binding a second, universally conserved subunit, cpSRP54 (Richter et al., 2008).

After cTP cleavage from LHCP by SPP, a specific region of protein-interaction motifs in the cpSRP43 binds with a 18 amino acid region (L18) located between the second and third transmembrane domains of mLHCP (Stengel et al., 2008). cpSRP43 and cpSRP54 are then thought to fold around the mLHCP creating a 'transit complex' that allows the highly hydrophobic mLHCP to traverse the stroma to the thylakoid membrane (Schünemann, 2004). Here, cpSRP interacts with its membrane bound receptor, cpFtsY (chloroplast filamentous temperature sensitive Y), creating a large membrane bound complex. This complex is thought to move through the thylakoid membrane (Moore et al., 2003) until it reaches the insertase Alb3 (for Albino3; Eichacker and Henry, 2001; Yuan et al., 2002). Hydrolysis of guanosine tripohosphate (GTP) is catalysed by the GTPase domains of cpSRP54 and cpFtsY, and precedes the insertion of mLHCP into the membrane by Alb3 (Kirst and Melis, 2013).

Some aspects of the SRP-pathway are not yet fully understood, for example, ATP is necessary for the mechanism, yet no ATP-binding protein has been identified as a component (Schünemann, 2004). We also do not yet understand the insertion mechanism by Alb3 that integrates mLHCP into the membrane (Falk et al., 2010). Other components might also be involved, for example, with delivering LHCP to the SRP pathway after cTP removal (Ouyang et al., 2011). However, there is no evidence to show that the SRP-pathway involves any cleavage mechanism, nor that it involves any chloroplast-encoded factor which could cause an incompatibility in the *Nt*(*Hn*) cybrid.

Currently, it is not known how the mLHCP N-terminal domain is bound in the transit complex (Gao et al., 2015; Stengel et al., 2008). We cannot therefore rule out the possibility that the mLHCP N-terminus is sufficiently exposed in the stroma for targeting by stromally-located chloroplast proteases, during transportation to the thylakoid by cpSRP. Indeed, most schematic diagrams, depict the N-terminus as protruding into the stroma (Akopian et al., 2013; Kirst and Melis, 2013; Wang and Dalbey, 2011). This presents the potential for an interaction between a *H. niger*-encoded proteolytic factor, with the N-terminus of the *N. tabacum*-encoded LHCP in *Nt*(*Hn*), and subsequent mis-processing.

### The chloroplast Clp stromal protease

Proteases are abundant and varied in the chloroplast (Nishimura and van Wijk, 2014). A single chloroplast-encoded component has been identified in the plastid protease system (Adam et al., 2001) and has been demonstrated to be essential for plant development (Kuroda and Maliga, 2003). This is the proteolytic ClpP1 (caseinolytic protease P1) subunit of the chloroplast Clp protease complex (Adam et al., 2001), which comprises several other subunits all of which are nuclear-encoded. In plastids, Clp is located in the stroma, and is responsible for the degradation of both soluble and membrane-bound proteins, (Adam, 2000; Adam et al., 2001).

There is no direct evidence that LHC proteins are a substrate for Clp proteolytic activity *in vivo* (Nishimura and van Wijk, 2014). LHC breakdown products have however been found in mutants of the non-catalytic nuclear-encoded subunit, ClpR2 of the Clp complex (*clpR2-1*), although the authors (Rudella et al., 2006) suggest that this is most likely due to a concomitant upregulation of other thylakoid bound proteases, albeit that the identity of these proteases and their substrates are also as yet unknown.

Surprisingly, in the *clpR2-1* mutant were also found low levels of pLHCP inserted into the thylakoid membranes. Rudella et al. (2006) states that the direct involvement of Clp in cTP removal is highly unlikely, and suggests that a general imbalance in the plastid proteome homeostasis resulted in suboptimal processing by SPP. The inclusion of pLHCP in the thylakoid membrane *in vivo* suggests that the presence of the cTP does not affect the SRP-pathway, supporting the possibility that the N-terminal domain in general, does not impact either LHCII transfer across the stroma or the insertion mechanism, leaving open the possibility that the *Nt*(*Hn*) LHCP N-terminus was removed before membrane insertion.

A BLAST search of the *N. tabacum* ClpP1 gene (*ClpP*; UniProt accession no. P12210) revealed high sequence similarity (94.9 %) with *H. niger ClpP1* (UniProt accession no. A0A059Q656). Despite the lack of evidence for interaction between Clp and LHCP under normal conditions, and the high similarity of the chloroplast-encoded ClpP1 component between *N. tabacum* and *H. niger*, there remains the possibility that in the *Nt*(*Hn*) cybrid, the *H. niger*-encoded ClpP1 could cause novel proteolytic activity against the *N. tabacum*-encoded LHCP, perhaps during LHCP transit to the thylakoid, if the N-terminus was sufficiently exposed, or once in its final place within the membrane.

#### 6.5.1.2 mLHCP N-terminal cleavage as a regulatory mechanism

In addition to those reported in cybrid research, there are other accounts of N-terminally truncated mLHCP elsewhere in the literature (described below). Most of these findings are explained in terms of regulatory acclimation, although no specific pathway, acclimative function, or cleaving protein have been identified.

Early investigation of LHCP chloroplast import and proteolytic modification, used *in vitro* methods in which pLHCP transcribed from a single wheat *lhcb* gene was incubated with wheat chloroplasts (Lamppa and Abad, 1987; Clark et al., 1989). Two mature forms of  26 kDa and  25 kDa were found to be associated with the thylakoid membranes (Lamppa and Abad, 1987). Additional experiments by Clark et al. (1989), in which wheat pLHCP was also incubated with 'organelle free' wheat extract (essentially a membrane free chloroplast lysate) demonstrated that the two mLHCP forms resulted from two separate LHCP cleavage events and that the lower MW mLHCP was due to truncation about 10 aa downstream from the mLHCB N-terminus, indicating the presence of a second cleavage site at this position (Clark et al., 1989).

Similar findings were made in pea (Cline and Henry, 1996; Kohorn and Yakir, 1990) and tomato (Pichersky et al., 1987). Indeed, initial reports based on experiential work for the determination of the junction between the transit peptide and the mature protein, first identified the site to be several amino acids downstream from the position now recognised to be at about residues  34-35 of the pLHCB (Abad et al., 1989). In Clark et al. (1989)'s experiments, wheat LHCP incubation with chloroplast extract, yielded only the 25 kDa form, not the 26 kDa peptide. The findings implied that cleavage at the first site, for the removal of the cTP, was dependent upon the presence of a membrane bound component, which Clark et al. (1989) suggests, might be a membrane-bound factor that confers on the pLHCP a conformation favourable to cleavage at both sites, and which was absent in the chloroplast extracts. Cleavage at the second site, yielding the 25 kDa polypeptide, is indicated to be by a soluble protease and seemed not to be dependent on cleavage of the cTP (Clark et al., 1989).

Differentially N-terminally processed lhcb forms have also been shown to exist *in vivo* in the algae *Chlamydomonas reinhardtii* (Stauber et al., 2003). Both *lhcbm6* and *lhcbm3* gene products (pertaining to lhcb1.3 and lhcb1 in higher plants respectively; Forsberg et al., 2005) have been found in two forms with different MW and pI, due to post-translational modification (PTM). Caffarri et al. (2005) also reported lhcb proteins of various length in *Zea mays* after various light and temperature treatments. Although they consider the various lhcb proteins to be independent gene products, they do not rule out the possibility that the

diversity of the lhcb proteins might instead (or also) be due to differential cleavage by a processing peptidase (Caffarri et al., 2005).

Forsberg et al. (2005), describes two proteolytic events against lhcb1 *in vitro*. In their work, they are able to ascribe the different proteolytic activity to two proteases discovered in pea (*Pisum sativum* L.) chloroplasts during *in vitro* experiments. The proteases catalysed endo-proteolytic cleavage of the N-terminus of pea lhcb1. One protease was stromally located and suggested to be involved with LHCP degradation. The other protease was shown to be thylakoid-associated, and by the addition of various inhibitors and other factors, was found to be different from the chloroplast proteases that had already described, although its identity was unsolved. Remarkably, the thylakoid localised protease cleaved at only one site, between residues 9 and 10 of the mature protein (Forsberg et al., 2005).

The work outlined above (Lamppa and Abad, 1987; Abad et al., 1989; Clark et al., 1989; Stauber et al., 2003; Forsberg et al., 2005; Cline and Henry, 1996; Kohorn and Yakir, 1990; Pichersky et al., 1987) conclusively reveals differential N-terminal processing of lhcb forms *in vitro*, with evidence that the same phenomenon occurs *in vivo* in algae (Stauber et al., 2003), and there is an indication that it also occurs in higher plants *in vivo* (Caffarri et al., 2005). That this type of post-translational modification (PTM) in lhcb proteins might have so far evaded detection in wildtype plant species, seems possible given that the lhcb protein content of the thylakoid is not often fully and conclusively identified, due at least in part to the large number of the lhcb protein types, the large number of isoforms and the similarity in sequence and MW throughout. It therefore seems reasonable to suggest that the variation in the lhcb proteins that are present in wildtype thylakoids could be, to some extent, due to differential N-terminal processing, rather than being solely the products of individual genes.

In several cases the cryptic cleavage site was found to be between 9-10 residues of the mature lhcb (Abad et al., 1989; Lamppa and Abad, 1987; Clark et al., 1989; Forsberg et al., 2005). Additionally, Forsberg et al. (2005) also newly describe a thylakoid-bound protease, although unidentified, that specifically cleaves between residues 9-10 of the lhcb protein. Stauber et al. (2003) and Forsberg et al. (2005) both suggest that as the lhcb N-terminal deletion observed in their investigations, led to the removal of the phosphorylation site that is involved in state transitions, their results might indicate a novel regulatory mechanism, and Forsberg et al. (2005) implicates the thylakoid bound protease as an important component.

This work (Lamppa and Abad, 1987; Abad et al., 1989; Clark et al., 1989; Stauber et al., 2003; Forsberg et al., 2005; Cline and Henry, 1996; Kohorn and Yakir, 1990; Pichersky et al., 1987) also describes systems in which the LHCP and the chloroplast are of the same specific origin. The work also Notably, in

systems where 'alien' or non-native components were used together, N-terminal truncation of the mLHCP have also been reported, although the cleavage site usually deviated from the 10 aa reported in 'native' systems. As already discussed, Babiychuk et al. (1995) reported truncation of the lhcb1 protein of *Nt*(*Ab*) cybrid plants, to be at 11-12 aa. While in the *Nt*(*Hn*) cybrid, we reported the cleavage at 5-8 aa from the N-terminus. To try and explain the LHC alterations observed in their *Nt*(*Ab*) cybrid, Babiychuk et al. (1995) suggests the involvement of a chloroplast-encoded accessory factor associated to the cleaving protease, that is responsible for recognising the cleavage site. Could the unidentified thylakoid-bound protease described by Forsberg et al. (2005) include a chloroplast-encoded factor that in cybrid plants might confer a novel proteolytic regulatory action on the nuclear-encoded lhcb?

If so, we might then explain the novel MW bands observed in the cybrid lhcb gel separations in this work and elsewhere (Babiychuk et al., 1995; Kushnir et al., 1987; Peter et al., 1999), to be the result of mis-identification, not of the cTP-mLHCP junction, but of a second cryptic cleavage site that appears to be utilised in a, as yet poorly understood, regulatory mechanism and which takes place in the thylakoid membrane. Under these circumstances we could then regard the cybrid plant as a useful model for further investigation of such a mechanism, as it is precisely the misprocessing of the lhcb proteins in the cybridised plant, manifested as novel MW bands compared to wildtype species, that allows for the detection of N-terminal deletion of the mLHCP.

Some of the reports are at odds with each other as to the location of the protease for the second cleavage site. The *in vitro* work by Lamppa and Abad (1987); Clark et al. (1989) suggests that the second cleavage site depends upon a stromally located protease, while Forsberg et al. (2005) concludes that the second N-terminal deletion is performed by a thylakoid-associated protease. Throughout the work however, the site of cleavage between residues 9-10, is consistent, suggesting that the same site might be acted upon by various proteases located in the thylakoid or the stroma.

Additionally, the suggestion by Forsberg et al. (2005) and Stauber et al. (2003) that the N-terminal removal might be a regulatory mechanism for the control of the state transitions mechanism is contradicted by reports from Kuttkat et al. (1995) in which the proteolytic N-terminal removal of LHCII is reported to occur only in monomers, while trimers are resistant, suggesting that in trimers, the N-terminal domain is shielded from the protease. Clearly there is a need for much more research regarding the existence, function and mechanism of possible lhcb regulation through N-terminal cleavage and the implications for both state transition and NPQ mechanisms.

# Chapter 7

# General discussion

The aim of this project was to begin an investigation of the regulatory and acclimative abilities of the *Nt*(*Hn*) cybrid plant to the light environment. We examined *Nt*(*Hn*) acclimation to long-term growth under LL and HL, at the level of the whole plant, leaf, cell, chloroplast, thylakoid, protein and pigment content. We also explored the responses to short-term (seconds to minutes) light changes in terms of regulatory molecular mechanisms: NPQ and state transitions. As far as we are aware, no other investigation of either light acclimation or light harvesting regulation by molecular mechanisms in cybrid plants, has been made.

The ability of a plant to plastically couple its structural and functional phenotypes to the abiotic light environment is crucial. The observable plant phenotype is the result of an immensely complex and poorly understood regulatory signalling network of retrograde and anterograde communication systems and feedback networks between subgenomes (Woodson and Chory, 2008). The expression and degradation of proteins must be tightly coordinated for optimal photosynthetic acclimation to long-term light conditions (Yang et al., 2000). A combination of regulated gene expression, post-transcriptional and post-translational modifications serve to build a proteome suitable for the prevailing environment. It is therefore unlikely that straight forward deductions regarding regulatory pathways, can be made from simple observed alterations within the phenotype alone.

The strong coupling of function and regulation between the chloroplast genome and the nuclear genes that encode chloroplast proteins is likely to pose strong limitations on their independent evolution (Greiner et al., 2011; Greiner and Bock, 2013). Ultimately, the nuclear-chloroplast incompatibility that is observed as an inhibited, sometimes deleterious, phenotype of a cybridised plant, is considered to arise because of the coevolution between the nuclear and chloroplast genomes of each of the parent plant species. Cybrid plants offer an intriguing model for investigation of plant regulation against the flux of natural light, both at the level of

the thylakoid membrane where the novel combination of inter-specific proteins are structurally and functionally bound to each other, and at the level of inter-specific, concerted genome and proteome regulation, for acclimation to the prevailing light environment.

In Chapter 3, we made a general presentation of the *Nt*(*Hn*) cybrid germination, growth and flowering characteristics. The outward aspect of the *Nt*(*Hn*) cybrid was predominantly of *N.tabacum*, although some novel developmental and physical traits were observed. Most notably, there was a large reduction in the proportion of viable seeds, a two-three week delay in germination and reduced growth rates that put the *Nt*(*Hn*) cybrid about three-four weeks behind *N. tabacum* in terms of overall size. In comparing plants of the same age (no. of days from seed sown), although much smaller in size, the number of leaves on the *Nt*(*Hn*) cybrid was comparable to *N.tabacum*. The disturbed phenotype of *Nt*(*Hn*) was therefore due to non-proportional growth, which resembled dwarfism, where leaf size, but not leaf number had been effected by cybridisation. The difference in size between *N. tabacum* and *Nt*(*Hn*) had almost disappeared in the mature plants, indicating that the factors inhibiting leaf size were transient during development.

Cell isolation of *N.tabacum* at 8 weeks and *Nt*(*Hn*) at 12 weeks (Chapter 4) recovered only loose clusters of chloroplasts in both preparations. This was presumably because of incomplete cell maturation, leading to cell wall disintegration during the preparation. The findings suggest that at the cellular level, development was at a similar stage between *N.tabacum* and *Nt*(*Hn*), despite the age difference. A possible explanation may be that cellular maturation and maturation in terms of leaf number, are governed differently, with the former being disturbed due to cybridisation.

Plant growth, and subsequently plant architecture, is largely regulated by hormone signalling. The *Nt*(*Hn*) cybrid exhibited morphological disturbance presumably due to altered hormone signalling. However we cannot know whether the plant dwarfism, resulted from genetic disturbance or from environmental stresses that caused stunting, due directly to sustained damage or to stress- or damage-induced hormone response (Zhang and Turner, 2008). If *Nt*(*Hn*) had an increased sensitivity to the light environment the extra stress may have resulted in altered hormone signals. Alternatively, if the factors involved in hormone signalling combined chloroplast and nuclear encoded factors, then there is the possibility that an incompatibility between them caused a breakdown in the pathway and subsequently in the hormone release.

Unexpectedly, we found abnormal flower morphology in some of the wildtype *N.tabacum* plants. They were similar to the *Nt*(*Hn*) cybrid flower abnormalities in terms of varying petal number, sometimes within one inflorescence. In two separate

cases, there were extreme deformities in the flower head. *N.tabacum* is a species of plant that is well suited to genetic studies and has been used in laboratories extensively. This is particularly true of the cultivar Wisconson38 (W38), that was used in this study and so it seems probable that the lineage was subject to transgenic studies in the past.

Transgenic manipulation is known to be a cause for genetic, somatic mosaicism (Vig, 1978). This means that adjacent cells in a tissue layer can have different genomes. Genetic mosaicism can incur chromosomal aberrations or organeller recombination. The mechanisms and causes of inactivation of genes behind some forms of mosaicism are still unknown (Loginova et al., 2012). In our analyses of other traits in *N. tabacum* including vegetative growth, cell, chloroplast and thylakoid structure, protein and pigment content and ETR, we did not observe any other obvious abnormalities. The observable effects of possible mitochondrial recombination in wildtype *N. tabacum*, were apparently limited to flower morphology and flower development.

Long-term acclimation of the *Nt*(*Hn*) cybrid was assessed in Chapter 4. The most notable phenotypic alterations caused by cybridisation, were the increased number of chloroplasts under LL as compared to *N. tabacum*, a large starch accumulation in both LL and HL plants that seemed also to severely disrupt the thylakoid membranes and a reduced chloroplast size despite a greater number of layers in each grana.

In a study by Labate et al. (2004), the *Lhcb*1-2 gene from pea (*Pisum sativum*) was inserted into *N. tabacum* and constitutively expressed alongside *N. tabacum* encoded LHCs. The pea transgene was first modified by fusing the DNA sequence encoding the mature portion of the pea *Lhcb*1-2 protein, with the DNA transit peptide sequence of pea small subunit ribulose-1, 5-bisphosphate carboxylase (Rbcs; Labate et al., 2004). In the established transgenic *N. tabacum* plant lines, the presence of both pea and *N. tabacum* lhcb1-2 proteins was confirmed in the thylakoid membranes.

Labate et al. (2004) reported stress-related phenotypes in their transgenic plants that closely matched those found in the *Nt*(*Hn*) cybrid of this study, including changes in the whole plant, increased starch content in cells, disturbed thylakoid arrangements and an increased qE (Labate et al., 2004). Although the study did not report the presence of novel MW lhcb proteins. In the system used by Labate et al., 2004, with the exception of the lhcb1-2 protein, the whole plant, including the plastid, was of a single specific origin. This work raises the possibility that the phenotype that we observe in the *Nt*(*Hn*) cybrid might arise due only to the introduction of an alien (*N. tabacum*) lhcb into a *H. niger* chloroplast, while the other novel interactions between *N. tabacum* and *H. niger* encoded components

might have little impact.

The lack of any modification to the MW of the pea LHC proteins (Labate et al., 2004) might indicate that PTM or mis-processing of the LHC polypeptides is dependent on a chloroplast-encoded factor. In other words, perhaps it was because the protease system in Labate et al. (2004)'s experiment was of single specific origin that there was no mis-identification of the cleavage site, even though the proteolytic activity was against an 'alien' lhcb protein. This is consistent with the notion that an incompatibility between a chloroplast-encoded and a nuclear-encoded factor created the novel MW lhcb in *Nt*(*Hn*).

In Chapter 6, we present evidence that indicates the deletion of the N-terminus of the *N. tabacum* lhcb1/2 protein in *Nt*(*Hn*) and we put forward the hypothesis that the removal of the threonine at the N-terminus was responsible for the near total inhibition of state transitions that was reported in Chapter 5. The LHCII N-terminal domain has also been demonstrated to be essential or important in several other processes. As well as being the site of phosphorylation to activate transition from state I to state II, the LHC N-terminus has also been found to be necessary for grana stacking, LHC aggregation (Ruban and Horton, 1992), trimerisation (Hobe et al., 1995) and LHC proteolysis (Zybailov et al., 2008).

Hobe et al. (1995) found that the N-terminal domain was involved in stabilising the LHCII trimer, although the first 15 amino acid residues of the mature LHC were shown to be unnecessary for trimerisation, residues 17-21, were found to be essential. In the alignment of MS/MS peptide fragments of the *Nt*(*Hn*) LHC proteins with online LHC sequences, the N-terminus was only absent by a maximum of 8 residues in the mature protein sequence. It is therefore unlikely that N-terminal removal affected trimerisation of the lhcb monomers.

The arrangement of trimeric LHCII complexes in the thylakoid membrane is depicted in Fig 7.1. The arrangement within the surface allows complimentary binding with the facing thylakoid surface, a feature necessary for the stacking of and stability of the thylakoids into granal structures. Correct development and stability of the thylakoids is dependent amongst other things, upon the protrusion of the N-terminus of the LHCII proteins into the stroma. The shortening of the N-terminal domain by 5-8 aa, does not seem to have inhibited the formation of grana, in fact, interestingly, the grana contained more layers in *Nt*(*Hn*).

LHCP proteolysis, requires recognition of, and binding to the N-terminus by factors of the chloroplast protease system (Zybailov et al., 2008). Proteolysis is crucial for the maintenance of a stoichiometrically balanced assemblage of thylakoid membrane proteins (Yang et al., 2000). The expression and degradation of proteins must be tightly coordinated for optimal photosynthetic acclimation to long-term light conditions (Yang et al., 2000). From FPLC elution profiles, we can determine

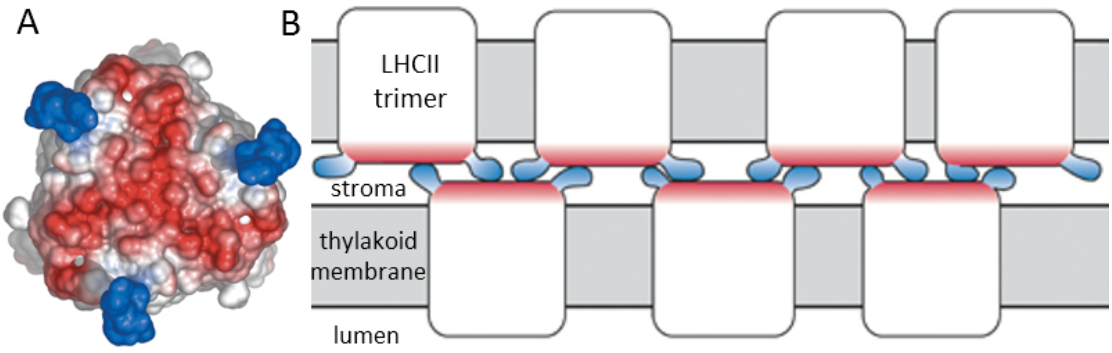


**Figure 7.1: A)** The distribution of negativly charged (*red*) areas and positively charged (*blue*) areas at the N-terminus, on the stromal surface of the LHCII trimer. **B)** Alternating negative and positive areas of trimeric LHCII form a zip-like, non-specific interaction with trimeric LHCII in the adjacent membrane. The N-terminus of each LHCII monomer is positively charged (*blue*) while the remaining areas are negatively charged (*red*) and Figure is taken from Standfuss et al. (2005).

that the relative LHCII content of *Nt*(*Hn*) was well within the range of the wildtype plants, indicating that proteolytic action for the degradation of LHCP was not affected by N-terminal removal.

The absence of an N-terminus was found by Ruban et al. (1992) to enhance NPQ. In the experiment they treated isolated LHCII with trypsin, which cleaved the N-terminus of the mature protein, they found that LHCII aggregation was increased, and they reported a concomitant increase in NPQ. It was this work, that led to our suggestion that the increased NPQ capacity measured in the *Nt*(*Hn*) cybrids in the first half of the study, might be a result of LHCII N-terminal truncation. However, our later investigation of quenching in isolated LHCII, revealed in fact a decrease in quenching capacity, although the *Nt*(*Hn*) plants used for quenching experiments, were also found to have a reduced NPQ capacity, in contrast to those measured previously.

The inconsistency of the NPQ results imply that other factors affected the NPQ response in *Nt*(*Hn*). As already discussed, Labate et al. (2004) found that the expression of just a single pea lhcb1-2 gene in *N. tabacum*, caused an increase in qE. Labate et al. (2004)'s work presents the possibility that changes in the capacity for qE in *Nt*(*Hn*), might arise due to a general sensitivity to the environment rather than, as previously suggested, due to the truncation of the N-terminus. A

heightened environmental sensitivity would serve to explain the broad range in the NPQ data.

It should be mentioned that *Nt*(*Hn*) LHC separation by MW always presented the same banding patterns with seven bands matching the *N. tabacum* banding pattern and an eighth novel, lower MW band. LHC separations were performed through out the study. The change in NPQ capacity cannot therefore be attributed to a change in *Nt*(*Hn*) LHC modification. This demonstrates that LHCII truncation was persistent in *Nt*(*Hn*), and supports the suggestion that another factor was influential in the qE response in *Nt*(*Hn*).

An alternative explanation for newly observed traits in the *Nt*(*Hn*) cybrid might be made in regards to altered post-transcriptional modification of plastid mRNA by nuclear-encoded proteins. Schmitz-Linneweber et al. (2005) investigated the genes that underlie nuclear-organellar incompatibility manifested as albinism in the *Ab*(*Nt*) cybrids, described in §1.6. They found that the *A.belladonna* nuclear genome was unable to support effective editing of the *N.tabacum* ATPase $\alpha$-subunit RNA transcript in the *N.tabacum* plastid. The editing site in the plastid mRNA was *N. tabacum*-specific and its misprocessing by the *A. belladonna* editotype was the primary cause of the observed pigment deficiency. Other editing defects were also uncovered and suggested as possible contributors to smaller scale incompatibility such as dwarfism (Schmitz-Linneweber et al., 2005).

Impaired or lost editing capabilities might arise in cybrid plants due to an absence of nuclear genes coding for species-specific editing factors of the alien organellar genomes (Schmitz-Linneweber et al., 2005). Multiple nuclear-encoded, editing factors have been identified for RNA editing in both plastid and mitochondria organelles (Takenaka et al., 2012). If differences exist in the genes encoding editing factors in *H.niger* and *N.tabacum*, it could explain nuclear–organellar incompatibility as a result of impaired nuclear protein – chloroplast RNA interactions.

Editing site evolution is observed to be extremely labile Shields and Wolfe (1997); Tillich et al. (2005), it follows that there must exist equally labile co-evolution between editing sites and editing activity (Shikanai, 2006). This rapid evolution could play a role in interspecific divergence, manifesting in the *Nt*(*Hn*) plants as nuclear-organellar incompatibility ultimately caused by defective editing of *H. niger* mRNA by the *N. tabacum* editing factors.

As well as post-transcriptional modification and PTM, the direct regulation of gene expression is an important process which has the potential for causing incompatibilities or altered gene expression in the cybrid plant. Interestingly, the *Nt*(*Hn*) FPLC elution profile of prepared thylakoid membrane protein was similar to *H. niger* rather than *N. tabacum*. Indicating that the photosystem:lhc ratios

more closely matched the chloroplast parent than the nuclear parent. Plastid-nucleus retrograde signalling is known to regulate nuclear gene expression with chloroplast function. Several signalling factors have been identified (Koussevitzky et al., 2007).

A comparative analysis of the *N.tabacum* and *H.niger* chloroplast genomes To date, the sequences of 683 plastid genomes are published in the NCBI database and this number is likely to increase quickly due to the recent development of new, rapid sequencing techniques (Shi, Hu, Huang, Gao, Zhao and Gao, 2012; Stull et al., 2013; Yang et al., 2014). Despite the high rate of speciation, remarkable similarity in both structure and gene content is found to exist between chloroplast genomes (Peschek, 2008; Schmitz-Linneweber et al., 2002). With few exceptions, the chloroplast genome exhibits a quadripartite structure and a similar set of genes mainly encoding the for constituents of the photosynthetic and genetic machineries (Schmitz-Linneweber et al., 2002).

**Table 7.1:** Characteristics of plastid genomes of *N.tabacum* and *H.niger*. Data taken from the Chloroplast Genome Database at http://chloroplast.cbio.psu.edu

| | **NCBI acc.no.** | **Genome size (kb)** | **Total genes** | **Protein coding genes** | **tRNA genes** | **rRNA genes** |
|---|---|---|---|---|---|---|
| ***N.tabacum*** | NC 001879.2 | 155 943 | 148 | 102 | 37 | 8 |
| ***H.niger*** | KF 248009.1 | 155 720 | 124 | 80 | 30 | 4 |

The *N.tabacum* chloroplast genome was first determined by Shinozaki et al. (1986), with two further updates by Wakasugi et al. (1998) and Yukawa et al. (2005), indeed this was the first complete chloroplast genome sequence for a higher plant (Howe et al., 2008). Towards the end of this project, the chloroplast genome of *H.niger* was also published by Sanchez-Puerta and Abbona (2014).

A comparison between *N.tabacum* and *H.niger* chloroplast genomes found a high level of similarity (96.9 %; Sanchez-Puerta and Abbona, 2014). With most notable differences occurring as editing sites, supporting the findings of Schmitz-Linneweber et al. (2005). In Table 7.1 we summarise the characteristics of the plastid genomes of *N.tabacum* and *H.niger* and in Fig 7.2, chloroplast genome maps are presented for each parent species. There are a few differences. The number of protein coding genes in *H.niger* cpDNA is 22 less than *N.tabacum*. The number of tRNA and rRNA genes are also reduced.

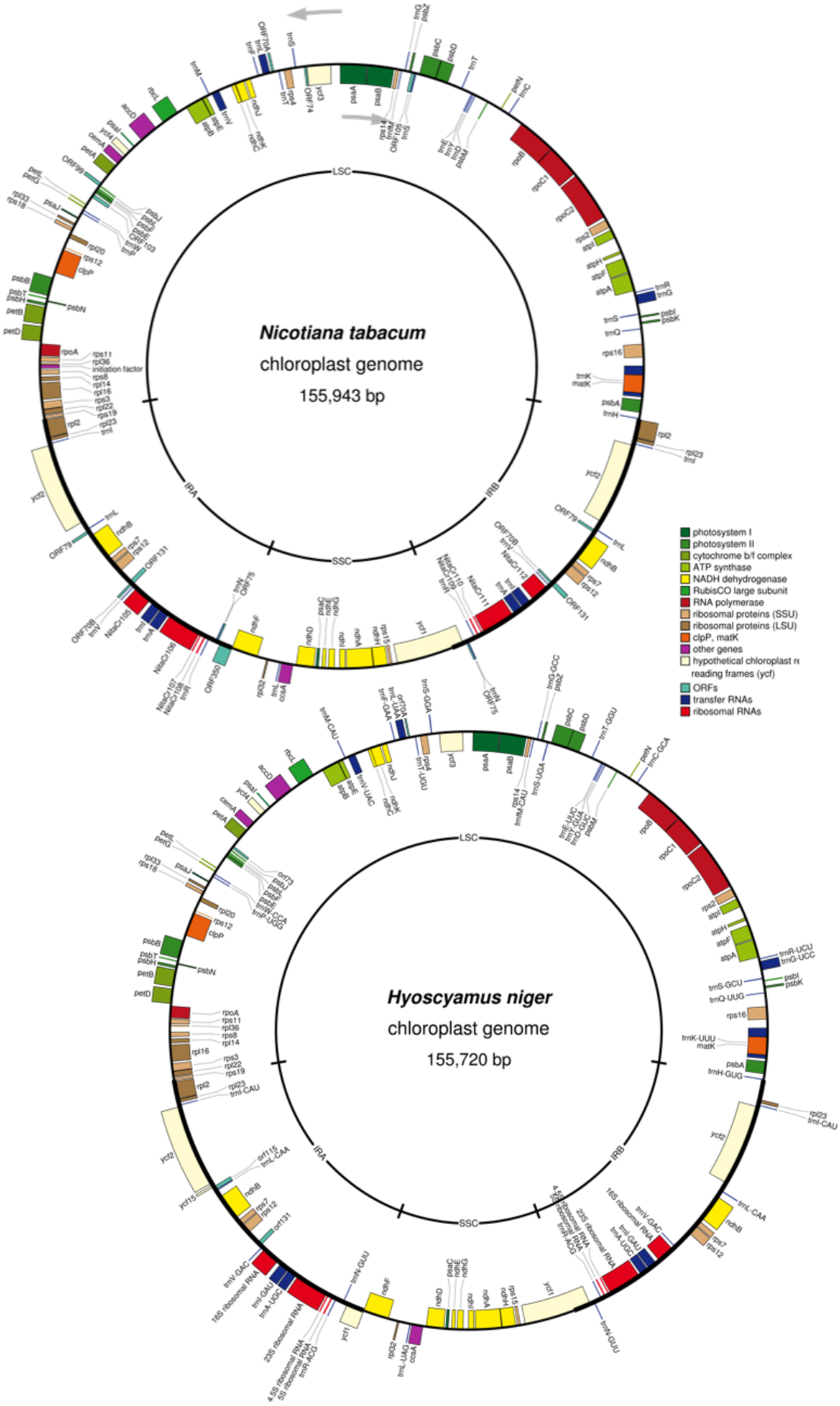


**Figure 7.2:** *See next page*

**Figure 7.2:** *...continued from previous page.* Gene organisation maps of the *N.tabacum* and *H.niger* circular plastid chromosomes. Genes drawn on the inside of the circle are transcribed in a clockwise direction while those drawn on the outside are transcribed in an anti-clockwise direction. Large (LSC) and small single copy regions (SSC) are separated by the inverted repeat (IR) sequences, IRA and IRB. Genes belonging to different functional groups are colour-coded, see the legend for details. The chloroplast genome maps were created using OrganellarGenomeDRAW (Lohse et al., 2013).

Although the *N. tabacum* and *H. niger* chloroplast genomes have high sequence similarity, the differences are a reflection of the strict co-evolution with the nuclear genome, and represent possible points of difference that could be potentially fatal when coupled with the nuclear genome of another plant species. It is remarkable how the expression of a single pea *lhcb1-2* gene, expressed in *N. tabacum*, can cause widespread phenotypic disturbance, yet the incorporation of an entire *H. niger* chloroplast against a *N. tabacum* nuclear background causes an apparently similar level of disturbance.

# Bibliography


Abad, M. S., Clark, S. E. and Lamppa, G. K. (1989), 'Properties of a chloroplast enzyme that cleaves the chlorophyll *a/b* binding protein precursor optimization of an organelle-free reaction', *Plant physiology* **9**0(1), 117–124.

Abrahams, J. P., Leslie, A. G., Lutter, R. and Walker, J. E. (1994), 'Structure at 2.8 Å resolution of F1-ATPase from bovine heart mitochondria', *Nature* **3**70(6491), 621–628.

Adam, Z. (2000), 'Chloroplast proteases: possible regulators of gene expression?', *Biochimie* **8**2(6), 647–654.

Adam, Z., Adamska, I., Nakabayashi, K., Ostersetzer, O., Haussuhl, K., Manuell, A., Zheng, B., Vallon, O., Rodermel, S. R., Shinozaki, K. et al. (2001), 'Chloroplast and mitochondrial proteases in Arabidopsis. A proposed nomenclature', *Plant Physiology* **1**25(4), 1912–1918.

Adams III, W., Demmig-Adams, B., Logan, B., Barker, D. and Osmond, C. (1999), 'Rapid changes in xanthophyll cycle-dependent energy dissipation and photosystem II efficiency in two vines, *Stephania japonica* and *Smilax australis*, growing in the understory of an open *Eucalyptus* forest', *Plant, Cell & Environment* **2**2(2), 125–136.

Akopian, D., Shen, K., Zhang, X. and Shan, S.-o. (2013), 'Signal Recognition Particle: An essential protein targeting machine', *Annual review of biochemistry* **8**2, 693.

Allen, J. F. (2003), 'State transitions - a question of balance', *Science* **2**99(5612), 1530–1532.

Allen, J. F., de Paula, W. B. M., Puthiyaveetil, S. and Nield, J. (2011), 'A structural phylogenetic map for chloroplast photosynthesis', *Trends in Plant Science* **1**6(12), 645–655.

Amunts, A., Drory, O. and Nelson, N. (2007), 'The structure of a plant photosystem I supercomplex at 3.4 Å resolution', *Nature* **4**47(7140), 58–63.

Amunts, A. and Nelson, N. (2009), 'Plant photosystem I design in the light of evolution', *Structure* **1**7(5), 637–650.

Amunts, A., Toporik, H., Borovikova, A. and Nelson, N. (2010), 'Structure determination and improved model of plant Photosystem I', *Journal of Biological Chemistry* **2**85(5), 3478–3486.

Anderson, J. M. and Aro, E.-M. (1994), 'Grana stacking and protection of photosystem II in thylakoid membranes of higher plant leaves under sustained high irradiance: an hypothesis', *Photosynthesis Research* **4**1(2), 315–326.

Anderson, J. M., Chow, W. and Goodchild, D. (1988), 'Thylakoid membrane organisation in sun/shade acclimation', *Functional Plant Biology* **1**5(2), 11–26.

Anderson, J. M., Chow, W. S. and Park, Y.-I. (1995), 'The grand design of photosynthesis: acclimation of the photosynthetic apparatus to environmental cues', *Photosynthesis Research* **4**6(1-2), 129–139.

Andreeva, A. S., Busheva, M. C., Stoitchkova, K. V. and Tzonova, I. K. (2010), Photoinduced changes in photosystem II pigments, *in* 'Journal of Physics: Conference Series', Vol. 253, IOP Publishing.

Andrizhiyevskaya, E. G., Chojnicka, A., Bautista, J. A., Diner, B. A., van Grondelle, R. and Dekker, J. P. (2005), 'Origin of the F685 and F695 fluorescence in photosystem II', *Photosynthesis research* **8**4(1-3), 173–180.

Arimura, S.-i., Yamamoto, J., Aida, G. P., Nakazono, M. and Tsutsumi, N. (2004), 'Frequent fusion and fission of plant mitochondria with unequal nucleoid distribution', *Proceedings of the National Academy of Sciences of the United States of America* **1**01(20), 7805–7808.

Arnon, D. I., Allen, M. B. and Whatley, F. (1954), 'Photosynthesis by isolated chloroplasts', *Nature* **1**74, 394–396.

Aro, E., Suorsa, M., Rokka, A., Allahverdiyeva, Y., Paakkarinen, V., Saleem, A., Battchikova, N. and Rintamäki, E. (2005), 'Dynamics of photosystem II: a proteomic approach to thylakoid protein complexes', *Journal of Experimental Botany* **5**6(411), 347–356.

Artimo, P., Jonnalagedda, M., Arnold, K., Baratin, D., Csardi, G., De Castro, E., Duvaud, S., Flegel, V., Fortier, A., Gasteiger, E. et al. (2012), 'ExPASy: SIB bioinformatics resource portal', *Nucleic acids research* **4**0(1), 597–603.

Austin, J. R. and Staehelin, L. A. (2011), 'Three-dimensional architecture of grana and stroma thylakoids of higher plants as determined by electron tomography', *Plant Physiology* **1**55(4), 1601–1611.

Babiychuk, E., Schantz, R., Cherep, N., Weil, J. H., Gleba, Y. and Kushnir, S. (1995), 'Alterations in chlorophyll $a/b$ binding proteins in *Solanaceae* cybrids', *Molecular & General Genetics* **2**49(6), 648–654.

Bailey, S., Walters, R. G., Jansson, S. and Horton, P. (2001), 'Acclimation of *Arabidopsis thaliana* to the light environment: the existence of separate low light and high light responses', *Planta* **2**13(5), 794–801.

Bajaj, Y. P. S. (1994), Somatic hybridisation - a rich source of genetic variability, *in* Y. Bajaj, ed., 'Somatic Hybridization in Crop Improvement I', Vol. 1 of *Biotechnology in Agriculture and Forestry*, Springer, Berlin Heidelberg, pp. 3–18.

Balakrishna, A. M., Seelert, H., Marx, S.-H., Dencher, N. A. and Gruber, G. (2014), 'Crystallographic structure of the turbine c-ring from spinach chloroplast F-ATP synthase', *Bioscience reports* **3**4(2), 147–154.

Ballottari, M., Girardon, J., Dall'Osto, L. and Bassi, R. (2012), 'Evolution and functional properties of Photosystem II light harvesting complexes in eukaryotes', *Biochimica et Biophysica Acta (BBA)-Bioenergetics* **1**817(1), 143–157.

Baniulis, D., Yamashita, E., Zhang, H., Hasan, S. and Cramer, W. (2008), 'Structure–function of the cytochrome *b*6*f* complex', *Photochemistry and photobiology* **8**4(6), 1349–1358.

Barber, J. (1995), 'Molecular basis of the vulnerability of photosystem II to damage by light', *Functional Plant Biology* **2**2(2), 201–208.

Barber, J. (2006), 'Photosystem II: an enzyme of global significance', *Biochemical Society Transactions* **3**4, 619–631.

Barber, J. (2014), 'Photosystem II: Its function, structure, and implications for artificial photosynthesis', *Biochemistry* **7**9(3), 185–196.

Barr, C. M., Neiman, M. and Taylor, D. R. (2005), 'Inheritance and recombination of mitochondrial genomes in plants, fungi and animals', *New Phytologist* **1**68(1), 39–50.

Bassi, R. and Dainese, P. (1992), 'A supramolecular light-harvesting complex from chloroplast photosystem-II membranes', *European Journal of Biochemistry* **2**04(1), 317–326.

Bassi, R., Pineau, B., Dainese, P. and Marquardt, J. (1993), 'Carotenoid-binding proteins of photosystem II', *European Journal of Biochemistry* **2**12(2), 297–303.

Bassi, R., Silvestri, M., Dainese, P., Moya, I. and Giacometti, G. M. (1991), 'Effects of a non-ionic detergent on the spectral properties and aggregation state of the light-harvesting chlorophyll *a/b* protein complex (LHCII)', *Journal of Photochemistry and Photobiology* **9**(3), 335–353.

Batlla, D., Kruk, B. and Benech-Arnold, R. (2000), 'Very early detection of canopy presence by seeds through perception of subtle modifications in red: far red signals', *Functional Ecology* **1**4(2), 195–202.

Beddard, G. and Porter, G. (1976), 'Concentration quenching in chlorophyll', **2**60, 366–367.

Belgio, E. (2009), The Photosystem II: spectral analysis of the low energy chlorophylls of the antenna complex CP29 and thermodynamic studies., PhD thesis, Universita' Degli Studi di Milano.

Belgio, E., Duffy, C. D. and Ruban, A. V. (2013), 'Switching light harvesting complex II into photoprotective state involves the lumen-facing apoprotein loop', *Physical Chemistry Chemical Physics* **1**5(29), 12253–12261.

Belgio, E., Johnson, M. P., Jurić, S. and Ruban, A. V. (2012), 'Higher plant Photosystem II light-harvesting antenna, not the reaction center, determines the excited-state lifetime, - both the maximum and the nonphotochemically quenched', *Biophysical journal* **1**02(12), 2761–2771.

Bellafiore, S., Barneche, F., Peltier, G. and Rochaix, J.-D. (2005), 'State transitions and light adaptation require chloroplast thylakoid protein kinase STN7', *Nature* **4**33(7028), 892–895.

Belliard, G., Vedel, F. and Pelletier, G. (1979), 'Mitochondrial recombination in cytoplasmic hybrids of *Nicotiana tabacum* by protoplast fusion'.

Benning, C. (2009), 'Mechanisms of lipid transport involved in organelle biogenesis in plant cells', *Annual Review of Cell and Developmental* **2**5, 71–91.

Berg, J., Stryer, L. and Tymoczko, J. (2002), *Biochemistry*, international version, 5th edn, W. H. Freeman.

Bergthorsson, U., Adams, K. L., Thomason, B. and Palmer, J. D. (2003), 'Widespread horizontal transfer of mitochondrial genes in flowering plants', *Nature* **4**24(6945), 197–201.

Blankenship, R. E. (2002), *Molecular mechanisms of photosynthesis*, Blackwell Science, Oxford.

Boardman, N. (1977), 'Comparative photosynthesis of sun and shade plants', *Annual review of plant physiology* **2**8(1), 355–377.

Boasson, R., Bonner, J. J. and Laetsch, W. (1972), 'Induction and regulation of chloroplast replication in mature tobacco leaf tissue', *Plant physiology* **4**9(1), 97–101.

Boekema, E. J., van Roon, H., Calkoen, F., Bassi, R. and Dekker, J. P. (1999), 'Multiple types of association of photosystem II and its light-harvesting antenna in partially solubilized photosystem II membranes', *Biochemistry* **3**8(8), 2233–2239.

Boeshore, M. L., Lifshitz, I., Hanson, M. R. and Izhar, S. (1983), 'Novel composition of mitochondrial genomes in petunia somatic hybrids derived from cytoplasmic male sterile and fertile plants', *Molecular and General Genetics MGG* **1**90(3), 459–467.

Böttcher, B. and Gräber, P. (2000), 'The structure of the $H^+$-ATP synthase from chloroplasts and its subcomplexes as revealed by electron microscopy', *Biochimica et Biophysica Acta (BBA)-Bioenergetics* **1**458(2), 404–416.

Bowers, P. and Porter, G. (1967), Quantum yields of triplet formation in solutions of chlorophyll, *in* 'Proceedings of the Royal Society of London A: Mathematical, Physical and Engineering Sciences', Vol. 296, The Royal Society, pp. 435–441.

Bricker, T. M. and Frankel, L. K. (2002), 'The structure and function of CP47 and CP43 in photosystem II', *Photosynthesis research* **7**2(2), 131–146.

Bricker, T. M. and Frankel, L. K. (2011), 'Auxiliary functions of the PsbO, PsbP and PsbQ proteins of higher plant photosystem II: a critical analysis', *Journal of Photochemistry and Photobiology B: Biology* **1**04(1), 165–178.

Bricker, T. M., Roose, J. L., Fagerlund, R. D., Frankel, L. K. and Eaton-Rye, J. J. (2012), 'The extrinsic proteins of photosystem II', *Biochimica et Biophysica Acta (BBA)-Bioenergetics* **1**817(1), 121–142.

Brody, S. S. and Rabinowitch, E. (1957), 'Excitation lifetime of photosynthetic pigments *in vitro* and *in vivo*', *Science* **1**25, 555.

Brooks, M. D., Sylak-Glassman, E. J., Fleming, G. R. and Niyogi, K. K. (2013), 'A thioredoxin-like/$\beta$-propeller protein maintains the efficiency of light harvesting

in Arabidopsis', *Proceedings of the National Academy of Sciences* **1**10(29), E2733–E2740.

Bruce, B. D. (2001), 'The paradox of plastid transit peptides: conservation of function despite divergence in primary structure', *Biochimica et Biophysica Acta (BBA)-Molecular Cell Research* **1**541(1), 2–21.

Busch, A. and Hippler, M. (2011), 'The structure and function of eukaryotic photosystem I', *Biochimica et Biophysica Acta (BBA)-Bioenergetics* **1**807(8), 864–877.

Butler, P. and Kühlbrandt, W. (1988), 'Determination of the aggregate size in detergent solution of the light-harvesting chlorophyll *a/b*-protein complex from chloroplast membranes', *Proceedings of the National Academy of Sciences* **8**5(11), 3797–3801.

Butler, W. L. (1978), 'Energy distribution in the photochemical apparatus of photosynthesis', *Annual Review of Plant Physiology* **2**9(1), 345–378.

Buvinger, W. E., Michel, H. and Bennett, J. (1989), 'A truncated analog of a pre-light-harvesting chlorophyll *a/b* protein II transit peptide inhibits protein import into chloroplasts.', *Journal of Biological Chemistry* **2**64(2), 1195–1202.

Caffarri, S., Frigerio, S., Olivieri, E., Righetti, P. G. and Bassi, R. (2005), 'Differential accumulation of Lhcb gene products in thylakoid membranes of *Zea mays* plants grown under contrasting light and temperature conditions', *Proteomics* **5**(3), 758–768.

Caffarri, S., Kouřil, R., Kereïche, S., Boekema, E. J. and Croce, R. (2009), 'Functional architecture of higher plant photosystem II supercomplexes', *The EMBO journal* **2**8(19), 3052–3063.

Calvin, M. (1962), 'The path of carbon in photosynthesis', *Angewandte Chemie International Edition in English* **1**(2), 65–75.

Canfield, D. E. (2014), *Oxygen: A Four Billion Year History*, Princeton University Press.

Carlson, P. S., Smith, H. H. and Dearing, R. D. (1972), 'Parasexual interspecific plant hybridization', *Proceedings of the National Academy of Sciences* **6**9(8), 2292–2294.

Casal, J. J. (2012), 'Shade avoidance', *The Arabidopsis Book, American Society of Plant Biologists* **1**0.

Cavanaugh, C. M. (1983), 'Symbiotic chemoautotrophic bacteria in marine invertebrates from sulphide-rich habitats'.

Cave, G., Tolley, L. C. and Strain, B. (1981), 'Effect of carbon dioxide enrichment on chlorophyll content, starch content and starch grain structure in Trifolium subterraneum leaves', *Physiologia Plantarum* **5**1(2), 171–174.

Clark, S. E., Abad, M. and Lamppa, G. (1989), 'Mutations at the transit peptide-mature protein junction separate two cleavage events during chloroplast import of the chlorophyll *a/b*-binding protein.', *Journal of Biological Chemistry* **2**64(29), 17544–17550.

Cline, K. and Henry, R. (1996), 'Import and routing of nucleus-encoded chloroplast proteins', *Annual review of cell and developmental biology* **1**2(1), 1–26.

Cramer, W., Zakharov, S., Saif Hasan, S., Zhang, H., Baniulis, D., Zhalnina, M., Soriano, G., Sharma, O., Rochet, J., Ryan, C. et al. (2011), 'Membrane proteins in four acts: Function precedes structure determination', *Methods* **5**5(4), 415–420.

Croce, R. and van Amerongen, H. (2014), 'Natural strategies for photosynthetic light harvesting', *Nature chemical biology* **1**0(7), 492–501.

Damkjaer, J. T., Kereiche, S., Johnson, M. P., Kovacs, L., Kiss, A. Z., Boekema, E. J., Ruban, A. V., Horton, P. and Jansson, S. (2009), 'The photosystem II light-harvesting protein Lhcb3 affects the macrostructure of photosystem II and the rate of state transitions in *Arabidopsis*', *The Plant Cell Online* **2**1(10), 3245–3256.

Daum, B. and Kühlbrandt, W. (2011), 'Electron tomography of plant thylakoid membranes', *Journal of experimental botany* **6**2(7), 2393–2402.

Daum, B., Nicastro, D., Austin, J., McIntosh, J. R. and Kühlbrandt, W. (2010), 'Arrangement of photosystem II and ATP synthase in chloroplast membranes of spinach and pea', *The Plant Cell Online* **2**2(4), 1299–1312.

Davies, P. J. (2010), The plant hormones: their nature, occurrence, and functions, *in* 'Plant hormones', Springer, pp. 1–15.

de Alda, J. A. O., Esteban, R., Diago, M. L. and Houmard, J. (2014), 'The plastid ancestor originated among one of the major cyanobacterial lineages', *Nature communications* **5**.

Debus, R. J., Barry, B. A., Babcock, G. T. and McIntosh, L. (1988), 'Site-directed mutagenesis identifies a tyrosine radical involved in the photosynthetic oxygen-evolving system', *Proceedings of the National Academy of Sciences* **8**5(2), 427–430.

Dekker, J. P. and Boekema, E. J. (2005), 'Supramolecular organization of thylakoid membrane proteins in green plants', *Biochimica et Biophysica Acta (BBA)-Bioenergetics* **1**706(1), 12–39.

Demmig-Adams, B. (1990), 'Carotenoids and photoprotection in plants: a role for the xanthophyll zeaxanthin', *Biochimica et Biophysica Acta (BBA)-Bioenergetics* **1**020(1), 1–24.

Demmig-Adams, B., Ebbert, V., Zarter, C. R. and Adams III, W. W. (2006), Characteristics and species-dependent employment of flexible versus sustained thermal dissipation and photoinhibition, *in* 'Photoprotection, Photoinhibition, Gene Regulation, and Environment', Springer, pp. 39–48.

Demmig-Adams, B., Gilmore, A. and Adams, W. (1996), 'Carotenoids 3: *in vivo* function of carotenoids in higher plants.', *The FASEB Journal* **1**0(4), 403–412.

Demmig, B., Winter, K., Krüger, A. and Czygan, F.-C. (1987), 'Photoinhibition and zeaxanthin formation in intact leaves a possible role of the xanthophyll cycle in the dissipation of excess light energy', *Plant Physiology* **8**4(2), 218–224.

Des Marais, D. J. et al. (2000), 'When did photosynthesis emerge on Earth?', *Science* **2**89(5485), 1703–1705.

Dixon, J. M., Taniguchi, M. and Lindsey, J. S. (2005), 'Photochemcad 2: A refined program with accompanying spectral databases for photochemical calculations', *Photochemistry and photobiology* **8**1(1), 212–213.

Du, H., Fuh, R. C. A., Li, J., Corkan, L. A. and Lindsey, J. S. (1998), 'Photochemcad: A computer aided design and research tool in photochemistry', *Photochemistry and photobiology* **6**8(2), 141–142.

Duffy, C. (2009), Photoprotection: Possible Mechanisms for the Regulation of Light Harvesting in Higher Plants, PhD thesis, Sheffield University.

Duffy, C., Chmeliov, J., Macernis, M., Sulskus, J., Valkunas, L. and Ruban, A. (2012), 'Modeling of fluorescence quenching by lutein in the plant light-harvesting complex LHCII', *The Journal of Physical Chemistry B* **1**17(38), 10974–10986.

Dunlap, J. C. (1999), 'Molecular bases for circadian clocks', *Cell* **9**6(2), 271–290.

Duysens, L. and Sweers, H. (1963), 'Mechanism of two photochemical reactions in algae as studied by means of fluorescence', *Studies on microalgae and photosynthetic bacteria* pp. 353–372.

Edner, C., Li, J., Albrecht, T., Mahlow, S., Hejazi, M., Hussain, H., Kaplan, F., Guy, C., Smith, S. M., Steup, M. et al. (2007), 'Glucan, water dikinase activity stimulates breakdown of starch granules by plastidial $\beta$-amylases', *Plant Physiology* **1**45(1), 17–28.

Eichacker, L. and Henry, R. (2001), 'Function of a chloroplast SRP in thylakoid protein export', *Biochimica et Biophysica Acta (BBA)-Molecular Cell Research* **1**541(1), 120–134.

Eilers, P. and Peeters, J. (1988), 'A model for the relationship between light intensity and the rate of photosynthesis in phytoplankton', *Ecological modelling* **4**2(3), 199–215.

Ellis, R. J. (2010), 'Biochemistry: Tackling unintelligent design', *Nature* **4**63(7278), 164–165.

Emerson, R. and Arnold, W. (1932), 'The photochemical reaction in photosynthesis', *The Journal of general physiology* **1**6(2), 191–205.

Evans, J. R., Caemmerer, S., Setchell, B. A. and Hudson, G. S. (1994), 'The relationship between $CO_2$ transfer conductance and leaf anatomy in transgenic tobacco with a reduced content of Rubisco', *Functional Plant Biology* **2**1(4), 475–495.

Falk, S., Ravaud, S., Koch, J. and Sinning, I. (2010), 'The C terminus of the Alb3 membrane insertase recruits cpSRP43 to the thylakoid membrane', *Journal of Biological Chemistry* **2**85(8), 5954–5962.

Farber, A., Young, A. J., Ruban, A. V., Horton, P. and Jahns, P. (1997), 'Dynamics of xanthophyll-cycle activity in different antenna subcomplexes in the photosynthetic membranes of higher plants (the relationship between zeaxanthin conversion and nonphotochemical fluorescence quenching)', *Plant Physiology* **1**15(4), 1609–1618.

Farmaki, T., Sanmartín, M., Jiménez, P., Paneque, M., Sanz, C., Vancanneyt, G., León, J. and Sánchez-Serrano, J. J. (2007), 'Differential distribution of the lipoxygenase pathway enzymes within potato chloroplasts', *Journal of experimental botany* **5**8(3), 555–568.

Ferreira, K. N., Iverson, T. M., Maghlaoui, K., Barber, J. and Iwata, S. (2004), 'Architecture of the photosynthetic oxygen-evolving center', *Science* **3**03(5665), 1831–1838.

Forsberg, J. and Allen, J. F. (2001), 'Protein tyrosine phosphorylation in the transition to light state 2 of chloroplast thylakoids', *Photosynthesis research* **6**8(1), 71–79.

Forsberg, J., Ström, J., Kieselbach, T., Larsson, H., Alexciev, K., Engström, Å. and Åkerlund, H.-E. (2005), 'Protease activities in the chloroplast capable of cleaving an LHCII N-terminal peptide', *Physiologia Plantarum* **1**23(1), 21–29.

Förster, T. (1948), 'Zwischenmolekulare energiewanderung und fluoreszenz', *Annalen der physik* **4**37(1-2), 55–75.

Förster, T. (2012), 'Energy migration and fluorescence. An english translation of Förster's 1948 paper: Zwischenmolekulare energiewanderung und fluoreszenz', *Journal of biomedical optics* **1**7(1), 21–210. Translated by Klaus Suhling.

Fuks, B. and Schnell, D. J. (1997), 'Mechanism of protein transport across the chloroplast envelope.', *Plant physiology* **1**14(2), 405.

Funk, C., Adamska, I., Green, B. R., Andersson, B. and Renger, G. (1995), 'The nuclear-encoded chlorophyll-binding photosystem II-S protein is stable in the absence of pigments', *Journal of Biological Chemistry* **2**70(50), 30141–30147.

Futai, M. and Kanazawa, H. (1983), 'Structure and function of proton-translocating adenosine triphosphatase ($F_0F_1$): biochemical and molecular biological approaches.', *Microbiological reviews* **4**7(3), 285.

Ganeteg, U., Klimmek, F. and Jansson, S. (2004), 'Lhca5– An LHC-type protein associated with photosystem I', *Plant molecular biology* **5**4(5), 641–651.

Gao, F., Kight, A. D., Henderson, R., Jayanthi, S., Patel, P., Murchison, M., Sharma, P., Goforth, R. L., Kumar, T. K. S., Henry, R. L. et al. (2015), 'Regulation of structural dynamics within a signal recognition particle promotes binding of protein targeting substrates', *Journal of Biological Chemistry* pp. jbc–M114.

Garab, G. and Mustárdy, L. (2000), 'Role of LHCII-containing macrodomains in the structure, function and dynamics of grana', *Functional Plant Biology* **2**7(3), 279–279.

Genty, B., Briantais, J.-M. and Baker, N. R. (1989), 'The relationship between the quantum yield of photosynthetic electron transport and quenching of chlorophyll

fluorescence', *Biochimica et Biophysica Acta (BBA)-General Subjects* **9**90(1), 87–92.

Gernand, D., Rutten, T., Varshney, A., Rubtsova, M., Prodanovic, S., Brüß, C., Kumlehn, J., Matzk, F. and Houben, A. (2005), 'Uniparental chromosome elimination at mitosis and interphase in wheat and pearl millet crosses involves micronucleus formation, progressive heterochromatinization, and DNA fragmentation', *The Plant Cell Online* **1**7(9), 2431–2438.

Ghanotakis, D. F. and Yocum, C. F. (1986), 'Purification and properties of an oxygen-evolving reaction center complex from photosystem II membranes: a simple procedure utilizing a non-ionic detergent and elevated ionic strength', *FEBS letters* **1**97(1), 244–248.

Gibbons, C., Montgomery, M. G., Leslie, A. G. and Walker, J. E. (2000), 'The structure of the central stalk in bovine F1-ATPase at 2.4 Å resolution', *Nature Structural & Molecular Biology* **7**(11), 1055–1061.

Giovagnetti, V., Ware, M. A. and Ruban, A. V. (2015), 'Assessment of the impact of photosystem I chlorophyll fluorescence on the pulse-amplitude modulated quenching analysis in leaves of *Arabidopsis thaliana*', *Photosynthesis research* pp. 1–11.

Givnish, T. J. (1988), 'Adaptation to sun and shade: a whole-plant perspective', *Functional Plant Biology* **1**5(2), 63–92.

Golbeck, J. (2003), 'Photosynthetic reaction centers: So little time, so much to do', *Biophysics textbooks online (http://www.biophysics.org)* .

Gómez, S. M., Bil, K. Y., Aguilera, R., Nishio, J. N., Faull, K. F. and Whitelegge, J. P. (2003), 'Transit peptide cleavage sites of integral thylakoid membrane proteins', *Molecular & Cellular Proteomics* **2**(10), 1068–1085.

Govindjee (1995), '63 years since Kautsky chlorophyll *a* fluorescence', *Australian Journal of Plant Physiology* **2**2(2), 131–160.

Govindjee (2004), Chlorophyll *a* fluorescence: a bit of basics and history, *in* G. C. Papageorgiou and Govindjee, eds, 'Chlorophyll *a* Fluorescence. A Signature of Photosynthesis', Vol. 19 of *Advances in Photosynthesis and Respiration*, Springer, pp. 1–42.

Greiner, S. and Bock, R. (2013), 'Tuning a ménage à trois: Co-evolution and co-adaptation of nuclear and organellar genomes in plants', *BioEssays* **3**5(4), 354–365.

Greiner, S., Rauwolf, U., Meurer, J. and Herrmann, R. G. (2011), 'The role of plastids in plant speciation', *Molecular ecology* **2**0(4), 671–691.

Groth, G. and Pohl, E. (2001), 'The structure of the chloroplast F1-ATPase at 3.2 Å resolution', *Journal of Biological Chemistry* **2**76(2), 1345–1352.

Groves, M. R., Mant, A., Kuhn, A., Koch, J., Dübel, S., Robinson, C. and Sinning, I. (2001), 'Functional characterization of recombinant chloroplast signal recognition particle', *Journal of Biological Chemistry* **2**76(30), 27778–27786.

Hager, A. (1969), 'Lichtbedingte pH-erniedrigung in einem chloroplasten-kompartiment als ursache der enzymatischen violaxanthin→ zeaxanthin-umwandlung; beziehungen zur photophosphorylierung', *Planta* **8**9(3), 224–243.

Hager, A. and Holocher, K. (1994), 'Localization of the xanthophyll-cycle enzyme violaxanthin de-epoxidase within the thylakoid lumen and abolition of its mobility by a (light-dependent) pH decrease', *Planta* **1**92(4), 581–589.

Hall, D., Rao, K. and of Biology, I. (1999), *Photosynthesis*, Institute of Biology's studies in biology, Cambridge University Press.

Hankamer, B., Morris, E. and Barber, J. (1999), 'Cryoelectron microscopy of photosystem two shows that CP43 and CP47 are located on opposite sides of the D1/D2 reaction centre proteins', *Nat. Struct. Biol* **6**, 560–564.

Hanson, M. R. (1991), 'Plant mitochondrial mutations and male sterility', *Annual review of genetics* **2**5(1), 461–486.

Hanson, M. R. and Bentolila, S. (2004), 'Interactions of mitochondrial and nuclear genes that affect male gametophyte development', *The Plant Cell Online* **1**6(suppl 1), S154–S169.

Hasegawa, K., Yukawa, Y., Sugita, M. and Sugiura, M. (2002), 'Organization and transcription of the gene family encoding chlorophyll $a/b$ binding proteins in *Nicotiana sylvestris*', *Gene* **2**89(1), 161–168.

Hejazi, M., Steup, M. and Fettke, J. (2012), 'The plastidial glucan, water dikinase (GWD) catalyses multiple phosphotransfer reactions', *FEBS Journal* **2**79(11), 1953–1966.

Hensel, M. (2006), 'Synthetic life architectures: ramifications and potentials of a literal biological paradigm for architectural design', *Architectural Design* **7**6(2), 18–25.

Hobe, S., Foerster, R., Klingler, J. and Paulsen, H. (1995), 'N-proximal sequence motif in light-harvesting chlorophyll $a/b$-binding protein is essential for the trimerization of light-harvesting chlorophyll $a/b$ complex', *Biochemistry* **3**4(32), 10224–10228.

Horton, P. (1996), Nonphotochemical quenching of chlorophyll fluorescence, *in* R. C. Jennings, G. Zucchelli, F. Ghetti and G. Colombetti, eds, 'Light as an energy source and information carrier in plant physiology', Vol. 287, Springer Science & Business Media, pp. 99–112.

Horton, P. and Ruban, A. (2005), 'Molecular design of the photosystem II light-harvesting antenna: photosynthesis and photoprotection', *Journal of experimental botany* **5**6(411), 365–373.

Horton, P., Ruban, A., Rees, D., Pascal, A., Noctor, G. and Young, A. (1991), 'Control of the light-harvesting function of chloroplast membranes by aggregation of the LHCII chlorophyll—protein complex', *FEBS letters* **2**92(1), 1–4.

Horton, P., Wentworth, M. and Ruban, A. (2005), 'Control of the light harvesting function of chloroplast membranes: the LHCII-aggregation model for non-photochemical quenching', *Febs Letters* **5**79(20), 4201–4206.

Howe, C., Barbrook, A., Nisbet, R., Lockhart, P. and Larkum, A. (2008), 'The origin of plastids', *Philosophical Transactions of the Royal Society B: Biological Sciences* **3**63(1504), 2675–2685.

Huot, Y. and Babin, M. (2010), Overview of fluorescence protocols: theory, basic concepts, and practice, *in* 'Chlorophyll *a* fluorescence in aquatic sciences: Methods and applications', Springer, pp. 31–74.

Ido, K., Nield, J., Fukao, Y., Nishimura, T., Sato, F. and Ifuku, K. (2014), 'Cross-linking evidence for multiple interactions of the PsbP and PsbQ proteins in a higher plant photosystem II supercomplex', *Journal of Biological Chemistry* **2**89(29), 20150–20157.

Iwai, M., Takizawa, K., Tokutsu, R., Okamuro, A., Takahashi, Y. and Minagawa, J. (2010), 'Isolation of the elusive supercomplex that drives cyclic electron flow in photosynthesis', *Nature* **4**64(7292), 1210–1213.

Jahns, P. and Junge, W. (1990), 'Dicyclohexylcarbodiimide-binding proteins related to the short circuit of the proton-pumping activity of photosystem II', *European journal of biochemistry* **1**93(3), 731–736.

Jahns, P., Latowski, D. and Strzalka, K. (2009), 'Mechanism and regulation of the violaxanthin cycle: the role of antenna proteins and membrane lipids', *Biochimica et Biophysica Acta (BBA)-Bioenergetics* **1**787(1), 3–14.

Jaillais, Y. and Chory, J. (2010), 'Unraveling the paradoxes of plant hormone signaling integration', *Nature structural & molecular biology* **1**7(6), 642–645.

Jarvis, P. (2008), 'Targeting of nucleus-encoded proteins to chloroplasts in plants', *New Phytologist* **1**79(2), 257–285.

Jarvis, P. and López-Juez, E. (2013), 'Biogenesis and homeostasis of chloroplasts and other plastids', *Nature Reviews Molecular Cell Biology* **1**5(12), 787–802.

Johnson, M. P. and Ruban, A. V. (2009), 'Photoprotective energy dissipation in higher plants involves alteration of the excited state energy of the emitting chlorophyll (s) in the light harvesting antenna II (LHCII)', *Journal of Biological Chemistry* **2**84(35), 23592–23601.

Johnson, M. P. and Ruban, A. V. (2010), '*Arabidopsis* plants lacking PsbS protein possess photoprotective energy dissipation', *The Plant Journal* **6**1(2), 283–289.

Jordan, P., Fromme, P., Witt, H. T., Klukas, O., Saenger, W. and Krauß, N. (2001), 'Three-dimensional structure of cyanobacterial photosystem I at 2.5 Å resolution', *Nature* **4**11(6840), 909–917.

Kashino, Y., Takahashi, T., Inoue-Kashino, N., Ban, A., Ikeda, Y., Satoh, K. and Sugiura, M. (2007), 'Ycf12 is a core subunit in the photosystem II complex', *Biochimica et Biophysica Acta (BBA)-Bioenergetics* **1**767(11), 1269–1275.

Kautsky, H., Appel, W. and Amann, H. (1959), 'Chlorophyll fluorescence and carbon assimilation. Part XIII. the fluorescence and the photochemistry of plants.', *Biochemische Zeitschrift* **3**32, 277–292.

Kautsky, H. and Hirsch, A. (1931), 'Neue versuche zur kohlensäureassimilation', *Naturwissenschaften* **1**9(48), 964–964.

Kendrick, R. E. and Kronenberg, G. (1994), *Photomorphogenesis in plants*, Springer.

Keren, N. and Krieger-Liszkay, A. (2011), 'Photoinhibition: molecular mechanisms and physiological significance', *Physiologia plantarum* **1**42(1), 1–5.

Kim, S., Sandusky, P., Bowlby, N. R., Aebersold, R., Green, B. R., Vlahaskis, S., Yocum, C. F. and Pichersky, E. (1992), 'Characterization of a spinach *psbS*

cDNA encoding the 22 kDa protein of photosystem II', *FEBS letters* **3**14(1), 67–71.

Kirchhoff, H., Sharpe, R. M., Herbstova, M., Yarbrough, R. and Edwards, G. E. (2013), 'Differential mobility of pigment-protein complexes in granal and agranal thylakoid membranes of C3 and C4 plants', *Plant physiology* **1**61(1), 497–507.

Kirst, H. and Melis, A. (2013), 'The chloroplast signal recognition particle (cp-SRP) pathway as a tool to minimize chlorophyll antenna size and maximize photosynthetic productivity', *Biotechnology advances* **3**2(1), 66–72.

Klimmek, F., Sjödin, A., Noutsos, C., Leister, D. and Jansson, S. (2006), 'Abundantly and rarely expressed lhc protein genes exhibit distinct regulation patterns in plants', *Plant physiology* **1**40(3), 793–804.

Klughammer, C. and Schreiber, U. (2008), 'Saturation pulse method for assessment of energy conversion in PSI', *PAM application notes* **1**, 11–14.

Kochevenko, A., Ratushnyak, Y., Kornyeyev, D., Stasik, O., Porublyova, L., Kochubey, S., Suprunova, T. and Gleba, Y. (2000), 'Functional cybrid plants of *Lycopersicon peruvianum* var'*dentatum*' with chloroplasts of *Lycopersicon esculentum*', *Plant Cell Reports* **1**9(6), 588–597.

Kohorn, B. and Yakir, D. (1990), 'Movement of newly imported light-harvesting chlorophyll-binding protein from unstacked to stacked thylakoid membranes is not affected by light treatment or absence of amino-terminal threonines.', *Journal of Biological Chemistry* **2**65(4), 2118–2123.

Kombrink, E. (2012), 'Chemical and genetic exploration of jasmonate biosynthesis and signaling paths', *Planta* **2**36(5), 1351–1366.

Kouřil, R., Dekker, J. P. and Boekema, E. J. (2012), 'Supramolecular organization of photosystem II in green plants', *Biochimica et Biophysica Acta (BBA)-Bioenergetics* **1**817(1), 2–12.

Koussevitzky, S., Nott, A., Mockler, T. C., Hong, F., Sachetto-Martins, G., Surpin, M., Lim, J., Mittler, R. and Chory, J. (2007), 'Signals from chloroplasts converge to regulate nuclear gene expression', *Science* **3**16(5825), 715–719.

Krause, G. (1974), 'Changes in chlorophyll fluorescence in relation to light-dependent cation transfer across thylakoid membranes', *Biochimica et Biophysica Acta (BBA)-Bioenergetics* **3**33(2), 301–313.

Krause, G. H. and Weis, E. (1984), 'Chlorophyll fluorescence as a tool in plant physiology', *Photosynthesis Research* **5**(2), 139–157.

Krause, G., Somersalo, S., Osmond, C., Briantais, J.-M. and Schreiber, U. (1989), 'Fluorescence as a tool in photosynthesis research: application in studies of photoinhibition, cold acclimation and freezing stress', *Philosophical Transactions of the Royal Society of London. B, Biological Sciences* **3**23(1216), 281–293.

Krause, G. and Weis, E. (1991), 'Chlorophyll fluorescence and photosynthesis: the basics', *Annual review of plant biology* **4**2(1), 313–349.

Krieger, A., Rutherford, A. W., Vass, I. and Hideg, É. (1998), 'Relationship between activity, D1 loss, and Mn binding in photoinhibition of photosystem II', *Biochemistry* **3**7(46), 16262–16269.

Krieger-Liszkay, A. (2005), 'Singlet oxygen production in photosynthesis', *Journal of Experimental Botany* **5**6(411), 337–346.

Krüger, T. P., Novoderezhkin, V. I., Romero, E. and van Grondelle, R. (2014), Photosynthetic energy transfer and charge separation in higher plants, *in* J. Golbeck and A. van der Est, eds, 'The Biophysics of Photosynthesis', Vol. 11 of *Biophysics for the Life Sciences*, Springer New York, pp. 79–118.

Kuchuk, N., Sytnyk, K., Vasylenko, M., Shakhovsky, A., Komarnytsky, I., Kushnir, S. and Gleba, Y. (2006), 'Genetic transformation of plastids of different *Solanaceae* species using tobacco cells as organelle hosts', *Theoretical and applied genetics* **1**13(3), 519–527.

Kurisu, G., Zhang, H., Smith, J. L. and Cramer, W. A. (2003), 'Structure of the cytochrome $b_6f$ complex of oxygenic photosynthesis: tuning the cavity', *Science* **3**02(5647), 1009–1014.

Kuroda, H. and Maliga, P. (2003), 'The plastid clpP1 protease gene is essential for plant development', *Nature* **4**25(6953), 86–89.

Kushnir, S., Babiychuk, E., Bannikova, M., Momot, V., Komarnitsky, I., Cherep, N. and Gleba, Y. (1991), 'Nucleo-cytoplasmic incompatibility in cybrid plants possessing an *Atropa* genome and a *Nicotiana* plastome', *Molecular and General Genetics MGG* **2**25(2), 225–230.

Kushnir, S. G., Shlumukov, L. R., Pogrebnyak, N. J., Berger, S. and Gleba, Y. (1987), 'Functional cybrid plants possessing a *Nicotiana* genome and an *Atropa* plastome', *Molecular & General Genetics* **2**09(1), 159–163.

Kuttkat, A., Grimm, R. and Paulsen, H. (1995), 'Light-harvesting chlorophyll *a/b*-binding protein inserted into isolated thylakoids binds pigments and is assembled into trimeric light-harvesting complex', *Plant physiology* **1**09(4), 1267–1276.

Kyle, D. J. (1985), 'The 32000 Dalton $Q_b$ protein of photosystem II', *Photochemistry and photobiology* **4**1(1), 107–116.

Labate, M., Ko, K., Ko, Z., Pinto, L., Real, M., Romano, M., Barja, P., Granell, A., Friso, G., Wijk, K. et al. (2004), 'Constitutive expression of pea *Lhcb 1–2* in tobacco affects plant development, morphology and photosynthetic capacity', *Plant molecular biology* **5**5(5), 701–714.

Laemmli, U. K. (1970), 'Cleavage of structural proteins during the assembly of the head of bacteriophage T4', *Nature* **2**27(5259), 680–685.

Lamppa, G. K. and Abad, M. S. (1987), 'Processing of a wheat light-harvesting chlorophyll *a/b* protein precursor by a soluble enzyme from higher plant chloroplasts', *The Journal of cell biology* **1**05(6), 2641–2648.

Latimer, P., Bannister, T. and Rabinowitch, E. (1956), 'Quantum yields of fluorescence of plant pigments.', *Science (New York, NY)* **1**24(3222), 585–586.

Leitch, I. J. and Leitch, A. R. (2013), *Genome size diversity and evolution in land plants*, Springer.

Lever, M. A., Rouxel, O., Alt, J. C., Shimizu, N., Ono, S., Coggon, R. M., Shanks, W. C., Lapham, L., Elvert, M., Prieto-Mollar, X. et al. (2013), 'Evidence for microbial carbon and sulfur cycling in deeply buried ridge flank basalt', *Science* **3**39(6125), 1305–1308.

Li, H. (2006), Organization and function of chlorosome proteins in the green sulfur bacterium *Chlorobium tepidum*, PhD thesis, Pennsylvania State University.

Li, X.-P., Björkman, O., Shih, C., Grossman, A. R., Rosenquist, M., Jansson, S. and Niyogi, K. K. (2000), 'A pigment-binding protein essential for regulation of photosynthetic light harvesting', *Nature* **4**03(6768), 391–395.

Li, X.-P., Gilmore, A. M., Caffarri, S., Bassi, R., Golan, T., Kramer, D. and Niyogi, K. K. (2004), 'Regulation of photosynthetic light harvesting involves intrathylakoid lumen pH sensing by the PsbS protein', *Journal of Biological Chemistry* **2**79(22), 22866–22874.

Li, X.-P., Müller-Moulé, P., Gilmore, A. M. and Niyogi, K. K. (2002), 'PsbS-dependent enhancement of feedback de-excitation protects photosystem II from

photoinhibition', *Proceedings of the National Academy of Sciences* **9**9(23), 15222–15227.

Lichtenthaler, H., Buschmann, C., Döll, M., Fietz, H.-J., Bach, T., Kozel, U., Meier, D. and Rahmsdorf, U. (1981), 'Photosynthetic activity, chloroplast ultrastructure, and leaf characteristics of high-light and low-light plants and of sun and shade leaves', *Photosynthesis research* **2**(2), 115–141.

Lin, M. T., Occhialini, A., Andralojc, P. J., Parry, M. A. and Hanson, M. R. (2014), 'A faster RuBisCO with potential to increase photosynthesis in crops', *Nature* **5**13(7519), 547–550.

Linke, B. and Börner, T. (2005), 'Mitochondrial effects on flower and pollen development', *Mitochondrion* **5**(6), 389–402.

Linke, B., Nothnagel, T. and Börner, T. (2003), 'Flower development in carrot CMS plants: mitochondria affect the expression of MADS box genes homologous to GLOBOSA and DEFICIENS', *The Plant Journal* **3**4(1), 27–37.

Liu, J., Xu, X. and Deng, X. (2005), 'Intergeneric somatic hybridization and its application to crop genetic improvement', *Plant cell, tissue and organ culture* **8**2(1), 19–44.

Liu, Z., Yan, H., Wang, K., Kuang, T., Zhang, J., Gui, L., An, X. and Chang, W. (2004), 'Crystal structure of spinach major light-harvesting complex at 2.72 Å resolution', *Nature* **4**28(6980), 287–292.

Loginova, D., Men'shanov, P. and Deineko, E. (2012), 'Analysis of mosaic expression of the *nptII* gene in transgenic tobacco plant lines contrasting in mosaicism', *Russian Journal of Genetics* **4**8(11), 1097–1102.

Lohse, M., Drechsel, O., Kahlau, S. and Bock, R. (2013), 'OrganellarGenomeDRAW—a suite of tools for generating physical maps of plastid and mitochondrial genomes and visualizing expression data sets', *Nucleic acids research* p. 289.

Lolkema, J. S. and Boekema, E. J. (2003), 'The A-type ATP synthase subunit K of *Methanopyrus kandleri* is deduced from its sequence to form a monomeric rotor comprising 13 hairpin domains', *FEBS letters* **5**43(1), 47–50.

Long, S., Humphries, S. and Falkowski, P. G. (1994), 'Photoinhibition of photosynthesis in nature', *Annual review of plant biology* **4**5(1), 633–662.

Lumsden, P. J. and Millar, A. J. (1998), *Biological rhythms and photoperiodism in plants*, Bios Scientific Publishers Oxford.

Makaroff, C. A. and Palmer, J. D. (1988), 'Mitochondrial dna rearrangements and transcriptional alterations in the male-sterile cytoplasm of ogura radish.', *Molecular and cellular biology* **8**(4), 1474–1480.

Margulis, L. (1970), *Origin of eukaryotic cells: evidence and research implications for a theory of the origin and evolution of microbial, plant, and animal cells on the Precambrian earth*, Yale University Press New Haven.

Martin, W. and Kowallik, K. (1999), 'Annotated english translation of mereschkowsky's 1905 paper 'über natur und ursprung der chromatophoren impflanzenreiche", *European Journal of Phycology* **3**4(3), 287–295.

Matsubara, S., Krause, G. H., Aranda, J., Virgo, A., Beisel, K. G., Jahns, P. and Winter, K. (2009), 'Sun-shade patterns of leaf carotenoid composition in 86 species of neotropical forest plants', *Functional Plant Biology* **3**6(1), 20–36.

Maxwell, K. and Johnson, G. N. (2000), 'Chlorophyll fluorescence a practical guide', *Journal of experimental botany* **5**1(345), 659–668.

Mazor, Y., Borovikova, A. and Nelson, N. (2015), 'The structure of plant photosystem I super-complex at 2.8 Å resolution', *eLife* p. e07433.

McAlister, E. D. and Myers, J. (1940), *The time course of photosynthesis and fluorescence observed simultaneously*, Smithsonian institution.

McDonald, M. S. (2003), *Photobiology of higher plants*, John Wiley & Sons.

McFadden, G. I. and van Dooren, G. G. (2004), 'Evolution: red algal genome affirms a common origin of all plastids', *Current Biology* **1**4(13), R514–R516.

McWatters, H. G., Bastow, R. M., Hall, A. and Millar, A. J. (2000), 'The ELF3 zeitnehmer regulates light signalling to the circadian clock', *Nature* **4**08(6813), 716–720.

Meier, T., Morgner, N., Matthies, D., Pogoryelov, D., Keis, S., Cook, G. M., Dimroth, P. and Brutschy, B. (2007), 'A tridecameric c ring of the adenosine triphosphate (ATP) synthase from the thermoalkaliphilic *Bacillus* sp. strain TA2. A1 facilitates ATP synthesis at low electrochemical proton potential', *Molecular microbiology* **6**5(5), 1181–1192.

Melkozernov, A. N. and Blankenship, R. E. (2005), 'Structural and functional organization of the peripheral light-harvesting system in photosystem I', *Photosynthesis research* **8**5(1), 33–50.

Menczel, L., Nagy, F., Kiss, Z. R. and Maliga, P. (1981), 'Streptomycin resistant and sensitive somatic hybrids of *Nicotiana tabacum* + *Nicotiana knightiana*: correlation of resistance to *N. tabacum* plastids', *Theoretical and applied genetics* **5**9(3), 191–195.

Müh, F. and Renger, T. (2014), Structure-based calculation of pigment–protein and excitonic pigment–pigment coupling in photosynthetic light-harvesting complexes, *in* J. Golbeck and A. van der Est, eds, 'The Biophysics of Photosynthesis', Vol. 11 of *Biophysics for the Life Sciences*, Springer New York, pp. 3–44.

Michel, H., Griffin, P., Shabanowitz, J., Hunt, D. and Bennett, J. (1991), 'Tandem mass spectrometry identifies sites of three post-translational modifications of spinach light-harvesting chlorophyll protein II. proteolytic cleavage, acetylation, and phosphorylation.', *Journal of Biological Chemistry* **2**66(26), 17584–17591.

Minagawa, J. (2013), 'Dynamic reorganization of photosynthetic supercomplexes during environmental acclimation of photosynthesis', *Frontiers in plant science* **4**.

Moberg, P., Ståhl, A., Bhushan, S., Wright, S. J., Eriksson, A., Bruce, B. D. and Glaser, E. (2003), 'Characterization of a novel zinc metalloprotease involved in degrading targeting peptides in mitochondria and chloroplasts', *The Plant Journal* **3**6(5), 616–628.

Moore, M., Goforth, R. L., Mori, H. and Henry, R. (2003), 'Functional interaction of chloroplast SRP/FtsY with the ALB3 translocase in thylakoids substrate not required', *The Journal of cell biology* **1**62(7), 1245–1254.

Morgan, A. and Maliga, P. (1987), 'Rapid chloroplast segregation and recombination of mitochondrial DNA in Brassica cybrids', *Molecular and General Genetics MGG* **2**09(2), 240–246.

Morosinotto, T. and Bassi, R. (2007), Antenna system of higher plants' Photosystem I and its interaction with the core complex, *in* G. Renger, ed., 'Primary Processes of Photosynthesis, Part 1: Principles and Apparatus', Vol. 1 of *Comprehensive Series in Photochemical & Photobiological Sciences*, Royal Society of Chemistry, chapter 7, pp. 301–323.

Müller, M. G., Slavov, C., Luthra, R., Redding, K. E. and Holzwarth, A. R. (2010), 'Independent initiation of primary electron transfer in the two branches of the photosystem I reaction center', *Proceedings of the National Academy of Sciences* **1**07(9), 4123–4128.

Müller, P., Li, X.-P. and Niyogi, K. K. (2001), 'Non-photochemical quenching. A response to excess light energy', *Plant Physiology* **1**25(4), 1558–1566.

Mullet, J. E. and Arntzen, C. J. (1980), 'Simulation of grana stacking in a model membrane system. Mediation by a purified light-harvesting pigment-protein complex from chloroplasts', *Biochimica et Biophysica Acta (BBA)-Bioenergetics* **5**89(1), 100–117.

Munekage, Y., Hashimoto, M., Miyake, C., Tomizawa, K.-I., Endo, T., Tasaka, M. and Shikanai, T. (2004), 'Cyclic electron flow around photosystem I is essential for photosynthesis', *Nature* **4**29(6991), 579–582.

Munekage, Y., Hojo, M., Meurer, J., Endo, T., Tasaka, M. and Shikanai, T. (2002), 'PGR5 is involved in cyclic electron flow around photosystem I and is essential for photoprotection in *Arabidopsis*', *Cell* **1**10(3), 361–371.

Murashige, T. and Skoog, F. (1962), 'A revised medium for rapid growth and bio assays with tobacco tissue cultures', *Physiologia plantarum* **1**5(3), 473–497.

Murchie, E. H. and Niyogi, K. K. (2011), 'Manipulation of photoprotection to improve plant photosynthesis', *Plant physiology* **1**55(1), 86–92.

Mustárdy, L., Buttle, K., Steinbach, G. and Garab, G. (2008), 'The three-dimensional network of the thylakoid membranes in plants: quasihelical model of the granum-stroma assembly', *The Plant Cell Online* **2**0(10), 2552–2557.

Nagata, T. and Bajaj, Y. (2001), *Somatic Hybridization in Crop Improvement II: II*, Biotechnology in Agriculture and Forestry, Springer Berlin Heidelberg.

Nelson, D. L., Lehninger, A. L. and Cox, M. M. (2008), *Lehninger Principles of Biochemistry*, 5th edn, Macmillan.

Nelson, N. and Ben-Shem, A. (2004), 'The complex architecture of oxygenic photosynthesis', *Nature Reviews Molecular Cell Biology* **5**(12), 971–982.

Nelson, N. and Yocum, C. F. (2006), 'Structure and function of photosystems I and II', *Annu. Rev. Plant Biol.* **5**7, 521–565.

Nickelsen, J. and Rengstl, B. (2012), 'Photosystem II assembly: from cyanobacteria to plants.', *Annual review of plant biology* **6**4, 609–635.

Nield, J. and Barber, J. (2006), 'Refinement of the structural model for the Photosystem II supercomplex of higher plants', *Biochimica et Biophysica Acta (BBA)-Bioenergetics* **1**757(5), 353–361.

Nield, J., Orlova, E. V., Morris, E. P., Gowen, B., van Heel, M. and Barber, J. (2000), '3D map of the plant photosystem II supercomplex obtained by cryo-electron microscopy and single particle analysis', *Nature Structural & Molecular Biology* **7**(1), 44–47.

Nilkens, M., Kress, E., Lambrev, P., Miloslavina, Y., Müller, M., Holzwarth, A. R. and Jahns, P. (2010), 'Identification of a slowly inducible zeaxanthin-dependent component of non-photochemical quenching of chlorophyll fluorescence generated under steady-state conditions in Arabidopsis', *Biochimica et Biophysica Acta (BBA)-Bioenergetics* **1**797(4), 466–475.

Nishimura, K. and van Wijk, K. J. (2014), 'Organization, function and substrates of the essential Clp protease system in plastids', *Biochimica et Biophysica Acta (BBA)-Bioenergetics* .

Niyogi, K. K. (1999), 'Photoprotection revisited: genetic and molecular approaches', *Annual review of plant biology* **5**0(1), 333–359.

Nobel, P. S. (2009), *Physicochemical and environmental plant physiology*, 4th edn, Academic press.

Noctor, G., Rees, D., Young, A. and Horton, P. (1991), 'The relationship between zeaxanthin, energy-dependent quenching of chlorophyll fluorescence, and trans-thylakoid pH gradient in isolated chloroplasts', *Biochimica et Biophysica Acta (BBA)-Bioenergetics* **1**057(3), 320–330.

Oblong, J. E. and Lamppa, G. K. (1992), 'Identification of two structurally related proteins involved in proteolytic processing of precursors targeted to the chloroplast.', *The EMBO journal* **1**1(12), 4401.

Oguchi, R., Hikosaka, K. and Hirose, T. (2003), 'Does the photosynthetic light-acclimation need change in leaf anatomy?', *Plant, Cell & Environment* **2**6(4), 505–512.

Ostroumov, E. E., Khan, Y. R., Scholes, G. D. et al. (2014), Photophysics of photosynthetic pigment-protein complexes, *in* B. Demmig-Adams, G. Garab, W. Adams III et al., eds, 'Non-Photochemical Quenching and Energy Dissipation in Plants, Algae and Cyanobacteria', Springer, pp. 97–128.

Ouyang, M., Li, X., Ma, J., Chi, W., Xiao, J., Zou, M., Chen, F., Lu, C. and Zhang, L. (2011), 'LTD is a protein required for sorting light-harvesting chlorophyll-binding proteins to the chloroplast SRP pathway', *Nature communications* **2**, 277.

Oxborough, K. and Horton, P. (1988), 'A study of the regulation and function of energy-dependent quenching in pea chloroplasts', *Biochimica et Biophysica Acta (BBA)-Bioenergetics* **9**34(1), 135–143.

Pagliano, C., Barera, S., Chimirri, F., Saracco, G. and Barber, J. (2012), 'Comparison of the $\alpha$ and $\beta$ isomeric forms of the detergent n-dodecyl-d-maltoside for solubilizing photosynthetic complexes from pea thylakoid membranes', *Biochimica et Biophysica Acta (BBA)-Bioenergetics* **1**817(8), 1506–1515.

Paila, Y. D., Richardson, L. G. and Schnell, D. J. (2015), 'New insights into the mechanism of chloroplast protein import and its integration with protein quality control, organelle biogenesis and development', *Journal of molecular biology* **4**27(5), 1038–1060.

Palmer, J. D. (2000), 'Molecular evolution: A single birth of all plastids?', *Nature* **4**05(6782), 32–33.

Pan, X., Li, M., Wan, T., Wang, L., Jia, C., Hou, Z., Zhao, X., Zhang, J. and Chang, W. (2011), 'Structural insights into energy regulation of light-harvesting complex CP29 from spinach', *Nature structural & molecular biology* **1**8(3), 309–315.

Pelletier, G. and Budar, F. (2007), 'The molecular biology of cytoplasmically inherited male sterility and prospects for its engineering', *Current Opinion in biotechnology* **1**8(2), 121–125.

Pelletier, G., Primard, C., Vedel, F., Chetrit, P., Remy, R., Renard, M. et al. (1983), 'Intergeneric cytoplasmic hybridization in Cruciferae by protoplast fusion', *Molecular and General Genetics MGG* **1**91(2), 244–250.

Pental, D., Hamill, J. D., Pirrie, A. and Cocking, E. C. (1986), 'Somatic hybridization of *Nicotiana tabacum* and *Petunia hybrida*', *Molecular and General Genetics MGG* **2**02(3), 342–347.

Peschek, G. A. (2008), 'Electron transport chains in oxygenic cyanobacteria', *Primary Processes of Photosynthesis: Principles and Applications* **2**, 383–415.

Peter, G. F. and Thornber, J. P. (1991), 'Biochemical composition and organization of higher plant photosystem II light-harvesting pigment-proteins.', *Journal of Biological Chemistry* **2**66(25), 16745–16754.

Peter, S., Spang, O., Medgyesy, P. and Schäfer, C. (1999), 'Consequences of intergeneric chloroplast transfers on photosynthesis and sensitivity to high light', *Functional Plant Biology* **2**6(2), 171–177.

Petrou, K., Belgio, E. and Ruban, A. V. (2013), 'pH sensitivity of chlorophyll fluorescence quenching is determined by the detergent/protein ratio and the state of LHCII aggregation', *Biochimica et Biophysica Acta (BBA)-Bioenergetics* .

Pfündel, E. E., Klughammer, C., Meister, A. and Cerovic, Z. G. (2013), 'Deriving fluorometer-specific values of relative PSI fluorescence intensity from quenching of $F_o$ fluorescence in leaves of *Arabidopsis thaliana* and *Zea mays*', *Photosynthesis research* **1**14(3), 189–206.

Pichersky, E., Hoffman, N. E., Malik, V. S., Bernatzky, R., Tanksley, S. D., Szabo, L. and Cashmore, A. R. (1987), 'The tomato Cab-4 and Cab-5 genes encode a second type of CAB polypeptides localized in photosystem II', *Plant molecular biology* **9**(2), 109–120.

Pietrzykowska, M., Suorsa, M., Semchonok, D. A., Tikkanen, M., Boekema, E. J., Aro, E.-M. and Jansson, S. (2014), 'The light-harvesting chlorophyll *a/b* binding proteins Lhcb1 and Lhcb2 play complementary roles during state transitions in Arabidopsis', *The Plant Cell Online* **2**6(9), 3646–3660.

Porra, R. J., Thompson, W. A. and Kriedemann, P. E. (1989), 'Determination of accurate extinction coefficients and simultaneous equations for assaying chlorophylls *a* and *b* extracted with four different solvents - verification of the chlorophyll standards by atomic absorption spectroscopy', *Biochimica et Biophysica Acta* **9**75(3), 384–394.

Pribil, M., Leister, D. et al. (2014), 'Structure and dynamics of thylakoids in land plants', *Journal of experimental botany* p. eru090.

Puthiyaveetil, S., Ibrahim, I. M. and Allen, J. F. (2012), 'Oxidation-reduction signalling components in regulatory pathways of state transitions and photosystem stoichiometry adjustment in chloroplasts', *Plant Cell and Environment* **3**5(2), 347–359.

Pyke, K. (2009), *Plastid Biology*, Cambridge University Press.

Pyke, K. (2011), Analysis of plastid number, size, and distribution in Arabidopsis plants by light and fluorescence microscopy, *in* 'Chloroplast Research in Arabidopsis', Springer, pp. 19–32.

Pyke, K. and Leech, R. (1987), 'The control of chloroplast number in wheat mesophyll cells', *Planta* **1**70(3), 416–420.

Ralph, P. J. and Gademann, R. (2005), 'Rapid light curves: a powerful tool to assess photosynthetic activity', *Aquatic Botany* **8**2(3), 222–237.

Rappaport, F., Guergova-Kuras, M., Nixon, P. J., Diner, B. A. and Lavergne, J. (2002), 'Kinetics and pathways of charge recombination in photosystem II', *Biochemistry* **4**1(26), 8518–8527.

Raven, J. A. and Geider, R. J. (2003), Adaptation, acclimation and regulation in algal photosynthesis, *in* 'Photosynthesis in Algae', Springer, pp. 385–412.

Rees, D., Noctor, G., Ruban, A. V., Crofts, J., Young, A. and Horton, P. (1992), 'pH dependent chlorophyll fluorescence quenching in spinach thylakoids from light treated or dark adapted leaves', *Photosynthesis research* **3**1(1), 11–19.

Rees, D., Young, A., Noctor, G., Britton, G. and Horton, P. (1989), 'Enhancement of the ΔpH-dependent dissipation of excitation energy in spinach chloroplasts by light-activation: correlation with the synthesis of zeaxanthin', *FEBS letters* **2**56(1), 85–90.

Remelli, R., Varotto, C., Sandonà, D., Croce, R. and Bassi, R. (1999), 'Chlorophyll binding to monomeric light-harvesting complex a mutation analysis of chromophore-binding residues', *Journal of Biological Chemistry* **2**74(47), 33510–33521.

Renger, G. (2007), Overview of primary processes of photosynthesis, *in* G. Renger, ed., 'Primary Processes of Photosynthesis, Part 1: Principles and Apparatus', Vol. 1 of *Comprehensive Series in Photochemical & Photobiological Sciences*, Royal Society of Chemistry, pp. 7–30.

Rhee, K.-H., Morris, E. P., Barber, J. and Kühlbrandt, W. (1998), 'Three-dimensional structure of the plant photosystem II reaction centre at 8 Å resolution', *Nature* **3**96(6708), 283–286.

Rhee, K.-H., Morris, E. P., Zheleva, D., Hankamer, B., Kühlbrandt, W. and Barber, J. (1997), 'Two-dimensional structure of plant photosystem II at 8-Å resolution', *Nature* **3**89(6650), 522–526.

Richter, C. V., Träger, C. and Schünemann, D. (2008), 'Evolutionary substitution of two amino acids in chloroplast SRP54 of higher plants cause its inability to bind SRP RNA', *FEBS letters* **5**82(21), 3223–3229.

Richter, S., Zhong, R. and Lamppa, G. (2005), 'Function of the stromal processing peptidase in the chloroplast import pathway', *Physiologia Plantarum* **1**23(4), 362–368.

Ritte, G., Lloyd, J. R., Eckermann, N., Rottmann, A., Kossmann, J. and Steup, M. (2002), 'The starch-related R1 protein is an $\alpha$-glucan, water dikinase', *Proceedings of the National Academy of Sciences* **9**9(10), 7166–7171.

Ruban, A. and Horton, P. (1992), 'Mechanism of $\delta$pH-dependent dissipation of absorbed excitation energy by photosynthetic membranes. I. Spectroscopic analysis of isolated light-harvesting complexes', *Biochimica et Biophysica Acta (BBA)-Bioenergetics* **1**102(1), 30–38.

Ruban, A., Rees, D., Noctor, G., Young, A. and Horton, P. (1991), 'Long-wavelength chlorophyll species are associated with amplification of high-energy-state excitation quenching in higher plants', *Biochimica et Biophysica Acta (BBA)-Bioenergetics* **1**059(3), 355–360.

Ruban, A., Rees, D., Pascal, A. and Horton, P. (1992), 'Mechanism of $\delta$pH-dependent dissipation of absorbed excitation energy by photosynthetic membranes. II. The relationship between LHCII aggregation in vitro and qE in isolated thylakoids', *Biochimica et Biophysica Acta (BBA)-Bioenergetics* **1**102(1), 39–44.

Ruban, A. V. (2009), 'Plants in light', *Commun Integr Biol* **2**(1), 50–55.

Ruban, A. V. (2012), *The photosynthetic membrane: molecular mechanisms and biophysics of light harvesting*, John Wiley & Sons.

Ruban, A. V. and Horton, P. (1994), 'Spectroscopy of non-photochemical and photochemical quenching of chlorophyll fluorescence in leaves; evidence for a role of the light harvesting complex of photosystem II in the regulation of energy dissipation', *Photosynthesis research* **4**0(2), 181–190.

Ruban, A. V. and Horton, P. (1999), 'The xanthophyll cycle modulates the kinetics of nonphotochemical energy dissipation in isolated light-harvesting complexes, intact chloroplasts, and leaves of spinach', *Plant Physiology* **1**19(2), 531–542.

Ruban, A. V. and Johnson, M. P. (2009), 'Dynamics of higher plant photosystem cross-section associated with state transitions', *Photosynthesis research* **9**9(3), 173–183.

Ruban, A. V., Johnson, M. P. and Duffy, C. D. (2012), 'The photoprotective molecular switch in the photosystem II antenna', *Biochimica et Biophysica Acta (BBA)-Bioenergetics* **1**817(1), 167–181.

Ruban, A. V. and Murchie, E. H. (2012), 'Assessing the photoprotective effectiveness of non-photochemical chlorophyll fluorescence quenching: a new approach', *Biochimica et Biophysica Acta (BBA)-Bioenergetics* **1**817(7), 977–982.

Ruban, A. V., Young, A. J., Pascal, A. A. and Horton, P. (1994), 'The effects of illumination on the xanthophyll composition of the photosystem II light-harvesting complexes of spinach thylakoid membranes', *Plant physiology* **1**04(1), 227–234.

Rudella, A., Friso, G., Alonso, J. M., Ecker, J. R. and Van Wijk, K. J. (2006), 'Downregulation of ClpR2 leads to reduced accumulation of the ClpPRS protease complex and defects in chloroplast biogenesis in Arabidopsis', *The Plant Cell* **1**8(7), 1704–1721.

Sanchez-Puerta, M. V. and Abbona, C. C. (2014), 'The chloroplast genome of *Hyoscyamus niger* and a phylogenetic study of the tribe Hyoscyameae (Solanaceae)', *PloS one* **9**(5), e98353.

Sanchez-Puerta, M., Zubko, M. K. and Palmer, J. D. (2014), 'Homologous recombination and retention of a single form of most genes shape the highly chimeric mitochondrial genome of a cybrid plant', *New Phytologist* .

Santner, A. and Estelle, M. (2009), 'Recent advances and emerging trends in plant hormone signalling', *Nature* **4**59(7250), 1071–1078.

Sapozhnikov, D., Krasovskaya, T. and Maevskaya, A. (1957), Change in the interrelationship of the basic carotenoids of the plastids of green leaves under the action of light, *in* 'Dokl Akad Nauk USSR', Vol. 113, pp. 465–467.

Scheer, H. (2008), Chlorophylls, *in* G. Renger, ed., 'Primary Processes of Photosynthesis, Part 1: Principles and Apparatus', Vol. 1 of *Comprehensive Series in Photochemical & Photobiological Sciences*, Royal Society of Chemistry, pp. 101–151.

Schirrmeister, B. E., de Vos, J. M., Antonelli, A. and Bagheri, H. C. (2013), 'Evolution of multicellularity coincided with increased diversification of cyanobacteria and the Great Oxidation Event', *Proceedings of the National Academy of Sciences* **1**10(5), 1791–1796.

Schmitz-Linneweber, C., Kushnir, S., Babiychuk, E., Poltnigg, P., Herrmann, R. G. and Maier, R. M. (2005), 'Pigment deficiency in nightshade/tobacco cybrids is caused by the failure to edit the plastid ATPase $\alpha$-subunit mRNA', *The Plant Cell Online* **1**7(6), 1815–1828.

Schmitz-Linneweber, C., Regel, R., Du, T. G., Hupfer, H., Herrmann, R. G. and Maier, R. M. (2002), 'The plastid chromosome of *Atropa belladonna* and its comparison with that of *Nicotiana tabacum*: the role of RNA editing in generating divergence in the process of plant speciation', *Molecular biology and evolution* **1**9(9), 1602–1612.

Schöttler, M. A., Albus, C. A. and Bock, R. (2011), 'Photosystem I: its biogenesis and function in higher plants', *Journal of plant physiology* **1**68(12), 1452–1461.

Schreiber, U. (2004), Pulse-amplitude-modulation (PAM), *in* G. C. Papageorgiou and Govindjee, eds, 'Chlorophyll *a* Fluorescence. A Signature of Photosynthesis', Vol. 19 of *Advances in Photosynthesis and Respiration*, Springer, pp. 279–319.

Schreiber, U., Klughammer, C. and Kolbowski, J. (2012), 'Assessment of wavelength-dependent parameters of photosynthetic electron transport with a new type of multi-color PAM chlorophyll fluorometer', *Photosynthesis research* **1**13(1-3), 127–144.

Schöttler, M. A. and Toth, S. Z. (2014), 'Photosynthetic complex stoichiometry dynamics in higher plants: environmental acclimation and photosynthetic flux control', *Frontiers in Plant Science* **5**(188).

Schünemann, D. (2004), 'Structure and function of the chloroplast signal recognition particle', *Current genetics* **4**4(6), 295–304.

Seelert, H., Poetsch, A., Dencher, N. A., Engel, A., Stahlberg, H. and Müller, D. J. (2000), 'Structural biology: proton-powered turbine of a plant motor', *Nature* **4**05(6785), 418–419.

Shepard, J. F. and Totten, R. E. (1977), 'Mesophyll cell protoplasts of potato isolation, proliferation, and plant regeneration', *Plant Physiology* **6**0(2), 313–316.

Shi, C., Hu, N., Huang, H., Gao, J., Zhao, Y.-J. and Gao, L.-Z. (2012), 'An improved chloroplast DNA extraction procedure for whole plastid genome sequencing', *PloS one* **7**(2), e31468.

Shi, L.-X., Hall, M., Funk, C. and Schröder, W. P. (2012), 'Photosystem II, a growing complex: updates on newly discovered components and low molecular mass proteins', *Biochimica et Biophysica Acta (BBA)-Bioenergetics* **1**817(1), 13–25.

Shields, D. C. and Wolfe, K. H. (1997), 'Accelerated evolution of sites undergoing mRNA editing in plant mitochondria and chloroplasts.', *Molecular biology and evolution* **1**4(3), 344–349.

Shikanai, T. (2006), 'RNA editing in plant organelles: machinery, physiological function and evolution', *Cellular and Molecular Life Sciences CMLS* **6**3(6), 698–708.

Shimoni, E., Rav-Hon, O., Ohad, I., Brumfeld, V. and Reich, Z. (2005), 'Three-dimensional organization of higher-plant chloroplast thylakoid membranes revealed by electron tomography', *The Plant Cell Online* **1**7(9), 2580–2586.

Shinozaki, K., Ohme, M., Tanaka, M., Wakasugi, T., Hayashida, N., Matsubayashi, T., Zaita, N., Chunwongse, J., Obokata, J., Yamaguchi-Shinozaki, K. et al. (1986), 'The complete nucleotide sequence of the tobacco chloroplast genome: its gene organization and expression', *The EMBO journal* **5**(9), 2043.

Sidorov, V., Zubko, M., Kuchko, A., Komarnitsky, I. and Gleba, Y. (1987), 'Somatic hybridization in potato: use of $\gamma$-irradiated protoplasts of *Solanum pinnatisectum* in genetic reconstruction', *Theoretical and applied genetics* **7**4(3), 364–368.

Siefermann, D. and Yamamoto, H. Y. (1975), 'Properties of NADPH and oxygen-dependent zeaxanthin epoxidation in isolated chloroplasts: a transmembrane model for the violaxanthin cycle', *Archives of biochemistry and biophysics* **1**71(1), 70–77.

Smith, A. M., Zeeman, S. C. and Smith, S. M. (2005), 'Starch degradation', *Annu. Rev. Plant Biol.* **5**6, 73–98.

Soll, J. and Schleiff, E. (2004), 'Protein import into chloroplasts', *Nature Reviews Molecular Cell Biology* **5**(3), 198–208.

Standfuss, J., Terwisscha van Scheltinga1, A. C., Lamborghini, M. and Kuhlbrandt, W. (2005), 'Mechanisms of photoprotection and nonphotochemical quenching in pea light harvesting complex at 2.5 Å resolution', *The EMBO Journal* **2**4, 919–928.

Stauber, E. J., Fink, A., Markert, C., Kruse, O., Johanningmeier, U. and Hippler, M. (2003), 'Proteomics of *Chlamydomonas reinhardtii* light-harvesting proteins', *Eukaryotic Cell* **2**(5), 978–994.

Stengel, K. F., Holdermann, I., Cain, P., Robinson, C., Wild, K. and Sinning, I. (2008), 'Structural basis for specific substrate recognition by the chloroplast signal recognition particle protein cpSRP43', *Science* **3**21(5886), 253–256.

Strasser, R. J., Tsimilli-Michael, M. and Srivastava, A. (2004), *Analysis of the chlorophyll a fluorescence transient*, Springer.

Stull, G. W., Moore, M. J., Mandala, V. S., Douglas, N. A., Kates, H.-R., Qi, X., Brockington, S. F., Soltis, P. S., Soltis, D. E. and Gitzendanner, M. A. (2013), 'A targeted enrichment strategy for massively parallel sequencing of angiosperm plastid genomes', *Applications in Plant Sciences* **1**(2).

Sugiura, M., Ozaki, Y., Nakamura, M., Cox, N., Rappaport, F. and Boussac, A. (2014), 'The D1-173 amino acid is a structural determinant of the critical interaction between D1–Tyr161 (Tyr Z) and D1–His190 in Photosystem II', *Biochimica et Biophysica Acta (BBA)-Bioenergetics* .

Sundberg, M. D. (1992), An introduction to stereological analysis: morphometric techniques for beginning biologists, *in* 'Tested Studies for Laboratory Teaching. Proceedings of the 6th Workshop Conference of the Association for Biology Laboratory Education, Toronto', pp. 51–72.

Suorsa, M., Rantala, M., Danielsson, R., Järvi, S., Paakkarinen, V., Schröder, W. P., Styring, S., Mamedov, F. and Aro, E.-M. (2013), 'Dark-adapted spinach thylakoid protein heterogeneity offers insights into the photosystem II repair cycle', *Biochimica et Biophysica Acta (BBA)-Bioenergetics* .

Süss, K.-H. and Schmidt, O. (1982), 'Evidence for an $\alpha$ 3, $\beta$ 3, $\gamma$, $\delta$, I, II, $\varepsilon$, III 5 subunit stoichiometry of chloroplast ATP synthetase complex ($CF_1$- $CF_o$)', *FEBS Letters* **1**44(2), 213–218.

Svyatyna, K. and Riemann, M. (2012), 'Light-dependent regulation of the jasmonate pathway', *Protoplasma* **2**49(2), 137–145.

Takenaka, M., Zehrmann, A., Verbitskiy, D., Kugelmann, M., Härtel, B. and Brennicke, A. (2012), 'Multiple organellar RNA editing factor (MORF) family proteins are required for RNA editing in mitochondria and plastids of plants', *Proceedings of the National Academy of Sciences* **1**09(13), 5104–5109.

Teixeira, P. F. and Glaser, E. (2013), 'Processing peptidases in mitochondria and chloroplasts', *Biochimica et Biophysica Acta (BBA)-Molecular Cell Research* **1**833(2), 360–370.

Terashima, I., Miyazawa, S.-I. and Hanba, Y. T. (2001), 'Why are sun leaves thicker than shade leaves?—consideration based on analyses of $CO_2$ diffusion in the leaf', *Journal of Plant Research* **1**14(1), 93–105.

Tillich, M., Funk, H. T., Schmitz-Linneweber, C., Poltnigg, P., Sabater, B., Martin, M. and Maier, R. M. (2005), 'Editing of plastid RNA in *Arabidopsis thaliana* ecotypes', *The Plant Journal* **4**3(5), 708–715.

Umena, Y., Kawakami, K., Shen, J.-R. and Kamiya, N. (2011), 'Crystal structure of oxygen-evolving photosystem II at a resolution of 1.9 Å', *Nature* **4**73(7345), 55–60.

Valladares, F. and Niinemets, Ü. (2008), 'Shade tolerance, a key plant feature of complex nature and consequences', *Annual Review of Ecology, Evolution, and Systematics* pp. 237–257.

van Amerongen, H. and Croce, R. (2007), Structure and function Photosystem II light harvesting proteins (lhcb) of higher plants, *in* G. Renger, ed., 'Primary Processes of Photosynthesis, Part 1: Principles and Apparatus', Vol. 1 of *Comprehensive Series in Photochemical & Photobiological Sciences*, Royal Society of Chemistry, chapter 8, pp. 329–354.

van Niel, C., Ruben, S., Carson, S., Kamen, M. and Foster, J. (1942), 'Radioactive carbon as an indicator of carbon dioxide utilization: VIII. the role of carbon dioxide in cellular metabolism', *Proceedings of the National Academy of Sciences of the United States of America* **2**8(1), 8.

van Roon, H., van Breemen, J. F., de Weerd, F. L., Dekker, J. P. and Boekema, E. J. (2000), 'Solubilization of green plant thylakoid membranes with n-dodecyl-$\alpha$, D-maltoside. implications for the structural organization of the Photosystem II, Photosystem I, ATP synthase and Cyt $b_6f$ complexes', *Photosynthesis research* **6**4(2-3), 155–166.

Vass, I., Styring, S., Hundal, T., Koivuniemi, A., Aro, E. and Andersson, B. (1992), 'Reversible and irreversible intermediates during photoinhibition of photosystem II: stable reduced $Q_A$ species promote chlorophyll triplet formation', *Proceedings of the National Academy of Sciences* **8**9(4), 1408–1412.

Vig, B. K. (1978), 'Somatic mosaicism in plants with special reference to somatic crossing over', *Environmental health perspectives* **2**7, 27.

von Ballmoos, C., Wiedenmann, A. and Dimroth, P. (2009), 'Essentials for ATP synthesis by F1F0 ATP synthases', *Annual review of biochemistry* **7**8, 649–672.

Wakasugi, T., Sugita, M., Tsudzuki, T. and Sugiura, M. (1998), 'Updated gene map of tobacco chloroplast DNA', *Plant Molecular Biology Reporter* **1**6(3), 231–241.

Walker, D. (1992), *Energy, plants and man*, University Science Books.

Walters, R. G. (2005), 'Towards an understanding of photosynthetic acclimation', *Journal of experimental botany* **5**6(411), 435–447.

Walters, R. G., Ruban, A. V. and Horton, P. (1994), 'Higher plant light-harvesting complexes LHCIIa and LHCIIc are bound by dicyclohexylcarbodiimide during inhibition of energy dissipation', *European journal of biochemistry* **2**26(3), 1063–1069.

Wang, L., Pan, Z.-Y. and Guo, W.-W. (2010), 'Proteomic analysis of leaves from a diploid cybrid produced by protoplast fusion between satsuma mandarin and pummelo', *Plant Cell, Tissue and Organ Culture (PCTOC)* **1**03(2), 165–174.

Wang, P. and Dalbey, R. E. (2011), 'Inserting membrane proteins: the YidC/Oxa1/Alb3 machinery in bacteria, mitochondria, and chloroplasts', *Biochimica et Biophysica Acta (BBA)-Biomembranes* **1**808(3), 866–875.

Wasternack, C. and Hause, B. (2013), 'Jasmonates: biosynthesis, perception, signal transduction and action in plant stress response, growth and development. An update to the 2007 review in Annals of Botany', *Annals of Botany* **1**11(6), 1021–1058.

Waterhouse, A. M., Procter, J. B., Martin, D. M., Clamp, M. and Barton, G. J. (2009), 'Jalview version 2. A multiple sequence alignment editor and analysis workbench', *Bioinformatics* **2**5(9), 1189–1191.

Wedell, N., Klein, R., Ljungberg, U., Andersson, B. and Herrmann, R. (1992), 'The single-copy gene *psbS* codes for a phylogenetically intriguing 22 kDa polypeptide of photosystem II', *FEBS letters* **3**14(1), 61–66.

White, A. J. and Critchley, C. (1999), 'Rapid light curves: a new fluorescence method to assess the state of the photosynthetic apparatus', *Photosynthesis Research* **5**9(1), 63–72.

Wicke, S., Schneeweiss, G. M., Müller, K. F., Quandt, D. et al. (2011), 'The evolution of the plastid chromosome in land plants: gene content, gene order, gene function', *Plant molecular biology* **7**6(3-5), 273–297.

Wientjes, E., van Amerongen, H. and Croce, R. (2013), 'LHCII is an antenna of both photosystems after long-term acclimation', *Biochimica et Biophysica Acta (BBA)-Bioenergetics* **1**827(3), 420–426.

Wild, A. and Wolf, G. (1980), 'The effect of different light intensities on the frequency and size of stomata, the size of cells, the number, size and chlorophyll content of chloroplasts in the mesophyll and the guard cells during the ontogeny of primary leaves of *Sinapis alba*', *Zeitschrift für Pflanzenphysiologie* **97**(4), 325–342.

Wollman, F.-A. (2001), 'State transitions reveal the dynamics and flexibility of the photosynthetic apparatus', *The EMBO journal* **20**(14), 3623–3630.

Woodson, J. D. and Chory, J. (2008), 'Coordination of gene expression between organellar and nuclear genomes', *Nature Reviews Genetics* **9**(5), 383–395.

Wraight, C. A. and Crofts, A. R. (1970), 'Energy-dependent quenching of chlorophyll a fluorescence in isolated chloroplasts', *European Journal of Biochemistry* **17**(2), 319–327.

Yamamoto, H. Y., Kamite, L. and Wang, Y.-Y. (1972), 'An ascorbate-induced absorbance change in chloroplasts from violaxanthin de-epoxidation', *Plant physiology* **49**(2), 224–228.

Yang, D.-H., Paulsen, H. and Andersson, B. (2000), 'The N-terminal domain of the light-harvesting chlorophyll $a/b$-binding protein complex (LHCII) is essential for its acclimative proteolysis', *FEBS letters* **466**(2), 385–388.

Yang, J.-B., Li, D.-Z. and Li, H.-T. (2014), 'Highly effective sequencing whole chloroplast genomes of angiosperms by nine novel universal primer pairs', *Molecular ecology resources* .

Yuan, J., Kight, A., Goforth, R. L., Moore, M., Peterson, E. C., Sakon, J. and Henry, R. (2002), 'ATP stimulates signal recognition particle (SRP)/FtsY-supported protein integration in chloroplasts', *Journal of Biological Chemistry* **277**(35), 32400–32404.

Yukawa, M., Tsudzuki, T. and Sugiura, M. (2005), 'The 2005 version of the chloroplast DNA sequence from tobacco (*Nicotiana tabacum*)', *Plant Molecular Biology Reporter* **23**(4), 359–365.

Yukawa, M., Tsudzuki, T. and Sugiura, M. (2006), 'The chloroplast genome of *Nicotiana sylvestris* and *Nicotiana tomentosiformis*: complete sequencing confirms that the *Nicotiana sylvestris* progenitor is the maternal genome donor of *Nicotiana tabacum*', *Molecular Genetics and Genomics* **275**(4), 367–373.

Zhang, Y. and Turner, J. G. (2008), 'Wound-induced endogenous jasmonates stunt plant growth by inhibiting mitosis', *PLoS One* **3**(11), e3699–e3699.

Zia, A., Johnson, M. P. and Ruban, A. V. (2011), 'Acclimation- and mutation-induced enhancement of PsbS levels affects the kinetics of non-photochemical quenching in *Arabidopsis thaliana*', *Planta* **2**33(6), 1253–1264.

Zivcak, M., Brestic, M., Kalaji, H. M. et al. (2014), 'Photosynthetic responses of sun-and shade-grown barley leaves to high light: is the lower PSII connectivity in shade leaves associated with protection against excess of light?', *Photosynthesis research* **1**19(3), 339–354.

Zubko, M. K., Zubko, E. I., Adler, K., Grimm, B. and Gleba, Y. Y. (2003), 'New CMS-associated phenotypes in cybrids *Nicotiana tabacum* L.(+ *Hyoscyamus niger* L.)', *Annals of botany* **9**2(2), 281–288.

Zubko, M. K., Zubko, E. I., Patskovsky, Y. V., Khvedynich, O. A., Fisahn, J., Gleba, Y. Y. and Schieder, O. (1996), 'Novel 'homeotic' CMS patterns generated in Nicotiana via cybridization with *Hyoscyamus* and *Scopolia*', *Journal of Experimental Botany* **4**7(301), 1101–1110.

Zubko, M. K., Zubko, E. I., Ruban, A. V., Adler, K., Mock, H. P., Misera, S., Gleba, Y. Y. and Grimm, B. (2001), 'Extensive developmental and metabolic alterations in cybrids *Nicotiana tabacum* (plus *Hyoscyamus niger*) are caused by complex nucleo-cytoplasmic incompatibility', *Plant Journal* **2**5(6), 627–639.

Zubko, M., Zubko, E. and Kapranov Ph, V. (1991), 'Induction of chlorophyll-deficient tobacco mutants as markers for cell engineering', *Biopolymers and Cell* **7**, 72–9.

Zybailov, B., Rutschow, H., Friso, G., Rudella, A., Emanuelsson, O., Sun, Q. and van Wijk, K. J. (2008), 'Sorting signals, N-terminal modifications and abundance of the chloroplast proteome', *PloS one* **3**(4), 1–19.